REPUBLIQUE DU CAMEROUN
Paix-Travail-Patrie

UNIVERSITE DE YAOUNDE I

CENTRE DE RECHERCHE ET DE FORMATION DOCTORALE EN SCIENCES, TECHNOLOGIES ET GEOSCIENCES

UNITE DE RECHERCHE ET DE FORMATIONDOCTORALEEN PHYSIQUES ETAPPLICATIONS

B.P 812 Yaoundé
Email: crfd_stg@uy1.uninet.cm

REPUBLIC OF CAMEROON
Peace-Work-Fatherland

THE UNIVERSITY OF YAOUNDE I

POSTGRADUATE SCHOOL OF SCIENCES, TECHNOLOGY AND GEOSCIENCES

RESEARCH AND POSTGRADUATE TRAINING UNIT FOR PHYSICS AND APPLICATIONS

P.O. Box 812 Yaoundé
Email: crfd_stg@uy1.uninet.cm

Laboratoire de Physique Nucléaire, Atomique, Moléculaire et Biophysique

Laboratory of Physics of Radiation, Atomic, Molecular and Biophysics

COMPLEX AND RICH FEATURES OF cAMP WAVES PATTERNS IN DICTYOSTELIUM DISCOIDEUM AMOEBA CELLS

THESIS

Submitted and defended in fulfillment of the requirements for the award of the Degree of Doctorat/Ph.D. in Physics,
Option: **Biophysics**

By

ZAORO Rodax Nelson

Registration Number: 12W1986

Master of Science in Physics

Under the Direction of:

TABI Conrad Bertrand

Professor

BIUST, Botswana

And under the Supervision of:

EKOBENA FOUDA Henri Paul

Professor

University of Yaoundé I

YEAR: 2022

UNIVERSITE DE YAOUNDE I
UNIVERSITY OF YAOUNDE I

FACULTE DES SCIENCES
FACULTY OF SCIENCE

DEPARTEMENT DE PHYSIQUE
DEPARTMENT OF PHYSICS

ATTESTATION DE CORRECTION DE LA THESE DE DOCTORAT/Ph.D

Nous, Professeur **BEN-BOLIE Germain Hubert** et Professeurs **SAÏDOU** et **HONA Jacques** respectivement Président et Examinateurs du jury de la Thèse de Doctorat/Ph.D de Monsieur **ZAORO Rodax Nelson** Matricule **12W1986**, préparée sous la co-direction des Professeurs **EKOBENA FOUDA Paul Henri** et **TABI Conrad Bertrand,** intitulée : «**Complex and rich features of cAMP waves patterns in Dictyostelium discoideum amoeba cells**», soutenue le **mercredi, 21 décembre 2022**, en vue de l'obtention du grade de Docteur/Ph.D en Physique, Spécialité **Physique des rayonnements et Biophysique** attestons que toutes les corrections demandées par le Jury de soutenance ont été effectuées.

En foi de quoi, la présente attestation lui est délivrée pour servir et valoir ce que de droit.

Fait à Yaoundé le : 22 DEC 2022

Les Examinateurs

Pr. HONA Jacques

Pr. SAÏDOU

Le Président du Jury

Pr. BEN-BOLIE Germain Hubert

Le Chef de Département de Physique

UNIVERSITE DE YAOUNDE I * FACULTE DES SCIENCES * DEPARTEMENT DE PHYSIQUE
Le Chef de Département
Ndjaka Jean-Marie Bienvenu
Professeur

Complex and Rich Features of cAMP Waves Patterns in Dictyostelium Discoideum Amoeba Cells

Submitted and defended in fulfilment of the requirements
for the award of the Degree of Doctorat/Ph.D in Physics,
Option: **Biophysics**

by

ZAORO Rodax Nelson
M. Sc. in Physics
Registration Number: **12W1986**

Under the supervision of

EKOBENA FOUDA Paul Henri
Professor
and
Tabi Conrad Bertrand
Professor

December 26, 2022

Dedication

To my Saviour and Lord Jesus Christ.

Acknowledgments

Obviously, no human work can be done without the manifestation of the will of Almighty God. To this end, I thank God for allowing me to begin and complete the work of this thesis. Throughout this process, the Eternal Almighty God has blessed me with health, peace, stability and especially with inspiring new ideas that have given me the desire and determination to do research. To God alone, be the glory of eternity in eternity.

Also I would like to express my gratitude to all the people who contributed, in whatever manner, to the success of this work, since a work like this needs many helpers. First of all, I want to thank my two supervisors, Professor **EKOBENA Fouda Henri Paul** and Professor **TABI Conrad Bertrand** for devoting their valuable time and cognitive resources in order to make this work perfect. Especially, I express my deepest thanks to Professor **TABI** who allowed me not only to discover but also to integrate this rich and fascinating area of biophysics, I named chimiotaxis or simply the science of the movement cellular. Absolutely, this transdisciplinary field that includes biology, chemistry, mathematics, bioinformatics as well as chimiotaxix has allowed me to better understand the mechanisms of signals transmission by cAMP in a well organized network. Thanks to the ingenuity of this "Master" of nonlinear, I quickly integrated a novel research world where a few years earlier I would not have risked it. His passion for research, his love of a job well done, his diligence in the finalization of a project, his ardor and perseverance in the search for original and aesthetic results, his particular interest in the transfer of skills and autonomy, here are so many other virtues that I have received from this great hero of biophysics. Excellently, Professor **EKOBENA Fouda Henri Paul** has well coordinated the follow-up of all works of this Thesis through very relevant orientations and appreciations. I would like to express my deep gratitude to them since they are considered as the precursors of the laboratory of Biophysics of the University of Yaoundé I which during a few years, not only welcomed and trained many students, but also enhanced the image of

our institution through remarkable scientific contributions.

I wish to express my deepest gratitude to my thesis advisor Professor **KOFANE Timoléon Crépin**. This thesis would not have been possible without the many great ideas he so freely and generously gave out. His intellectual prowess and his energy have been inspirational. **Timoléon** allows his students wide latitude to explore interesting research ideas yet pays close attention to keep progress on track. His gentle encouragement and firm guidance have been instrumental in the completion of this work.

Now, I would like to think about my long years of academic training and cordially thank some of the teachers who gave me scientific knowledge. They are: **Pr BEN-BOLIE Germain Hubert**, **Pr SAÏDOU**, **Pr DIKANDE Alain Moïse**, **Pr WOAFO Paul**, **Pr OWONO OWONO Luc Calvin**, **Pr NDJAKA Jean-Marie**, **Pr MOHAMADOU Alidou**, **Pr KENFACK JIOTSA Aurelien**, **Pr PEMHA Elkana**, **Pr TCHAWOUA Clément**, **Pr ZEKENG Serge**, **Pr NDJOMO Donatien**, **Pr MANGUELE Dikoum Eléazar**, **Pr OWONO ATEBA**, **Pr NANA NBENJO**, **Pr ESSIMBI ZOBO**, **Pr EYEBE FOUDA Armand**, **Pr HONA Jacques**, **Pr MBANE BIOUELE**, **Pr SIEWE SIEWE Martin**, **Pr FEWO Serges Ibraid**, **Pr NJANDJOCK NOUCK Philippe**, **Pr DJUIDJE KENMOE Germaine**, **Pr ENYEGUE A NYAM Françoise**, **Pr BODO Bertrand**, **Pr VONDOU DEBERTINI Appolinaire**, **Pr MVOGO Alain**, **Dr WOULACHE Rosalie Laure**, **Pr TALLA Eric Tabue**, **Dr BEYALA ATEBA Jean Félix**, **Dr MVONDO Stanislas**.

I also take this opportunity to thank all my academic elders who shared with me their experience on calculation methods, the use of software essential for the research and interpretation of some complex phenomena. They are: **Dr ETEME Armand Sylvin**, **Dr Bansi Kamdem Christel Delphun**, **Dr NDZANA Fabien II**, **Dr MAÏNA Ibrahim**, **Dr KOL Guy**, **Dr ADAMOU DANG Koko**, **Dr TOGUEU Alain Bertrand**, **Dr MENGUE MENGUE Armand Didier**, **Dr OKALY Joseph Brizar**, **Dr PANGUETNA Cherif Souleman**, **Dr ISSA Sali**, **Dr TAKEMBO Ntahkie Clovis**, **Dr OMON Yves**

Additionally, I would like to thank my classmates who supported me with various actions throughout my academic career. I am thinking mainly of: Mr **KOSH KOMBA NDJAKA Tom Johnny** (for his very motivational encouragement), Mr **LABE Prudent Achille**, Mr **GOÏMASSE Rodrigue**, Mr **SENGHA Gerard Ghislain**, Mrs **CHARA-DACKOU Venant**, Mr **GAZAMBETI Yvon**.

I address my gratitude to all the leaders of the University of Bangui, in particular

Pr. SYSSA MAGALE Jean-Laurant, **Pr SYLLA Sembala**, **Pr BASSIA Jean-Marie**, **Pr ROUAULD Joachim**, **Pr SONGUELE Julien**, the Head of Department of physics **Dr MBESSE Yvon**, **Pr OMAROU Sanda**, **Pr KONDJI Yvon Symplice**, **Pr M'BOLIGAPA Jean**, **Dr MBAIKOA Timoleon**, **Dr KOAGOU PANGASSI Thiery**, **Pr MALEGUIZA**, **Dr GBEBRI**

My gratitude to the man of God, **Pastor GONITOUA Leonard Matchide**, by his prayers and his advice which gives me a blessing for the accomplishment of this work as well to all the deacons and pastors of the **MPTN** Church. My particular thanks are addressed to: Pastor **NGAIDONON Flavien**, Pastor **FEIMONAZOUI Merlin**, Pastor **NZENGOU Diana**, Pastor **MAGBODIATE Amede**, Pastor **BOKOSSY**. I do not forget all the Brothers and Sisters who accompanied me during this long process by their ceaseless prayers. I express my deep thanks with all the pastorale team of **CEMIRE of Yaoundé**, **Rev. Dr GWET Alain** for their boundless spiritual support.

Furthermore, I wish to express my heartfelt thanks to the parents, brothers, sisters and friends who have distinguished themselves by their immeasurable commitments throughout my academic training. First of all, my late mother, **BEMBE Emillienne**, who did everything and gave everything before the world separated us. My father **ZAORO Rodax Albert**, my uncles **NAKOMBO Gros Raimand Emil**, **KORONDO Gilbert**, **NDOUBE Apolinaire**, **BEMBE Edgar**. My great brothers **YANOE Emery** and **PANGO Armand Elie**, **ZAORO Monou**, also deserve to be thanked at the highest level because their psychological and material supports have largely contributed to the realization of this work.

I also say thank you to my mother-in-law **NEKINGUA Louise** for the peace and stability she brought me. I do not forget my brothers-in-law and my sisters-in-law for their immeasurable multidimensional supports.

Finally, a special thank you to my beloved and sweetheart **ZAORO née Ella Edwige SONGOHOUTOU** for his unyielding commitment to my side as well as our son **ZAORO Otsem Prémice**. Together we have done and will continue to make prowess.

Contents

Dedication i

Acknowledgments ii

Contents v

List of Figures ix

List of Tables xviii

List of Abbreviations xix

Résumé xx

Abstract xxi

General Introduction 1

0.1 Context of the thesis 1

0.2 Problematic and objectives of the thesis 5

0.3 Organization of the Thesis 5

Chapter 1 Literature review on Cyclic AMP, cyclic AMP in dictyostelium discoideum amoebas and cyclic AMP models 7

Introduction 7

1.1 cAMP 8

1.1.1 Anatomie of the cAMP system 8

1.1.1.1 Effectors and signaling pathways 9

1.1.1.2 cAMP signal compartmentalization 10

1.1.2 Functions 11

1.1.2.1 cAMP and enzymatic activity 11

1.1.2.2 cAMP in the bacteria 12

1.1.2.3 cAMP and lymphocyte function 13
1.2 cAMP in the Dictyostelium discoideum amoebae 15
1.2.1 Dictyostelium discoideum like model of study 15
1.2.2 Cellular Motility of Dictyostelium discoideum 18
1.2.3 Modes of cAMP signaling in dictyostelium discoideum cells 19
1.2.3.1 Excitable behavior 19
1.2.3.2 From oscillations to waves of cAMP 20
1.2.3.3 Exact adaptation 21
1.2.4 Waves of cAMP in dictyostelium discoideum cells 23
1.2.5 Frequency encoding of cAMP pulses in intercellular communication 24
1.3 Mathematical cAMP models 26
1.3.1 Goldbeter-Segel Model 27
1.3.2 Martiel-Goldbeter Model 28
1.3.3 Monk-Othmer Model 28
1.3.4 Tang-Othmer model 30
1.3.5 FitzHugh-Nagumo Model 33
1.3.6 Difference and Similitude between the Various Models 34
Conclusion 34

Chapter 2 Models of cAMP in Dictostelium-discoideum and methodologie 36

Introduction 36
2.1 Mathematical modeling 38
2.1.1 Reaction-Diffusion Systeme 38
2.1.1.1 Generalities 38
2.1.1.2 Activator-Inibitor 39
2.1.2 Model and kinetic equations MG 40
2.1.2.1 Description of the Model 40
2.1.2.2 Kinetic equations 42
2.1.3 Two-component MG model with advection 49
2.1.4 Two-dimensional FHN model 51
2.1.5 Long-range diffusive FHN model 53
2.2 Analytical and Numerical methods 55

2.2.1 Multiple scale expansion in the continuum approximation with derivation of two-dimensional CGL equation . . . 55
2.2.2 Semi-discrete approximation with derivation of two-Dimensional CGL equations for two different frequency modes . . . 58
2.2.3 Linear stability analysis . . . 64
2.2.3.1 Linear stability analysis on the 2D CGL equations . . . 64
2.2.3.2 Linear stability analysis on the 2D CGL equations for two different frequency modes . . . 65
2.2.3.3 Bifurcation theory . . . 67
2.2.4 Runge-Kutta numerical intégration method. . . . 67
Conclusion . . . 69

Chapter 3 Results and Discussion **71**
Introduction . . . 71
3.1 Unstable cAMP wave patterns during aggregation of Dictyostelium discoideum . . . 72
3.1.1 Analytical analysis of MI . . . 72
3.1.1.1 The MI growth rate versus the wavenumbers of perturbations 72
3.1.1.2 The MI growth rate versus the longitudinal wavenumber of perturbations . . . 74
3.1.2 Numerical analysis of MI . . . 75
3.1.2.1 Bifurcation-like behaviors of the MG model . . . 75
3.1.2.2 Dynamic Media . . . 76
3.1.2.3 Excitable Dynamics . . . 77
3.1.2.4 cAMP oscillations in absence of the advective flow . . . 79
3.1.2.5 cAMP oscillations in present of the advective flow . . . 80
3.1.3 Concluding remarks . . . 82
3.2 Complex patterns in Dictyostelium discoideum cells with frequency mode excitations . . . 83
3.2.1 Analytical features of MI . . . 83
3.2.2 Numerical analysis of MI . . . 83
3.2.2.1 The synchronization factor R . . . 85
3.2.2.2 Patterns cAMP waves in HF mode . . . 85
3.2.2.3 Patterns cAMP waves in LF mode . . . 87

3.2.3 Concluding remarks 87
3.3 Long-range interaction of multi-spiral cAMP waves in Dictyostelium discoideum aggregation. 92
3.3.1 Numerical results 92
3.3.1.1 stability of multi-spiral waves under effects of weak LRI . 92
3.3.1.2 stability of multi-spiral waves under effects of Coulomb LRI 95
3.3.1.3 stability of multi-spiral waves under effects of strong LRI . 96
3.3.1.4 stability of multi-spiral waves under effects of ultra LRI . 98
3.3.2 Concluding remarks 99
3.4 Conclusion 101

General Conclusion **103**

Bibliography **106**

List of publication **124**

Appendix **125**

List of Figures

Figure 1.1 Structure of cyclic AMP, with chimical formula $C_{10}H_{11}N_5O_6P$ and molar mass=329.206 g/mol [57] 9

Figure 1.2 Activation of the proteins dependent cAMP kinase by the cyclic AMP. The cyclic AMP activates the proteins kinase by dissociating the complex of under units regulating and catalytic. [72] 12

Figure 1.3 Diagram showing a Dictyostelium discoideum amoeba responds to cAMP. 1: cAMP reception at the cell membrane activates a G-protein. 2: G-protein stimulates adenylate cyclase. 3: cAMP diffuses out of cell into. 4: Internal cAMP inactivates the external cAMP receptor. 5: A different g-protein stimulates Phospholipase C. 6: IP_3 induces calcium ion release. 7: Calcium ions act on the cytoskeleton to induc the extension of pseudopodia. [106]. 16

Figure 1.4 The cycle of Dictyostelium discoideum. The starvation induced the synthesis and the excretion of cAMP by amoeba. intervenes at all the stages of the pluricellular phase: aggregation, slug, culmination, constitution of the spores [72]. 17

Figure 1.5 Model of the cycle of cellular movement for Dictyostelium cells. There gray arrow indicates the direction of movement. In gray, zones where the cell exerts forces (black arrows) to deform its membrane. Points of adhesion with the substrate are represented in black. according to [109]. 18

Figure 1.6 Excitable cAMP signalling. a: Schematic of the extracellular space, above the double red line (plasma membrane) and the inside of a containing the main components to produce cAMP oscillations and cellmovement. b: schematic of temporal changes in cAMPsynthesis and adaptation in response to a constant stimulus of cAMP (stippled blue line) [117] 21

Figure 1.7 Oscillations of cAMP in amoebae dictyostelium discoideum. The panel represents the periodic variation of intracellular cAMP within a suspension of synthesized cells. The extracellular cAMP (not shown) varies with the same period [135]. 22

Figure 1.8 Wave patterns observed during aggregation in wildtype and mutant strains. Strain Ax3 shows spiral waves, strain DH1 makes many concentric waves, the cAR3 strain is a mutant that expresses a lower affinity cAMP receptor and produces large spiral waves. The N272 strain expresses even lower affinity cAMP receptors, makes chaotic waves. They are not able to set up stable centres since the wave period is so slow that the cells disperse between waves, see [142] for further details 25

Figure 1.9 A schematic of the Calcium-cyclic AMP control network in dictyostelium discoideum proposed in (I) and (II) and modified herein. Solid arrows indicate the chimical reaction and transport pathways, broken lines indicate the control pathways. Ac, adenylate cyclase; ATP, adenosine triphosphate; C_0, concentration of extracellular cyclic AMP; C_i, concentration of cytosol cyclic AMP; Ca_0, concentration of extracellular calcium; Ca_1, concentration of cytosol calcium; Ca_s, concentration of sequestered intracellular calcium; ePDE, extracellular free phosphodiesterase; iPDE, cytoplasmic phosphodiesterase; mPDE, membrane bound extracellular phosphodiesterase. 31

Figure 1.10 A schematic diagram of the activation of adenylate cyclase via G_s proteins. H_s denotes the stimulus signal, R_s, the stimulus receptor, $\alpha_s GDP\beta\gamma$ unactivated G_s, protein, and UC unactivated adenylate cyclase. It is believed that upon binding of H_s, with R_s, G_s, is activated by the H_sR_s complex. This involves the release of the $\beta\gamma$ subunits and the addition of GTP to the α_s chain. $\alpha_s GTP$, which is denoted by $\alpha_s^{'}$ in this figure, then activates adenylate cyclase, which catalyzes the conversion of ATP to CAMP. 32

Figure 2.1 Model based on receptor desensitization for the cAMP signaling system of the slime mold Dictyostelium discoideum. Extracellular cAMP binds to the active state (R) of the receptor and thereby activates adenylate cyclase (C) which produces cAMP from intracellular ATP. The transition from the active to the desensitized state (D) of the receptor may in principle occur through a simple conformational change or though covalent modification. The latter situation appears to prevail in D. discoideum where the R and D states correspond to the dephosphorylated and phosphorylated forms of the cAMP receptor. Arrows indicate transport of cAMP into the extracellular medium and cAMP hydrolysis by the intracellular and extracellular forms of phosphodiesterase. The kinetics of the cAMP production in well-stirred suspensions of D. d. cells are well described by the MG model [2], which is based on the relevant kinetic rate laws and the interaction between cAMP and its membrane receptor 41

Figure 2.2 The angular wave frequency ω and the group velocity v_g are plotted against the wavenumber k. The influence of the degradation rate of extracellular cAMP by the enzyme phosphodiesterase k_e is studied for a fixed value $\sigma = 0.2\ \text{min}^{-1}$ of the production rate of intercellular cAMP. 59

Figure 2.3 Variations of the coefficients of the CGL Eq. (2.46) versus the wavenumber k, with changing the degradation rate of extracellular cAMP by the enzyme phosphodiesterase k_e. The dispersion coefficient P_1, P_2, as well the dissipative coefficients R_r and R_i remain positive for any k and k_e. However, the real and imaginary parts of the nonlinearity coefficient Q_r and Q_i are positives for some values of k and negatives for others. All the panels have been plotted for a fixed value $\sigma = 0.2\ \text{min}^{-1}$ of maximum activity of adenylate cyclase. 60

Figure 2.4 The angular wave frequency ω and the group velocity v_g are plotted against the wavenumber p. In all the figures, the blue line represents the HF mode and the red dashed-line pictures the low-frequency mode. We have fixed $k_g = 4.7$, $k_r = 1.5$, $a = 0.05$ and $D_{0X} = D_{0Y} = 2$. 62

Figure 2.5 The panels show the variations the coefficients of the CGL Eq.(2.59) versus the wavenumber p. The dispersion coefficient $P_1^{l_0}$, $P_2^{l_0}$, as well the dissipative coefficients and R^{l_0} remain positive for any p. The two modes are considered: the high-frequency mode (solid blue line) and the HF mode. We have fixed $k_g = 4.7$, $k_r = 1.5$, $a = 0.05$ and $D_{0X} = D_{0Y} = 2$. 63

Figure 3.1 The MI growth rate $\Gamma(K_1, K_2)$ versus the wavenumbers K_1 and K_2. Panels $(\text{aj})_{j=1,2,3}$ corresponds to $\sigma = 0.2\text{min}^{-1}$, panels $(\text{bj})_{j=1,2,3}$ to $\sigma = 0.3\text{min}^{-1}$ and panels $(\text{cj})_{j=1,2,3}$ gives the MI growth rate for $\sigma = 0.6\text{min}^{-1}$. From top to bottom, the different rows have been, respectively, computed for $k_e = 2.6\text{min}^{-1}$ $(j = 1)$, 2.8min^{-1} $(j = 2)$ and 3.1min^{-1} $(j = 3)$. 73

Figure 3.2 The MI growth rate $\Gamma(K_1, K_2)$ versus the longitudinal wavenumber K_1, with $K_2 = 0.1\pi$. Each panel corresponds to a fixed value of σ, while Γ is plotted for three different values of k_e. Panel (a) corresponds to $\sigma = 0.2\text{min}^{-1}$ and panel (b) to $\sigma = 0.6$ min^{-1}. $\Gamma > 0$ is delimited by the intervals $0 < K_1 < K_{1,cr}$, where the plane wave is expected to be unstable under slight modulation. 74

Figure 3.3 The bifurcation diagrams of cAMP extracellular concentration $\gamma(50, 50)$ in the $(k_e, t)-$plane with increasing σ (i.e, higher activity of the enzyme adenylate cyclase) as: $\sigma = 0.1$ min^{-1} in panel (a), $\sigma = 0.15$ min^{-1} in panel (b) and $\sigma = 0.2$ min^{-1} in panel (c). The diagrams allow to find the threshold value k_e above which the dynamical activity of D. *discoideum* is switched on. 76

Figure 3.4 The phase portraits in the $(\gamma, \rho)-$plane are depicted in panels $(\text{aj})_{j=1,2}$. Time series for cAMP concentration γ are displayed in panels $(\text{bj})_{j=1,2}$, while time series for the fraction of receptors in the active state ρ are shown in panels $(\text{cj})_{j=1,2}$. The features are obtained in absence of the advective flow, with $\sigma = 0.2\text{min}^{-1}$ and k_e taking the values 2.8min^{-1} $(j = 1)$ and 3.1min^{-1} $(j = 2)$. 78

Figure 3.5 The phase portraits in the $(\gamma, \rho)-$plane are depicted in panels $(\mathrm{aj})_{j=1,2}$. Time series for cAMP concentration γ are displayed in panels $(\mathrm{bj})_{j=1,2}$, while time series for the fraction of receptors in the active state ρ are shown in panels $(\mathrm{cj})_{j=1,2}$. These results have been obtained in the absence of the advective flow, with $\sigma = 0.25\mathrm{min}^{-1}$ and k_e taking the values $2.8\mathrm{min}^{-1}$ $(j = 1)$ and $3.1\mathrm{min}^{-1}$ $(j = 2)$. 79

Figure 3.6 The panels show the manifestation of MI through pattern formation in absence of the external flow, for different values of the degradation rate of the intracellular cAMP k_e: (a) $k_e = 2.6\mathrm{min}^{-1}$, (b) $k_e = 2.8\mathrm{min}^{-1}$ and (c) $k_e = 3.1\mathrm{min}^{-1}$, with $\sigma = 0.3\mathrm{min}^{-1}$. All the panels have been recorded at time $t = 60\mathrm{min}$. 80

Figure 3.7 Two-dimensional patterns of cAMP concentration $\gamma(x, y, t)$. Panels $(\mathrm{aj})_{j=1,2,3}$ show results for $k_e = 2.6\mathrm{min}^{-1}$ and panels $(\mathrm{bj})_{j=1,3}$ correspond to $k_e = 3.1\mathrm{min}^{-1}$. From left to right, panels in each set correspond respectively to $V_f = 0.2\mathrm{mm.min}^{-1}$, $1\mathrm{mm.min}^{-1}$ and $1.8\mathrm{mm.min}^{-1}$, with $\sigma = 0.3\mathrm{min}^{-1}$ and $t = 60\mathrm{min}$. 81

Figure 3.8 The MI growth rate instability $\Gamma(K_1, K_2)$ versus the waves number K_1 and K_2. Panels $((aj) - (bj)_{j=1,2})$ and $((cj) - (dj)_{j=1,2})$ corresponding for HF and LF regimes. We have fixed $p = 0.25\pi$, $\phi_0 = 0.1$ $k_r = 1.5$, $a = 0.05$ and $D_{0X} = D_{0Y} = 2$, with k_g taking respectively the values 4.7 $((a)_1 - (c)_1)$ and 5 $((a)_2 - (c)_2)$, the same for the stability/instability diagrams, where red regions are for instability and the blue ones are those where the plane wave solution is expected to remain stable under modulation. 84

Figure 3.9 Bands diagrams of synchronisation factor R versus the rate of cAMP production k_g for both HF (a) and LF (b) modes. (a) when $k_g \in [4.7 - 5.15]$ the feature illustrates asynchrony state of oscillations cAMP concentration as R decreases towards 0, at $k_g > 5.15$ the cAMP oscillations stretch at this synchronized when R increasing. (b) synchronisation factor R is raising the cAMP oscillations illustrates the values synchronous in their propagating. We have fixed $k = 0.25\pi$, $k_r = 1.5$, $a = 0.05$, $\tau = 4.8$, $D_x = 2$ and $D_y = 2$. 86

Figure 3.10 Time series of cAMP concentration $g(n, m, t)$ according to the HF mode at various node (200,200) for line blue and (350,350) line red. We varying the parameter k_g from top to bottom as: (a) $k_g = 5$, (b) $k_g = 4.86$, (c) $k_g = 4.7$. We have fixed $k = 0.25\pi$, $k_r = 1.5$, $a = 0.05$, $\tau = 4.8$, $D_x = 2$ and $D_y = 2$. 87

Figure 3.11 Space-time plots of cAMP concentration $g_{n,m}(t)$ in $(n, t)-$ plane according to the HF mode, under the change of the $m-space$ in the tranverse direction as $m = 100$ in columns (A), $m = 200$ in columns (B) and $m = 350$ in columns (c). We have fixed $k = 0.25\pi$, $k_r = 1.5$, $a = 0.05$, $\tau = 4.8$, $D_x = 2$ and $D_y = 2$. We varying the parameter k_g from top to bottom as: line (A) $k_g = 5$, line (D) $k_g = 4.86$, line (G) $k_g = 4.7$. 88

Figure 3.12 Space-temporal patterns of cAMP concentration $g_{n,m}(t)$ in 400×400 according to the HF mode array at different times: $t = 100$ in columns (A), $t = 500$ in columns (B) and $t = 900$ in columns (c). We have fixed $k = 0.25\pi$, $k_r = 1.5$, $a = 0.05$, $\tau = 4.8$, $D_x = 2$ and $D_y = 2$. We varying the parameter k_g from top to bottom as: line (A) $k_g = 5$, line (D) $k_g = 4.86$, line (G) $k_g = 4.7$. 89

Figure 3.13 Time series of cAMP concentration $g(n, m, t)$ according to the LF mode at various node (200,200) for line blue and (350,350) line red. We varying the parameter k_g from top to bottom as: (a) $k_g = 5$, (b) $k_g = 4.86$, (c) $k_g = 4.7$. We have fixed $k = 0.25\pi$, $k_r = 1.5$, $a = 0.05$, $\tau = 4.8$, $D_x = 2$ and $D_y = 2$. 89

Figure 3.14 Space-time plots of cAMP concentration $g_{n,m}(t)$ in $(n, t)-$ plane according to the LF mode, under the change of the $m-space$ in the tranverse direction as $m = 100$ in column (A), $m = 200$ in column (B) and $m = 350$ in column (c). We have fixed $k = 0.25\pi$, $k_r = 1.5$, $a = 0.05$, $\tau = 4.8$, $D_x = 2$ and $D_y = 2$. We varying the parameter k_g from top to bottom as: line (A) $k_g = 5$, line (D) $k_g = 4.86$, line (G) $k_g = 4.7$. 90

Figure 3.15 Space-temporal patterns of cAMP concentration $g_{n,m}(t)$ in 400×400 according to the LF mode array at different times: $t = 100$ in columns (A), $t = 500$ in columns (B) and $t = 900$ in columns (c). We have fixed $k = 0.25\pi$, $k_r = 1.5$, $a = 0.05$, $\tau = 4.8$, $D_x = 2$ and $D_y = 2$. We varying the parameter k_g from top to bottom as: line (A) $k_g = 5$, line (D) $k_g = 4.86$, line (G) $k_g = 4.7$. 91

Figure 3.16 Bands diagrams of synchronisation factor R versus the rate of cAMP production k_g panel (A), long-range interaction parameter s panel (B) and amplitude of periodic signal A_0 panel (C). We have fixed $f_0 = 1$, $k_g = 4.72$ $k_r = 1.35$, $a = 0.05$, $\tau = 4.82$,and $D = 0.26$. . 93

Figure 3.17 Time series of cAMP concentration $g_{n,m}(t)$ recorded for node (100,100) for line blue and (150,150) line red. We varying the long-range parameter s from top to bottom as: (A) $s = 0$, (B) $s = 1$, (C) $s = 3$, (D) $s = 10$. We have fixed $A_0 = 0.38$, $f_0 = 1$, $k_g = 4.72$, $k_r = 1.35$, $a = 0.05$, $\tau = 4.82$, and $D = 0.26$. The values of A_0 and k_g were selected in agreement with the synchronization diagrams of FIG.1. . 94

Figure 3.18 The phase portraits show the evolution of the cAMP concentration g versus the the number of desensitized cAMP receptors r while considering node (100,100). We varying the long-range parameter s from top to bottom as: (A) $s = 0$, (B) $s = 1$, (C) $s = 3$, (D) $s = 10$. We have fixed $A_0 = 0.38$, $f_0 = 1$, $k_g = 4.72$, $k_r = 1.35$, $a = 0.05$, $\tau = 4.82$, and $D = 0.26$. The obtained features reflect the same scenarios as in FIG.2. The chaotic attractorlike profiles of these features highly predict the asynchronous states within amoebae population. 94

Figure 3.19 Spatiotemporal patterns of cAMP concentration $g_{n,m}(t)$ in (n,t)-plan under the change of the cell number m in the transverse direction as m = 50 in panel (A), m = 100 in panel (B), m = 150 in panel (C) and m = 180 in panel (D). The features are obtained in the case of strong LR $s = 10$. We observe the emergence of nonlinear patterns by random pulsations. 95

Figure 3.20 Evolution of multi-spirals waves cAMP concentration $g_{n,m}(t)$ in 200×200 cells array at different times:(A) $t = 500$, (B) $t = 1000$, (C) $t = 1500$ and (D) $t = 1800$. The features are obtained in the case of weak interaction $s = 10$. We have fixed $f_0 = 1$, $k_r = 1.35$, $a = 0.05$, $\tau = 4.82$, $D = 0.26$. As time increases, the spatiotemporal dynamics of cAMP concentration in medium becomes more excitable. 96

Figure 3.21 Spatiotemporal patterns of cAMP concentration $g_{n,m}(t)$ in (n,t)-plan under the change of the cell number m in the transverse direction as m = 50 in panel (A), m = 100 in panel (B), m = 150 in panel (C) and m = 180 in panel (D). The features are obtained in the case of strong LR $s = 3$. We observe asynchronous nonlinear patterns show a collision between two or more waves followed by new pulsations in the cAMP concentration. 97

Figure 3.22 Evolution of multi-spirals waves cAMP concentration $g_{n,m}(t)$ in 200×200 cells array at different times:(A) $t = 500$, (B) $t = 1000$, (C) $t = 1500$ and (D) $t = 1800$. The features are obtained in the case for nearest neighbors interaction $s = 3$. We have fixed $f_0 = 1$, $k_r = 1.35$, $a = 0.05$, $\tau = 4.82$, $D = 0.26$. As time increases, the spatiotemporal dynamics of cAMP concentration in medium show emergence of excitability. 97

Figure 3.23 Spatiotemporal patterns of cAMP concentration $g_{n,m}(t)$ in (n,t)-plan under the change of the cell number m in the transverse direction as m = 50 in panel (A), m = 100 in panel (B), m = 150 in panel (C) and m = 180 in panel (D). The features are obtained in the case for nearest neighbors interaction $s = 1$. We observe the emergence of asynchronous structures which are localized in some space regions over the time. 98

Figure 3.24 Evolution of multi-spirals waves cAMP concentration $g_{n,m}(t)$ in 200×200 cells array at different times:(A) $t = 500$, (B) $t = 1000$, (C) $t = 1500$ and (D) $t = 1800$. The features are obtained in the case for strong interaction $s = 1$. We have fixed $f_0 = 1$, $k_r = 1.35$, $a = 0.05$, $\tau = 4.82$, $D = 0.26$. As time increases, we observed less excitation in medium of cAMP concentration. 99

Figure 3.25 Spatiotemporal patterns of cAMP concentration $g_{n,m}(t)$ in (n,t)-plan under the change of the cell number m in the transverse direction as m = 50 in panel (A), m = 100 in panel (B), m = 150 in panel (C) and m = 180 in panel (D). The features are obtained in the case of weak LR $s = 0$. The change of cell number m gives a qualitative insight on the heterogeneous nature of the network, which remains asynchronous during a time, and could be considered as the true precursors of multi-spiral waves. 100

Figure 3.26 Evolution of multi-spirals waves cAMP concentration $g_{n,m}(t)$ in 200×200 cells array at different times:(A) $t = 500$, (B) $t = 1000$, (C) $t = 1500$ and (D) $t = 1800$. The features are obtained in the case for global interaction $s = 0$. We have fixed $f_0 = 1$, $k_r = 1.35$, $a = 0.05$, $\tau = 4.82$, $D = 0.26$. As time increases, we observed a disintegration of the multi-spiral wave in the spatiotemporal dynamics of cAMP concentration in medium. 100

Figure 3.27 Simulation results of spatially extended multi-spiral waves at different values of the parameters long-range interaction at time t = 1900. The features presents influence of parameters long-range: (A) $s = 10$ (see Fig.8.D), (B) $s = 3$ (see Fig.9.D), (C)$s = 1$ (see Fig.10.D), (D) $s = 0$(see Fig.11.D). 101

List of Tables

Tableau 1.1 *The meaning of the chemical magnitudes* 29

Tableau 1.2 *The expression of the parameters, appearing in (1.2), in terms of the chemical magnitudes of Table 1.* 30

Tableau 2.1 *State variables of some representative excitable media [179, 230]* 39

Tableau 3.1 *The numerical values of the parameters considered in the model* 75

List of Abbreviations

Initials	Meaning	**Initials**	Meaning
dd	dicryostelium discoideum	**cAMP**	cyclic Acide MonoPhosphate
MG	Martiel-Golbeter	**S-cAMP**	Signaux cyclic Acide MonoPhosphate
GS	Goldbeter-Segel	**CGL**	Complex Ginzburg-Landau
FHN	FitzHugh-Nagumo	**cAMP-O**	cyclic Acide MonoPhosphate Oscillation
MO	Monk-Othmer	**CCGL**	Coupled complex Ginzburg-Landau
TO	Tang-Othmer	**ODEs**	Ordinary differential equations
LRI	Long-Range Interaction	**CEDI**	Cellular differenciation
MI	Modulational instability	**RK4**	Fourth-order Runge-Kutta
NA	Neuronal activity	**NS**	Neuronal synchronization
CNS	Central nervous system	**EPSPs**	Excitatory post synaptic potentials
NMDA	N-methyl-D-aspartic acid	**GABA**	G-Amino-Butyric Acid
DNA	Desoxyribonucleic acid	**WP**	Waves propagation
CEDI	Cellular differenciation	**PDE**	Phosphodiestrase Extracellular
cGMP	cyclic Guanine Mono-Phosphate	**ARN**	Acid Ribonucleic
PKA	Protein Kinase A	**EPAC**	Exchange Protein directly Activated by cAMP
PKB	Protein Kinase B	**CNG**	Cyclic Nucleotid Gated channel
HCN	Hyperpolarization-activated Cyclic Nucleotide-gated	**AKAP**	A-kinase Anchoring Proteine
AC	Adenylate Cyclase	**TCR**	T-Cell Receptor

Résumé

Dans cette thèse nous étudions la dynamique non linéaire de l'adénosine monophosphate cyclique (AMPc) et son rôle dans le processus d'agrégation des amibes dictyostelium discoideum (dd). Ce phénomène d'agrégation demeure un défi majeur non seulement pour les chimistes (chimiotaxie) et les biologistes (différenciation cellulaire), mais aussi pour les physiciens (propagation d'onde). Ce profond intérêt est suscité d'une part par l'importance biologique de cette macromolécule, et d'autre part par le fait que la molécule d'AMPc soit à l'origine une entité dynamique, de par les phénomènes de régulation et de transcription. A cet effet, les modèles de Martiel-Goldbeter et FitzHugh-Nagumo modifier permettent de comprendre l'impact de certains paramètres dans l'environnement. Grâce à la méthode des échelles multiples, nous réduisons les équations génériques, à l'équation de Ginzburg-Landau complexe. Cette dernière est explorée dans l'analyse de la stabilité linéaire conduisant ainsi à la dérivation de l'amplitude critique ou du gain d'instabilité modulationnelle. La méthode de Runge-Kutta d'ordre quatre nous permet d'intégrer numériquement nos modèles génériques afin de vérifier la validité des résultats analytiques. Les résultats suggèrent que l'absence et la présence d'écoulement dans le processus d'agrégation fait apparaître des motifs comme : les ondes quasi-périodiques, les grains en spirales et les motifs chaotiques. Un autre résultat intéressant est la mise en évidence de deux régimes de fréquence qui régissent théoriquement la dynamique d'AMPc. Le régime haute fréquence caractérisé par la formation des ondes spirales et le régime basse fréquence responsable des ondes circulaires. Plus remarquablement encore, nous montrons que le phénomène d'interaction à longue portée contribue à l'ajustement de la communication cellule-cellule avec l'apparition des structures asynchrones en forme de spirales.

Mots clés: cAMP; amibe Dictyostelium discoideum; advection; Conduit d'écoulement; modèle de Martiel-Goldbeter; modèle de FitzHugh-Nagumo; propagation d'onde; instabilité modulationnelle; formation des motifs; équation complexe de Ginzburg-Landau.

Abstract

In this thesis we study the nonlinear dynamics of the cyclic adenosine monophosphate (cAMP) and its role in the process of aggregation of the amoebas dictyostelium discoideum (dd). This phenomenon of aggregation remains a major challenge not only for the chemists (chemotaxy) and the biologists (cellular differentiation), but also for physicists (wave propagation). This deep interest is caused on the one hand by the biological importance of this macromolecule, and on the other hand by the fact that the molecule of cAMP is in the beginning a dynamic entity, from the phenomena of regulation and of transcription. To this end, the models Martiel-Goldbeter and FitzHugh-Nagumo to modify makes it possible to understand the impact of certain parameters in the environment. Thanks to the method of multiple scales, we reduce the generic equations, with the complex Ginzburg-Landau equation. This last is explored in the analysis of the linear stability thus leading to derivation of the critical amplitude or the profit of modulational instability. The method of Runge-Kutta of order four enables us to integrate our generic models numerically in order to check the validity of the analytical results. The unstable formation of the reasons for lead to flow of cAMP reveals reasons like: Quasi-periodic waves, spiral seeds and chaotic patterns. Another interesting result is the highlighting of two frequency regimes which theoretically govern the cAMP dynamics. The high frequency mode characterized by the formation of waves spirals and the low frequency mode responsible for circular waves. more remarkably again, we show that the phenomenon of long-range interaction contributes to the adjustment of cell-cell communication with the appearance of asynchronous spiral structures.

Keywords: cAMP; Dictyostelium discoideum amoeba; advection; Flow-driven; Martiel-Goldbeter model; FitzHugh-Nagumo model; wave propagation complex Ginzburg-Landau equation; pattern formation; modulational instability

General Introduction

The aggregation process of dictyostelium discoideum (dd) amoeba is a very complex biological phenomenon, which involves the dynamics of cAMP waves. The cAMP signaling system that controls aggregation is also capable of excitable behavior, which consists in the transient amplification of suprathreshold pulses of extracellular cAMP. To understand how D.d amoebae interact within a aggregation surface, simplified mathematical models are used, which aim to apprehend the essence of their underlying dynamics. The three-dimensional Martiel-Goldbeter (MG) model and FitzHugh-Nagumo (FHN) model falls into this class of simplified cAMP models. This models are able to describe oscillations in the cAMP level in cell suspensions as well as cAMP WP in a dispersed cell population through a system of ODEs where the main variable is the cAMP concentration extracellular. When this model is subjected to natural influences, therefore analytical and numerical techniques can be applied to study the phenomena of spatio-temporal pattern formation.

0.1 Context of the thesis

Many different models of cell-to-cell communication in Dictyostelium have been proposed over the years. The most famous include Goldbeter and Segel (GS) model [1], Martiel and Goldbeter (MG) model [2], Monk-Othmer (MO) model [3], Tang-Othmer (TO) model [4] and The FitzHugh-Nagumo (FHN) model [5–7]. Of all the cAMP mathematical models, MG and TO models have a biophysical meaning not only because their parameters are experimentally measurable but also because they allow to investigate questions related to the excitability, adaptation and oscillation by Dictyostelium cells [8]. In contrast they have either a great number of variables or a large number of parameters which are expressed by hyperbolic or exponential functions endowed with infinite and increasing nonlinearity. This makes them analytically less tractable, or computationally more expensive. However, the MG and FHN models are known in principle, to produce all different types of firing pattern that have been shown to exist in aggregation surface of D.D. cells [5, 6, 9].

Beyond its role in controlling cell aggregation after starvation, the cAMP signaling system in

D.d provides a prototype for the onset of a biological rhythm in the course of development.The notion of a developmental path suggests that aggregation centers are those cells that are the first to enter into the domain of sustained of cAMP-O [10]. In the absence of oscillations, when the steady state is stable, it is possible to trigger a pulse of cAMP if the initial effect of the extracellular signal is to lower instantaneously the level of intracellular cAMP below the steady state level. Then, if the steady state is a stable focus, the system responds to a decrease of cAMP by making a loop in the phase plane before returning to steady state. The wavelike patterns observed during dd. aggregation represent one of the most beautiful and best understood examples of spatiotemporal self-organization at the cellular level. The wavelike nature of aggregation results from the existence of a cellular rhythm in the production of cyclic AMP (cAMP), the molecule that controls chemotaxis in the course of aggregation [11]. cAMP-O soon became a topic of choice for theoretical modeling. The oscillations and waves of cAMP in the slime mold D.D. represent one of the most striking examples of spatiotemporal self-organization at the cellular level, and provide a prototype for pulsatile intercellular communication in higher organisms, for example, pulsatile hormone secretion. Dictyostelium also represents an organism of choice for studying development and differentiation [12–14].

Transport-coupled nonlinear dynamics is fundamental to most types of spatiotemporal self-organization. The rich physics of these processes is not only of basic interest, but holds the key to understanding biological phenomena such as cell motion, embryogenesis, dynamical diseases, and patterns in bacterial systems [15–19]. Important examples are found in reaction-diffusion media, which have provided valuable insights into systems as diverse as the patterned shells of mollusks, neuronal networks, and the human heart [20, 21]. Usually in these reaction-diffusion systems transport coupling in the form of molecular diffusion or diffusionlike electric processes is considered. In contrary, transport coupling by fluid flow has received little attention, with experiments focusing mainly on the Belousov-Zhabotinsky (BZ) reaction [22–25]. In reactionŰdiffusion systems, an advective flow can induce unique emergent phenomena. One well known example is the differential flow induced chemical instability (DIFICI) that destabilizes an otherwise spatially homogeneous state of a system. The basic idea behind DIFICI is that the reacting species flow at different speeds. This differential transport can initiate instabilities of the homogeneous steady state that induce propagating wave trains moving in the flow direction. Instabilities in the homogeneous distribution can arise if phytoplankton and zooplankton move with different velocities, regardless of which one is faster. This mechanism of generating spatial structures is free from the restrictions of the Turing mechanism [26], which requires a large difference in diffusion coefficients of the two species involved.

In the natural environment, d.d. cells can be exposed to an external fluid flow which would be expected to significantly change the wave generation processes. Recently, Gholamie et al have

conducted experiments and performed numerical simulations to study flow-driven waves in a biological system, namely quasi one-dimensional colonies of signaling amoeba D. discoideum [27]. In these experiments with chemotactically competent D. discoideum cells, a straight flow-through microfluidic channel was used. Starved cells were allowed to settle on the substrate before a laminar flow of buffer was switched on. The flow advected extracellular cAMP downstream but was not strong enough to detach the cells from the substrate. This differential transport of extracellular cAMP induced macroscopic wave trains that had a unique period and propagated with a velocity proportional to the imposed flow velocity downstream. This behavior was studied theoretically [28, 29] using the two-component reaction- diffusion model proposed by Martiel-Goldbeter [2] for the production and relay of cAMP. While the theoretical results could explain much of the experimental observations, there were still open questions regarding the generation of a self supporting wave train at the inlet of the microfluidic channel and only small flow rates of up to 5 mm/min were studied. Furthermore, the state of the cells was assumed to be constant in the convectively unstable regime, lacking a way to verify this experimentally. The effects of an external electric field on pulse waves have been widely studied in the chemical excitable system formed by the Belousov-Zhabotinski (BZ) reaction medium both experimentally and by means of mathematical modelling [31–36]. The effects include both the decrease and increase of the pulse propagation velocity, annihilation of the pulse, breaking of continuous circular pulses into fragments, enhancement or suppression of spiral wave formation, the drift of spiral centers through the system, and phenomena resulting from a modified refractoriness of the medium, namely the reversal of the direction of the pulse propagation and pulse splitting (i.e., the back firing of new pulses from the back of the existing one). Effects of an external electric field on the propagation of excitable cAMP pulses in aggregating cells of D.D. have been studied by Linder et al [37]. There is a growing interest in understanding the way electric field interact with the cells, especially their effect on some fundamental immunitary functions.

In all these cases, it appears that pulsatile signals can be encoded in terms of their frequency on the basis of desensitization in target cells. Low frequency (LF) oscillations modulate activities over broad spatial areas and across long temporal windows, while high frequency (HF) oscillations are restrained to small regions and short temporal windows. Besides pulsatile patterns of hormone secretion [38], the best example of pulsatile signaling in intercellular communication is that of cyclic AMP (cAMP) signals which control aggregation and differentiation of the cellular slime mold Dictyostelium discoideum [12]. Pulsatile cAMP signals of appropriate frequency prove more effective than constant stimuli in promoting Dictyostelium development [11] Thus, cAMP pulses applied at 5-6 min intervals are effective , in contrast to pulses given every 2 min or at random intervals [39, 40]. experimental findings indicate that the phenomenon of pulsatile signaling observed in Dictyostelium is a general property shared by many, if not most,

hormones, that might also extend to a number of growth factors. In all these cases, it appears that desensitization in target cells allows for the frequency encoding of signals in intercellular communication. As evidenced by pulsatile hormonal therapy , this conclusion is also of clinical relevance for chronopharmacology as it bears on the search for optimal patterns of drug delivery [41,42]. Using one-dimensional model, it has not been possible, to the best of our knowledge, to differentiate LF and HF modes. In this regard, it is widely accepted that cAMP, in order to discern their collective behaviors, should be connected in networks. the FHN model will be developed to describe the oscillations of cAMP in frequency mode.

In the most biological systems, long-range cell-to-cell interaction appears to be a trustworthy pathway for a perfect intercellular communication [43–45]. Paolo and its coworkers [46] have showed that local cell-to-cell coupling in social Dd amoebae via secreted chemicals may be tuned into a critical value, resulting in emergent long-range communication and heightened sensitivity. This issue has been demonstrated by means of cell-cell correlations showing evidence of self-organization at the onset of aggregation. In the same direction, Singer et al. [47] have argued that propagating cAMP not only control the initial aggregation process but continue to be the long-range cell-cell communication mechanism guiding cell movement during multicellular Dictyostelium morphogenesis at the mound and slugs stages. Agreengly, cAMP waves not only propagate through local coupling for relaying nearest-neighbor cellto- cell information, but also across global coupling necessary for long-range intercellular communication. However some physical situations that highlight global effect of long-range parameter deserve to be well-understood.

The modulational instability (MI) technique is nowadays well-documented as it has been extensively applied to a broad range of physical settings including nonlinear optics [48], hydrodynamics [49], biophysics [50–53], just to name a few. The phenomenon of wave modulation appears by taking account of the space-time , and both are useful in the understanding appearance of the structures space-time in the systems out of equilibrium in the nature. The evidence that these waves are nonlinear being well-established, it remains however important to clearly elucidate the conditions and mechanisms leading to their formation and propagation during aggregation of D.d cells. In some recent contributions, wave modulation, through the activation of MI, has been addressed by Tabi et al. [54], there is a strong relationship between the MI process and the emergence of spiral waves in a FHN model that includes intracellular magnetic flow effects, with application to cardiac excitations. Therefore, MI is one of the direct mechanisms that lead to the formation of solitons and train of waves in systems where there are competitive effects between nonlinearity and dispersion [45, 49, 51–53, 55].

0.2 Problematic and objectives of the thesis

Communication of amoebae D.D by cAMP signaling results to the formation of localized nonlinear waves and appearance of patterns. However, the analytical and numerical research of such structures is even less considered. In this thesis, the combination of analytical and numerical methods is used to study waves propagation and the aggregation phenomena in the context of the transport and transfer of S-cAMP in colony of amoebae DD. This implies the development of new cAMP mathematical models, the MG model that reproduces the essential properties of the signaling system, such as excitability, oscillation, and adaptation. The model present of an external flow, the extracellular cAMP spreads out in the extracellular medium by both molecular diffusion and advection, the FHN model, these equations are commonly used to describe a prototype excitable medium. Some analytical techniques such as multiple scaling method and linear stability analysis of plane waves will be then applied. The multiple scales method in the discrete approximation will lead to a complex Ginzburg-Landau (CGL) equations. Through these, we derive a reductive partial differential equations, find instability criteria and elaborate analytical expressions of MI growth rates. Finally numerical solutions will be presented using the fourth-order Runge-Kutta (RK4) computational scheme.

0.3 Organization of the Thesis

This thesis is divided into three chapters that are outlined as follows:

✠ The first chapter focuses on the structure and properties of cAMP in colony of amoeba D.D as a basic unit of communication processing and moovement cellular by chemiotatic as macroscopic structures for the transport and transfer of S-cAMP. In this chapter some of the most prominent cAMP signaling models in amoeba are presented and resulting in the choice of the MG model whose properties are well discussed and the FHN model discrete.

✠ The second chapter presents the improved mathematical models developed in this thesis as well as the analytical and numerical methods used. Some immediate applications are made in order to facilitate the understanding of the used methods. Interestingly, a complex Ginzburg-Landau (CGL) equations are derived from generic model and allow to find analytical expression of some MI functions such as critical amplitude or MI gain along with instability criterion.

✠ The third chapter is devoted to results and interpretations. We first discuss the effects of flow in the aggregation process of Dictyostelium discoideum Then the low and high frequency modes are studied in a discrete model of two-dimensional FHN network. We end with the study of Long-range interaction of multi-spiral cAMP waves in Dictyostelium discoideum aggregation.

The thesis ends with a general conclusion including the summary of the main results and the

futures orientations.

Chapter 1

Literature review on Cyclic AMP, cyclic AMP in dictyostelium discoideum amoebas and cyclic AMP models

Introduction

Due to its action as second messenger of the intracellular hormones and the control exerted on the activity of certain genes,cyclic adenosine 3' -5' Monophosphate (cAMP) appears as a relevant molecule for investigations the laboratories. cAMP is elaborate in various fields such as chemistry (chemotaxis), biology (transmission of the hormonal signal), and biophysics (oscillation of the waves) [56]. In the amoebas dictyostelium discoideum, the aggregation centers emit signals of cAMP for few minutes. Each cAMP signal is relayed and starts a chemotaxis response. Consequently, the amoebas incorporate themselves around the centers by forming a wave of cellular motion for each pulsation of cAMP. The microscopic scale observations show that these waves can be concentric or of spiral forms. The waves of cellular movement of the amoeba dictyostelium are superimposed on the waves of cAMP. These waves are due to the pulsating secretion of cAMP by the centers of aggregation and to the relay of these signals which propagate through the area of aggregation. The cAMP waves astonishingly resemble the chemical waves observed in absence of mixture, on a solid frame, in the Belousov-Zhabotinsky reaction; one of the well known examples of oscillating chemical reaction. The interaction of the cAMP waves in the area of aggregation with the waves of cellular motion generates oscillations which lead to the patterns formation. The understanding of biological as well as chemical formation of patterns provides us with information that nature hides in the macroscopic scale as in microscopic one alike. This information allows us to understand the temporal evolution of the cells, how

they differentiate themselves from one to another and their modes of communication with each other. The oscillation of cAMP secreted by the amoeba dictyostelium discoideum in the area of aggregation is one of the phenomena which explain the formation of the patterns in biology. This mechanism initially explains the identification of the variables and their interactions. Once the variables are identified, one investigates the reason of their growth or decrease in the course of time. The essential point is the derivation of a model which describes cAMP oscillations in suspensions of cells as well as the propagation of wave of cAMP in a population of the dispersed cells.

Many mathematical models were derived to understand the dynamics of the cAMP waves in the colony of the amoebas dictyostelium discoideum during their aggregation. The kinetic mechanism of the concentration of cAMP is presented firstly in the form of an oscillating reaction. An oscillating reaction is a reaction in which the concentrations of the various reagents are functions of time. Thus the study of the nonlinear kinetics of the reaction allows, on the one hand, to check the validity of the model and on the other hand, to predict the dynamic properties of the reaction like the period of the oscillations and the duration of the phenomenon. The kinetic equations giving the concentration of the reagents with respect to time are differential equations. In the second place the diffusion of the elements in all the system, it is this displacement which produces the waves. The development of these mathematical models of the indication of cAMP, gives a clear comprehension finally studied its behavior.

This work is divided into three principal parts. The first part is devoted to cAMP, a presentation of its structure, its various functions and its modes of indication. The second part relates to the behavior of cAMP in the colony of the amoebas dictyostelium discoideum, namely the effects cAMP in the differentiation of amoebas D.D. chemotaxis and the cellular movement. Finally a comment clarifies mathematical models in their quantitative and qualitative forms in view of describing the wave propagation of cAMP in the colony of amoebas dictyostelium discoideum.

1.1 cAMP

1.1.1 Anatomie of the cAMP system

Cyclic adenosine monophosphate (cAMP) is a second messenger molecule comprised of an adenine ribonucleotide bearing a phosphate group bound to the oxygen molecules at the 3' and 5' positions of the sugar moiety (see Fig. 1.1). Cyclic AMP, which is synthesized from ATP by the intracellular enzyme adenylate cyclase, modulates the activity of several hormone-dependent signal transduction pathways.

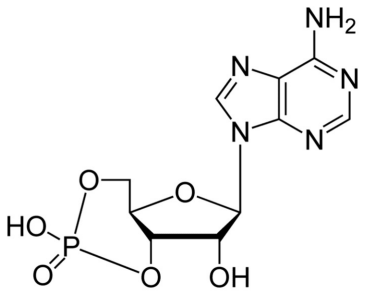

Figure 1.1: Structure of cyclic AMP, with chimical formula $C_{10}H_{11}N_5O_6P$ and molar mass=329.206 g/mol [57]

1.1.1.1 Effectors and signaling pathways

• **Phosphodiestrase (PDE)**

The PDE are the enzymes responsible for the hydrolysis of the cyclic nucle otides (cAMP and cGMP) Although in certain cells like the cardiomyocytes, cAMP can be transported out of the cell by channels of the family of the MRP (Multidrug Protein Resistance), the catalytic activity of the PDE constitutes the only way of elimination of cAMP in the majority of cellular types. It is mainly the activity of the PDE which will bring a dimension space-time of the cAMP signal.

Described for the first time in 1962 by Butcher and Sutherland [58], the superfamilly of the PDE contains currently more than 90 members gathered into 11 families according to their structural, enzymatic, pharmacological properties like their regulation of mode. Each family is coded by 1 to 4 genes which can undergo alternative splicing, which explains the 96 listed PDE. A nomenclature was proposed in order to classify different the isoformes, one can thus identify the family of PDE, coding gene for the isoforme as well as the alternative splicing. With titre this example the PDE 4 D3 corresponds has the PDE of family 4, coded by the gene D and produced by the alternate third épissage of the ARN resulting from this same gene.

The PDE of families 4,7 and 8 are capable of degrader selectively cAMP, where as the isoformes of family 5, 6 and 9 are specific of cGMP. Families 1, 2, 3,10 and 1 can to hydrolyze two cyclic nucleotides indifferently. From a structure point of view, the PDE divide a common structural organization container: a catalytic field preserves of a family has the other and locates has the end C-final and of the fields of regulation and addressing locate primarily in the part N-final. The majority of the PDE function out of dimer or oligomer [59].

The D.d amoebas also have will PDE, which of degrade cAMP. Two forms coexist. First is intracellular, while second is secreted by the cells in the extracellular medium. If the two shapes of the enzyme degrade cAMP, the function of the extracellular PDE is significant because it makes it possible to avoid its accumulation in the exterior medium.

• **cAMP effectors**

Parallel to the canonical way implying the PKA like principal effector, two other effector of this way were described. It is about protein EPAC as well as channels ionic CNG and HCN. Together or separately, these various branches of indication cAMP, tend to modulate various cellular functions.

-Protein Kinase A (PKA)

In the inactive state, the PKA is a formed heteromastigate of 4 sub-units: 2 sub-units catalytic (c) and 2 pennies regulating units (r) cAMP while binding to under - units R, dissociates and releases the sub-units C which become active. The sub-units C of the PKA have for function of phosphorated the proteins target on the level of a reason whose sequence is made of two aa basic followed by a neutral aa then of a serine or a threonine phosphorylase: RRXS / T. The ATP is here the donor of phosphate and energy.

-The EPAC exchange factor

The discovery of protein EPAC like new intracellular target of cAMP suggest that the mechanism of indication of cAMP is much more complex than than one believed before. Thus, most of the effects induced by cAMP, which were allotted with the only action of the PKA, are partly ascribable with EPAC and does not imply branch PKA cAMP way. To date, it was shown that protein EPAC is implied in one multitude of cellular functions as cellular adhesion [60, 61], the junctions cell-cell [62], the exocytosis and secretion [63], differentiation [64], and cellular proliferation [65].

-The channels regulated by cyclic nucleotides: CNG et HCN

Channels CNG are expressed mainly in the photoreceptor of the retina and olfactory neurons. The functional forms are heterotetramere composed of two under unit α and two pennies unit β [66]. The opening of these channels is controlled as well by the connection of a molecule of cAMP like cGMP. During the fixing of the one from these two nucleotides cyclic, the pore of the channel becomes permeant with calcium and the monovalent cations. Thus the opening of this channel induces a depolarization of the membrane plasmic of the cell leading to a massive entry of ions calcium. It the last by binding the calmodulin module of many intracellular targets of which channels CNG them even. This feedback negative, constitutes with the PDE the principal mechanism of regulation negative of channels CNG.

1.1.1.2 cAMP signal compartmentalization

It is increasingly allowed that the various protagonists of the way of indication cAMP are not distributed in a diffuse way within the plasmic membrane or in the cytosol but are gathered in signalosome thanks to AKAP (A - Kinase Anchoring Protein) [67]. Signalosome can thus gather all the partners of indication: PDE, AKAP, AC, and PKA or the EPAC [68]. This complex provides one thus space control of the effector of cAMP in addition to the temporal control of

indication via one specific cytosolic distribution of PDE [68–70].

• **AKAP importance**

The family of the AKAP counts about fifty member today. Members of this family share of advantage a common function that a common structure. In spite of this structural diversity, to be regarded as a AKAP, a protein must answer 3 criteria. All the AKAP present a field of connection to under regulating unit of the PKA. Then, AKAP presents a field of specific addressing which imposes one to him " bulk-heading " has a cellular compartment gives. With titred' example, the AKAP 79/150 present a peptide sequence which enables him to interact with phospholipids of the membrane plasmic, whereas the AKAP - WAVE1 (WisKott- Aldrich VErprolin-homology protein 1) interacts with the cytosquelette of actine or the membranes mitochondrials Lastly, AKAP must be able to interact with many proteins of indication cAMP (proteins phosphatases, GSK, protein Kinase...) and thus Co-locate the effector of way (PKA or EPAC) with these various partners within " signalosome ". The AKAP thus seem to act like platforms of anchoring of the different protagonists of indication, at the same time those implied in transduction and those which induce the stop, that they maintain has proximity from/to each other [71].

1.1.2 Functions

Adenosine 3'-5' monophosphate (cAMP) is the second messenger of the action of the polypeptide hormones at the higher organizations, but also an essential effector of cellular operation at all alive beings, of the most elementary, nucleate unicellular organization or not (yeast, protist, bacterium) with the most complex eucaryote. cAMP thus seems a major regulator of the expression genes, able to control at the same time their transcription and the activity proteins for which they code [72].

1.1.2.1 cAMP and enzymatic activity

Work of Sutherland made it possible to identify cAMP like the second messenger of the action of many hormones [73]. The first messenger is the hormone it even. The cells targets are cells which have in their plasmic membrane of the receivers for this hormone. The connection of the hormone with its specific receptor led to the activation of the AC which is, it also, related to the membrane. This activation is not direct, it is transmitted by a regulating protein binding the GTP, the protein G. cAMP is then formed from the ATP. Thus, the hormone does not have to penetrate in the cell to play its biological role. But how cAMP exerts it its effects? It is striking to note that the mechanism of action of cAMP is common to all the organizations eucaryotes and appears accurately preserved during the evolution. cAMP activates a protein kinase capable to phosphorylate of proteins. In the case of the metabolism hepatic, the protein

cAMP kinase dependent phosphoryl as well enzymes of the glycolysis and of glycogenosynthesis (that it inactive) that those of the glycogenolyses and of the gluconeogenesis (that it activates). It in results an integrated biological effect in response to glucagon (via cAMP) at the time of the fast: mobilization hepatic glycogen and inhibition of its synthesis, saves and production of glucose by ů the liver for the peripheral bodies. The mechanism of activation of protein kinase by cAMP is maintaining well-known. This enzyme consists of two types sub-units, regulator from 49 to 52 kcal which can to bind to cAMP, and of the sub-unit catalytic of 38 kcal. In the absence of cAMP, sub-units regulating and catalytic, form a complex R2C2, deprived of activity enzymatic. The connection of cAMP with the regulating sub-units conduit with the dissociation of the complex R2C2 in a dimer R2 related to 4 molecules of cAMP and in 2 sub-unit C These catalytic sub-units free are then endowed with activity enzymatic [73]. Thus, there connection of cAMP to the sub-units regulating inhibition raises that these last exerted on the sub-unit catalytic (see Fig. 1.2)

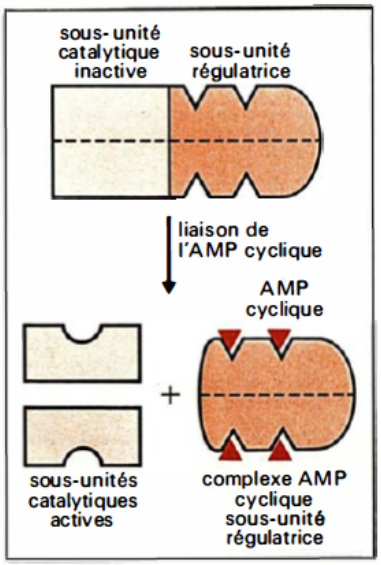

Figure 1.2: Activation of the proteins dependent cAMP kinase by the cyclic AMP. The cyclic AMP activates the proteins kinase by dissociating the complex of under units regulating and catalytic. [72]

1.1.2.2 cAMP in the bacteria

One has just seen how cAMP stimulate or inhibits the activity of enzymes implied in the metabolism glycogen by modifications post-translation of these enzymes. If the researchers have summer put on the track of other levels of regulation by cAMP, the merit in be allocated to the microbiologists. Those know since some years already that cAMP, product by the bacteria when they are deprived of glucose, is able of to stimulate the transcription of some genes which

contribute to the exploitation other sources of energy [74]. In this case, the activation of the transcription bacterial genome by cAMP is not mediated by one protein dependent cAMP kinase: at the bacterium indeed, cAMP synthesized in the absence of glucose bind to the CAPE (Catabolite Gene Activating Protein) or CRP (ACMcP Receptor Protein) which is a protein dimeric (sub-unit = 22 kdal). The CAP-cAMP complex (but not the CAPE only) stimulates the transcription while binding to a sequence (containing the element in particular TGTGA) located upstream of the promoter who controls the expression of the catabolic opéron. Moreover, one change in the sequence consensus TGTGA or in the genes which code for the adenylate cyclase or CRP breaks down the transcription of catabolic gene in the absence of glucose [74]. It is thought now that there sequence consensus TGTGA is it site of connection of one of the sub-units from the CAPE with the ADN, the second sub-unit recognizing another sequence located 6 bases further, sometimes symmetrical, sometimes very different first. The distance who separates the sequence consensus TGTGA of the site of initiation of transcription is very variable of one opéron catabolic with the other. In the case of let us operate inducible by cAMP, the sequence consensus is found far upstream from the site of initiation transcription (enters - 100 and - 60). The connection of the ARN polymerase with the promoter, very weak in the absence of cAMP, is considerably increased in presence CAP-cAMP complex. There transcription is then initiated and it gene takes a configuration known as opened. The connection of the complex CAP-cAMP with the ADN does not lead not with an unfolding of the ADN nor with a unmasking of the sites cryptic but the formation of one allows complex stable and highly closely connected ARN polymerase with the promoter bacterial most powerful. However the model of activation transcriptional by cAMP must to take into account the fact that one do not find in the promoters of let us operate inducible by cAMP there Pribnow Box, homologous with sequence consensus TATA of eucaryotes (see médecine/sciences, 1985; 1: 48). These facts, joints with discovered remarkable interactions protein-protein enters it complex CAP-cAMP and the ARN polymerase, give rise to think that this complex, once fixed on gene, provides itself the sites necessary to the interaction of the ARN polymerase with the ADN thus with the initiation of the transcription [74].

1.1.2.3 cAMP and lymphocyte function

- **Lymphocyte T**

The role of cAMP like inhibitor of the lymphocyte T was very indeed shown [75–77]. More precisely, the intracellular increase in cAMP in these cells induces an inhibition of their activation [76] and of their proliferation [78]. Results showed that, in T mature, the increase intracellular cAMP induced by one cascade implying kinase Csk (COOH-terminal Src Kinase) lead to a inactivation of cascade of indication downstream from the TCR [79].

cAMP decreases also the cytotoxic activity of T thanks to a significant reduction of production

of many cytokines, such as IL 2, the TNF-α and the IFN -γ by the Th1 lymphocytes (Th→ Lymphocyte T helper; Th1 and Th2: under populations 1 and 2 differentiated on the basis from cytokines secreted [80].

Parallel to these immunosuppresseurs effects, certain studies bring back effects rather opposite contributing to a immunoactivation supported for example by an increase in the secretion of the cytokines by Th2 under the action of cAMP [**?**, 81–84]. It also has highlighted a transitory increase in cAMP at the center lymphocytes T, following their adhesion with DC. This increase in cAMP [85] contributes to increase the sensitivity of the cell T to the antigens following the contact Lymphocyte. DC describes by same team [86].

• **Lymphocyte B**

cAMP and its effector, PKA and EPAC, play a significant role in the regulation of the activity of the lymphocyte B. The current data do not make it possible to formulate distinctly the respective contribution of these effector but show a preferential share of the PKA on cellular functions of the mature lymphocytes B and by the means of protein EPAC in immature cellular forms. The use of the analogue of cAMP, sensitive PKA (6-Bnz-AMP), on mature lymphocytes B of spleen of mouse, the way ERK1/2, that inhibits independently activation of S receivers of lymphocyte B (BCR), which is reflected on the functions of these cells and conduit with a reduction in the immunizing answer humoral [87, 88].

With the difference of the mature lymphocytes B, the effect of cAMP in the immature forms is rather dependant EPAC. In these cells, the increase in intracellular AMPc is translated by an inhibition of way PKB and that independamment of the activation of the PKA. Moreover, it has demontré summer that cAMP, by the means of protein EPAC, modulates the process of selection negative of the immature lymphocytes B, with an effect mainly pro-apoptotic. Us let us know that the response of the immature cells B has the activation of the BCR by a antigene depend balance between signals pro-apoptotics, passing mainly by ERK1/2 [89, 90] and anti-apoptotics passer by way PI3K/PKB [91, 92].

• **cAMP in the pathophysiology: Lymphocyte and HIV**

Some studies carried out in vitro show that an infection of lines lymphocytaires by the HIV leads has an increase in the cellular concentration of cAMP [93–95]. Moreover, of the studies ex vivo show that cells T of seropositive patients contain twice more cAMP than those exits of seronegative people [94, 95].

This increase in intracellular cAMP seems to pass by the activation of the PKA under influence of the glycoproteins gp 120 contained in the viral envelope [94, 96, 99]. The mechanism by which this protein increases cAMP Concentration is still unknown. A study tends to associate this effect with receivers chimiokinergic and more particularly with CXCR4 [96].

Several studies showed that the activation of the cAMP way in the infected cells T contribute

to inhibit the immunizing answer and thus to support the infection. The adhesion of the virus by the means of the gp 120 on the CXCR4 decreases significantly the proliferation of the lymphocytes T $CD4^+$ and T $CD8^+$ This effect is in connection with an activation of the PKA and CREB [94,96] With reverse, the reduction in cAMP restores there proliferation and cytotoxicity of these cells [94,98], cAMP also acts on T regulators : during infection HIV, one attend a suppression of the potentiation of these cells by an increase in the level of CTLA-4 (Cytotoxic T - L ymphocyte A ntigen 4) [99]. This protein is known to be one controlled negative of immunity.

All of these studies describe cAMP signaling as a key component of process of infection of T lymphocytes with HIV particularly by suppressing the response immune. Nevertheless, it seems that its role is even more complex. Several studies report an inhibitory effect of cAMP on the ability of the virus to replicate. A raise cAMP, either through activation of AC by FSK, or after blockade of cAMP degradation by treatment with rolipram, a specific inhibitor of PDE4, is correlated with a decrease in viral transcription as well as a decrease in the level of the HIV $p24^{Gag}$ protein in T lymphocytes [100,101]. Similarly, a study shows that in naive T cells, cAMP significantly decreases nuclear import, translocation and replication of viral DNA, by comparison with memory T cells. An effect on the expression of HIV receptors is also reported, CCR5 and CXCR4 [102,103].

Taken together, these data suggest that the cAMP / PKA pathway affects infection with HIV on both the pre- and post-integration stages. Thus the role of cAMP during infection with HIV and more generally in the immune response seems to go beyond the simple function of immunosuppressant. This knowledge can help establish new therapeutic targets in antiretroviral therapy or identify target molecules with immunoregulatory potential, which could help restore immune dysfunction in this pathology.

1.2 cAMP in the Dictyostelium discoideum amoebae

1.2.1 Dictyostelium discoideum like model of study

Dictyostelium discoideum is a unicellular organization eucaryote discovered in the years 1930 by Raper [104](see Fig.1.3). The genome of this amoeba, haploid, was entirely sequenced [105]. It is composed of 34 Megabases, distributed on 6 chromosomes, and contains approximately 12500 genes. By way of comparison, it is twice as much as the yeast Saccharomyses cerevisiae (6000 genes approximately), and almost as much as certain pluricellular organizations like Drosophila melanogaster (14000 genes approximately). At the phylogenetic level, Dictyostelium discoideum diverged after plant/animals separation, but before that between animals and mushrooms. Nevertheless, because of an evolution slower, the distance between Dictyostelium and the man is less

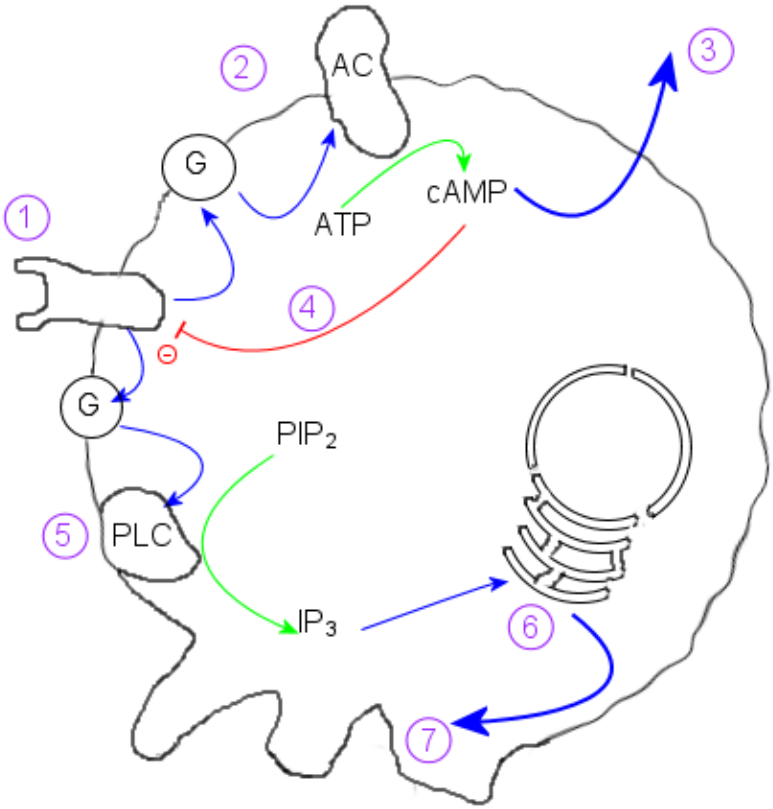

Figure 1.3: Diagram showing a Dictyostelium discoideum amoeba responds to cAMP. 1: cAMP reception at the cell membrane activates a G-protein. 2: G-protein stimulates adenylate cyclase. 3: cAMP diffuses out of cell into. 4: Internal cAMP inactivates the external cAMP receptor. 5: A different g-protein stimulates Phospholipase C. 6: IP_3 induces calcium ion release. 7: Calcium ions act on the cytoskeleton to induc the extension of pseudopodia. [106].

than that between the man and the yeast S. cerevisiae. In particular, about thirty genes orthologists to genes implied in human diseases were identified, of which 5 miss yeast genomes [105].

In nature, Dictyostelium discoideum lives in the basements timbered while being nourished bacteria by phagocytosis. The stocks used at the laboratory underwent changes which them also allow to nourish by macropinocytose medium axenic (not containing bacteria) [107]. In the presence of nutriments, Dictyostelium exists and multiplies in the shape of cells insulated, of approximately $10\mu m$ of diameter. This phase of growth of the cells is known as phase vegetative. In the event of nutritive deficiency, the cells cease dividing and engage in one process of development (Fig. 1.4), for a review to see [108]: the cells produce and relay a signal of cAMP,

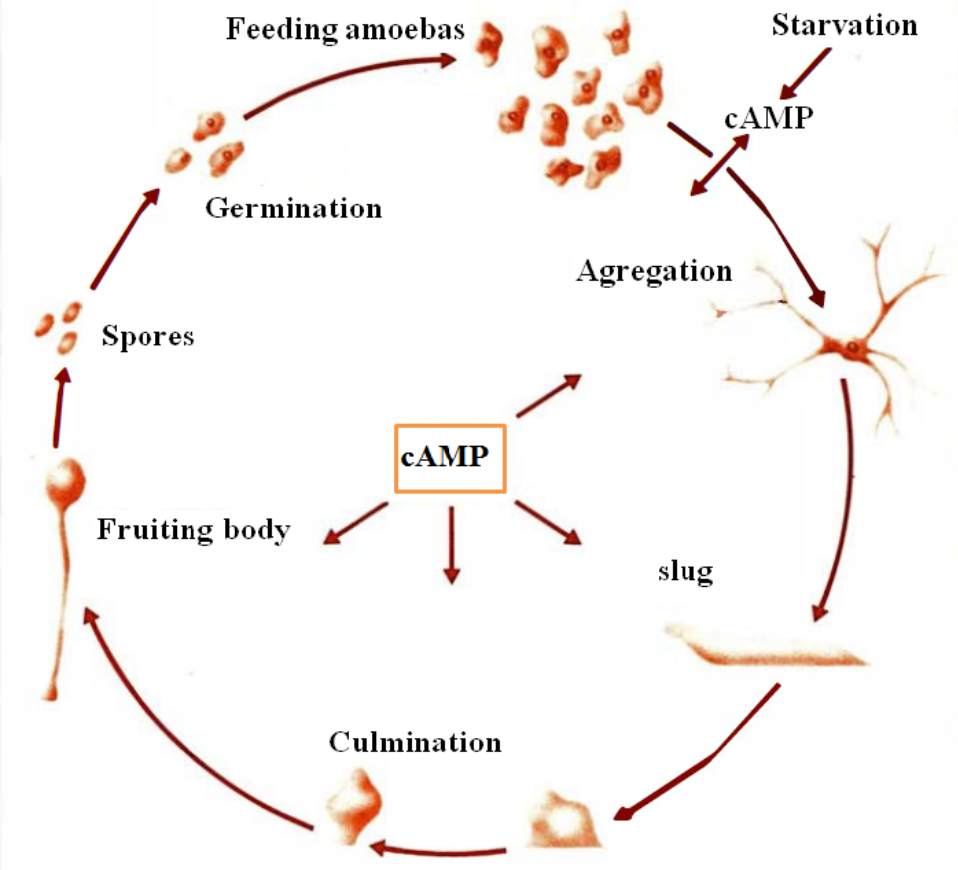

Figure 1.4: The cycle of Dictyostelium discoideum. The starvation induced the synthesis and the excretion of cAMP by amoeba. intervenes at all the stages of the pluricellular phase: aggregation, slug, culmination, constitution of the spores [72].

and move towards the source of this signal by chemotactism. In this manner, aggregates of 10^5 cells approximately are formed between 5 and 10 hours after the beginning of the deficiency. Each aggregate then will evolve/move to form a lengthened structure known as of snail, able of to move. Within this structure, the cells are different in two distinct types, of cells known as pre-stems (approximately 25 % of the cells) and pre-spores (approximately 75% of the cells). Lastly, the snail will be raised to form final fructification: a stem of dead cells surmounted by a cluster of cells known as spores, very resistant and likely to give again vegetative cells if the nutritive conditions become again favorable.

During these different life cycles, the Dictyostelium amoeba is therefore able to move spontaneously or by chemotaxis (towards folic acid in the vegetative phase and towards cAMP in the aggregative phase), to phagocyte particles, to differentiate into two types cells, and to form organized structures.

We now will evoke the mechanisms which allow Dictyostelium of to drive.

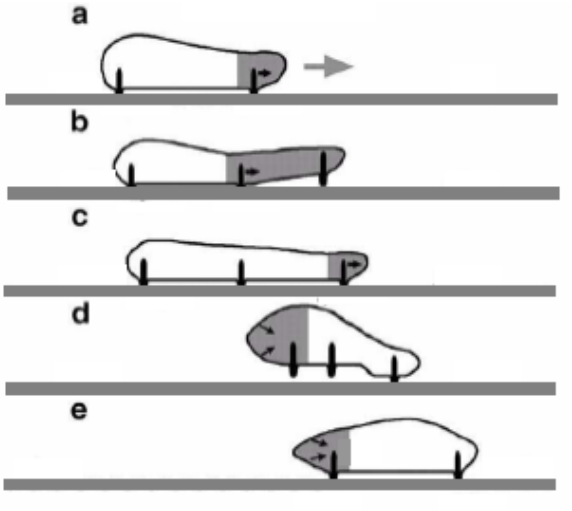

Figure 1.5: Model of the cycle of cellular movement for Dictyostelium cells. There gray arrow indicates the direction of movement. In gray, zones where the cell exerts forces (black arrows) to deform its membrane. Points of adhesion with the substrate are represented in black. according to [109].

1.2.2 Cellular Motility of Dictyostelium discoideum

The amoeba Dictyostelium discoideum is able to move on a surface at a speed of the order of 10ìm/mn. This motility known as amoebic can be broken up into a cycle comprising three phases (Fig. 1.5):

- **The emission of protrusions to the face before cell (a and b)**I.e. a deformation of the membrane which can have various forms. The cell thus must to exert forces on the membrane to move it. These forces are obtained thanks to the polymerization of filaments of actine.

- **The adhesion of these protrusions on the substrate (c).** The adhesion of protrusions on the substrate makes it possible to exert forces to draw the cell forwards. The cellular adhesion brings into play many molecular assemblies, among which proteins of the intégrine type.

- **The detachment and the retraction of the face postpone cell (d and e).** Once the cell stretched well on surface, it must contract before being able to extend to new. This phase requires to exert forces of contraction to the back of the cell. It puts more particularly concerned assemblies of myosine II and filaments of actine. The three phases are not independent: temporal and space coordination between various phases is an essential element so that the cell advances correctly. To move, the cell must be able to push its membrane with before and to draw this one with the back, and thus to exert forces. The existence of these forces can be put in obviousness by depositing the cells on a deformable substrate [109]. In what follows, we will be interested in the ways of indication which control and coordinate their actions.

1.2.3 Modes of cAMP signaling in dictyostelium discoideum cells

1.2.3.1 Excitable behavior

- **The Mechanism and Role of Chemotaxis**

  The aggregation of Dictyostelium cells has been extensively studied and shown to involve chemotaxis to 3'-5'cyclic AMP (cAMP), produced by the aggregating cells themselves. Chemotaxis is the process by which cells move either up or down gradients of diffusible signalling molecules. The mechanism of chemotaxis arose very early in evolution and was used by primitive single celled organisms including bacteria to translocate to sources of food. In multicellular organism chemotaxis is a key mechanism to generate complex cell migration patterns necessary to build complex structures during the embryonic development of most animals. In eukaryotic cells movement involves cycles of pseudopod or lamellipod extension at the front end of a migrating cell driven by localised actin filament formation, coupled with retraction of the actin-myosin network in the rear end of the cell. During chemotaxis cells measure gradients of the chemo-attractant along the length of the cell via attractant specific cell surface receptors that signal to the actin-myosin cytoskeleton to result in directional movement. High concentrations of the attractant promote and stabilise new protrusions in the direction of the increasing gradient and coordinate retraction of the cell at the low end of the gradient, resulting in net translocation up the gradient giving rise to directed cell movement [110].

- **Starving Cells Are Produced and Respond to Pulses of the Chemo-Attractant cAMP**

  Starvation triggers changes in gene expression that results in cells becoming able to detect cAMP via specific transmembrane cAMP receptors and they also acquire the ability to make and secrete cAMP using a specific starvation induced adenylate cyclase (ACA) [111]. cAMP is degraded by a secreted cAMP specific phosphodiesterase [112]. Cells in an aggregation center start to periodically produce and secrete cAMP. This cAMP diffuses to neighboring cells, which detect and amplify the signal and pass it on to their neighbours, resulting in a periodic cAMP wave propagation process [113]. The cAMP waves propagate from the aggregation center outwards and guide the chemotactic movement of the cells towards the aggregation center resulting in the aggregation of up to hundreds of thousands of cells. Although the underlying biochemistry of this excitable signalling system is rather complicated, we will briefly describe the main process and components here [114]. Binding of cAMP to the seven transmembrane cAMP receptors results in stimulation of a signal transduction cascade that leads to the activation of an ACA, that within tens

of seconds produces cAMP part of which is secreted to the outside. The secreted cAMP binds to the cAMP receptor and thus is part of an autocatalytic feedback loop resulting in a rapid increase of cAMP production. However stimulation of the receptor also activates an adaptation process that, with a small time delay, results in inhibition of adenylyl cyclase activity and thus in a cessation of cAMP production. Since cAMP diffuses away into the extracellular medium and is also degraded by internal and secreted cAMP phosphodiesterase, this results in a drop in internal and external cAMP levels. This drop in extracellular cAMP in turn results in de-adaptation of the cells (Fig. 1.6). This scheme has been the basis for many mathematical models for the cAMP oscillator that can describe key experimental results and the transition of excitable to oscillatory cAMP synthesis during development [115]. The details of the underlying biochemistry of the cAMP oscillator is rather complex and contains many components. Especially the biochemical basis for adaptation is not yet completely understood in molecular detail [116].

1.2.3.2 From oscillations to waves of cAMP

The wavelike aggregation of D. discoideum cells after starvation provides a striking example of spatiotemporal organization at the supracellular level. In their pioneering paper of 1970 Keller and Segel showed that the initial homogeneous cell spatial distribution becomes unstable when the rate of secretion of chemotactic factor by the cells exceeds a critical value. A key result of this analysis, which applies particularly well to D. minutum, was that no heterogeneity in cell function-i.e., no center-is needed to trigger aggregation. Not considered explicitly in this first study was the wavelike nature of aggregation in D. discoideum cells. The periodic nature of aggregation in this species is directly linked to the oscillatory synthesis of cAMP, which is released in the form of periodic pulses by cells behaving as aggregation centers (Fig. 1.7). Experimental observations indicate that aggregating cells form either concentric or spiral waves [11, 118, 119]. The waves of cellular movement are superimposed on waves of the chemoattractant, cAMP. Much work has been devoted to understanding the onset of spatio-temporal self-organization [120] and the transition from concentric to spiral patterns of wavelike aggregation, both experimentally and theoretically [121–123]. Building on the notion of developmental path which was initially proposed for the transitions in dynamic behavior observed for the cAMP signaling system, [124, 125] investigated the effect of desynchronization of cells following the developmental path in parameter space. The results indicate that concentric waves of cAMP form first when cells enter the domain of autonomous oscillations, while neighboring cells are in an excitable state and relay these signals. However, the heterogeneity in parameter values, due to the distribution of cells on the developmental path, creates defects that eventually lead to breaks in concentric waves. From

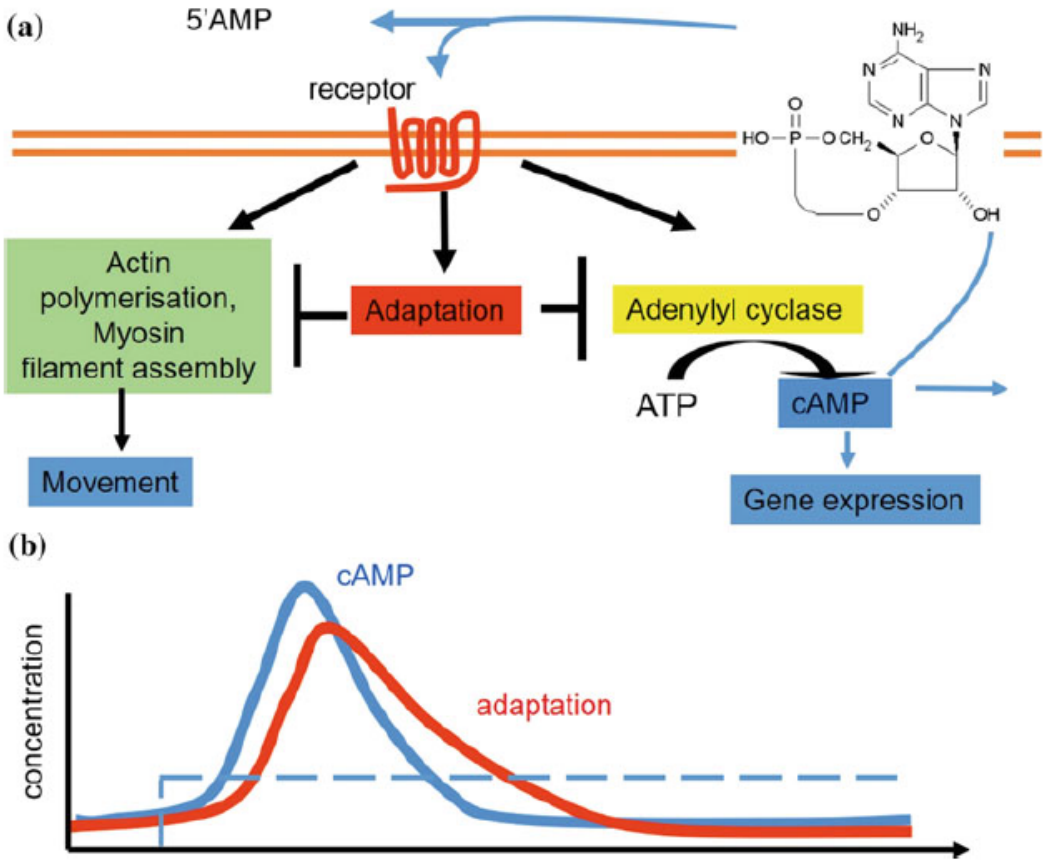

Figure 1.6: Excitable cAMP signalling. a: Schematic of the extracellular space, above the double red line (plasma membrane) and the inside of a containing the main components to produce cAMP oscillations and cellmovement. b: schematic of temporal changes in cAMPsynthesis and adaptation in response to a constant stimulus of cAMP (stippled blue line) [117]

these defects spiral patterns arise, which are maintained even when all cells have become excitable and no one is capable any more of sending out periodic pulses of cAMP. Besides desynchronization other factors may favor the transition from concentric to spiral waves. The transition is likely facilitated by the chemotactic movement of cells, which further amplifies heterogeneities within the aggregation field [122].

1.2.3.3 Exact adaptation

In many sensory systems the response triggered by an external stimulus decreases in the course of time and returns to basal levels even though the stimulus is maintained at a high value. This physiological process is called adaptation. Adaptation can be partial or exact. In the latter case, the system returns precisely to the same steady state regardless of the level

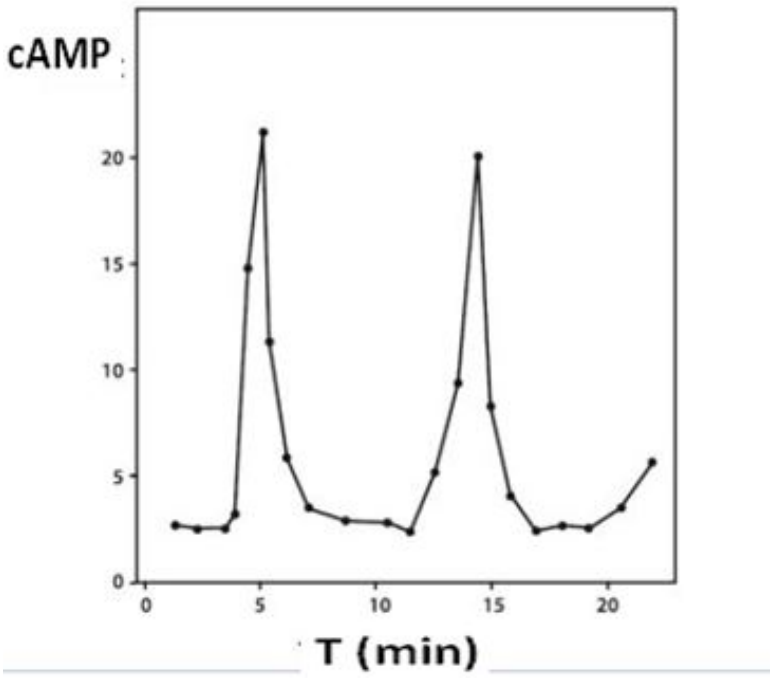

Figure 1.7: Oscillations of cAMP in amoebae dictyostelium discoideum. The panel represents the periodic variation of intracellular cAMP within a suspension of synthesized cells. The extracellular cAMP (not shown) varies with the same period [135].

of stimulation. Exact adaptation is observed in bacterial chemotaxis [126], and in the cAMP relay response in Dictyostelium [127]. In the summer of 1985 Peter Devreotes and I joined Lee Segel at the Weizmann Institute to work on this problem. Building on previous work devoted to adaptation of the bacterial chemotactic response [128], we considered a two-state receptor model, with a ligand that binds with different affinities to these two states, which are in conformational equilibrium. We assumed that a certain activity is generated by a linear combination of the four liganded or free receptor states to which an activity coefficient is attributed. The mathematical problem was to determine whether, for a given set of parameter values, it is possible to find a set of activity coefficients that would ensure that the total activity generated upon ligand binding to the receptor returns to the same steady state, regardless of the magnitude of the stepwise increase in ligand concentration. We found, to our delight, that a unique set of activity coefficients satisfying this constraint indeed exists. Lee was instrumental in carrying out the mathematical derivations that led to this surprising result [129] Alternative molecular mechanisms for exact adaptation have since been proposed [130] . A recent modeling study was specifically devoted to a detailed analysis of the intracellular biochemical events mediating the chemotactic response in Dictyostelium cells [131].

Although the underlying biochemistry of this excitable signalling system is rather compli-

cated, we will briefly describe the main process and components here [132]. Binding of cAMP to the seven transmembrane cAMP receptors results in stimulation of a signal transduction cascade that leads to the activation of anACA, that within tens of seconds produces cAMP part of which is secreted to the outside (Fig. 1.6a). The secreted cAMP binds to the cAMP receptor and thus is part of an autocatalytic feedback loop resulting in a rapid increase of cAMP production. However stimulation of the receptor also activates an adaptation process that, with a small time delay, results in inhibition of adenylyl cyclase activity and thus in a cessation of cAMP production. Since cAMP diffuses away into the extracellular medium and is also degraded by internal and secreted cAMP phosphodiesterases, this results in a drop in internal and external cAMP levels. This drop in extracellular cAMP in turn results in de-adaptation of the cells (Fig. 1.6b). This scheme has been the basis for many mathematical models for the cAMP oscillator that can describe key experimental results and the transition of excitable to oscillatory cAMP synthesis during development [133]. The details of the underlying biochemistry of the cAMP oscillator is rather complex and contains many components. Especially the biochemical basis for adaptation is not yet completely understood in molecular detail [134].

1.2.4 Waves of cAMP in dictyostelium discoideum cells

- **Visualising cAMP Wave Propagation**

  During the synchronised chemotactic movement phase the cells elongate slightly, while during the falling phase of the waves the cells stop moving and take on a less polarised shape. These locally synchronised cell behaviours can be visualised as changes in light scattering that reflect the propagating cAMP waves (Fig. 1.8) [118]. cAMP waves have also been measured directly using isotope dilution fluorography and these measurements showed that the optical density waves reflected the cAMP waves and that the concentrations varied between 10-9 and 10-6 M which is well within the Kd of the cAMP receptors [136]. Nowadays cAMP dependent cell-cell signalling can be measured directly by dynamic measurements of intracellular cAMP genetically engineered cAMP binding proteins using the principle of Fluorescence Resonance Energy Transfer (FRET) [137]. Furthermore it is possible to dynamically measure various components of the cAMP signal transduction machinery to cAMP relay and the actin-myosin cytoskeleton in single cells but also at the population level. These measurements can therefore not only be used to study the spatiotemporal dynamics of signal transduction but also to indirectly visualise the dynamics of cAMP wave propagation. Most recently it has been shown that a transcription factor gatC shuttles between the cytoplasm and the nucleus in response to cAMP stimulation and that this is a key part of the mechanism of pulsatile induced gene expression [138].

- **Competition Between Aggregation Centres**

  Observation of wave forms during aggregation reveals that there are essentially two types of waves that can be observed during aggregation. These are patterns of concentric waves that are periodically initiated by the aggregation center and spiral waves (Fig. 1.8). In both cases the cAMP waves propagate over a large distance of up to several centimeters and pass over hundreds of thousands of cells. The period of the waves is initially quite long, in the order of 8 min but gradually goes to down to $\sim 3min$, while the wave propagation speed is initially high ($\sim 1mm/min$) but then drops down as the cells come into closer contact. Centres arise at different times and oscillate with different frequencies [118]. Due to the fact that colliding waves annihilate each other faster oscillating centres can encroach on slower oscillating centres and can finally wipe them out. It has been described that spiral centres normally wipe out concentric centres [139]. Concentric centres can only exist when the cells in the center are in an oscillatory mode, however spiral waves can exist both in excitable and oscillatory systems. In spiral waves the waves rotate around a central core, periodically re-stimulate themselves and are likely to run at the maximum frequency that the excitable or oscillatory medium can sustain and therefore are likely to dominate [140]. Different strains show typically different types of waves during the aggregation stage. This is likely dependent on the exact composition of the molecular components making up the cAMP oscillatory machinery, which is not known in detail for all of the components in all of the strains.

1.2.5 Frequency encoding of cAMP pulses in intercellular communication

Key experiments published independently in 1975 by two groups showed that cAMP signals in Dictyostelium are frequency encoded. In a mutant of D. discoideum unable to aggregate, cAMP pulses administered at the physiological frequency of one pulse every 5 min are capable of rescuing the mutant and lead to multicellular aggregation [141] . In contrast, continuous stimulation by cAMP does not lead to aggregation. In the wild type, the administration of cAMP pulses after starvation accelerates development in the phase leading to aggregation. This effect is obtained with cAMP pulses delivered every 5 min but not when the interval between pulses is reduced to 2min, or when the cAMP signal becomes continuous [39] . Pulses of cAMP administered at random intervals in wild type are likewise less effective [144]. These observations demonstrate the importance of the frequency of pulsatile cAMP signals.

The model based on receptor desensitization provides a unified explanation for these experimental observations. It shows that when the pulse is given at regular intervals, the receptor

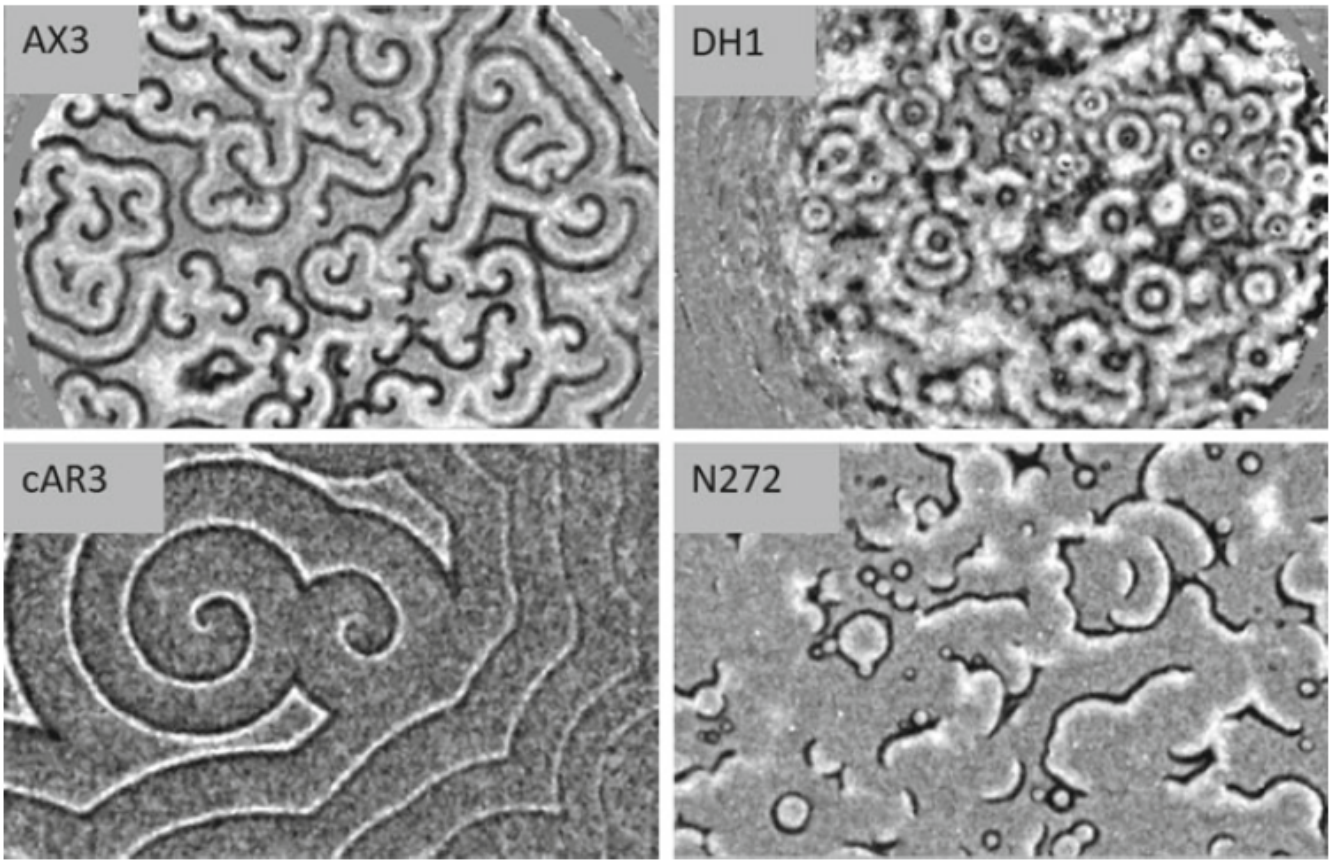

Figure 1.8: Wave patterns observed during aggregation in wildtype and mutant strains. Strain Ax3 shows spiral waves, strain DH1 makes many concentric waves, the cAR3 strain is a mutant that expresses a lower affinity cAMP receptor and produces large spiral waves. The N272 strain expresses even lower affinity cAMP receptors, makes chaotic waves. They are not able to set up stable centres since the wave period is so slow that the cells disperse between waves, see [142] for further details

has sufficient time to resensitize during a 5-min interval, but not during a 2-min interval. In the latter case, when the next pulse arrives the amount of active receptor will not be sufficient to produce a large-amplitude response. In these conditions the synthesis of cAMP elicited by repetitive pulses of extracellular cAMP will be reduced, while it is nearly maximum when the pulse is given every 5 min. For the same reason, continuous stimulation by cAMP causes receptor desensitization and permanent attenuation of the cAMP response [2].

The model further predicts the existence of an optimal pattern of pulsatile stimulation by cAMP, which maximizes cellular responsiveness, i.e. the amount of cAMP synthesized in a given time in response to cAMP pulses. For the experimentally determined values of the rate constants measuring receptor desensitization and resensitization, the model predicts that the optimal pulsatile signal of cAMP should have a duration of about 4min, with an interpulse

interval of about 3 min [145]. Increasing or decreasing the values of these rate constants should change the characteristics of the optimal pattern of pulsatile stimulation, a subject that could be easily explored with mutants.

The cAMP signaling system in Dictyostelium provides a useful prototype for pulsatile intercellular communication in higher organisms. It can be viewed as a primitive hormonal communication system, in which cAMP plays the role of both the hormone and the intracellular second messengerŮthis duality underlies the self-amplification property that is the hallmark of cAMP synthesis in Dictyostelium. The link with hormonal signaling goes beyond this analogy. Most hormones are indeed released in a pulsatile manner, and the frequency of pulsatile secretion often governs the efficacy of the hormonal signal.

The study of a general model of a receptor undergoing reversible desensitization shows that when the hormone that binds to the receptor is applied in a pulsatile manner, there exists an optimal pattern of periodic stimulation that maximizes target cell responsiveness [146] . The results account for the existence of such an optimal pattern of stimulation for the hormone GnRH, which is secreted by the hypothalamus in the form of a 5-min pulse every hour. The model further shows that the optimal periodic signal is more efficient than pulses delivered in a random or chaotic manner [147]. This is very similar to Dictyostelium.

1.3 Mathematical cAMP models

Cellular slime moulds are unique organisms positioned between uni- and multi-cellular life in the evolutionary tree. The amoebae of the cellular slime mould Dictyostelium discoideum normally live as single cells in forest soil and feed on bacteria. They multiply by binary fission. Cyclic adenosine monophosphate (cAMP) is the primary chemoattractant for the D. discoideum cells during early aggregation. cAMP is emitted from the aggregation centers in a pulsatile manner and surrounding cells detect it by highly specific cAMP receptors. Many different models of cell-to-cell communication in Dictyostelium have been proposed over the years. The earliest models were necessarily a little crude because essential biochemical information about the signaling system was lacking. Modeling cAMP wave propagation in agar-surface cultures introduces spatial dependencies and is much more complicated than modeling oscillations and signal relaying in cell-suspension cultures because as well as the signal-relaying system we now have to account for random diffusion of cAMP in the extracellular milieu, and chemotactic motion of the amoebae. The models in this category are able to describe oscillations in the cAMP level in cell suspensions as well as cAMP wave propagation in a dispersed cell population.

1.3.1 Goldbeter-Segel Model

There is general agreement that the cAMP signalling system in Dictyostelium contains the following elements:

1. cAMP receptors on the exterior of the cell;
2. a coupling between the receptors and the membrane-bound enzyme adenylate cyclase;
3. synthesis of cAMP by the cyclase whose catalytic activity increases in response to exterior CAMP signals;
4. a secretion of newly synthesized cAMP to the cell exterior where it is hydrolyzed by the enzyme phosphodiesterase.

In the model, the receptor-enzyme complex is treated as a membrane-bound allosteric protein with catalytic and regulatory (receptor) sites facing, respectively, the inside volume of the cell and the extracellular medium.

In homogeneous conditions which correspond to the experiments in continuously stirred suspensions of D. discoideum cells, the system is described by three ordinary differential equations:

$$\frac{d\alpha}{dt} = V - \sigma\varphi - k'\alpha, \tag{1.1a}$$

$$\frac{d\beta}{dt} = q\sigma\varphi - k_t\beta, \tag{1.1b}$$

$$\frac{d\gamma}{dt} = (k_t\beta/h) - k\gamma, \tag{1.1c}$$

with

$$\varphi = \alpha(1+\alpha)(1+\gamma)^{2/}[L + (1+\alpha)^2(1+\gamma)^2] \tag{1.1d}$$

The variables α, β and γ denote the normalized concentrations of intracellular ATP, intracellular CAMP, and extracellular cAMP divided, respectively, by K_s, K_p and K_p where K_s and K_p are the Michaelis constant of adenylate cyclase for ATP and the dissociation constant of the cAMP receptor. Also $q = K_s/K_p$ while σ and V are the maximum cyclase activity and a constant ATP input, divided by K_s. The apparent first order rate constants k_t, and k relate to the cAMP transport across the cell membrane and to the phosphodiesterase reaction, which are both considered as linear processes (both the extracellular and membrane-bound forms of phosphodiesterase are lumped together into parameter k); L is the allosteric constant of adenylate cyclase; h is a dilution factor (see ref. [1] and [148] for further details). The term $-k\alpha$ in the evolution equation for a represents a modification of the system originally considered in [1]. This term relates to the utilization of ATP in reactions other than that catalyzed by adenylate cyclase.

Alternatively, when combined with parameter $V = k\alpha_0$, it gives the term $k(\alpha_0 - \alpha)$ which can be viewed as expressing a possible transport of ATP from a constant intracellular pool (α_0) to the site of cAMP synthesis at the membrane.

1.3.2 Martiel-Goldbeter Model

Martiel and Goldbeter (1987) proposed a model for cAMP signaling based on receptor desensitization. This model incorporates both a positive and a negative feedback by extracellular cAMP. Binding of cAMP to its receptor triggers the activation of adenylate cyclase as well as the transition of the receptor into a desensitized (phosphorylated) state. In this three-variable model, the explosive rise in cAMP synthesis is limited by the drop in the fraction of active receptor. Desensitization begins as soon as the level of extracellular cAMP starts to increase. Once the level of cAMP has dropped to a minimum, the receptor resensitizes through dephosphorylation. A new cycle of oscillations begins upon binding of extracellular cAMP to the receptor in its active state. As in the previous model, relay of suprathreshold pulses of cAMP occurs in a parameter domain adjacent to the domain in which sustained oscillations occur. The dynamics of the cAMP signaling system is then governed by the three differential, where the various functions and parameters remain defined as:

$$\partial_t \rho = -f_1(\gamma)\rho + f_2(\gamma)(1-\rho), \tag{1.2a}$$

$$\partial_t \beta = q\sigma\alpha\phi(\rho,\gamma)/(1+\alpha) - \beta \tag{1.2b}$$

$$\partial_t \gamma = (k_t\beta/h) - \gamma \tag{1.2c}$$

with,

$f_1(\gamma) = \frac{k_1+k_2\gamma}{1+\gamma}$; $f_2(\gamma) = \frac{k_1L_1+k_2L_2c\gamma}{1+c\gamma}$; $\phi(\rho\gamma\alpha) = \frac{\alpha(\lambda\theta+\epsilon Y^2)}{1+\alpha\theta+\epsilon Y^2(1+\alpha)}$; $Y = \frac{\rho\gamma}{1+\gamma}$

In the above equations, ρ denotes the total fraction of receptor in the active state; β and γ denote the intracellular and extracellular concentrations of cAMP divided by the dissociation constant KR; α is the intracellular ATP concentration. The constants k_t, k_e, q and k_i, are rate constants associated with the metabolism of cAMP, and h is the ratio of extracellular volume to intracellular volume. The rate functions $f_1(\gamma)$ and $f_2(\gamma)$ describe the kinetics of the receptor box, and $\phi(\rho\gamma\alpha)$ describes the activation of adenylate cyclase by bound and active receptor.

1.3.3 Monk-Othmer Model

The Monk-Othmer model developed previously for signal relay and adaptation in the cellular slime mould Dictyostelium discoideum is shown to account for the observed oscillations calcium and cyclic AMP in cellular suspensions.

Magnitudes	Definition
k_1	Rate constant for modification step $R \rightarrow D$
k_2	Rate constant for modification step $cAMPe - R \rightarrow cAMPe - D$.
k_{-1}	Rate constant for demodification step $D \rightarrow R$.
k_{-2}	Rate constant for demodification step $cAMPe - D \rightarrow cAMPe - R$.
K_R	Dissociation constant of cAMP-receptor complex in R state.
K_D	Dissociation constant of cAMP-receptor complex in D state.
$K_{m,cyclase}$	Michaelis constant of the form AC of adenylate cyclase.
$K'_{m,cyclase}$	Michaelis constant of the form IC of adenylate cyclase.
$V_{m,cyclase}$	The rate of the maximum adenylate cyclase activity.
k_i	Apparent first-order rate constant for iPDE.
k_t	Apparent first-order rate constant for cAMP transport into extracellular medium.
h	Ratio of extracellular to intracellular volumes.
$V_{m,PDE}$	Maximum activity for ePDE.
$K_{m,PDE}$	Michaelis constant of ePDE for cAMP.
ATP	The intracellular level of ATP.
k_5	Catalytic constant of the form IC of adenylate cyclase.
k_4	Catalytic constant of the form AC of adenylate cyclase.
ϵ	Coupling constant for activation of IC by cAMPe-R.

Table 1.1: *The meaning of the chemical magnitudes*

The network of the major processes and the control pathways in the expended model is shown in (Fig. 1.9). A qualitative argument is given which explains how the oscillations arise. The model described by the equations intracellular and extracellular dynamics are given by:

- **The equations for the intracellular dynamics**

  The equations for the intracellular variables are independent of whethere or not the concentration of extracellular cyclic AMP is clamped. the velocity of the transport intracellular concentration is given by:

$$\overline{g_2}(Ca_0, C_o) - \overline{g_1}(Ca_i, C_o) = \overline{R_1}(C_o)\frac{Ca_0}{K_{FCa} + Ca_o} - V_{pump}\frac{Ca_i^{q_4}}{K_{pump}^{q_4} + Ca_i^{q_4}} \tag{1.3}$$

  Where $\overline{R_1}(C_o)$ is an increasing function, the form:

$$\overline{R_1}(C_o) = V_{m1} = \left(\frac{R_I + k_I C_o}{1 + k_I C_o}\right)\left(\frac{R_{I1} + k_{I1} C_o}{1 + k_{I1} C_o}\right) \tag{1.4}$$

$L_1 = k_{-1}/k_1$	$q = K_{m,cyclase}/K_R$	$\alpha = ATP/K_{m,cyclase}$
$L_2 = k_{-2}/k_2$	$\sigma = V_{m,cyclase}/K_{m,cyclase}$	$\theta = K_{m,cyclase}/K'_{m,cyclase}$
$c = K_R/K_D$	$k_e = V_{m,PDE}/K_{m,PDE}$	$\lambda = k_5/k_4$

Table 1.2: *The expression of the parameters, appearing in (1.2), in terms of the chemical magnitudes of Table 1.*

The functions $\overline{g_1}$ and $\overline{g_2}$ are the rate of transport of cytoplasmic calcium to exterior compartment and exterior calcium to cytoplasm respectively. For the other parameters (see [3]).

- **The equations for the extracellular dynamics**

  The dimensionless equations governing the concentration of extracellular cyclic AMP are as follows:

$$
\begin{aligned}
&\frac{dx_1}{d\tau} = R_c\big(\frac{\rho}{1-\rho}\big)(R_H f_2(x_2) - V_{PO}(\frac{x_1^\alpha}{1+x_1^\alpha}) + HR_H(R_H x_2 - x_1) \\
&- V_{PE}(\frac{x_1}{R_e + x_1}) \\
&\frac{dx_2}{d\tau} = V(x_1, x_3) + H(x_1 - R_H x_2) - f_2(x_2) - V_{PI}(\frac{x_2}{1+x_2}) \\
&\frac{dx_3}{d\tau} = R_1(x_1)(\frac{x_6}{K_F + x_6}) - V_{PU}(\frac{x_3^{q_4}}{K_{PU}^{q_5} + x_3^{q_4}}) \\
&+ V_s(\frac{R_S + K_S x_2}{1 + K_S x_2})(x_4 - x_3) - V_{SA}(\frac{x_3^{q_5}}{1 + x_3^{q_5}}) \\
&\frac{dx_4}{d\tau} = (\frac{R_c}{1-R_c})(V_{SA}(\frac{x_3^{q_5}}{1+x_3^{q_5}}) - V_s(\frac{R_s + K_s x_2}{1 + K_s x_2})(x_4 - x_3)) \\
&x_6 = (\frac{1}{1-\rho})(\overline{x_6} - R_c\rho x_3 - (1-R_c)\rho x_4)
\end{aligned}
\tag{1.5}
$$

  Here $x_1, ..., x_6$ denote the dimensionless concentrations of extracellular cyclic AMP and calcium. The definition of each of the dimensionless parameters in the above equations is given in [3].

1.3.4 Tang-Othmer model

The Tang and Othmer model is based on signal transduction via G proteins for adaptation of the signal relay process in the cellular slime mold Dictyostelium discoideum. The kinetic constants involved in the model are estimated from Dictyostelium discoideum and other systems.

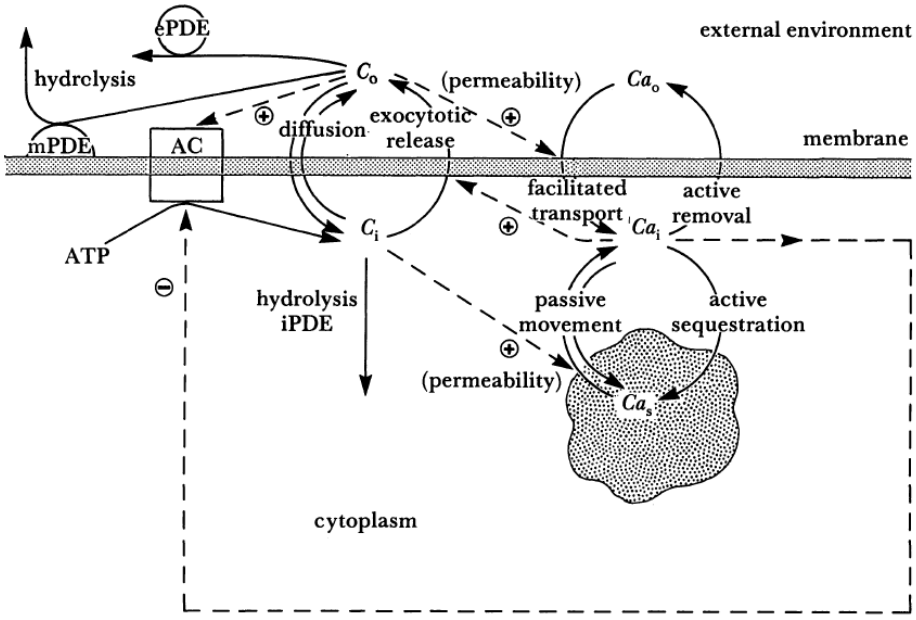

Figure 1.9: A schematic of the Calcium-cyclic AMP control network in dictyostelium discoideum proposed in (I) and (II) and modified herein. Solid arrows indicate the chimical reaction and transport pathways, broken lines indicate the control pathways. Ac, adenylate cyclase; ATP, adenosine triphosphate; C_0, concentration of extracellular cyclic AMP; C_i, concentration of cytosol cyclic AMP; Ca_0, concentration of extracellular calcium; Ca_1, concentration of cytosol calcium; Ca_s, concentration of sequestered intracellular calcium; ePDE, extracellular free phosphodiesterase; iPDE, cytoplasmic phosphodiesterase; mPDE, membrane bound extracellular phosphodiesterase.

A typical scheme for signal transduction is shown in (Figure 1.10) . Upon binding of agonist to a receptor, the agonist-receptor complex H_sR_s catalyzes the conversion of G_s, from the inactive GDP-binding state, to the active GTP-binding state, with the release of GDP and the $\beta\gamma$ subunits. Binding of the active G_s, protein, who is denote by $G_s^{'}$ or $\alpha_s GTP$, with the unactivated adenylate cyclase, which we denote UC, converts the latter into the activated cyclase AC. $\alpha_s GTP$ is deactivated by the intrinsic GTPase activity of α_s. Modulo the basal rate for the unactivated cyclase, the rate at which CAMP is produced is proportional to the amount of agonist present, and a constant level of stimulus can sustain a constant level of CAMP production in the absence of adaptation.

- **The differential equations for quantities in the stimulus pathway are:**

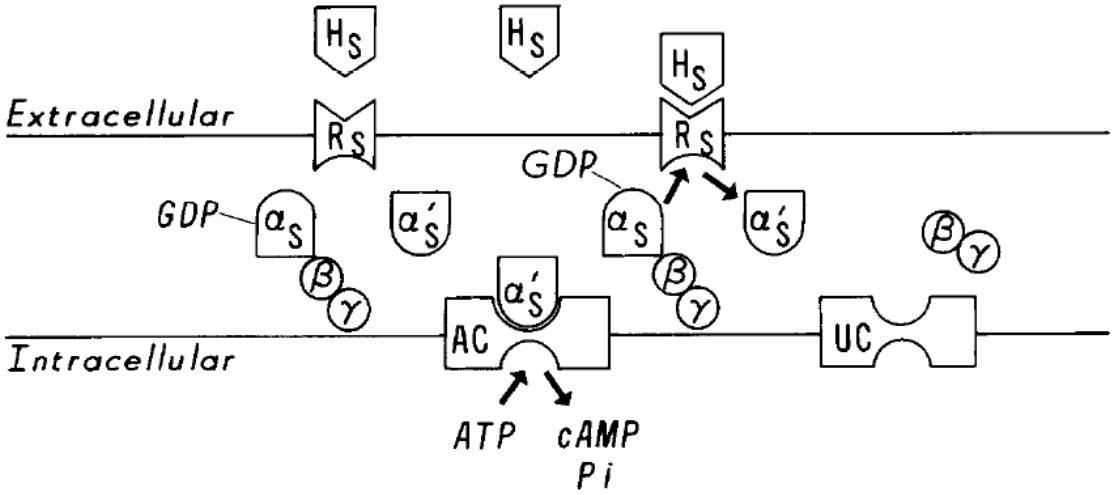

Figure 1.10: A schematic diagram of the activation of adenylate cyclase via G_s proteins. H_s denotes the stimulus signal, R_s, the stimulus receptor, $\alpha_s GDP\beta\gamma$ unactivated G_s, protein, and UC unactivated adenylate cyclase. It is believed that upon binding of H_s, with R_s, G_s, is activated by the H_sR_s complex. This involves the release of the $\beta\gamma$ subunits and the addition of GTP to the α_s chain. $\alpha_s GTP$, which is denoted by $\alpha_s^{'}$ in this figure, then activates adenylate cyclase, which catalyzes the conversion of ATP to CAMP.

$$
\begin{aligned}
\frac{dy_1}{dt} &= k_1 H_z z_1 - k_{-1} y_1 - k_2 y_1 z_2 + (k_{-2} + k_3) y_2 - h_4 y_1 y_8 + h_5 y_9, \\
\frac{dy_2}{dt} &= k_2 y_1 z_2 - (k_{-2} + k_3) y_2, \\
\frac{dy_3}{dt} &= k_3 y_2 - k_4 y_3 z_3 - k_5 y_3, \\
\frac{dy_4}{dt} &= k_4 y_3 z_3 - (k_5 + l_1) y_4 + (l_{-1} + l_2) y_{11}, \\
\frac{dy_5}{dt} &= k_5 (y_3 + y_4) - k_6 y_5 z_6,
\end{aligned}
\tag{1.6}
$$

- **differential equations for quantities in the inhibitory pathway are:**

$$\begin{aligned}
\frac{dy_6}{dt} &= h_1 H z_4 - h_{-1} y_6 - h_2 y_6 z_5 + (h_{-2} + h_3) y_7, \\
\frac{dy_7}{dt} &= h_2 y_6 z_6 - (h_{-2} + h_3) y_7, \\
\frac{dy_8}{dt} &= h_3 y_7 - h_4 y_1 y_8 - h_5 y_8 + h_6 y_9, \\
\frac{dy_9}{dt} &= -(h_5 + h_6) y_9 + h_4 y_1 y_8, \\
\frac{dy_{10}}{dt} &= h_5 (y_8 + y_9) - h_7 y_{10} z_6
\end{aligned} \tag{1.7}$$

- **The differential equations for the production and secretion of intracellular CAMP are:**

$$\begin{aligned}
\frac{dy_{11}}{dt} &= l_1 y_4 - (l_{-1} + l_2) y_{11}, \\
\frac{dy_{12}}{dt} &= l_2 y_{11} - l_5 y_{12} + l_{-3} y_{13} - l_3 y_{12} z_7 \\
\frac{dy_{13}}{dt} &= -(l_{-3} + l_4) y_{13} + l_3 y_{12} z_7, \\
\frac{dy^*_{14}}{dt} &= l_5 y_{12}
\end{aligned} \tag{1.8}$$

The definition of the concentration $y_1 - y_{14}$ in the differential equations and other parameter are given in [4]. The term asterisk $(*)$ is used to indicate the former.

1.3.5 FitzHugh-Nagumo Model

The FitzHugh-Nagumo (FHN) cyclic AMP model [5–7] is the equivalent reduced MG model. These equations are commonly used to describe a prototype excitable medium. The theory of nonlinear mechanics was used by the phase space method to obtain the derivative of FHN model. The two-component FitzHugh-Nagumo model system:

$$\dot{g} = D\big(g_{xx} + g_{yy}\big) - k_g g\big(g - a\big)\big(g - 1\big) - k_r r, \tag{1.9a}$$

$$\dot{r} = \big(g - r\big)/\tau \tag{1.9b}$$

The first equation describes the excitation of the medium, defined by the variable (g), over time. This variable is linked to the extra cellular cAMP concentration. The second equation defines the recovery process of the medium (r) and could be thought to describe the desensitisation

of the cAMP receptors. D is the diffusion coefficient for cAMP; τ is a time scaling factor for the variables r and g; k_g and k_r, define the rate of production and hydrolysis of cAMP by one cell and a is a coefficient.

1.3.6 Difference and Similitude between the Various Models

Many different models of cell-to-cell communication in Dictyostelium have been proposed over the years. The earliest models were necessarily a little crude because essential biochemical information about the signaling system was lacking. For instance, before the kinetic properties of the membrane receptor were characterized, Goldbeter and Segel (1980) suggested a model in which intracellular ATP, intracellular cAMP, and extracellular cAMP were the essential dynamical variables. the Goldbeter-Segel model was unable to account for adaptation of the cAMP response to repeated stimulation of Dictyostelium cells by external application of cAMP. Then model calculations agree in quantitative detail with experimental observations of the relay response of Dictyostelium cells in suspension, of adaptation to constant stimulation, and of the response of cells to periodic pulsatile and stepwise stimulation (Martiel and Goldbeter, 1987). The models Martiel-Goldbeter (MG) and Goldbeter-Segel (GS) are not able to explain the oscillations observed of calcium and the cyclic AMP in the cellular suspension. For that Monk and Othmer (1989) developed a model for the calcium-cyclic-AMP control network in Dictyostelium discoideum. In the enzymatic activity, Tang-Othmer (1995) proposed a model or the receptor dependent activation of activating and inhibitory G proteins controls the periodic cAMP production.The prototype FitzHugh-Nagumo (1997) system describe excitable and/or oscillatory media and is very similar to the models precedent. This models were developed to describe mathematically the cAMP relay kinetics of Dictyostelium amoebae. Some of them have biophysically meaningful and measurable parameters(GS, MG, MO, TO), and the other although not having biophysically meaningful, exhibit the most fundamental properties of the propagation waves of cyclic AMP (FHN).

Conclusion

This chapter has allowed us to understand the anatomy and physiology of the cyclic AMP signaling system in the amoebas dictyostelium discoideum. The good quantitative agreement between theory and experiment on cAMP waves during aggregation of Dictyostelium amoebae is very encouraging and provides reasonable cause for optimism in modeling the complete developmental process in this organism. Dictyostelium aggregation is in many respects a special case in that it is a simple process organized by traveling waves and a process for which we have a

good description of the kinetics of the biochemical reactions taking place. To explain a complex developmental process, unfolding in space and time, it is necessary but not sufficient to study the individual pieces of the molecular machinery. Eventually these pieces must be put together into a mathematical model, and the model must be studied by analytical and numerical methods to demonstrate that the mechanism really can account for the developmental process in quantitative detail. The differents Mathematical models and numerical experimentation, of the sort we have reviewed here, are becoming increasingly important in developmental biology. Their ultimate success, however, will depend crucially on close interaction between biologists and theoreticians. Therefore, in the rest of this work, we propose to study the pulsatile communication in the amoebas dictyostelium discoideum.

Chapter 2

Models of cAMP in Dictostelium-discoideum and methodologie

Introduction

For a logical understanding of the communication between cells in the colony of amoebas dictyostelium discoideum, several models were proposed during years. The first models were too rough because certain biochemical information essential for the system signaling missed. Goldbeter and Segel [151] suggested a model in which intracellular adenosine triphosphate (ATP) and intracellular and extracellular Adénosine Monophosphate cyclic (AMPc) was essential dynamic variables. By assuming the positive feedback of extracellular cAMP on the activity of the cyclase of adenylate, Goldbeter and Segel could show oscillations and announce the relay in the model which was remarkably similar to the experimental observations in the well-stirred up suspension of cells. Unfortunately, the model of Goldbeter-Segel could not explain the adaptation of the cAMP response to the repeated stimulation of the cells of Dictyostelium by external application of cAMP [153, 154]. Modeling cAMP wave propagation in agar-surface cultures introduces spatial dependencies and is much more complicated than modeling oscillations and signal relaying in cell-suspension cultures because as well as the signal-relaying system we now have to account for random diffusion of cAMP in the extracellular milieu, random motion of the amoebae on the agar surface, and chemotactic motion of the amoebae. Martiel and Goldbeter [2] developed a complete model of cAMP signaling by adding several reactions recapitulating the synthesis of cAMP by adenylate cyclase, the cAMP transport through the plasma membrane, and the degradation of cAMP by the phosphodiestérase. By traditional methods of biochemical kinetics,

Martiel and Goldbeter derived a set of equations describing the dynamics of rates of interactions of intracellular cAMP, extracellular cAMP and the membrane receiver. For slightly different values of parameter, the model predicts that the cells answer the external cAMP impulse by amplifying the impulse of cAMP. The models for calculations are in agreement with the quantitative time with experimental observations of the response of relay in suspension of the cells of Dictyostelium, of adaptation to constant stimulation, and of the response of the cells to pulsatile stimulation and by stages périodique. Little time later, the MG model undergoes improvements, the extracellular diffusion of cAMP was injected by Tyson and its collaborateurs [9], the reaction-diffusion-migration worked out by Linder et al. [155] , Gholami and its collaborators improved by the addition of the advection in the model (reaction-diffusion-advection) [150]. These models are similar to the FitzHugh-Naguno prototype, often used in the excitable and oscillatoire mediums [5].

Several studies were carried out to improve the models of AMPc waves propagation within the colony the amoebas dictyostelium discoideum. This improvement of the models of AMPc signaling in the suspension of cells are due to certain influences in nature such as instability in pulsatile secretion of AMPc and the propagation of AMPc wave. The instability of the AMPc waves in the process of aggregation of the amoebas dictyostelium discoideum can be caused by various phenomena, the presence of an electric field in the area of aggregation of the dictyostelium discoideum, when this area of dictyostelium discoideum aggregation is exposed to a fluid flow (phenomenon of advection), etc. The modeling of the AMPc wave propagation allows the analytical and numerical control of parameters with the aim of studying the natural phenomena appearing in the process of aggregation of the dictyostelium discoideum and giving a biophysics meaning. In experiments the random movement of the amoebas towards the centers of aggregation while following the gradient of AMPc waves propagation presents coherent and incoherent dualism [2]. The analytical and numerical study of this dualism could moreover include the dynamics of the concentric and spiral waves of AMPc.

Highlighting experimental studies through the development of the mathematical models of complex systems produces coherent information between the experiment and theory. The analytical solutions of the elaborated mathematical models explicitly describe the temporal or spatiotemporelle dynamics of the studied systems.Indeed compared to their complexities, these generic models can be reduced to partial equations that give rise to specific soliton, and whose solutions can be obtained using well known analytical methods such as the expansions on multi-scales [156, 158, 159, 189] which lead to a generalized equation of Ginzburg-Landau [161–166]. Obtaining the reliable results which are in conformity with physical reality with these methods depend on the user. Primarily these models were mathematically developed to describe the kinetics of relay of AMPc of the amoebas dictyostelium discoideum. It is well-known that the model

suggested by Martiel-Goldbeter which is elaborate on the assumption of activation/inactivation of the receivers of AMPc plays an important role in this project, and the model established by FitzHugh-Nagumo, which is generally used to describe the prototype of the excitable medium. Both can describe the solitary wave propagation of AMPc as communication tool between cells. These waves result from the interaction between the properties of the medium, nonlinearity and dispersion. They very often involve the phenomenon of modulational instability (MI) which has been studied in various fields of physics such as: Nonlinear optical system [167], Nonlinear hydrodynamics [168], Nonlinear transmission lines (NTLs) [169–171] and biophysics [45, 51–53, 172].

The linear stability method of analysis is used to study the phenomenon of MI, but the limit of this method to envisage the manifestation of the long-term phenomena, called upon numerical methods. However, the numerical methods such as the integration method of Runge-Kunta of fourth order are generally exploited, to give not only validity to the analysis of linear stability, but to also indicate the model patterns. In this chapter we will present the model of AMPc signaling in a population of suspended cells of amoebas dictyostelium discoideum which we developed in this thesis. Moreover we will apply the analytical and numerical methods not only to simplify them, but to also solve them.

2.1 Mathematical modeling

2.1.1 Reaction-Diffusion Systeme

2.1.1.1 Generalities

The models of reaction diffusion type have received a lot of attention in the literature. This has been reflected in a deep knowledge of the subject and in an overwhelming quantity of papers. Some representative reviews and introductory books that treat this topic are [175–179, 226]. In the following we will give a brief description of this type of models. Reaction-diffusion models are systems of coupled partial differential equations (PDEs in the following) that can be written in the following way:

$$\partial_t X(x,t) = \underbrace{g\big(X(x,t)\big)}_{reaction} + \underbrace{D\nabla^2 X(x,t)}_{diffusion}, \tag{2.1}$$

where X is a (column) vector field. In the context of chemical reactions, the elements of this field represent the concentrations of different reactants. The functions in the vector $g\big(X(x,t)\big)$ are typically nonlinear. This portion of the Eq.(2.1) is usually called the reaction part. The

System	Activator	Inhibitor
Dictyostelium discoideum	cyclic AMP	membrane receptor
BZ reaction	bromous acid	oxidized catalyst
CO oxidation	coverage of the absorbed CO	structural change of the surface
Neuromuscular tissue	membrane potential	ionic conductance
Epidemics	infectious agent	level of immunity
Spiral galaxies	density of molecular cloud	temperature of molecular cloud

Table 2.1: *State variables of some representative excitable media [179, 230]*

diffusion matrix D is square and typically diagonal. This last portion of the Eq.(2.1) is called the diffusion part and accounts for the diffusion of the reactants. In this Thesis we will concentrate on cases where the physical space on which the reactants diffuse is *one-dimensional*. Consequently, in the following we will substitute the Laplacian operator ∇^2 by a one dimensional spatial (second) derivative ∂_x^2.

2.1.1.2 Activator-Inibitor

A well studied subgroup of reaction-diffusion systems are the so called activator-inhibitor models [175–177, 180, 226]. These models have been used in many different pattern forming systems ranging from chemical reactions [177, 180] to biological problems [181, 226] (such as population dynamics, epidemic spreading, and many others). The activator-inhibitor models consist of two variables (i.e. $X = \big(\gamma; \rho\big)^{Tr}$ in Eq.(2.1)) which diffuse in the medium. The first variable, γ, called activator and the second, ρ, inhibitor. The field γ is auto-catalytic. A small amount of its concentration triggers the production of more of it. The growth of γ is inhibited by the presence of a second field ρ.

The dynamics of the inhibitor ρ is such that the presence of a nonzero concentration of activator γ stimulates the γ production, i.e. γ acts as a catalysator for the ρ production. On the other hand a nonzero quantity of this second field ρ induces its decrease. Consequently a nonzero quantity of γ activates the production of both γ and ρ and, conversely, a nonzero quantity of ρ halts and reverses (i.e. inhibits) the production of both. This is the reason why the fields γ and ρ are called activator and inhibitor respectively. So far this description corresponds to the linear behavior. Typically (saturating) nonlinearities are introduced to limit the unbounded catalytic process.

2.1.2 Model and kinetic equations MG

2.1.2.1 Description of the Model

In the model proposed by Martiel and Goldbeter [2] (hereafter referred to as the MG model) it is assumed that the cells contain a large number of receptors (10^5-10^6 molecules/cell) that might be in either the active or desensitized state.The transition from active to desensitized state takes place by means of the phosphorylation of the cAMP receptor Eq.(2.1). In the derivation of this model several processes are assumed to play a role inside and outside the cell, namely:

$$R \rightleftharpoons D \tag{2.2a}$$

$$D + P \rightleftharpoons DP \tag{2.2b}$$

$$RP \rightleftharpoons DP \tag{2.2c}$$

$$2RP + C \rightleftharpoons E \tag{2.2d}$$

$$E + S \rightleftharpoons ES \rightleftharpoons E + P_i \tag{2.2e}$$

$$C + S \rightleftharpoons CS \rightleftharpoons C + P_i \tag{2.2f}$$

$$P_i \rightleftharpoons \tag{2.2g}$$

$$P_i \rightleftharpoons P \rightleftharpoons \tag{2.2h}$$

$$\rightleftharpoons S \rightleftharpoons \tag{2.2i}$$

The monomeric receptor, located on the outer face of the plasma membrane, exists in two conformational states, R and D. Extracellular cAMP (P) binds to these two conformations with different affinities (steps b and c). The transitions between the two states (steps a and d) may represent a simple conformational change, or a process of covalent modification; in the latter case, the modifying enzymes operate in the firstorder kinetic domain. Experimental evidence in D. discoideum suggests that these transitions are associated with desensitization through phosphorylation of the cAMP receptor [182]. The hypothesis that upon diffusion in the membrane, two molecules of active complex RP bind to adenylate cyclase (step e) and thereby activate the enzyme. Whether such a process occurs in Dictyostelium remains a conjecture; however, receptor dimerization required for activation of the cellular response has been demonstrated for the gonadotropin-releasing hormone receptor [183]. The reason for considering such cooperative process is that some form of nonlinearity is essential for oscillations (see, e.g., [184]). The cooperativity of step e replaces here the one previously located at the level of cAMP binding to a dimeric receptor [185]. Although positive cooperativity in binding is suggested by some

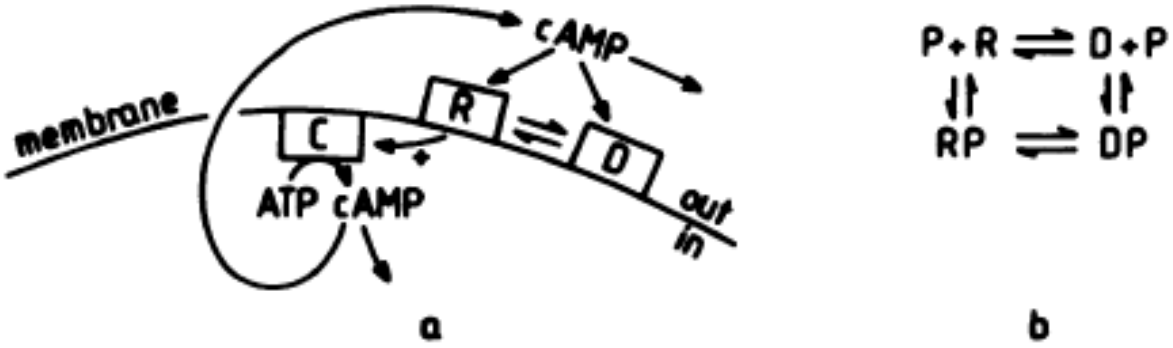

Figure 2.1: Model based on receptor desensitization for the cAMP signaling system of the slime mold Dictyostelium discoideum. Extracellular cAMP binds to the active state (R) of the receptor and thereby activates adenylate cyclase (C) which produces cAMP from intracellular ATP. The transition from the active to the desensitized state (D) of the receptor may in principle occur through a simple conformational change or though covalent modification. The latter situation appears to prevail in D. discoideum where the R and D states correspond to the dephosphorylated and phosphorylated forms of the cAMP receptor. Arrows indicate transport of cAMP into the extracellular medium and cAMP hydrolysis by the intracellular and extracellular forms of phosphodiesterase. The kinetics of the cAMP production in well-stirred suspensions of D. d. cells are well described by the MG model [2], which is based on the relevant kinetic rate laws and the interaction between cAMP and its membrane receptor

experiments [186], it is not apparent in the observations made with constant stimuli [187]. Both types of cooperativity yield similar results.

A global step e without including a more detailed mechanism for adenylate cyclase activation by the cAMP-receptor complex. This process likely involves a GTP-binding protein as in the activation of adenylate cyclase in higher organisms [188]. The nonlinearity of step e may thus be taken as reflecting also the amplification of the activation process due to interactions between the GTP-binding protein and adenylate cyclase.

In view of the results obtained for the β-adrenergic receptor [189],the modified form DP of the receptor cannot couple to the cyclase, and therefore represents an inactive, desensitized state. Such a hypothesis holds with suggestions based on experimental observations [190]- [182]. To account for the enhancement in cAMP synthesis that follows binding of extracellular cAMP, the receptor-adenylate cyclase complex E (step f) has a larger affinity for the substrate ATP (S) and/or a larger catalytic activity than the free form C of the enzyme (step g).

Part of intracellular cAMP (P_i) is hydrolyzed by an intracellular phosphodiesterase (step h), whereas part is transported across the plasma membrane into the extracellular medium where it is hydrolyzed by the membrane bound and extracellular forms of this enzyme (step i). In agreement with the experiments [191], these steps are each governed by an apparent first-order rate constant. A final assumption is that the substrate ATP is synthesized at a constant rate and used in a number of reactions besides that catalyzed by adenylate cyclase; a global rate constant $k^{'}$ characterizes the latter ATP consuming processes. The assumption of a constant rate of utilization in these processes would yield similar results (the ATP level will, in fact, be taken as constant after reduction of the model to a three-variable system).

2.1.2.2 Kinetic equations

The time evolution of the concentration of the various species appearing in the kinetic of Eq.(2.1) is governed by the following differential equations (2.3) In these equations $\rho = R/R_T$, $\delta = D/R_T$, $x = RP/R_T$, $\overline{e} = E/E_T$, $\overline{es} = ES/E_T$, $c = C/R_T$ and $\overline{cs} = CS/R_T$, where R_T and E_T represent the total amount of receptor and of adenylate cyclase; β and γ denote respectively the concentration of intracellular and extracellular cAMP divided by the dissociation constant $K_R = d_1/a_1$; α is the intracellular level of ATP normalized by the Michaelis constant $K_m = (d_4 + k_4)/a_4$. Moreover, $L_1 = k_{-1}/k_1$ is the equilibrium ratio of the states R and D in the absence of ligand, whereas $L_2 = k_{-2}/k_2$; $c = K_R/K_D$ with $K_D = d_2/a_2$ is the nonexclusive binding coefficient of extracellular cAMP for the two receptor states; $\upsilon = \upsilon_i/K_m$; h is the dilution

factor.

$$\frac{d\rho}{dt} = k_1(-\rho + L_1\delta) + d_1(-\rho\gamma + x)$$

$$\frac{d\delta}{dt} = k_1(\rho - L_1\delta) + d_1(-c\delta\gamma + y)$$

$$\frac{dx}{dt} = k_2(-x + L_2 y) + d_1(\rho\gamma - x) + (2\mu/h)d_3(-\epsilon x^2\overline{c} + \overline{e})$$

$$\frac{d\overline{c}}{dt} = d_3(-\epsilon x^2\overline{c} + \overline{e}) + (d_5 + k_5)(-\overline{c}\alpha\theta + \overline{cs})$$

$$\frac{d\overline{e}}{dt} = d_3(\epsilon x^2\overline{c} - \overline{e}) + (d_4 + k_4)(-\overline{e}\alpha + \overline{es}) \tag{2.3}$$

$$\frac{d\overline{es}}{dt} = (d_4 + k_4)(\overline{e}\alpha - \overline{es})$$

$$\frac{d\alpha}{dt} = \upsilon - k^{'}\alpha - \sigma(\overline{es} + \lambda\overline{cs}) + \theta_E((d_4 + k_4)$$
$$(-\overline{e}\alpha + \overline{es}) + (d_5 + k_5)(-\overline{c}\alpha\theta + \overline{cs}))$$

$$\frac{d\beta}{dt} = q\sigma(\overline{es} + \lambda\overline{cs}) - (k_i + k_t)\beta$$

$$\frac{d\gamma}{dt} = (k_t\beta/h) - k_e + \eta(d_1(-\rho\gamma + x) + d_2(-c\delta\gamma + y))$$

In deriving Eq.(2.2), we made use of the two conservation relations for the receptor and for adenylate cyclase:

$$\begin{aligned} R_T &= R + D + RP + DP + (2/h)(E + ES) \\ E_T &= E + ES + C + CS \end{aligned} \tag{2.4}$$

The assumption that RT and ET remain constant holds in first approximation, given that the time scale for the variation of these parameters is much longer than the time scale for relay and oscillations. The conservation relations Eq.(2.3) take into account the fact that the receptor and adenylate cyclase concentrations are defined with respect to the extracellular and intracellular

volumes, respectively. Eq.(2.3) yield the following expressions for y and $\overline{cs}$, which supplement Eq.(2.2):

$$\begin{aligned} y &= 1 - \rho - \delta - x - (2\mu/h)(\overline{e} + \overline{es}) \\ \overline{cs} &= 1 - \overline{c} - \overline{e} - \overline{es} \end{aligned} \tag{2.5}$$

In the limit of fast binding of extracellular cAMP to both forms of the receptor and fast association between RP and C, C and S, E and S, the following inequality on the rate constants for the reaction steps I holds

$$(k_1, k_{-1}, k_2, k_{-2}, k_i, k_t, k_e, \sigma, k^{'}) \ll (a_1, d_1, a_2, d_2, a_3, d_3, a_4, d_4, a_5, d_5) \tag{2.6}$$

As Eq.(2.2) contain both fast binding and slow modification terms, we introduce new variables to separate the nine differential Eq.(2.2) into two sets, one associated with the slower time scale governing the interconversion of the receptor forms, and another associated with the faster time scale governing the binding reactions. Let us define PT and 6r as the total fractions of the receptor in the active and inactive (modified) states, $\overline{Y}$ the total fraction of the receptor forms bound to cAMP, A as the total concentration of intracellular ATP (free plus bound to the two forms of adenylate cyclase), and r as the normalized total concentration of extracellular cAMP (free plus bound to the two receptor states). These new variables are expressed as a function of the old ones by Eq.(2.6).

$$\begin{aligned} \rho_T &= 1 - \delta_T = \rho + x + (2\mu/h)(\overline{e} + \overline{es}) \\ \overline{Y} &= x + y + (2\mu/h)(\overline{e} + \overline{es}) \\ A &= \alpha + \Theta_E(\overline{cs} + \overline{es}) \\ \Gamma &= \gamma + \eta(1 - \rho - \delta) = \gamma + \eta\overline{Y} \end{aligned} \tag{2.7}$$

The evolution equations for these new variables can now be obtained by taking their time derivative from Eq.(2.6) and inserting into the resulting relations the relevant equations from Eqs. Al. This procedure yields the new set of Eq.(2.7) in which the first four equations govern the evolution of slower variables, while the remaining equations relate to fast variables (system Eq.(2.7) can be complemented by one of the three equations for ρ, δ or x in (2.2) but these equations contain both fast and slow terms and will therefore not be used in the subsequent reduction).

$$\begin{aligned}
\frac{d\rho_T}{dt} &= k_1(-\rho + L_1\delta) + k_2(-x + L_2 y) \\
\frac{dA}{dt} &= \upsilon - k^{'}\alpha - \sigma(\overline{es} + \lambda\overline{cs}) \\
\frac{d\beta}{dt} &= q\sigma(\overline{es} + \lambda\overline{cs}) - (k_i + k_t)\beta \\
\frac{d\Gamma}{dt} &= (k_t\beta/h) - k_e \\
\frac{d\overline{Y}}{dt} &= k_1(\rho\gamma - x) + d_2(-c\delta\gamma - y) \\
\frac{d\overline{c}}{dt} &= d_3(-\epsilon x^2\overline{c} + \overline{e}) + (d_5 + k_5)(-\overline{c}\alpha\theta + \overline{cs}) \\
\frac{d\overline{e}}{dt} &= d_3(\epsilon x^2\overline{c} - \overline{e}) + (d_4 + k_4)(-\overline{e}\alpha + \overline{es}) \\
\frac{d\overline{es}}{dt} &= (d_4 + k_4)(\overline{e}\alpha - \overline{es})(-\overline{e}\alpha + \overline{es}) + (d_5 + k_5)(-\overline{c}\alpha\theta + \overline{cs}))
\end{aligned} \tag{2.8}$$

where y and $\overline{c}$ are still given by Eq.(2.4). We now require that, after an initial transient phase, the differential equations for the fastest variables $\overline{Y}$, $\overline{c}$, $\overline{e}$ and $\overline{es}$ reduce to algebraic equations corresponding to the quasi-steady-state hypothesis for these receptor and enzyme forms. This condition leads to Eq.(2.8).

$$\begin{aligned}
& d_1(\rho\gamma - x) + d_2(c\delta\gamma - y) = 0 \\
& \overline{e}\alpha - \overline{es} = 0 \\
& \overline{c}\alpha\Theta - \overline{cs} = 0 \\
& \epsilon x^2\overline{c} - \overline{e} = 0
\end{aligned} \tag{2.9}$$

In the first of these equations each of the two terms in parentheses vanishes since, when the quasi-steady-state regime holds, the set relations (2.8) must remain independent of the actual values of d, and d2. The five algebraic relations obtained from A7, plus the four kinetic equations

for the slow variables in (2.7), correspond to the nine degrees of freedom of the initial system (2.2. Taking into account the conservation relations (2.4) we obtain Eq.(2.9) for $\overline{c}$ as a function of α and x; similar relations are obtained for $\overline{e}$, $\overline{es}$, and $\overline{cs}$.

$$\overline{c} = [1 + \alpha\Theta + \epsilon x^2(1+\alpha)]^{-1} \tag{2.10}$$

The evolution equations for the remaining slow variables can now be transformed according to relations (2.8) and (2.9), yielding the four-variable differential system (2.10):

$$\begin{aligned}
\frac{d\rho_T}{dt} &= k_1(-\rho + L_1\delta) + k_2(-\rho\gamma + L_2 c\delta\gamma) \\
\frac{dA}{dt} &= \upsilon - k^{'}\alpha - \sigma\alpha(\lambda\theta + \epsilon\rho^2\gamma^2)/[1 + \alpha\Theta + \epsilon\rho^2\gamma^2(1+\alpha)] \\
\frac{d\beta}{dt} &= q\sigma\alpha(\lambda\theta + \epsilon\rho^2\gamma^2)/[1 + \alpha\Theta + \epsilon\rho^2\gamma^2(1+\alpha)] - (k_i + k_t)\beta \\
\frac{d\Gamma}{dt} &= (k_t/h)\beta - k_e\gamma
\end{aligned} \tag{2.11}$$

To express in these equations the old variables in terms of the new ones, we use the definitions (2.6) which take the form

$$\begin{aligned}
\rho_T &= \rho(1+\gamma) + (2\mu/h)[\epsilon\rho^2\gamma^2(1+\alpha)]/[1 + \alpha\Theta + \epsilon\rho^2\gamma^2(1+\alpha)] \\
A &= \alpha + \Theta_E[\alpha(\theta + \epsilon\rho^2\gamma^2)]/[1 + \alpha\Theta + \epsilon\rho^2\gamma^2(1+\alpha)] + \\
\Gamma &= \gamma + \eta(\rho\gamma + c\delta\gamma) + (2\mu/h)[\epsilon\rho^2\gamma^2(1+\alpha)]/[1 + \alpha\Theta + \epsilon\rho^2\gamma^2(1+\alpha)].
\end{aligned} \tag{2.12}$$

As experimentally observed (see Tables I and II), the parameters (mu/h), Θ_E and η are much smaller than unity. Neglecting the terms multiplied by these factors in Eq.(2.11), we obtain the simpler expressions for the new variables ρ_T. A, and Γ as a function of the original ones ρ, α, and γ:

$$\rho_T = \rho(1+\gamma); A = \alpha; \Gamma = \gamma \tag{2.13}$$

Inserting the expressions (2.8) into (2.12) and taking into account the conservation relations (2.4), we get

$$\rho = \rho_T/(1+\gamma); \Gamma = (1-\rho_T)/(1+c\gamma) \tag{2.14}$$

The four-variable system (2.10) takes the final form (2.14):

$$\begin{aligned}
\frac{d\rho_T}{dt} &= -\rho_T[(k_1+k_2)/(1+\gamma)] \\
\frac{d\alpha}{dt} &= \upsilon - k^{'}\alpha - \sigma\Phi(\rho_T,\gamma,\alpha) \\
\frac{d\beta}{dt} &= q\sigma\alpha\Phi(\rho_T,\gamma,\alpha) - (k_i+k_t)\beta \\
\frac{d\Gamma}{dt} &= (k_t/h)\beta - k_e\gamma
\end{aligned} \tag{2.15}$$

With $\Phi(\rho_T,\gamma,\alpha) = \alpha(\theta+\epsilon\rho^2\gamma^2)/[1+\alpha\Theta+\epsilon\rho^2\gamma^2(1+\alpha)]$; $Y = \rho_T\gamma/(1+\gamma)$.These equations are identical to the four-variable system (2) analyzed in the text. System 2 further reduces to the three-variable system (3) when considering that the ATP level (a) does not vary in time.

Eqs.(2.14) are valid in the limit of negligible (μ/h), Θ_E, and η (see Eqs.(2.12)). The values of the two first pararameters are generally smaller than that of the latter, which may reach 200 (see Table II). It may therefore be of interest to determine the behavior of the system when the cAMP bound to the receptor is taken into account (this amounts to keeping the term $\eta[\rho\gamma + c\delta\gamma]$ in Eqs.(2.11)). In the limit $(\mu/h) \to 0$, $\Theta_E \to 0$ and finite η we obtain, instead of Eqs.(2.12):

$$\begin{aligned}
\frac{d\rho_T}{dt} &= -\rho_T f_1(\gamma) + (1-\rho_T) f_2(\gamma) \\
\frac{d\alpha}{dt} &= \upsilon - k^{'}\alpha - \sigma\Phi(\rho_T,\gamma,\alpha) \\
\frac{d\beta}{dt} &= q\sigma\Phi(\rho_T,\gamma,\alpha) - (k_i+k_t)\beta \\
\frac{d\Gamma}{dt} &= (k_t/h)\beta - k_e\gamma
\end{aligned} \tag{2.16}$$

With $\Phi(\rho_T,\gamma,\alpha) = \alpha(\theta+\epsilon\rho^2\gamma^2)/[1+\alpha\Theta+\epsilon\rho^2\gamma^2(1+\alpha)]$; $Y = \rho_T\gamma/(1+\gamma)$; $f_1(\gamma) = (k_1+k_2\gamma)/(1+\gamma)$; $f_2(\gamma) = (k_1L_1+k_2L_2c\gamma)/(1+c\gamma)$; $\Gamma = \gamma+\eta(\rho\gamma+c\delta\gamma)+(2\mu/h)[\epsilon\rho^2\gamma^2(1+\alpha)]/[1+\alpha\Theta+\epsilon\rho^2\gamma^2(1+\alpha)]$. γ is given by the unique positive root of the third-degree polynomial:

$$-c\gamma^3 + (c\Gamma-1-\eta c)\gamma^2 + [(1+c)\Gamma-1-\eta c-\eta\rho_T(1-c)]\gamma+\Gamma = 0 \tag{2.17}$$

To simplify this system of nine differential equations, we consider all binding reactions 2.1b, 2.1c, 2.1e-2.1g as much more rapid than the slow transitions between the unmodified and modified receptor states in steps 2.1a and 2.1d. Due to the simultaneous presence of fast and slow terms in some of the Eq.(2.1), the obtainment of the quasi-steady-state equations is not straightforward. This property allows us to further reduce the number of variables by considering a as a parameter in Eq.(2.15). The dynamics of the cAMP signaling system is then governed by the three differential Eq.(2.17), where the various functions and parameters remain defined as in Eq.(2.15).

$$\begin{aligned}
\frac{d\rho_T}{dt} &= -\rho_T f_1(\gamma) + (1-\rho_T) f_2(\gamma) \\
\frac{d\beta}{dt} &= q\sigma\Phi(\rho_T,\gamma,\alpha) - (k_i+k_t)\beta \\
\frac{d\gamma}{dt} &= (k_t/h)\beta - k_e\gamma
\end{aligned} \tag{2.18}$$

Eqs.2.17 can be further reduced to a two-variable system for large values of q, k_t and k_i. Then a quasi-steady-state hypothesis for ,β can indeed be made. The advantage of a two-variable system is that the link between relay and oscillations can be demonstrated by phase plane analysis. As the experimental values available for k_t, and k_i, relative to q, are too low for such reduction to hold rigorously, we shall use the three-variable system governed by Eq.(2.17) for studying the dynamics of the signaling system.

2.1.3 Two-component MG model with advection

The MG Model is based on receptor desensitization for the cAMP signaling system of the slime mold Dictyostelium discoideum. The model takes into account both the desensitization of the cAMP receptor by reversible phosphorylation and the activation of adenylate cyclase that follows binding of extracellular cAMP to the unmodified receptor. The dynamics of the signaling system is studied in terms of three variables, namely, intracellular and extracellular cAMP, and the fraction of receptor in active state. Tyson et al. extended the model [9] and advection in the system is added by A. Gholami et al [150].

The main equations of the model in its three component version are as follows, where ρ stands for the percentage of active receptors on the cell membrane, γ, the extracellular concentration of cAMP, and β, the intracellular amount of cAMP. The receptor dynamics are given by

$$\partial_t \rho = -k_1 f_1(\gamma)\rho + k_1 f_2(\gamma)(1-\rho), \tag{2.19}$$

with

$$f_1(\gamma) = \frac{1+\kappa\gamma}{1+\gamma},\ f_2(\gamma) = \frac{L_1 + \kappa L_2 c\gamma}{1+c\gamma}, \tag{2.20}$$

where f_1 controls the receptor desensitization (change from active to inactive state) and f_2, the resensitization. The intracellular cAMP is increased by the cAMP production, which in turn depends on the extracellular cAMP and the active receptors. This production is tuned through the rate σ at which the activated ACA produces cAMP. The intracellular cAMP is diminished through degradation by intracellular phosphodiesterase at a rate k_i and passive transport outside of the cell at a rate k_t.

$$\partial_t \beta = q\sigma\alpha\phi(\rho,\gamma)/(1+\alpha) - (k_i + k_r)\beta \tag{2.21}$$

with

$$\phi(\rho,\gamma) = \frac{\lambda_1 + Y^2}{\lambda_2 + Y^2},\ Y = \frac{\rho\gamma}{1+\gamma}. \tag{2.22}$$

$\lambda_2 = (1+\alpha\theta)/(\epsilon(1+\alpha))$ and $\lambda_1 = \lambda\theta/\epsilon$. The extracellular concentration of cAMP γ is degraded at a rate k_e by the extracellular phosphodiesterase and is increased by the transport of cAMP from the intracellular medium

$$\partial_t\gamma = D\nabla^2\gamma + \upsilon\cdot\nabla\gamma + k_t\beta/h - k_e\gamma, \tag{2.23}$$

We nondimensionalize the system by introducing dimensionless time and space as $t' = t\times k_1$ and $x' = x\times k_1/\sqrt{k_eD}$ Dropping primes and setting $\epsilon_1 = k_1/k_e$, $\epsilon' = k_1/(k_i+k_t)$ and υ is the dimensionless flow velocity $\upsilon = V_f/\sqrt{k_eD}$,where V_f is the dimensional velocity. we arrive at

$$\partial_t\rho = -f_1(\gamma)\rho + f_2(\gamma)(1-\rho), \tag{2.24a}$$

$$\epsilon'\partial_t\beta = q\sigma\alpha\phi(\rho,\gamma)/(1+\alpha) - \beta \tag{2.24b}$$

$$\partial_t\gamma = \epsilon_1\nabla^2\gamma + \upsilon\cdot\nabla\gamma + (k_t\beta/(hk_e) - \gamma)/\epsilon_1 \tag{2.24c}$$

Finally, we reduce this system to a two component model which simplifies its theoretical treatment. For this, we assume ϵ' small, which means that the intracellular cAMP is instantaneously transmitted to the outside media. We then arrive at the two component Martiel-Goldbeter,

$$\partial_t\gamma = \epsilon_1\nabla^2\gamma + \vec{v}\cdot\vec{\nabla}\gamma + \frac{1}{\epsilon_1}[s\phi(\rho,\gamma) - \gamma], \tag{2.25a}$$

$$\partial\rho = -f_1(\gamma)\rho + f_2(\gamma)(1-\rho), \tag{2.25b}$$

where $s = qk_t\alpha\sigma/k_e(k_t+k_i)h(1+\alpha)$, for a discussion on the validity of this approximation, refer [9]- [150]).By combining Eqs.(2.19)-(2.21)-(2.23) followed with some simplifications without the loss of generality, we get:

$$\frac{\partial\gamma}{\partial t} = a_0 + a_1\gamma + a_2\gamma^2 - \gamma^3 + a_3(\gamma\rho)^2 + a_4\gamma(\gamma\rho)^2 + \upsilon\nabla\gamma + \epsilon_1\nabla^2\gamma, \tag{2.26a}$$

$$\frac{\partial\rho}{\partial t} = L_1 - b_1\rho + b_2\gamma + b_3\gamma^2 + b_4\gamma\rho + b_5\gamma^2\rho, \tag{2.26b}$$

where the constant parameters $(a_i)_{i=0,4}$ and $(b_j)_{j=1,5}$ are given in **Appendix A**. Nonlinear velocity of reactions together with conditions at the edges null or periodic flow, this system equations has a stationary and homogeneous solution (γ_0,ρ_0). This solution corresponds to the branch stable towards which the system in the absence of instability will evaluate. Let us consider now an open engine in which this uniform stationary state undergoes a small local perturbation (γ_1,ρ_1) of the concentration of intermediaries. Correspondingly we set

$$\gamma = \gamma_0 + \gamma_1, \tag{2.27a}$$

$$\rho = \rho_0 + \rho_1, \tag{2.27b}$$

to obtain the dynamical equations in γ_1 and ρ_1 as follow:

$$\dot{\gamma_1} = c_0 + c_1\gamma_1 + c_2\gamma_1^2 + c_3\gamma_1^3 + c_4\gamma_1\rho_1 + c_5\rho_1 + c_6\rho_1^2 + c_7\gamma_1^2\rho_1 + c_8\gamma_1\rho_1^2 + \upsilon\gamma_{1x} + \epsilon_1\triangle\gamma_1, \tag{2.28a}$$

$$\dot{\rho_1} = d_0 + d_1\rho_1 + d_2\gamma_1 + d_3\gamma_1^2 + d_4\gamma_1\rho_1 + d_5\gamma_1^2\rho_1, \tag{2.28b}$$

where the new constant parameters $(c_i)_{i=0,8}$ and $(d_j)_{j=0,5}$ are given in **Appendix B**. Let us now differentiate Eq.(3.1a) with respect to the time in order to eliminate the variable ρ_1 and keep only the variable γ_1. This is achieved by replacing $\dot{\rho}_1$ and ρ_1 by their corresponding expression extracted in Eqs.(3.1b) and (3.1a), respectively. Thus we obtain the following second order differential equation:

$$\begin{aligned}
&\ddot{\psi} + \Omega_0^2\psi + e_1\psi^2 + e_2\psi^3 + \big[\varepsilon^2 f_0 + f_1\psi + f_2\psi^2\big]\dot{\psi} + \big[g_0 + g_1\psi\big]\dot{\psi}^2 + g_2\dot{\psi}^3 + \\
&\big[\varepsilon^2 h_0 + h_1\psi + h_2\psi^2 + h_3\dot{\psi} + h_4\dot{\psi}^2 + h_5\psi\dot{\psi}\big]\psi' + \big[i_0 + i_1\psi + i_2\dot{\psi}\big](\psi')^2 + e_0 \\
&= \big[D_0 + D_1\psi + D_2\psi^2 + D_3\dot{\psi} + D_4\dot{\psi}^2 + D_5\psi\dot{\psi} + D_6\psi' + D_7\psi\psi' + D_8\dot{\psi}\psi'\big]\psi'' + \\
&\big[H_0 + H_1\psi + H_2\dot{\psi}\big](\psi'')^2 + \varepsilon^2\lambda_0\dot{\psi}' + \varepsilon^2\mu_0\dot{\psi}'',
\end{aligned} \tag{2.29}$$

To further proceed, we assume $\gamma_1 = \varepsilon\psi$, where parameters f_0, h_0, λ_0 and μ_0 have been considered to be perturbed at order ε^2, ε being a parameter smaller than 1 ($\varepsilon \ll 1$). In Eq.(2.28) $\gamma_1' = \nabla\gamma_1$ and $\gamma_1'' = \nabla^2\gamma_1$ and the constant parameters are given in **Appendix C**. It is important to stress that the above transformation does not fundamentally affect the original system, instead the approach allows us to conveniently write Eq.(2:24) in a Liénard form that is a second-order differential equation with a small damping term. Eq.(2:29) describes the dynamics of the cAMP concentration. However, some nearly-exact solutions may be obtained using perturbation methods. In the following, the system of Eq.(2:29) will be reduced into a CGL equation by applying the continuum approximation, while the version (2.24) will be numerically simulated using the RK4 method. Globally, the models will be used to show the existence of cAMP oscillations in Dictostelium-discoideum medium.

2.1.4 Two-dimensional FHN model

A paradigmatic example of an activator-inhibitor model is the so called FitzHugh-Nagumo system (FHN) [175, 176, 226]. This model was initially proposed independently by R. FitzHugh [195] and Nagumo et al. [196] as a mathematically tractable model for propagation of electrical signals in neurons (for a short introduction to this topic see Section 6.5 in [226] and references therein). The FHN model represents one of the simplest descriptions of an excitable media,

consequently it has been used as simplified or toy model in many other areas (see e.g. [175, 222]). A crucial feature that distinguishes the FHN model is that nonlinearities appear only in the dynamics of the activator field g. This saturating nonlinearity term has the form of a cubic function in g. A generic FHN model is given by:

$$\dot{g} = D\big(g_{xx} + g_{yy}\big) - k_g g\big(g - a\big)\big(g - 1\big) - k_r r, \tag{2.30a}$$

$$\dot{r} = \big(g - r\big)/\tau \tag{2.30b}$$

The first equation describes the excitation of the medium, defined by the variable (g), over time. This variable is linked to the extra cellular cAMP concentration. The second equation defines the recovery process of the medium (r) and could be thought to describe the desensitisation of the cAMP receptors. D_{xx} and D_{yy} are the diffusions coefficients for cAMP ; τ is a time scaling factor for the variables r and g; k_g and k_r, define the rate of production and hydrolysis of cAMP by one cell and a is a coefficient. their values numerical are given by: $k_g = 4.72$, $a = 0.05$, $k_r = 1.5$, $\tau = 5$, and $D = 1$. It is worth to notice that Eq.(2.30) only describes the propagation of cAMP withim a single cell. In order to investigate the cell-cell communication via the release-receiving cAMP process in a colony of amoebae, includes an external stimulus is proposed here and reads

$$\begin{aligned}\dot{g}_{n,m} &= D_x\big(g_{n+1,m} - 2g_{n,m} + g_{n-1,m}\big) + D_y\big(g_{n,m+1} - 2g_{n,m} + g_{n,m-1}\big) \\ &- k_g\big(g_{n,m} - a\big)\big(g_{n,m} - 1\big) - k_r r_{n,m} + R,\end{aligned} \tag{2.31a}$$

$$\dot{r}_{n,m} = \mu\big(g_{n,m} - r_{n,m}\big) \tag{2.31b}$$

Where $\mu = 1/\tau$ and the discrete index $n, m = 1, N$ denotes the number of cell in a ring of N total cells. The positive real R have been introduced to excite these cells in order to initiate cAMP waves in the extracellular medium. The first step of this process consists in differentiating Equation (2a) with respect to time, and substituting the derivative $\dot{r}_{n,m}$, into the obtained second-order ordinary differential equation. This leads to

$$\begin{aligned}&\ddot{g}_{n,m} + k_g a\dot{g}_{n,m} - 2k_g(1+a)g_{n,m}\dot{g}_{n,m} + 3k_g g_{n,m}^2\dot{g}_{n,m} + k_r\dot{r}_{n,m} = D_x(\dot{g}_{n+1,m} - 2\dot{g}_{n,m} + \dot{g}_{n-1,m}) \\ &D_y(\dot{g}_{n,m+1} - 2\dot{g}_{n,m} + \dot{g}_{n,m-1})\end{aligned} \tag{2.32}$$

As we can note, Equation (2.32) still contains some terms with $\dot{r}_{n,m}$. To get rid of them, we slightly perturb Equation (2:31) by considering $g_{n,m} \to \epsilon g_{n,m}$ and $r_{n,m} \to \epsilon r_{n,m}$, where ϵ is a parameter smaller than 1. We then extract the variable $r_{n,m}$ at order ϵ^1. Finally, going back to Equation (2:32) and replacing the variable $r_{n,m}$ by its expression lead to a second-order differential-difference equation which can be handled using a perturbation approach. For this purpose, we introduce a new variable $g_{n,m} = \epsilon G_{n,m}$, where ϵ is a small parameter that measures the strength of nonlinearity.

$$\begin{aligned}
&\ddot{G}_{n,m} + \Omega_0^2 G_{n,m} + \Omega_1 G_{n,m}^2 + \Omega_2 G_{n,m}^3 + [\epsilon^2\gamma_0 + \gamma_1 G_{n,m} + \gamma_2 G_{n,m}^2]\dot{G}_{n,m} = \\
&D_{0X}(G_{n+1,m} - 2G_{n,m} + G_{n-1,m}) + D_{0Y}(G_{n,m+1} - 2G_{n,m} + G_{n,m-1}) + \\
&\epsilon^2 D_{1X}(\dot{G}_{n+1,m} - 2\dot{G}_{n,m} + \dot{G}_{n-1,m}) + \epsilon^2 D_{1Y}(\dot{G}_{n,m+1} - 2\dot{G}_{n,m} + \dot{G}_{n,m-1})
\end{aligned} \tag{2.33}$$

With

$\Omega_0^2 = \mu(k_r + k_g a)$; $\Omega_1 = -\mu k_g(1+a)$; $\Omega_2 = \mu k_g$; $\gamma_0 = k_g a + \mu$; $\gamma_1 = -2k_g(1+a)$; $\gamma_2 = 3k_g$; $D_{0X} = \mu D_X$; $D_{0Y} = \mu D_Y$, $D_{1X} = D_X$ and $D_{1X} = D_X$.

Moreover, since we are interested in wave propagation in a weakly dissipative medium, we assume the parameters γ_0, D_{1X} and D_{1Y} perturbed at the order ϵ^2.

The nonlinear Eq.(2:32) describes the spatiotemporal dynamics of cAMP signaling in a given network and may be useful in understanding of some mechanisms such as aggregation of Dd amoebae which utilize cAMP signaling to communicate among them.

2.1.5 Long-range diffusive FHN model

Here the model is considered for N identical cAMP concentration mutually coupled not only to their nearest neighbors, but also to distant ones via LR interaction. In that framework, the dynamics of the *nth* cAMP concentration is described by the system:

$$\begin{aligned}
&\dot{g}_{n,m} = -k_g\big(g_{n,m} - a\big)\big(g_{n,m} - 1\big) - k_r r_{n,m} + \\
&\sum_{n\neq m}^{\infty} D_{nm}(x_n - x_m)\big(g_{n+j,m} + g_{n-j,m} + g_{n,m+j} + g_{n,m-1} - 4g_{n,m}\big) + A_0\sin(2\pi f_0 t),
\end{aligned} \tag{2.34a}$$

$$\dot{r}_{n,m} = \mu\big(g_{n,m} - r_{n,m}\big) \tag{2.34b}$$

Where $\mu = 1/\tau$ and the discrete index $1 \leq n \leq N$ and $1 \leq m \leq M$ denotes the number of cell in a ring of N and M total cells. Here $A_0 \sin(2\pi f_0 t)$ is a weak periodic signal, with A_0 and f_0 being the amplitude and frequency of the signal, respectively. The positive real A_0 have been introduced to excite these cells in order to initiate cAMP waves in the extracellular medium. The above FHN model is generalized due to the presence of the term $\sum_{n\neq m}^{\infty} D_{nm}(x_n - x_m)$. $D_{n,m}$ is then restricted to take a fixed value when amoebae m and n are coupled, and 0 otherwise. In our situation, values for $D_{n,m}$ are assumed to satisfy a power-law formula, which generalizes the prime idea and consider one amoebae to be coupled to all the other in the network except to itself. The coupling parameter in these conditions is then written

$$D_{n,m} = \frac{D}{\mid n - m \mid^s} \tag{2.35}$$

where D characterizes the coupling strength, s is a parameter introduced to cover different physical scenarios including the nearest-neighbor approximation ($s = \infty$), quadrupole-quadrupole interaction ($s = 5$), dipole-dipole interaction ($s = 3$), Coulomb interaction ($s = 1$) [198–200]. The distance-dependant coupling strength $D_{n,m}$ is restricted to the constant parameter D. Further simplifications can be brought to the model by considering $j = n - m$, which reduces the diffusive term to $\sum_{j=1}^{\infty} D \mid j \mid^{-s} \left(g_{n+j,m} + g_{n-j,m} + g_{n,m+j} + g_{n,m-1} - 4g_{n,m}\right)$ while all the other equations do not change. Index n, m and j are respectively, cAMP concentration number secret by amoebaes D.d on longitudinal (n), transversal (m) axial, and the range of interaction. Explicitly,$j = 1$ corresponds to interaction between amoebae n on longitudinal axial and amoebae m on transversal axial, and its nearest neighbors $n \pm 1$ and $m \pm 1$, $j = 2$ translate the interaction between amoebae n on longitudinal axial and amoebae m on transversal axial with its second neighbors $n \pm 2$ and $m \pm 2$ and so on. This does not change the substance of Eq.(2.31), but clearly picture the way cAMP interact and also facilitates numerical calculations. In summary, the model of FHN with power-law LR diffuse interaction is fully described by the following set of equations:

$$\begin{aligned} \dot{g}_{n,m} &= -k_g\big(g_{n,m} - a\big)\big(g_{n,m} - 1\big) - k_r r_{n,m} + \\ &\sum_{j=1}^{\infty} D \mid j \mid^{-s} \left(g_{n+j,m} + g_{n-j,m} + g_{n,m+j} + g_{n,m-1} - 4g_{n,m}\right) + A_0 \sin(2\pi f_0 t), \end{aligned} \tag{2.36a}$$

$$\dot{r}_{n,m} = \mu\big(g_{n,m} - r_{n,m}\big) \tag{2.36b}$$

Eq.(2.33) which contains nonlinear and long-range dispersive $\left(\sum_{j=1}^{\infty} D \mid j \mid^{-s} \left(g_{n+j,m} + g_{n-j,m} + g_{n,m+j} + g_{n,m-1} - 4g_{n,m}\right)\right)$ terms in Eq.(2:36a) constitute the long-range diffuse two-

dimensional FHN model. In the next paragraphs, it will numerically be studied in order to seek different spatiotemporal patterns shapes induced by the LRI.

2.2 Analytical and Numerical methods

2.2.1 Multiple scale expansion in the continuum approximation with derivation of two-dimensional CGL equation

Some natural processes have more than one characteristic length or time scales associated with them, for example, the turbulent flow consists of various length scales of the turbulent eddies along with the length scale of the objects over which the fluid flows. The failure to recognize a dependence on more than one space/time scale is a common source of nonuniformity in perturbation expansions. The method of multiple scales (also called the multiple-scale analysis) comprises techniques used to construct uniformly valid approximations to the solutions of perturbation problems in which the solutions depend simultaneously on widely different scales. This is done by introducing fast-scale and slow-scale variables for an independent variable, and subsequently treating these variables, fast and slow, as if they are independent. More specifically, the method generates a hierarchy of (small) scales for the space and time variations of the envelopes of a fundamental (linear) plane wave and all the overtones. The scale is moreover directly related to the (small) amplitude of the wave itself. The multiple scale method is quite appropriate for the study of boundary value problems and leads to a CGL equation (with reversed space-time), the goal being the study of a nonlinear dispersive chain with dispersion relation $\omega(k)$ where ω represents the wave frequency and k the wavenumber of the carried wave. The physical problem we are concerned with is the following: the first particle of the chain (say x = 0) is given an oscillation (or is submitted to an external force) at frequency ω. The principle of this method can be summarized as follow: given a continue differential equation in the form

$$F(\dot{U}(t), U(t), U_{xx}(t), U_{yy}(t), U_x(t), U_y(t), U^2(t), U^3(t)...) = 0 \tag{2.37}$$

With $U = (\gamma, \rho)$. One first seeks a solution of Eq.(2.29) in the form of a Fourier expansion in harmonics of the fundamental $A^l(x,t) = e^{il(kx-\omega t)}$, where the Fourier components are developed in a Taylor series in power of the small parameter . measuring the amplitude of the initial wave, that is to say

$$\begin{pmatrix} \gamma(x,y,t) \\ \rho(x,y,t) \end{pmatrix} = \begin{pmatrix} \gamma_0 \\ \rho_0 \end{pmatrix} + \sum_{p=1}^{\infty} \epsilon^p \sum_{l=-\infty}^{+\infty} \begin{pmatrix} \psi_l^{(p)}(\xi,\eta,\tau) \\ \phi_l^{(p)}(\xi,\eta,\tau) \end{pmatrix} A^l(x,t), \tag{2.38}$$

Note that the above serie includes all overtones $A^l(x,t) = e^{il(kx-\omega t)}$ up to order p. These are generated by the nonlinear terms which explain that the corresponding coefficients are of maximum order ϵ^p. Here we have the realvaluedness condition

$$\begin{aligned}(\psi_l^{(p)}(\xi,\eta,\tau)) &= (\psi_l^{(p)}(\xi,\eta,\tau))^* \\ (\phi_l^{(p)}(\xi,\eta,\tau)) &= (\phi_l^{(p)}(\xi,\eta,\tau))^*\end{aligned} \tag{2.39}$$

with the asterisk denoting complex conjugations. The slow variables $\xi = \varepsilon(x - v_g t)$, $\eta = \varepsilon y$ and $\tau = \varepsilon^2 t$

We then insert solution (2.37) into Eq.(2.29) to obtain a linear homogeneous system for $\psi_l^{(p)}(\xi,\eta,\tau)$ and $\phi_l^{(p)}(\xi,\eta,\tau)$ polynomial in $A^l(x,t)$. Finally we can proceed to collect and solve different orders of ϵ^p and harmonics l, order (p,l) in the obtained equation or system of equations. Note that it is enough to consider $l > 0$ as negative values follow from the reality condition (2.36). The culminating stage comes from order (3,1) where the cubic CGL equation is derived. In addition, the general formulas of this method are given as follows:

- The spatial derivative operators are given by:

$$\begin{aligned}\frac{\partial}{\partial x} &= \left(\epsilon\frac{\partial}{\partial \xi} + ilk\right) \\ \frac{\partial}{\partial y} &= \epsilon\frac{\partial}{\partial y} \\ \frac{\partial^2}{\partial x^2} &= \left(\epsilon^2\frac{\partial^2}{\partial \xi^2} + 2i\epsilon lk\frac{\partial}{\partial \xi} - l^2k^2\right) \\ \frac{\partial^2}{\partial y^2} &= \epsilon^2\frac{\partial^2}{\partial y^2}\end{aligned} \tag{2.40}$$

- The temporal derivative operators are given by:

$$\begin{aligned}\frac{\partial}{\partial t} &= \left(\epsilon^2\frac{\partial}{\partial \tau} - \epsilon v_g\frac{\partial}{\partial \xi} - il\omega\right) \\ \frac{\partial^2}{\partial t^2} &= \left(\epsilon^2 v_g^2\frac{\partial^2}{\partial \xi^2} - 2il\omega\epsilon^2\frac{\partial}{\partial \tau} + 2il\omega\epsilon v_g\frac{\partial}{\partial \xi} - l^2\omega^2\right)\end{aligned} \tag{2.41}$$

- The spatio-temporal derivative operators are given by:

$$\begin{aligned}\frac{\partial^2}{\partial x\partial t} &= \left(ilk\epsilon^2\frac{\partial}{\partial \tau} - \epsilon^2 v_g\frac{\partial^2}{\partial \xi^2} - il\omega\epsilon\frac{\partial}{\partial \xi} - il\omega\epsilon v_g\frac{\partial}{\partial \xi} + l^2k\omega\right) \\ \frac{\partial^3}{\partial x^2\partial t} &= \left(-l\omega\epsilon^2\frac{\partial}{\partial \tau} - l^2k^2\epsilon^2\frac{\partial}{\partial \tau} - 2il\epsilon^2 v_g\frac{\partial}{\partial^2\xi^2} + 2l^2k\omega\epsilon\frac{\partial}{\partial \xi} + l^2k^2\epsilon v_g\frac{\partial}{\partial \xi} + il^3k^2\omega\right)\end{aligned} \tag{2.42}$$

By substitution of solution (2.38) into (2.24) who leads to the form (2.28), we obtain a linear homogeneous system $\psi_p^{(l)}(\xi,\eta,\tau)$ polynomial $A^{(l)}(x,t)$ in Appendix D. When one expand the terms in exponential until the third order, it is possible from Eq.(2.46) to obtain the coefficients of the constant at different orders of ϵ:

$$\begin{aligned}
&\epsilon : \psi_1^{(0)} = 0;\\
&\epsilon^2 : \psi_0^2 = \frac{2}{\Omega_0^2}[g_0\omega^2 + h_3 + H_0k^4 - e_1 - i_0k^2 - D_1k^2]|\psi_1^{(1)}|^2 = m_1|\psi_1^{(1)}|^2\\
&\epsilon^3 : \psi_0^3 = 0
\end{aligned} \tag{2.43}$$

The coefficients of $A^{(1)}$, at different order of ϵ, give:

$$\begin{aligned}
&\epsilon : \omega^2 = \Omega_0^2 + D_0k^2;\\
&\epsilon^2 : \upsilon_g = \frac{D_0k}{\omega}\\
&\epsilon^3 : -i\omega\psi_1^{(3)} - \upsilon_g\frac{\partial\psi_1^{(2)}}{\partial\xi} + \frac{\partial\psi_1^{(1)}}{\partial\tau} + \Omega_0^2\psi_1^{(3)} + 2e_1\left(\psi_0^{(2)}\psi_1^{(1)} + \psi_2^{(2)}\psi_{-1}^{(1)}\right) + 3e_2|\psi_1^{(1)}|^2\psi_1^{(1)} + if_0\omega\psi_1^{(1)}\\
&- if_1\omega\psi_0^{(2)}\psi_1^{(1)} - if_2\omega|\psi_1^{(1)}|^2\psi_1^{(1)} + 2g_0\omega^2\psi_2^{(2)}\psi_{-1}^{(1)} - 3g_1\omega^2|\psi_1^{(1)}|^2\psi_1^{(1)} - 3g_2\omega^3|\psi_1^{(1)}|^2\psi_1^{(1)} + ih_0k\psi_1^{(1)} +\\
&ih_1k\psi_0^{(2)}\psi_1^{(1)} + ih_2k|\psi_1^{(1)}|^2\psi_1^{(1)} - h_3k\omega\psi_2^{(2)}\psi_{-1}^{(1)} - ih_4k\omega^2|\psi_1^{(1)}|^2\psi_1^{(1)} - h_5k\omega|\psi_1^{(1)}|^2\psi_1^{(1)} + 4i_0k^2\psi_2^{(2)}\psi_{-1}^{(1)}\\
&+ i_1k^2|\psi_1^{(1)}|^2\psi_1^{(1)} - 3ii_2k^2\omega|\psi_1^{(1)}|^2\psi_1^{(1)} + D_0k^2\psi_1^{(3)} - 2iD_0k\frac{\partial\psi_1^{(2)}}{\partial\xi} - D_0\frac{\partial^2\psi_1^{(1)}}{\partial\xi^2} + D_0\frac{\partial^2\psi_1^{(1)}}{\partial\eta^2} - 3D_1k^2\times\\
&\psi_2^{(2)}\psi_{-1}^{(1)} + 3D_2k^2|\psi_1^{(1)}|^2\psi_1^{(1)} - 6iD_3k^2\omega\psi_2^{(2)}\psi_{-1}^{(1)} + 3D_4k^2\omega^2|\psi_1^{(1)}|^2\psi_1^{(1)} - iD_5k^2\omega|\psi_1^{(1)}|^2\psi_1^{(1)} + iD_7k^3\times\\
&|\psi_1^{(1)}|^2\psi_1^{(1)} - D_8k^3\omega|\psi_1^{(1)}|^2\psi_1^{(1)} - 3H_1k^4 + iH_2k^4\omega|\psi_1^{(1)}|^2\psi_1^{(1)} + 6iD_6k^3\psi_2^{(2)}\psi_{-1}^{(1)} - 4H_0k^4\psi_2^{(2)}\psi_{-1}^{(1)} - \lambda_0\times\\
&k\omega\psi_1^{(1)} - i\mu_0k^2\omega\psi_1^{(1)} = 0
\end{aligned} \tag{2.44}$$

The coefficients of $A^{(2)}$, at different order of ϵ^2, give:

$$\begin{aligned}
&\psi_2^{(2)} = (m_r + im_i)(\psi_1^{(1)})^2\\
&m_r = \frac{1}{3(\omega^2 - D_0k^2)}\left(e_1 - g_0\omega^2 + h_3k\omega + D_1k^2 - H_0k^4 - i_0k^2\right);\\
&m_i = \frac{1}{3(\omega^2 - D_0k^2)}\left(h_1k + D_3\omega^2k^2 + D_6k^3 - \omega f_1\right)
\end{aligned} \tag{2.45}$$

With the expression of $\psi_2^{(2)}$ and ψ_0^2, Eq.(2.36) becoms

$$i\frac{\partial\psi}{\partial\tau}+\frac{P_1}{2}\frac{\partial^2\psi}{\partial\xi^2}+\frac{P_2}{2}\frac{\partial^2\psi}{\partial\eta^2}+(Q_r+iQ_i)\mid\psi\mid^2\psi+i\frac{(R_r+iR_i)}{2}\psi=0, \tag{2.46}$$

where the coefficient $P_1, P_2, Q_r, Q_i, R_r, R_i$ are given by

$$\begin{aligned}
P_1 &= \frac{1}{\omega}(D_0-v_g^2),\ \ P_2=\frac{D_0}{\omega},\\
Q_r &= \frac{1}{2\omega}[3g_1\omega^2+h_5k\omega+3D_4k^2\omega^2+D_8k^3\omega+3H_1k^4-3e_2-3D_2k^2\\
&- 2e_1m_1+(2h_3k\omega+3D_1k^2+4H_0k^4-2e_1-2g_0\omega^2-4i_0k^2)m_r\\
&+ 6m_i(D_6k^3-D_3k^2\omega)],\\
Q_i &= \frac{1}{2\omega}[\omega f_2+3g_2\omega^3+h_4k\omega^2+3i_2k^2\omega\\
&+ D_5k^2\omega-h_2k-D_7k^3-H_2k^4\omega+(\omega f_1-h_1k)m_1\\
&+ (2h_3k\omega+3D_1k^2+4H_0k^4-2e_1-2g_0\omega^2-4i_0k^2)m_i+6m_r(D_3k^2\omega-D_6k^3)]\\
R_r &= \frac{\omega f_0-h_0k+\mu_0k^2\omega}{\omega},\ \ R_i=\lambda_0k.
\end{aligned} \tag{2.47}$$

The frequency ω and the corresponding group velocity v_g are plotted in Fig.(2.2) versus the wavenumber k, for different values of the degradation rate of the intracellular cAMP k_e. For $k=0$, we have $\omega=\Omega_0$ which is not sensitive to the change in k_e. However, when $k\neq 0$, the frequency decreases with increasing k_e due to the parameter D_0 which depends on system parameters (see Fig.(2.2a). Although $v_g=0$ for $k=0$, its value is also found to be sensitive to the change in k_e for $k>0$. Fig.(2.2b) shows that v_g is a decreasing function of the degradation rate of the intracellular cAMP.

Except for P_1, P_2 all the other parameters are complex and the subscripts r and i denote their real and imaginary parts, respectively. They are plotted in Fig. 2.3, versus the wavenumber k, and show different features when k_e changes. In fact, except Q_r and Q_i that have some negative values, the rest of the coefficients remain positive. This shows that the found CGL equation remains linked to system parameters and gives credit to the linear stability analysis that will be performed. The CGL equation is a universal model that gives the possibility to predict pattern formation in reaction-diffusion models [192]. The applicability of the CGL equations goes far beyond reaction-diffusion systems to cover other research areas actually related to superconductivity, nonlinear optics, plasmas, Bose-Einstein condensates, and quantum field theories [193].

2.2.2 Semi-discrete approximation with derivation of two-Dimensional CGL equations for two different frequency modes

The SDA is a perturbation technique in which the carrier waves are kept discrete while the amplitude is treated in the continuum limit. Applying this method allows one to study the

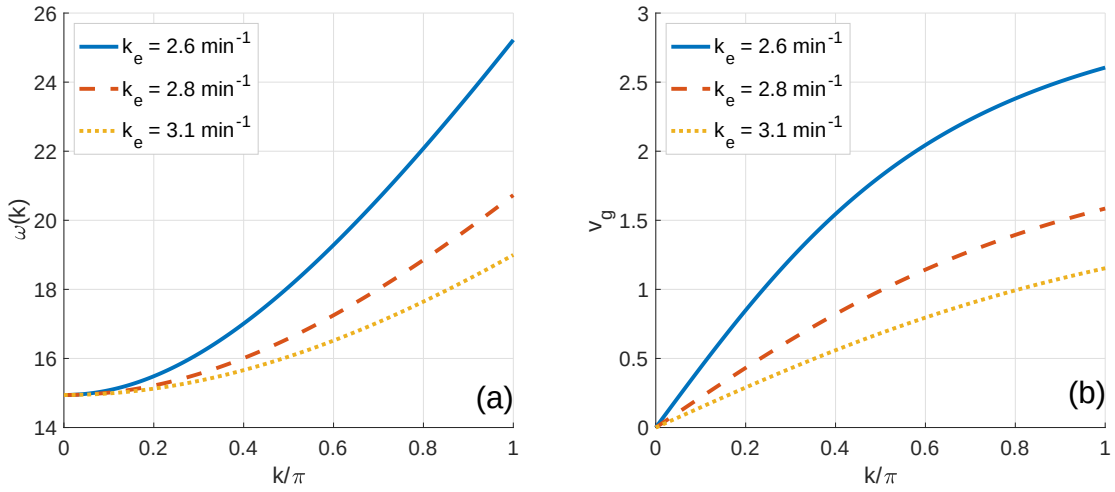

Figure 2.2: The angular wave frequency ω and the group velocity v_g are plotted against the wavenumber k. The influence of the degradation rate of extracellular cAMP by the enzyme phosphodiesterase k_e is studied for a fixed value $\sigma = 0.2$ min^{-1} of the production rate of intercellular cAMP.

modulation of a plane wave caused by nonlinear effects. Its principle is almost identical to the full-discrete approximation, but the derived amplitude equations are either the NLS type or the generalized CGL. In practice, having a nonlinear differential equation as in Eq.(2.12), one seeks solutions in the form:

$$g_n(t) = G(\xi,\tau)e^{i\theta_n} + G^*(\xi,\tau)e^{-i\theta_n} + \epsilon[H(\xi,\tau) + I(\xi,\tau)e^{2i\theta_n} + I^*(\xi,\tau)e^{-2i\theta_n}], \tag{2.48}$$

where the slow variables ξ and τ are related to fast ones n and t as

$$\xi = \epsilon(n - v_g t) \;\; and \;\; \tau = \epsilon^2 t \tag{2.49}$$

with $0 < \epsilon << 1$ and $\theta_n = kn - \omega t$. Note that index n denotes the cell number. Parameters k, v_g and ω, respectively stand for the wavenumber, group velocity and angular frequency and they are known to be related by the dispersion relation, or the solvability condition that determines the group velocity as.

$$v_g = \frac{\partial \omega}{\partial k} \tag{2.50}$$

Then such solution (2.48) is inserted into model of Eq.(2.33) which yields a linear homogeneous system for G, H and I polynomial in $e^{il\theta_n}$, $l = 0, 1, 2$ that will be solve later. In order to evaluate the diffusion term $g_{n+j}(t) - gu_n(t) + g_{n-j}(t)$, it is worthy to treat amplitudes G, H and I like the continuum functions such that $G(\xi_{n\pm j},\tau)$, $H(\xi_{n\pm j},\tau)$ and $I(\xi_{n\pm j},\tau)$ are developed up to order ϵ^2 in Taylor serie as

$$G(\xi_{n\pm j},\tau) = G(\xi,\tau) \pm \epsilon j \frac{\partial G(\xi,\tau)}{\partial \xi} + \frac{\epsilon^2 j^2}{2}\frac{\partial^2 G(\xi,\tau)}{\partial \xi^2} + O(\epsilon^2). \tag{2.51}$$

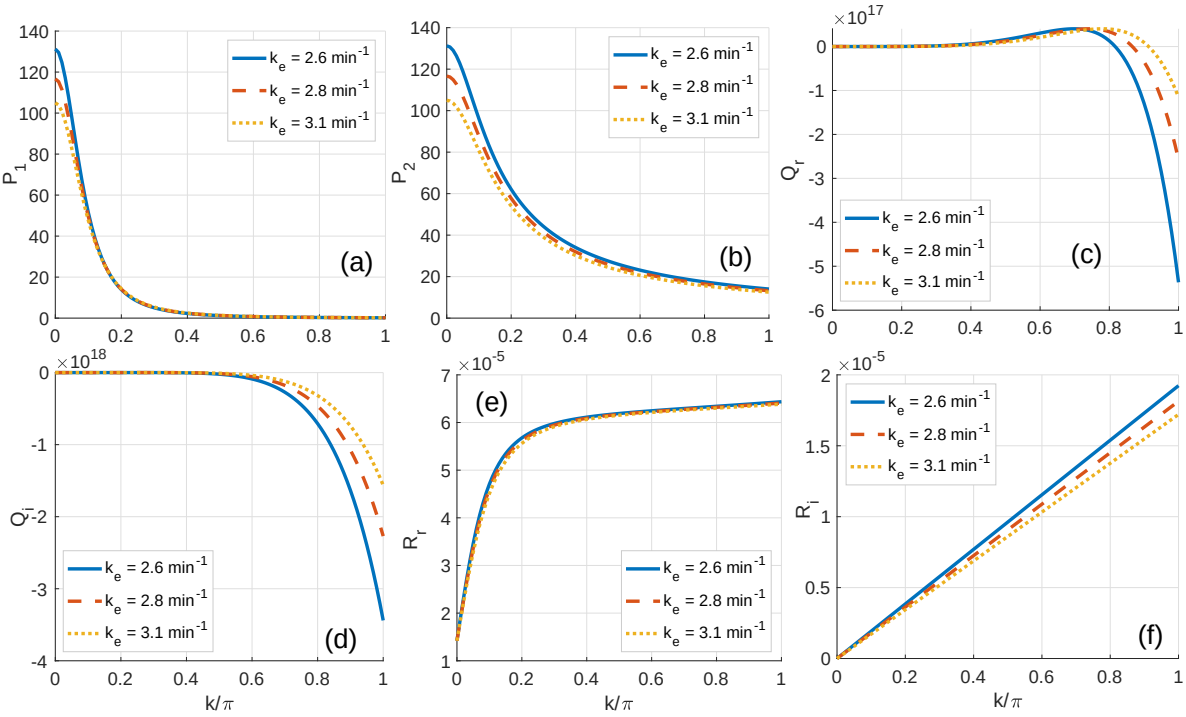

Figure 2.3: Variations of the coefficients of the CGL Eq. (2.46) versus the wavenumber k, with changing the degradation rate of extracellular cAMP by the enzyme phosphodiesterase k_e. The dispersion coefficient P_1, P_2, as well the dissipative coefficients R_r and R_i remain positive for any k and k_e. However, the real and imaginary parts of the nonlinearity coefficient Q_r and Q_i are positives for some values of k and negatives for others. All the panels have been plotted for a fixed value $\sigma = 0.2$ min^{-1} of maximum activity of adenylate cyclase.

Therefore, we obtain the following formula

$$\begin{aligned} g_{n+j} - 2g_n + g_{n-j} = &\left(2G\big(\cos(jk) - 1\big) + 2ij\epsilon \sin(jk)\frac{\partial G}{\partial \xi} + \epsilon j^2 \cos(jk)\frac{\partial^2 G}{\partial \xi^2}\right) e^{i\theta_n} \\ &+ \left(2\epsilon I\big(\cos(2jk) - 1\big) + 2ij\epsilon^2 \sin(2jk)\frac{\partial I}{\partial \xi}\right) e^{2i\theta_n} + c.c. + O(\epsilon^3) \end{aligned} \tag{2.52}$$

furthermore the temporal derivative operators are given by

$$\begin{aligned} \frac{\partial}{\partial t} &= \left(\epsilon^2 \frac{\partial}{\partial \tau} - \epsilon v_g \frac{\partial}{\partial \xi} - il\omega\right), \\ \frac{\partial^2}{\partial t^2} &= \left(\epsilon^2 v_g^2 \frac{\partial^2}{\partial \xi^2} - 2il\omega\epsilon^2 \frac{\partial}{\partial \tau} + 2il\omega\epsilon v_g \frac{\partial}{\partial \xi} - l^2\omega^2\right) + O(\epsilon^3). \end{aligned} \tag{2.53}$$

Here, we will attempt to apply the technique of the SDA on the model of Eqs.(2.33) whose trial solutions are given by:

$$\begin{aligned} G_{n,m} = G(\xi,\eta,\tau)e^{i\theta_{n,m}} + G^*(\xi,\eta,\tau)e^{-i\theta_{n,m}} + \epsilon(H(\xi,\eta,\tau) + \\ I(\xi,\eta,\tau)e^{2i\theta_{n,m}} + I^*(\xi,\eta,\tau)e^{-2i\theta_{n,m}}) \end{aligned} \tag{2.54}$$

where the change of variables $\xi = \epsilon(n - v_g t)$, $\eta = \epsilon m$ and $\tau = \epsilon^2 t$ has been applied, with v_g being the group velocity that will be defined later. We should however notice that according to the new variables, the direction n is the dominant one. In solutions (2.54), $\theta_{n,m} = kn + qm - \omega t$ is the phase of the carrier wave and *c.c.* represents the complex conjugate. We insert solution (2.54) into Eqs.(2.33) and we collect the coefficients of $e^{pi\theta_{n,m}}$ $(p = 0, 1, 2)$ at different orders of ϵ. The orders $\epsilon^0 e^{i\theta_{n,m}}$ and $\epsilon^1 e^{i\theta_{n,m}}$ give

$$\omega^2 = \Omega_0^2 + 4D_{0X}\sin^2\left(\frac{k}{2}\right) + 4D_{0Y}\sin^2\left(\frac{q}{2}\right), \tag{2.55a}$$

$$v_g = \frac{D_{0X}\sin(k)}{\omega}, \quad \text{and} \quad \sin(q) = 0, \tag{2.55b}$$

where $v_g = \frac{\partial \omega}{\partial k}$ is the group velocity in the n-direction. From Eq.(2.55b), the wavenumber q should fulfill some conditions for the investigated solutions to exist. Therefore, $\sin q = 0$ implies that the group velocity in the m-direction is null, therefore reinforcing that the direction n has priority over the $m-$direction for the nerve impulse propagation. In other words, the wavenumber q is such that $q = q_l = l\pi$ $(l \in Z)$, and one can get a simplified expression for the frequency as

$$\omega_{l_0}^2 = \Omega_0^2 + 4D_{0X}\sin^2\left(\frac{k}{2}\right) + 2D_{0Y}\left[1 - (-1)^{l_0}\right], \tag{2.56}$$

where $l_0 = 1$ for $q_l = (2l+1)\pi$ and $l_0 = 2$ for $q_l = 2l\pi$. It is therefore obvious that Eq.(2.56) defines two frequencies for the same wavenumber k, in the n-direction, and two different wavenumbers $q = (2l + l_0)\pi|_{l_0=1}$ and $q = (2l + l_0)\pi|_{l_0=2}$, in the m-direction. The case $l_0 = 1$ corresponds to

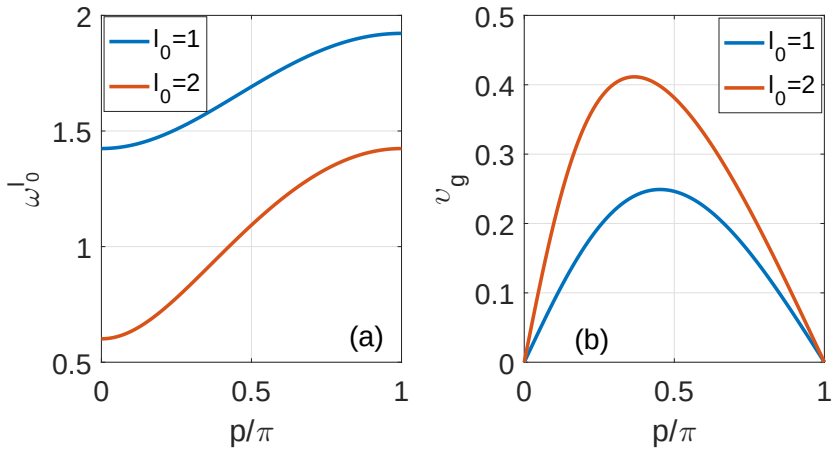

Figure 2.4: The angular wave frequency ω and the group velocity v_g are plotted against the wavenumber p. In all the figures, the blue line represents the HF mode and the red dashed-line pictures the low-frequency mode. We have fixed $k_g = 4.7$, $k_r = 1.5$, $a = 0.05$ and $D_{0X} = D_{0Y} = 2$.

the HF mode, while $l_0 = 2$ is related to the LF mode. This also implies that each of the frequencies modes has its corresponding group velocity. Both of then are shown in Fig.2.4 versus the wavenumber k, where we have considered two cases. One of the most obvious behaviors is that between the two frequencies there is a gap. In general, from Eq. (2.56), the lower cutoff frequencies are obtained for $k = 0$, i.e., $\omega_{l_0}^{min} = \omega_{l_0}(k = 0) = \sqrt{\Omega_0^2 + 2D_{0Y}\left[1 - (-1)^{l_0}\right]}$ and the upper cutoff frequencies are found for $k = \pi$, i.e., $\omega_{l_0}^{max} = \omega_{l_0}(k = \pi) = \sqrt{\Omega_0^2 + 4D_{0X} + 2D_{0Y}\left[1 - (-1)^{l_0}\right]}$. We have considered the cases $D_{0X} = D_{0Y} = 2$ and $D_{0X} = D_{0Y} = 0.05$. Comparing them, we observe that the gap between the two frequencies has increased for $D_{0X} = D_{0Y}$, making possible a better understanding of the difference between the two modes. The same phenomenon is visible for the group velocities, which are higher for the LF regimes. Under these considerations, the other coefficients of solutions (2.42) are obtained as follows:

$$H = \frac{-2\Omega_1}{\Omega_0^2} \mid G \mid^2 \tag{2.57}$$

$$I = \frac{1}{3\Omega_0^2 + 16D_{0X}sin^4(\frac{p}{2}) + 8D_{0Y}Zl_0}(-\Omega_1 + i\gamma_1\omega)G^2 \tag{2.58}$$

By making use of all the previous steps, canceling the third-order equations, withe $\epsilon^3 e^{i\theta_{n,m}}$,we finally get the 2D-CGL the equation.

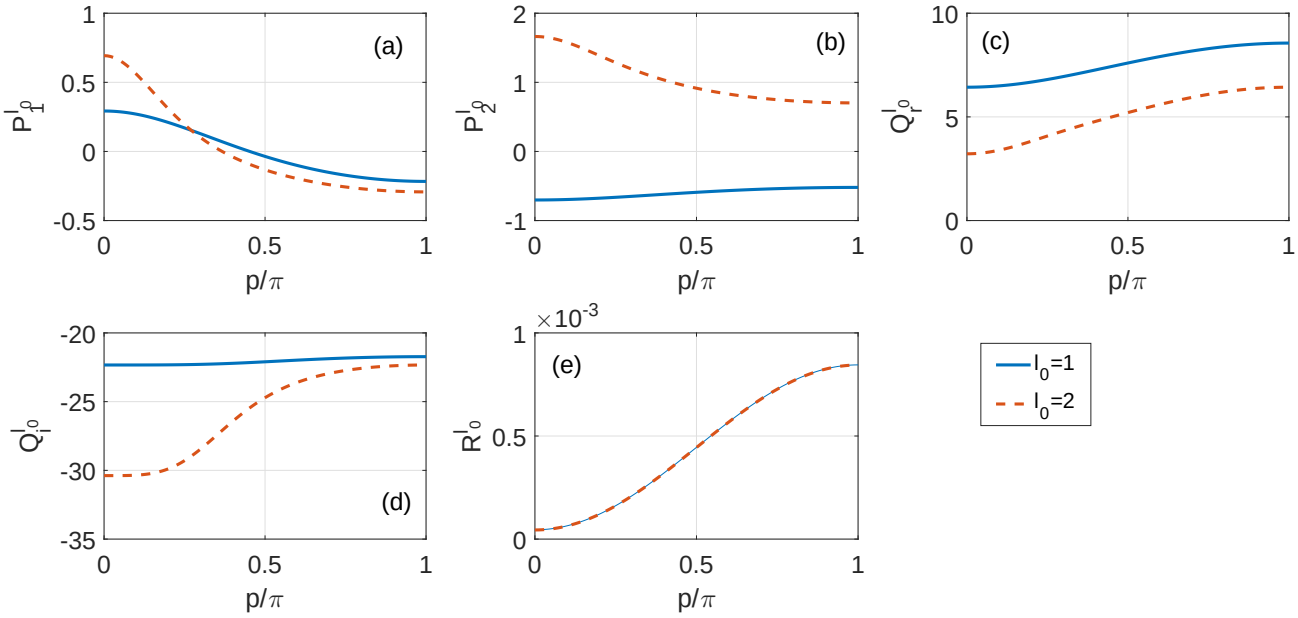

Figure 2.5: The panels show the variations the coefficients of the CGL Eq.(2.59) versus the wavenumber p. The dispersion coefficient $P_1^{l_0}$, $P_2^{l_0}$, as well the dissipative coefficients and R^{l_0} remain positive for any p. The two modes are considered: the high-frequency mode (solid blue line) and the HF mode. We have fixed $k_g = 4.7$, $k_r = 1.5$, $a = 0.05$ and $D_{0X} = D_{0Y} = 2$.

$$i\frac{\partial G}{\partial \tau} + \frac{P_1^{l_0}}{2}\frac{\partial^2 G}{\partial \xi^2} + \frac{P_2^{l_0}}{2}\frac{\partial^2 G}{\partial \eta^2} + (Q_r^{l_0} + iQ_i^{l_0}) \mid G \mid^2 G + i\frac{R^{l0}}{2}\psi = 0 \tag{2.59}$$

Eq.(2.59) is the 2D-CGL equation, with the parameters $P_1^{l_0}$, $P_2^{l_0}$, Q^{l_0}, and R^{l_0} given by

$P_1^{l_0} = \frac{1}{\omega^3}(D_{0X}cosq - D_{0X}^2 sin^2 p)$,

$P_2^{l_0} = \frac{(-1)^{l_0}}{\omega_{l_0}}$,

$Q_r^{l_0} = \frac{1}{2\omega}(\frac{4\Omega_1^2}{\Omega_0^2} + \frac{2\Omega_1^2}{3\Omega_0^2+16D_{0X}sin^4(\frac{p}{2})+8D_{0Y}Zl_0} - \Omega_2)$,

$Q_i^{l_0} = \frac{\gamma_2}{2} - \frac{\gamma_1\Omega_1}{\Omega_0^2} - \frac{\gamma_1\Omega_1}{3\Omega_0^2+16D_{0X}sin^4(\frac{p}{2})+8D_{0Y}Zl_0}$,

$R^{l_0} = \gamma_0 + 4D_{1X}sin^2\frac{p}{2} + 2D_{1Y}Zl_0$

Beforehand, we initially examine the variations of each coefficient of Equation (2.59) with respect to the wavenumber p and this, because the formation of solitonic structures in such systems depends essentially on the sign of their coefficients. This is done in Fig(2.5), where for each of the coefficients, plots corresponding to the two available modes of propagation are compared. In general, $Q_r^{l_0}$ and R^{l_0} are positive coefficients in both regimes. However $P_1^{l_0}$ has positive and negative values, respectively for $p < 0.45\pi$ and $p > 0.45\pi$. $P_2^{l_0}$ is positive for the LF mode and negative for the HF mode. In the HF and LF regime, $Q_i^{l_0}$ is exclusively negative

values and $Q_r^{l_0}$ positif values.

2.2.3 Linear stability analysis

Linear stability analysis is a technique that can analytically predict the development of MI phenomenon in a nonlinear and dispersive dynamical system. Generally performed on integrable equations, the procedure differs, however, when we move from discrete equations to continuous ones.

In a particular case of CGL equations, the linear stability analysis is usually carried out by means of the following scheme. First, we have to find an equilibrium state of the system of equations under investigation, which is simple and exact monochromatic wave solutions. Second, we have to add a small perturbation on the equilibrium state with a perturbation wavenumber and frequency, which are much smaller than those of the carrier wave. The small perturbation functions satisfy a set of equations from which one deduces the nonlinear dispersion relation. The latter is analyzed to obtain a complex frequency, revealing the growth of the amplitudemodulated wave packet. Finally the instability growth rate is derived such that MI appears in some privileged areas of space in which instability growth rate is different from zero and disappears elsewhere.

2.2.3.1 Linear stability analysis on the 2D CGL equations

Here, we perform the linear stability analysis on Eq.(2:38) that describes amplitude evolution of envelop soliton in two dimensions. A plane wave $\psi(\xi,\eta,\tau)=\phi_0 e^{i(q_1\xi+q_2\eta-\varpi\tau)}$ is assumed to be solution of the generalized equation Eq.(2.43), where the wavenumber q_1 and q_2, the frequency ϖ and the amplitude ϕ_0, after separating the real and imaginary parts, satisfy the relations

$$\varpi=\frac{P_1}{2}q_1^2+\frac{P_2}{2}q_2^2+\frac{Ri}{2}-Q_r\phi_0^2,\quad\text{and}\quad Q_i\phi_0^2+\frac{R_r}{2}=0. \tag{2.60}$$

Usually, a solution is said to be stable if it remains unchanged in the presence of small perturbations. For our particular case, the perturbed solution is taken to be $\psi(\xi,\eta,\tau)=[\phi_0+\Phi(\xi,\eta,\tau)]e^{i(q_1\xi+q_2\eta-\varpi\tau+\mu(\xi,\eta,\tau))}$, where $\Phi(\xi,\eta,\tau)$ and $\mu(\xi,\eta,\tau)$ are respectively the perturbation amplitude and the perturbation phase considered to be small in comparison to both amplitude and phase of the plane wave. Further replacing ψ by its perturbed expression into Eq.(2.43), and after splitting the real and imaginary parts, we obtain the following equations that govern the perturbations Φ and μ

$$-\phi_0\mu_\tau+\frac{P_1}{2}\Phi_{\xi\xi}+\frac{P_2}{2}\Phi_{\eta\eta}-P_1q_1\phi_0\mu_\xi-P_2q_2\phi_0\mu_\eta+2Q_r\phi_0^2\Phi=0 \tag{2.61a}$$

$$\phi_\tau+\frac{P_1}{2}\phi_0\mu_{\xi\xi}+\frac{P_2}{2}\phi_0\mu_{\eta\eta}+P_1q_1\Phi_\xi+P_2q_2\Phi_\eta-R_r\Phi=0 \tag{2.61b}$$

Solutions to the above equations can be assumed in the form $\Phi(\xi,\eta,\tau) = \Phi_0 e^{i(K_1\xi+K_2\eta-\nu\tau)} + cc.$, $\mu(\xi,\eta,\tau) = \mu_0 e^{i(K_1\xi+K_2\eta-\nu\tau)} + cc.$, with σ and δ being respectively the wavenumbers of the perturbations, in the K_1 and K_2 directions, and ν their respective angular frequencies. Making use of these, one finally gets to the homogeneous system

$$\begin{pmatrix} \left(2Q_r\phi_0^2 - \frac{P_1}{2}K_1^2 - \frac{P_2}{2}K_2^2\right) & i\phi_0\left(\nu - P_1q_1K_1 - P_2q_2K_2\right) \\ \left(R_r + i(\nu - P_1q_1K_1 - P_2P_2q_2K_2)\right) & \frac{\phi_0}{2}\left(P_1K_1^2 + P_2K_2^2\right) \end{pmatrix} \begin{pmatrix} \Phi_0 \\ \mu_0 \end{pmatrix} = \begin{pmatrix} 0 \\ 0 \end{pmatrix} \tag{2.62}$$

in Φ_0 and μ_0. The determinant of the system matrix should be null for non-trivial solutions to exist. This leads to the nonlinear dispersion relation

$$X^2 - iR_rX - \frac{P_1K_1^2 + P_2K_2^2}{4}\left(1 - \frac{4Q_r\phi_0^2}{P_1K_1^2 + P_2K_2^2}\right) = 0, \tag{2.63}$$

with $X = \nu - P_1q_1K_1 - P_2q_2K_2$. For MI to develop in the model, the angular frequency should be complex, with a non-zero imaginary part. More precisely, the discriminant $\Delta = \left(P_1K_1^2+P_2K_2^2\right)\left(1-\frac{4Q_r\phi_0^2}{P_1K_1^2+P_2K_2^2}\right)-R_r^2$ of Eq. (2.68), should be negative, so that the condition for instability $\frac{Q_r}{P_1K_1^2+P_2K_2^2} > 0$ be fulfilled. The corresponding solution will then be $X = i\frac{R_r^{l_0}}{2} + i\frac{\sqrt{-\Delta}}{2}$, i.e.,

$$\nu = P_1q_1K_1 + P_2q_2K_2 + i\left(\frac{R_r}{2} + \frac{\sqrt{-\Delta}}{2}\right), \tag{2.64}$$

and one easily gets the growth rate of MI in the form

$$\Gamma(K_1,K_2) = \frac{1}{2}\left[R_r + \sqrt{R_r^2 + \left(P_1K_1^2 + P_2K_2^2\right)\left(\frac{4Q_r\phi_0^2}{P_1K_1^2 + P_2K_2^2} - 1\right)}\right] \tag{2.65}$$

It is then obvious that for Γ to be positive, we should have $\frac{4Q_r\phi_0^2}{P_1K_1^2+P_2K_2^2} - 1 > 0$, and this will be possible only if the wave amplitude exceeds its threshold value $\phi_{0,cr}$, i.e.,

$$\phi_0^2 > \phi_{0,cr}^2 = \frac{P_1K_1^2 + P_2K_2^2}{4Q_r}. \tag{2.66}$$

2.2.3.2 Linear stability analysis on the 2D CGL equations for two different frequency modes

In order to study the stability of the plane wave $G(\xi,\eta,\tau) = \phi_0 e^{i(p\xi+q\eta-\varpi\tau)}$ solution of Equation (2.59), where the wavenumbers p and q, and the angular frequency ϖ verify the dispersion relations

$$\begin{aligned} \varpi &= \frac{P_1^{l_0}}{2}p^2 + \frac{P_2^{l_0}}{2}q^2 - Q_r^{l_0}\phi_0^2 \\ Q_i^{l_0}\phi_0^2 &+ \frac{R_r^{l_0}}{2} = 0 \end{aligned} \tag{2.67}$$

one can introduce small perturbations in its amplitude or phase, or in both. In general, there are regions where such a plane wave gets unstable, giving rise to a phenomenon known as MI. When the amplitude and the phase are both perturbed, the corresponding solution writes

$$G(\xi,\eta,\tau) = [\phi_0 + \Phi(\xi,\eta,\tau)]e^{i(p\xi+q\eta-\varpi\tau+\mu(\xi,\eta,\tau))} \tag{2.68}$$

where $\Phi(\xi,\eta,\tau)$ and $\mu(\xi,\eta,\tau)$ are respectively the perturbation amplitude and the perturbation phase. These two perturbations are small compared to the amplitude and the phase of the unperturbed plane wave. Inserting Equation (2.68) into Equation (2.59), and linearizing around the unperturbed plane wave solution lead to the set of equations

$$\begin{aligned} &-\phi_0\mu_\tau + \frac{P_1^{l_0}}{2}\Phi_{\xi\xi} + \frac{P_2^{l_0}}{2}\Phi_{\eta\eta} - P_1^{l_0}p\phi_0\mu_\xi - P_2^{l_0}q\phi_0\mu_\eta + 2Q_r^{l_0}\phi_0^2\Phi = 0 \\ &\phi_\tau + \frac{P_1^{l_0}}{2}\phi_0\mu_{\xi\xi} + \frac{P_2^{l_0}}{2}\phi_0\mu_{\eta\eta} + P_1^{l_0}p\Phi_\xi + P_2^{l_0}q\Phi_\eta - R_r^{l_0}\Phi = 0 \end{aligned} \tag{2.69}$$

Solutions to the above equations can be assumed in the form; $\Phi(\xi,\eta,\tau) = \Phi_0 e^{i(K_1\xi+K_2\eta-\nu\tau)} + cc...$; $\mu(\xi,\eta,\tau) = \mu_0 e^{i(K_1\xi+K_2\eta-\nu\tau)} + cc...$, with K_1 and K_2 being respectively the wavenumbers of the perturbations and ν thier respective angular frequencies. Making use of these, one finally gets to the homogeneous system in Φ_0 et μ_0.

$$\begin{pmatrix} (2Q_r^{l_0}\phi_0^2 - \frac{P_1^{l_0}}{2}K_1^2 - \frac{P_2^{l_0}}{2}K_2^2)\Phi_0 & i\phi_0(\nu - P_1^{l_0}pK_1 - P_2^{l_0}qK_2)\mu_0 \\ (R_r^{l_0} + i(\nu - P_1^{l_0}pK_1 - P_2^{l_0}qK_2)\Phi_0 & \frac{\phi_0}{2}(P_1^{l_0}K_1^2 - P_2^{l_0}K_2^2)\mu_0 \end{pmatrix} = 0 \tag{2.70}$$

The determinant of the system matrix should be null for non-trivial solutions to exist. This leads to the nonlinear dispersion relation

$$X^2 - iR_rX - \frac{P_1^{l_0}K_1^2 + P_2^{l_0}K_2^2}{4}(1 - \frac{4Q_r^{l_0}\phi_0^2}{P_1^{l_0}K_1^2 + P_2^{l_0}K_2^2}) = 0 \tag{2.71}$$

With $X = \nu - P_1^{l_0}pK_1 - P_2^{l_0}qK_2$. For MI to develop in the model, the angular frequency should be complex, with a nonzero imaginary part. More precisely, the discriminant $\Sigma = \left(P_1^{l_0}K_1^2 + P_2^{l_0}K_2^2\right)\left(1 - \frac{4Q_r^{l_0}\phi_0^2}{P_1^{l_0}K_1^2+P_2^{l_0}K_2^2}\right) - (R_r^{l_0})^2$ of Eq.(14), should be negative, so that the condition for instability $\frac{Q_r^{l_0}}{P_1^{l_0}K_1^2+P_2^{l_0}K_2^2} > 0$ be fulfilled. The corresponding solution will then be

$$X = P_1^{l_0}pK_1 + P_2^{l_0}qK_2 + i\left(\frac{R_r^{l_0}}{2} + \frac{\sqrt{-\Delta}}{2}\right) \tag{2.72}$$

and one easily gets the growth rate of MI in the form

$$\Gamma(K_1,K_2)=\frac{1}{2}[R_r^{l_0}+\sqrt{(R_r^{l_0})^2+(P_1^{l_0}K_1^2+P_2^{l_0}K_2^2)(\frac{4Q_r^{l_0}\phi_0^2}{P_1^{l_0}K_1^2+P_2^{l_0}K_2^2}-1)}] \tag{2.73}$$

It is then obvious that for Γ to be positive, we should have $\frac{4Q_r^{l_0}\phi_0^2}{P_1^{l_0}K_1^2+P_2^{l_0}K_2^2}-1>0$, and this will be possible only if the wave amplitude exceeds its threshold value $\phi_{0,cr}$, i.e.,

$$\phi_0^2>\phi_{0,cr}^2=\frac{P_1^{l_0}K_1^2+P_2^{l_0}K_2^2}{4Q_r^{l_0}}. \tag{2.74}$$

2.2.3.3 Bifurcation theory

The fundamental aspect of the study of dynamical systems is the bifurcation notion. A term that was introduced by Henri Poincaré at the beginning of the XX^e century in this work on differential systems. For certain critical values of control parameters of the system, the diagonal solution of the equation changes qualitatively: we say that there is a bifurcation. A first approach to the study of systems dynamics consists in finding the points of equilibrium, that is to say the stationary solutions which do not present the temporal evolution. The next step is to vary the system control settings. We watch as the points of equilibrium become, especially those that were stable before changing the system settings and bifurcations that appear. For the values of the parameters at which such qualitative changes appear, so-called bifurcation values, the construction of the portrait of phase requires adopted tools [194].

Mathematical models of deterministic physical systems typically consist of dynamical systems. These dynamical systems usually contain parameters. These parameters take explicitly into account the influence of either the internal properties of the system or other external features. Often, some subgroup of these parameters can be changed at will by varying some properties of the physical process or by other means. Such parameters are called control parameters. Frequently, as these control parameters are varied, the qualitative structure of the solutions of the dynamical system change. These changes are called bifurcations and the values of the control parameters for which they happen are called bifurcation values. Here we will concentrate our attention on numeric resolution of eqs (2.24) for obtain the bifurcatoin values.

2.2.4 Runge-Kutta numerical intégration method.

Numerical solution of ordinary differential equations is the most important technique in continuous time dynamics. Since most ordinary differential equations are not soluble analytically, numerical integration is the only way to obtain information about the trajectory. Many different methods have been proposed and used in an attempt to solve accurately various types of ordinary differential equations. However there are a handful of methods known and used universally

(i.e., Runge-Kutta, Adams-Bashforth and Backward Differentiation Formula methods). All these methods discretize the differential system to produce a discrete system of equation or map. The methods obtain different maps from the same differential equation, but they have the same aim; that the dynamics of the map should correspond closely to the dynamics of the differential equation. In this work, we use the fourth order Runge-Kutta algorithm and other numerical methods which depend on what we want to find.

The fourth order Runge-Kutta is a much more locally accurate method. Let's consider the following problem:

The fourth order Runge-Kutta is a much more locally accurate method. Let's consider the following problem

$$\begin{cases} \dfrac{dy}{dt} = f(t,y) \\ y(t_0) = \alpha \end{cases}; \tag{2.75}$$

and define h to be the normalized integration time step size and set $t_i = t_0 + ih$. Then the following sequence of operations

$$\begin{aligned} &U_0 = \alpha, \\ &U_{i+1} = U_i + \frac{h}{6}(k_1 + 2k_2 + 2k_3 + k_4), \quad \text{for i} = 0, 1, ..., \text{n} - 1 \end{aligned} \tag{2.76}$$

computes an approximate solution, that is $U_n \approx y(t_n)$. k_1, k_2, k_3 and k_4 are the coefficients which have to be evaluated in each stage of the loop (of the fourth order Runge-Kutta algorithm) by the formulas below:

$$\begin{aligned} k_1 &= f(t_i, U_i), \\ k_2 &= f(t_i + \frac{h}{2}, U_i + \frac{h}{2}k_1), \\ k_3 &= f(t_i + \frac{h}{2}, U_i + \frac{h}{2}k_2), \\ k_4 &= f(t_i + h, U_i + hk_3). \end{aligned} \tag{2.77}$$

In the case of differential equation of Filippov's type of which we are particularly concerned with in the framework of this dissertation, the above algorithm is slightly modified to take into account the piecewise definition of the differential equation. Consider the following Filippov type equation

$$\begin{cases} \dfrac{dy}{dt} = f(t,y) = \begin{cases} f^-(t,y), & \text{if } y < \beta \\ f^+(t,y), & \text{if } y > \beta \end{cases}; \\ y(0) = \alpha \end{cases} \tag{2.78}$$

where $y = \beta$ defined the switching boundary, that is the manifold of the state space on which the right-hand side ($f(t, y)$) of Eq.(2.75) changes discontinuously. The algorithm used to obtained the approximate solution of this equation (Eq.(2.75)) is given as follows:

$$\begin{aligned} &U_0 = \alpha, \\ &U_{i+1} = \begin{cases} U_i + \dfrac{h}{6}\left(k_1^- + 2k_2^- + 2k_3^- + k_4^-\right), & \text{if } U_i < \beta, \\ U_i + \dfrac{h}{6}\left(k_1^+ + 2k_2^+ + 2k_3^+ + k_4^+\right), & \text{if } U_i > \beta, \end{cases} \quad \text{for } i = 0, 1, ..., n-1 \end{aligned} \tag{2.79}$$

where

$$\begin{aligned} k_1^j &= f^j(t_i, U_i), \\ k_2^j &= f^j(t_i + \frac{h}{2}, U_i + \frac{h}{2}k_1), \\ k_3^j &= f^j(t_i + \frac{h}{2}, U_i + \frac{h}{2}k_2), \\ k_4^j &= f^j(t_i + h, U_i + hk_3), \\ j &\in \{-, +\}. \end{aligned} \tag{2.80}$$

The Runge-Kutta method is very widely favored as:

- It is easy to use and no equations need to be solved at each stage;
- It is highly accurate for moderate h values;
- It is a one step method, that is; U_{i+1} only depends on U_i;
- It is easy to start and easy to code.

In the special case when $f(t, y) = f(t)$, we have

$$y(t) = \int_{t_o}^{t} f(t)dt + y(t_0) \tag{2.81}$$

and the task of evaluating this integral accurately is called quadrature. To solve any differential equation with the fourth order Runge-Kutta algorithm, we need to put it into the standard form given by Eq.(2.75).

Conclusion

This chapter was devoted,on the one hand, to the modeling three improved to describe oscillations in the cAMP level in cell suspensions as well as cAMP wave propagation in a dispersed cell population including of the two-component MG model in the presence of diffusion and external flow, FHN model with frequency mode , FHN model with LRI and on the other hand, in addition, the analytical methods such as the multiple scale expansion, the linear stability analysis and the RK4 numerical integration method furnished the second part of the chapter.

Thanks to the SDA and DA, we have been able to reduce the insolvent generic equations to a CGL equations whose solutions have been extensively developed in the literature. Then the analysis of the linear stability led us either to the determination of the critical amplitude above which the plane wave would become unstable or to the derivation of the instability growth rate which predicts the manifestations of the phenomenon of MI under some instability criteria that have also been established. We are therefore interested not only in the various patterns induced by the MI phenomena, but also in the study of the different phenomena that are associated withe oscillations in the cAMP level in cell suspensions as well as cAMP wave propagation in a dispersed of D.D.

Chapter 3

Results and Discussion

Introduction

In the previous chapters, we have provided the generalities on the collective behavior of D. discoideum. During starvation, D. discoideum amoeba release periodic spikes of cAMP in response to extracellular cAMP levels and interact by propagating cAMP waves throughout space. We have also shown that the reaction-diffusion equations modeling the chemical cAMP concentration and cAMP receptors, can be reduced to a CGL equation. In the present chapter, we bring out our results on the study of the cAMP waves patterns during aggregation of Dictyostelium discoideum cells : Here we study communication within an amoebas colony through the MI technique, the effects of advection on the nonlinear patterns are investigated both analytically and numerically In Section 3.1 the effect of factors like the degradation rate of extracellular cAMP (k_e) and the production rate of cAMP (σ) is studied in presence of the flow on the emergence of nonlinear patterns is discussed analytically, via the MI. Some features of MI growth rate will be discused in term of the wavenumber for different values of the control parameters. Then numerical simulations of the model of Eqs. (2.25), the feature of patterns formation by using MI, additionally to the time series and phase portraits of cAMP concentration. To direct by the bifurcation method, the values of (k_e) and (σ) are explicitly selected. A relationship between the formation of self-modulated waves using MI will be established, and a strong correlation between analytical and numerical results, in presence of the flow. We examine in section 3.2 the two frequency regimes namely the HF and the LF, detected in a two-dimensional FHN model will be explored. The different features of MI gain, given by Eq.(2.73), will be studied. The various profiles of numerical solution will also be investigated with using the synchronization factor, along with their propagation in the two frequency regimes. In Section 3.3, we also study through numerical computations LR diffusive effects in a discrete FHN amoebae network. Their impact on the emergence of target and multi-spiral waves is discussed. Moreover, the main fea-

tures of cAMP waves are found to be qualitatively and quantitatively altered by the change of the long-range parameter.

3.1 Unstable cAMP wave patterns during aggregation of Dictyostelium discoideum

Here we study Flow-driven formation of unstable patterns of cyclic adenosine monophosphate (cAMP) through the MI technique. In that respect, effects of some parameters such as the the change of the extracellular cAMP degradation rate (k_e), the production rate of cAMP (σ) and the advection flow velocity (V_f). on the nonlinear patterns are investigated both analytically and numerically.

3.1.1 Analytical analysis of MI

Analytical study has revealed under the activation of MI phenomenon, the existence of the instability domain in a two-dimensional Martiel-Golbeter, also analytical expression of instability growth rate has been derived. In this section, we present the instability diagrams from the function which represents the MI gain $\Gamma(K_1, K_2)$.

3.1.1.1 The MI growth rate versus the wavenumbers of perturbations

This part we discuss the parameters where cAMP waves are unstable by the MI features obtained from Eq.(2.45). In order for Γ to be positive, we should have $\frac{4Q_r\phi_0^2}{P_1K_1^2+P_2K_2^2} - 1 > 0$, which will be possible only if the amplitude goes beyond a threshold $\phi_{0,cr}^2 = \frac{P_1K_1^2+P_2K_2^2}{4Q_r}$. When values for ϕ_0 are suitably chosen, we obtain the MI growth rate shown in Fig. 3.1, where panels $(\text{aj})_{j=1,2,3}$ corresponds to $\sigma = 0.2\text{min}^{-1}$, panels $(\text{bj})_{j=1,2,3}$ to $\sigma = 0.3\text{min}^{-1}$ and panels $(\text{cj})_{j=1,2,3}$ gives the MI growth rate for $\sigma = 0.6\text{min}^{-1}$. In the $(K_1, K_2)-$plane, it is obvious from the two sets of diagrams that the area of instability, i.e., where $\Gamma(K_1, K_2) > 0$, gets expanded with increasing k_e. However, regions of instability are more larger for $\sigma = 0.6\text{min}^{-1}$ than for the other values. This shows that both the production and degradation rates of cAMP may deeply influence pattern formation. However, for $k_e = 3.1\text{min}^{-1}$, there is marginal instability, which corresponds to what is shown in Fig. 3.1(c3). There are several regions of instability and this confirms the results of the previous investigation on amoeba communication in during aggregation.

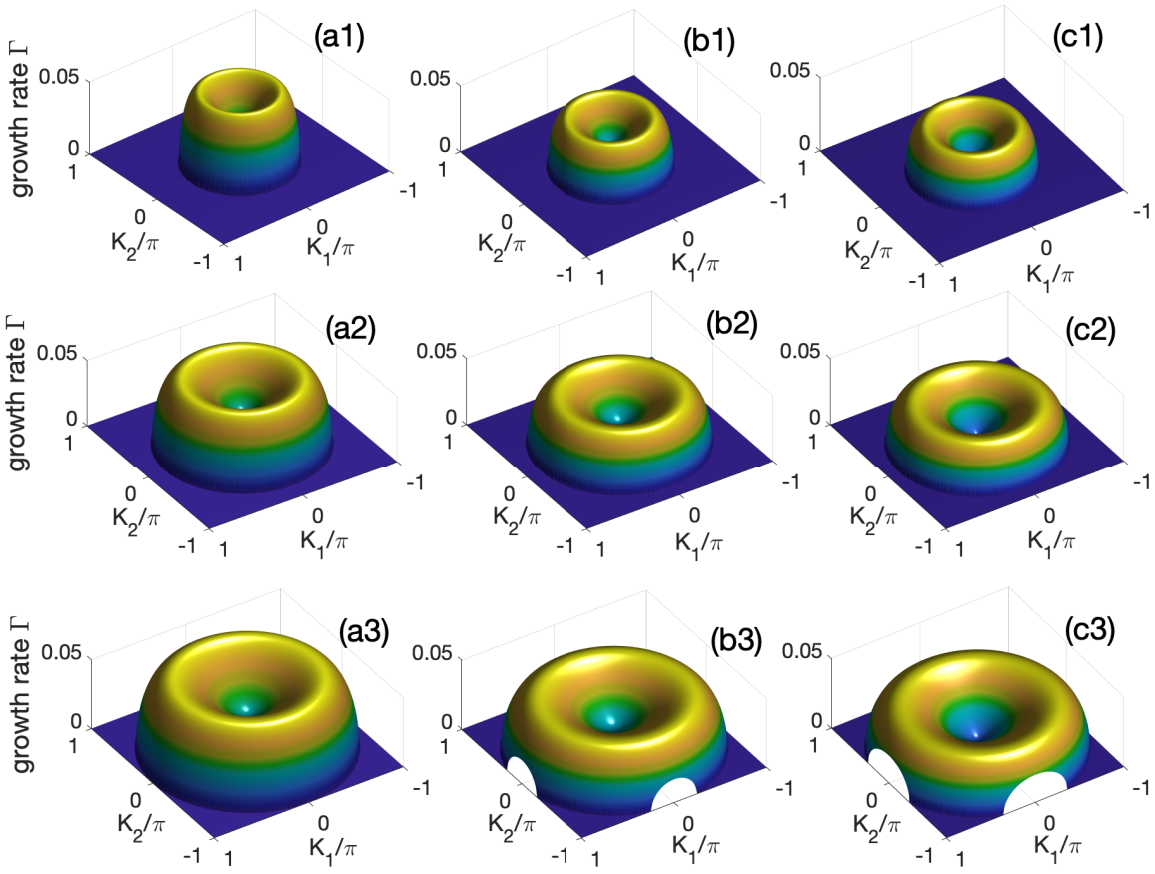

Figure 3.1: The MI growth rate $\Gamma(K_1, K_2)$ versus the wavenumbers K_1 and K_2. Panels $(\text{aj})_{j=1,2,3}$ corresponds to $\sigma = 0.2\text{min}^{-1}$, panels $(\text{bj})_{j=1,2,3}$ to $\sigma = 0.3\text{min}^{-1}$ and panels $(\text{cj})_{j=1,2,3}$ gives the MI growth rate for $\sigma = 0.6\text{min}^{-1}$. From top to bottom, the different rows have been, respectively, computed for $k_e = 2.6\text{min}^{-1}$ $(j = 1)$, 2.8min^{-1} $(j = 2)$ and 3.1min^{-1} $(j = 3)$.

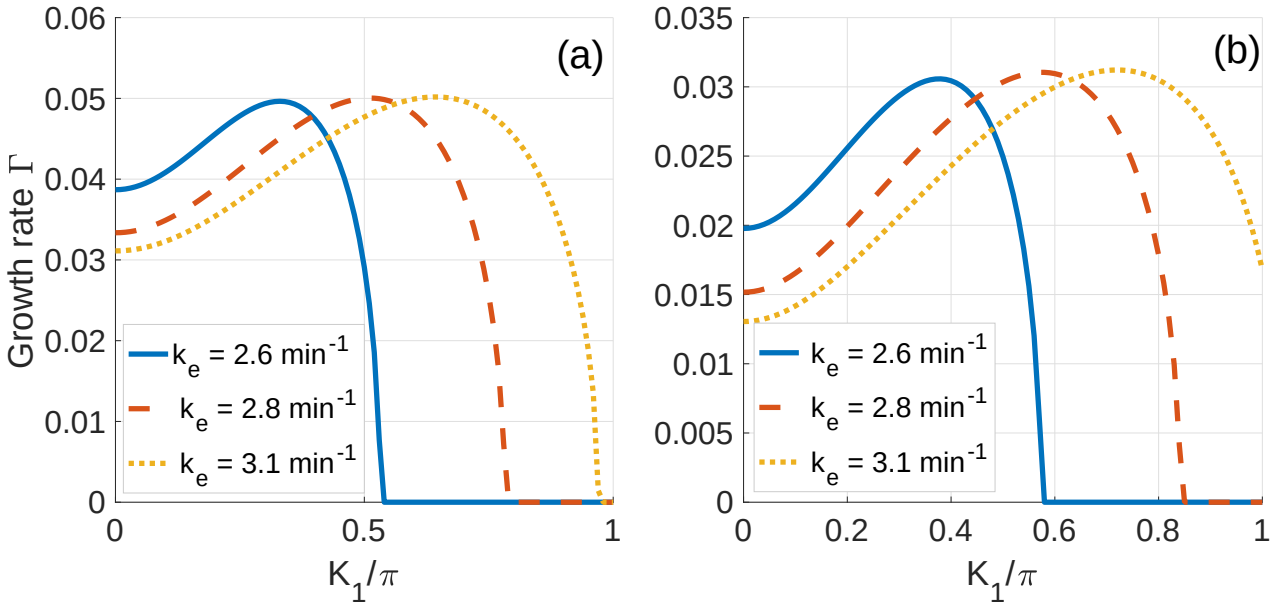

Figure 3.2: The MI growth rate $\Gamma(K_1, K_2)$ versus the longitudinal wavenumber K_1, with $K_2 = 0.1\pi$. Each panel corresponds to a fixed value of σ, while Γ is plotted for three different values of k_e. Panel (a) corresponds to $\sigma = 0.2\text{min}^{-1}$ and panel (b) to $\sigma = 0.6$ min^{-1}. $\Gamma > 0$ is delimited by the intervals $0 < K_1 < K_{1,cr}$, where the plane wave is expected to be unstable under slight modulation.

3.1.1.2 The MI growth rate versus the longitudinal wavenumber of perturbations

In this part we are interested in the features of the MI growth rate $\Gamma(K_1, K_2)$ plotted in longitudinal wavenumber K_1. Fixing $K_2 = 0.1\pi$, the same regions are clearly depicted in Fig. 3.2, where Γ is plotted versus K_1. Fig. 3.2(a) shows results for $\sigma = 0.2\text{min}^{-1}$, and $\Gamma > 0$ is delimited by the intervals $0 < K_1 < K_{1,cr}$, where the plane wave becomes unstable under slight modulations. $K_{1,cr}$, in Fig. 3.2(a), increases when k_e takes the respective value 2.6 min^{-1}, 2.8 min^{-1} and 3.1 min^{-1}. The same behaviors appear for $\sigma = 0.6\text{min}^{-1}$.

In summary, both the production rate of intercellular cAMP and degradation rate of extracellular cAMP influence the stability features of the system dynamics studied, but in the two detected cases, there are common regions of stability and instability, which is possible for specific values of the wavenumber k. Moreover, this also suggests that the two detected regimes might display different dynamical behaviors, depending of course on the value of the range parameter k_e, the extracelllar and σ the intracellular parameters.

Dimensionless parameter	Numerical value	Parameter	Numerical value
L_1	10	k_1	0.4min^{-1}
L_2	0.1	k_2	$0.004\ \text{min}^{-1}$
c	100	σ	$0.1 - 0.4\ \text{min}^{-1}$
q	4000	k_i	$1.7\ \text{min}^{-1}$
h	5	k_t	$0.9\ \text{min}^{-1}$
α	3	k_e	$2.5 - 12\ \text{min}^{-1}$
λ	0.01	D	$0.024\ \text{mm}^2\text{min}^{-1}$
θ	0.01		
ϵ	1		

Table 3.1: *The numerical values of the parameters considered in the model*

3.1.2 Numerical analysis of MI

Here we seek to show that cAMP oscillation and MI phenomena are in perfect correlation. According to the above analytical results based on linear stability analysis, the stability condition of an extended plane wave has been determined for the CGL equation (2.38) which is only an approximate description of the generic equation (2.24). The linear stability analysis cannot tell us the long-time evolution of a modulated extended nonlinear wave. Therefore, in order to check the validity of our analytical approach and to determine the evolution of the system taking into account the instability zone, we have performed numerical simulations of the MG model of Eqs.(2.24)with a given initial condition being the perturbed plane waves, with wavenumbers $K_1 = 0.4\pi$ and $K_2 = 0.1\pi$ belonging to the instability areas depicted in Figs. 3.1 and 3.2. No-flux boundary conditions have been considered in the Merson modification of the Runge-Kutta computational scheme, with a time step $\Delta t = 10^{-4}$min and spatial meshes $\Delta x = \Delta y = 0.01$mm. We chose as the initial condition a linear wave with a slightly modulated amplitude [201–203].

$$\gamma(t=0) = \phi_0\big[1 + 0.01cos(0.01cos(K_1x + K_2y))\big]cos(kx) \tag{3.1a}$$

$$\rho(t=0) = \phi_0\big[1 + 0.01cos(0.01cos(K_1x + K_2y))\big]cos(kx) \tag{3.1b}$$

The numerical values of the parameters are given in (Tab.3.1)

3.1.2.1 Bifurcation-like behaviors of the MG model

Simulation results giving lower and higher threshold values of k_e which support cAMP pattern formation via MI process are shown in the bifurcation diagram of Fig. 3.3, with red regions being

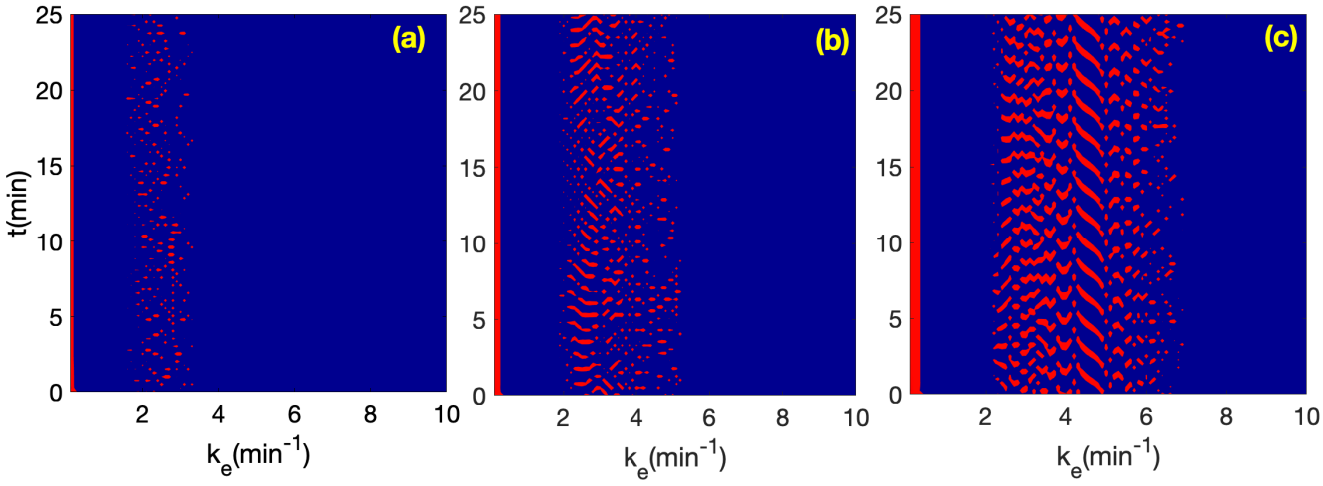

Figure 3.3: The bifurcation diagrams of cAMP extracellular concentration $\gamma(50, 50)$ in the $(k_e, t)-$plane with increasing σ (i.e, higher activity of the enzyme adenylate cyclase) as: $\sigma = 0.1$ min^{-1} in panel (a), $\sigma = 0.15$ min^{-1} in panel (b) and $\sigma = 0.2$ min^{-1} in panel (c). The diagrams allow to find the threshold value k_e above which the dynamical activity of D. *discoideum* is switched on.

where wave patterns are expected. The bifurcation behaviors of the system show clearly that the interval for active k_e is very sensitive to the change in σ, as expected, since the activity of adenylate cyclase, which produces intracellular cAMP, controls the rate at which the extracellular cAMP gets degraded. The balance between the two parameters may then play an important role in the occurrence of wave patterns.

3.1.2.2 Dynamic Media

A great deal of effort has been devoted to the study of complex spatiotemporal patterns during the last few years, which appear when a nonlinear system is driven away from the equilibrium. A variety of systems have been studied, in such diverse contexts as classical mechanics, hydrodynamics, chemistry, material science, biophysics and solid state physics [175,179,204–206]. All these systems are referred to as active media, among which excitable media are particularly important for describing many spatiotemporal patterns in biological systems. In this party, we introduce a classification of active media for the both generic features of excitable media and osscillatory, using the cAMP concentration in the colony of D.d as an example system.

The partial differential equations (2.25) describe reaction-diffusion-advection active media, which can be further classified as excitable, or oscillatory, depending on their stationary states [206]. In excitable media, each component typically has a single stationary state that is stable under small perturbations. If the perturbation exceeds a certain threshold, however, this compo-

nent produces a strong burst of activity. It undergoes a sequence of transitions and later returns to the initial state of rest. An oscillatory medium consists of elements that typically have one unstable steady state and perform stable limit-cycle. oscillations.

3.1.2.3 Excitable Dynamics

An excitable medium is a spatially distributed system of locally excitable elements. The interaction of neighboring elements by diffusive coupling can produce a number of distinctive types of wave propagation. If a local region of space is perturbed beyond the excitability threshold, then the autocatalytic production of the propagator species γ in that region causes its concentration to increase. Diffusing out into neighboring regions, it will cause the neighboring regions to exceed the threshold and thus cause the excitation to spread out. In one spatial dimension, one would observe a wave train of impulses. Two-dimensional excitable media exhibit two topologically distinct patterns: expanding concentric circular waves, called target patterns, and rotating spiral waves. In three dimensions, the corresponding spatiotemporal structures are expanding concentric spherical waves and rotating scroll waves.

There are many examples of excitable media, which support propagating waves of chemical, physical or biological activity. The most famous is the axonal membrane [207], which can support propagating electrical signals and was first characterized by Hodgkin and Huxley [208]. Other examples of biological excitable media include cardiac muscle [209–211, 222], among which epicardial, ventricular, and atrial muscle are useful for the study of the mechanism of fibrillation and tachycardia. Neuronal tissue supporting waves of spreading depression, which has been studied in rat cerebral cortex [213] and chicken retina [214], has provided insights into the mechanism of migraine disorder [215]. Another example of biochemical media includes the social amoebae Dictyostelium discoideum [216–218], a slime mold that supports waves of cyclic adenosine 3Š,5Š-monophosphate (cyclic AMP) activity. Another biological example is the Xenopus laevis oocyte [219], an intracellular milieu for studying Ca2+ signaling. Examples of chemical excitable systems including the BZ reaction [175, 179, 204–206, 220, 221] and the CO oxidation on single crystal Pt(110) [222, 223], which give rise to many kinds of spatiotemporal patterns in the excitable media. There are also many examples of macroscopic excitable media such as epidemic spreading in population biology [224–226] and spiral galaxies in the celestial system, whose rotating arms can be treated as traveling waves of star formation in an excitable medium of interstellar gas and dust [227–229]. Table 3.1 shows a comparison of some of the examples of excitable media by identifying their characteristic state variables, u and v [179, 230]. Among these excitable media, the biochemical systems have been most extensively used to study the properties of excitable media. One of the main advantages of biochemical systems is their ability to be controlled and their simplicity in comparison with biological or celestial systems. Among biochemical systems,

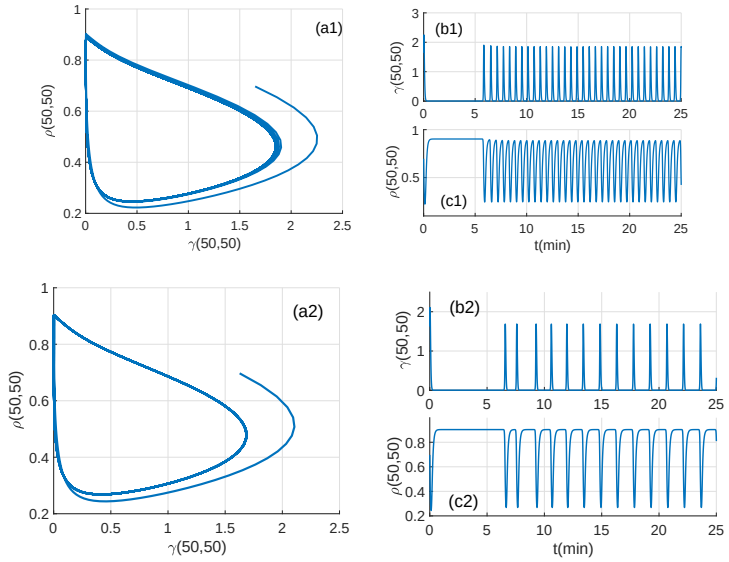

Figure 3.4: The phase portraits in the $(\gamma, \rho)-$plane are depicted in panels $(\mathrm{aj})_{j=1,2}$. Time series for cAMP concentration γ are displayed in panels $(\mathrm{bj})_{j=1,2}$, while time series for the fraction of receptors in the active state ρ are shown in panels $(\mathrm{cj})_{j=1,2}$. The features are obtained in absence of the advective flow, with $\sigma = 0.2\mathrm{min}^{-1}$ and k_e taking the values $2.8\mathrm{min}^{-1}$ $(j = 1)$ and $3.1\mathrm{min}^{-1}$ $(j = 2)$.

the D.d aggregation is the most widely studied excitable biochemical medium.

Based on the results of Fig. 3.3, the time series and phase diagrams describing the dynamics of both the cAMP concentration γ and the fraction of receptors in the active state ρ are depicted in Figs. 3.4 and 3.5. In order to get the results of Fig. 3.4, we have fixed $\sigma = 0.2\mathrm{min}^{-1}$, and values for k_e have been picked from the active region of Fig. 3.3. In this regard, Panels (a1), (b1) and (c1) of Fig. 3.4 have been obtained $k_e = 2.8\mathrm{min}^{-1}$, while panels (a2), (b2) and (c2) were obtained for $k_e = 3.1\mathrm{min}^{-1}$. The dynamics of γ and ρ is in general quasi-periodic, but with increasing the degradation rate of cAMP, the wave frequency drops. On the other hand, when the production rate of intercellular cAMP is increased to $\sigma = 0.25\mathrm{min}^{-1}$, the wave frequencies for γ and ρ increase, although there is some wave modulation for $k_e = 2.8\mathrm{min}^{-1}$, as depicted in Figs. 3.5(b1) and (c1), in the time interval $12\mathrm{min}<t<18\mathrm{min}$, followed by quasi-periodic oscillations of the concentration γ and ρ for $t < 18\mathrm{min}$. These modulations disappear when k_e increases to $3.1\mathrm{min}^{-1}$, and the wave amplitude decreases and becomes constant at $t > 12\mathrm{min}$ (see Figs. 3.5(b2) and (c2)). This shows the effect of each of the parameters, which may contribute to balance nonlinear and dispersive effects for nonlinear modes to emerge in the system. In the rest of this letter, we fixed $\sigma = 0.3\ \mathrm{min}^{-1}$ and used different values of k_e. Also, most of the simulations were recorded at time $t = 60\mathrm{min}$.

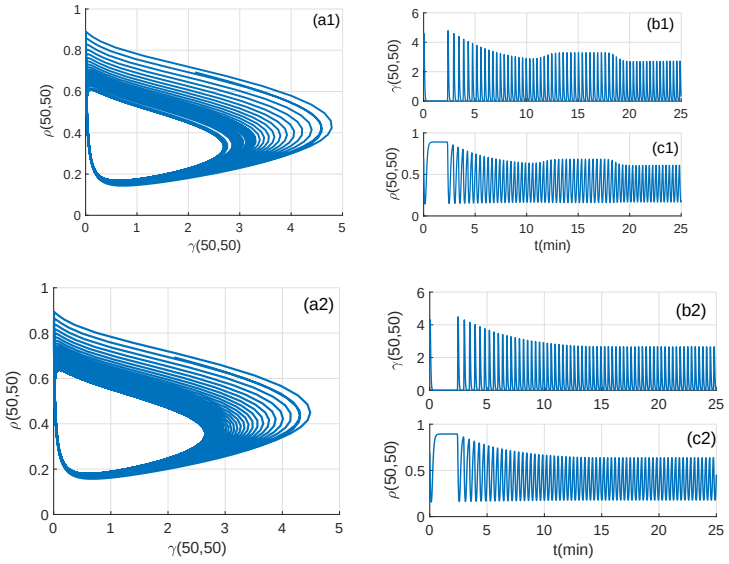

Figure 3.5: The phase portraits in the $(\gamma, \rho)-$plane are depicted in panels $(\mathrm{aj})_{j=1,2}$. Time series for cAMP concentration γ are displayed in panels $(\mathrm{bj})_{j=1,2}$, while time series for the fraction of receptors in the active state ρ are shown in panels $(\mathrm{cj})_{j=1,2}$. These results have been obtained in the absence of the advective flow, with $\sigma = 0.25\mathrm{min}^{-1}$ and k_e taking the values $2.8\mathrm{min}^{-1}$ $(j = 1)$ and $3.1\mathrm{min}^{-1}$ $(j = 2)$.

3.1.2.4 cAMP oscillations in absence of the advective flow

In absence of the advective flow, i.e., $V_f = 0$, typical examples of simulation results are given in Fig. 3.6, where panels (a), (b) and (c) correspond to the respective values 2.6 min^{-1}, $2.8\mathrm{min}^{-1}$ and $3.1\mathrm{min}^{-1}$ of k_e. Initially, as predicted by the linear stability analysis on the 2D CGL equation, the plane wave solution breaks up into wave patterns in panel (a), then forms localized patterns that are a mixed-up of unstable patterns and spiral seeds (see Fig. 3.6(b)). The later scenario tends to disappear when the degradation rate k_e increases, leading to erratic structures and sporadic bands along the boundaries of the system (see Fig. 3.6(c)). Also, one can still see some spots of high cAMP concentration that confirm the robust tendency of the amoeba to aggregate under any starvation situation.

Spiral wave is a unique self-organized and self-sustained pattern. The dynamics of the spiral wave is basically determined by its center (seed). As soon as a spiral seed emerges in the aggregation surface, the spiral wave starts to travel along expanding circular paths with some particular properties and capabilities. Since the dynamics of spiral wave is determined by its central part known as the spiral seed, we apply different values of degradation rate of extracellular cAMP (ke) the spiral seeds in three limited areas, specified in the previous section (Fig. 3.6). In this way, the maintenance or suppression of the existed spiral waves under degradation rate

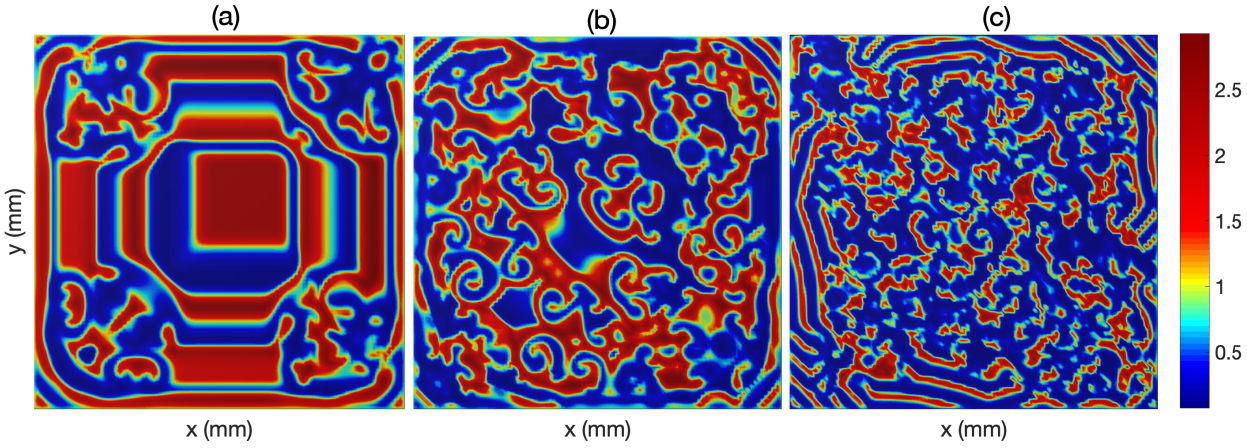

Figure 3.6: The panels show the manifestation of MI through pattern formation in absence of the external flow, for different values of the degradation rate of the intracellular cAMP k_e: (a) $k_e = 2.6\text{min}^{-1}$, (b) $k_e = 2.8\text{min}^{-1}$ and (c) $k_e = 3.1\text{min}^{-1}$, with $\sigma = 0.3\text{min}^{-1}$. All the panels have been recorded at time $t = 60\text{min}$.

of extracellular cAMP (k_e) can be investigated.The results confirm that continuance of rotating spiral seeds suffer from higher amplitude.

3.1.2.5 cAMP oscillations in present of the advective flow

We now consider a flow that goes from left to right, in the $x-$direction. Figs. 3.7(aj)$_{j=1,2,3}$ show the corresponding spatiotemporal behaviors of the dimensionless concentration of cAMP for $k_e = 2.6\text{min}^{-1}$, which corresponds to the case of Fig. 3.6(b). Panels (aj)$_{j=1,2,3}$ have been recorded, respectively, from left to right, for the flow velocities $V_f = 0.2\text{mm.min}^{-1}$, 1mm.min^{-1} and 1.8mm.min^{-1}. Obviously, the disintegration of the initial plane wave importantly depends on the imposed flow velocity. For example, in Fig. 3.7(a1), cooperative patterns appear in the system for $V_f = 0.2\text{mm.min}^{-1}$, with large spots of high cAMP concentration. By increasing the flow velocity to 1mm.min^{-1}, one obtains the wave patterns of Fig. 3.7(a2), characterized by trains of upstream peaks with flat tops, followed by a zone of erratic patterns of high cAMP concentration. Additionally, one can notice the disappearance of the spiral seeds, which corroborate the fact that advective flows are not favorable to spiral wave formation. This gets more pronounced in Fig. 3.7(a3), with $V_f = 1.8\text{mm.min}^{-1}$. This phenomenon, to our modest opinion, may be due to the fact that the production rate of cAMP being unchanged, the degradation rate which is increased, along with the flow velocity, brings about important changes in the balance between nonlinear and dispersive effects, and therefore affects the process of MI. This suitably agrees with the patterns of Figs. 3.7(bj)$_{j=1,2,3}$, where the degradation rate k_e has been increased to 3.1

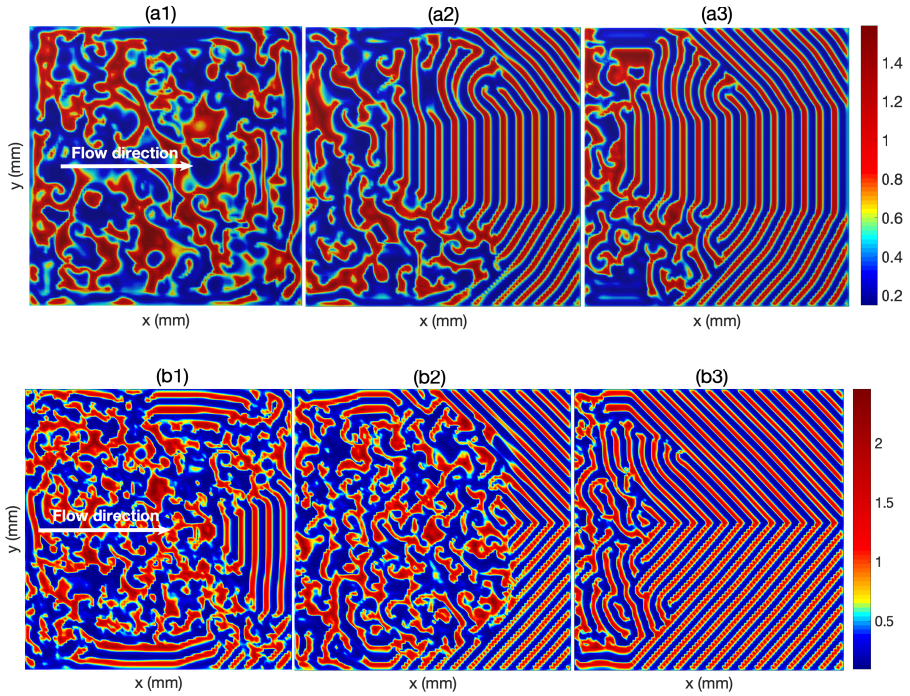

Figure 3.7: Two-dimensional patterns of cAMP concentration $\gamma(x, y, t)$. Panels $(\text{aj})_{j=1,2,3}$ show results for $k_e = 2.6\text{min}^{-1}$ and panels $(\text{bj})_{j=1,3}$ correspond to $k_e = 3.1\text{min}^{-1}$. From left to right, panels in each set correspond respectively to $V_f = 0.2\text{mm.min}^{-1}$, 1mm.min^{-1} and 1.8mm.min^{-1}, with $\sigma = 0.3\text{min}^{-1}$ and $t = 60\text{min}$.

min^{-1}. As in the previous case, the flow velocity takes the same values and increases from left to right. This case corresponds to Fig. 3.6(c), in absence of the advection flow. Obviously, the propagating cAMP waves respond to the flow. In this case, the spectrum of behaviors obtained in Fig. 3.7 remains, except that the trains of upstream peaks acquire a triangular shape, as a response to the high velocity of the flow. This was already predicted numerically by Edwards [231] and confirmed experimentally by Leconte et al. [232] in the case of an autocatalytic reaction. In general, when the flow velocity increases, the wave patterns are restrained to the left area of the medium, where there are probably multiple interactions between the upstream peaks and other types of patterns that are due to the instability of the initial plane wave solutions. Remarkably, all such modes of oscillation can be obtained through the activation of MI, but their long-time behaviors cannot be predicted by the linear stability analysis. However, when wave parameters are well-chosen in the area of instability, one expects some correlation between the analytical and numerical calculations, which is, once more, satisfactorily confirmed by the above-discussed results.

3.1.3 Concluding remarks

In this letter, the collective behavior of D. discoideumwas studied. During starvation, D. discoideum amoeba release periodic spikes of cAMP in response to extracellular cAMP levels and interact by propagating cAMP waves throughout space. Starting with the pioneering work by Martiel and Goldbeter [2], there has been several contributions on modeling the D. discoideum signaling network. We have considered the same model in the present work. We have shown that the reaction-diffusion equations modeling the chemical cAMP concentration and cAMP receptors, can be reduced to a CGL equation, on which we conducted the linear stability analysis of MI. Regions of parameters that support the MI process have been discussed via the MI growth rate. Additionally, numerical simulations have been performed in a square channel and two oscillation cases have been considered:(i)cAMP oscillations in absence of the advective flow and (ii) in presence of the flow. In the absence of the flow, we considered as control parameters the production rate of intercellular cAMP (σ) and degradation rate of extracellular cAMP (k_e) that are among important parameters governing the system dynamics. In the first case, in agreement with the calculations on the CGL equation, the plane wave solutions were found to disintegrate into wave patterns, that are very sensitive to the change in control parameters. In that context, we obtained erratic patterns and spiral seeds. On the other hand, in presence of the flow, especially when the flow velocity was increased, an instability appeared, which generated wave trains upstream, followed again by erratic patterns. For some values of the degradation rate of extracellular cAMP, one obtained upstream traveling peaks of different shapes, which is in agreement with several experiments. In fact, Gholami and coworkers already obtained such results either through experiment [27] or through direct numerical simulation [28]in straight microfluidic devices, where flow-driven waves with a parabolic and triangular flow profiles were reported. Under fast advective flows, Eckstein et al. [30] compared numerical and experimental results on pattern formation of self-organizing D. discoideumamoeba in a microfluidic setup, using a modified MG model, for a better understanding of the aggregation process, through waves patterns of cAMP of D. discoideumin its natural environment. However, our approach has shown that MG equations, when parameters related to MI are well-chosen, the same wave patterns of D. discoideum aggregation can be retrieved, which once more confirms their robustness in the studied system, and may give some substantial hint in this research field. In the next Section, we study different mode frequency in process aggregation of dictyostelium discoideum cells.

3.2 Complex patterns in Dictyostelium discoideum cells with frequency mode excitations

The linear stability analysis being carried out on the CGL Eq.(2.59) has revealed the existence of two frequency regimes in a two-dimensional FitzHugh-Nagumo Dictyostelium discoideum amoebae model , under the activation of MI phenomenon. In this section, we present the analitycal solutions instability diagrams from the function $\Gamma(K_1, K_2)$ which represents the MI gain, also the numerical solutions for two frenquency mode.

3.2.1 Analytical features of MI

In this part we are interested in the features of the MI growth rate $\Gamma(K_1, K_2)$, in Fig.3.8, we plot the growth rate of instability in the plane (K_1, K_2) both for the HF and LF regimes. The panels $((aj) - (bj)_{j=1,2})$ correspond to HF MI. For both cases, we have fixed $p = 0.25\pi$ and, on changing k_g. In the HF regime,for $k_g = 4.7$ and $k_g = 5$, increasing the region of instability in form X-shape. The panels $((cj) - (dj)_{j=1,2})$ correspond to LF MI. the region of instability increasing in form circular for both k_g values. One common behavior appears for $k_g = 4.7$ growth rate rather displays circular unstable regions, also unstable wave patterns are expected for $-0.29\pi < K_2 < 0.29\pi$ and $-0.11\pi < K_1 < 0.11\pi$ (see Fig.3.8$(c_1) - (d_1)$). On increasing $k_g = 5$ the region of instability increasing for $-0.31\pi < K_2 < 0.31\pi$ and $-0.12\pi < K_1 < 0.12\pi$ (see Fig.3.8$(c_2) - (d_2)$). This show that the patterns formation depend of frequency mode and the production rate of cAMP extracellular.

3.2.2 Numerical analysis of MI

From the linear stability analysis, we have performed direct numerical simulations. However, the analysis give a clear idea on the regions of parameters where pattern formation may be observed. The two dimensional FitzHugh-Nagumo model of Eqs. (2a) and (2b) has been used in the simulations, with the initial conditions being the perturbed plane waves, with wavenumbers $K_1 = 0.18\pi$ and $K_2 = 0.52\pi$ belonging to the instability areas depicted in Figs. 3.8 These equations have been integrated using the fourth-order Runge- Kutta computational scheme, with a time step $\Delta t = 5 \times 10^{-2}$ and space step $\Delta x = \Delta y = 1 \times 10^{-1}$, no-flux boundary conditions have been considered in the Merson modification. The reason for choosing such initial conditions is to observe the dynamics imposed to the system by the MI of two frequency regime.

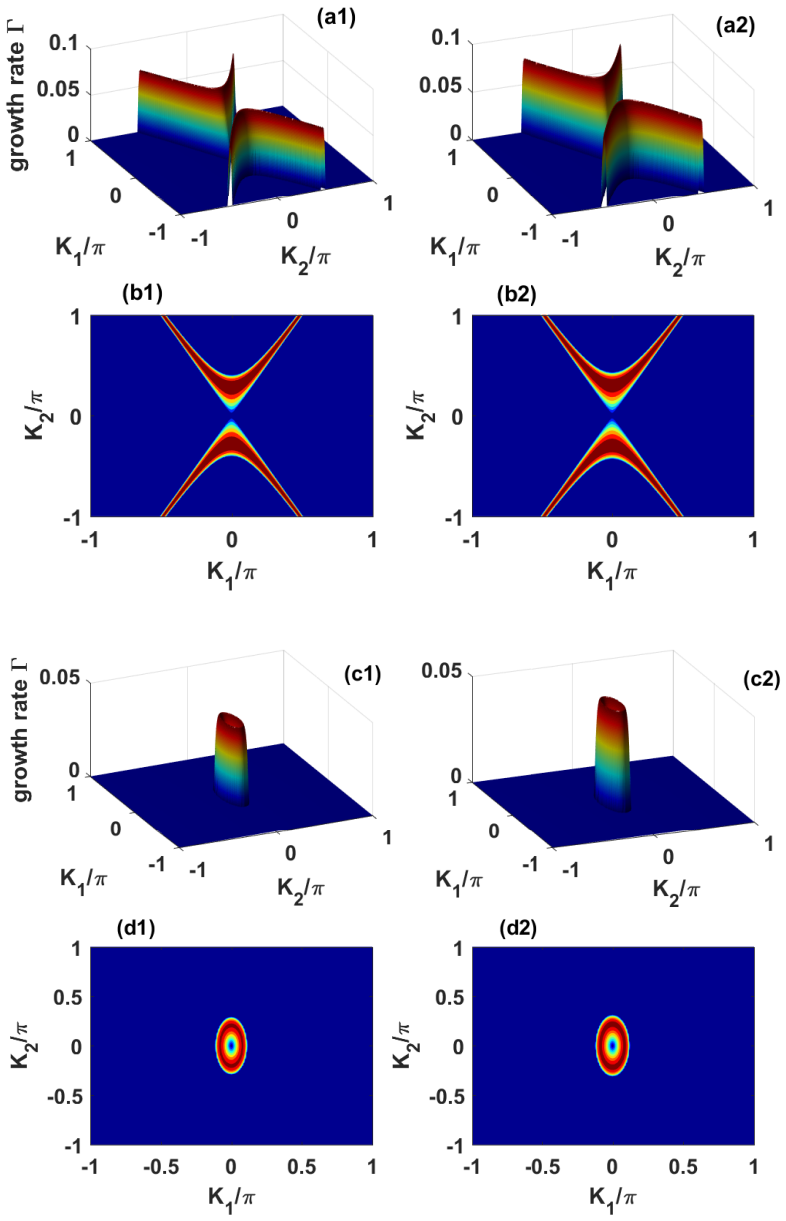

Figure 3.8: The MI growth rate instability $\Gamma(K_1, K_2)$ versus the waves number K_1 and K_2. Panels $((aj) - (bj)_{j=1,2})$ and $((cj) - (dj)_{j=1,2})$ corresponding for HF and LF regimes. We have fixed $p = 0.25\pi$, $\phi_0 = 0.1$ $k_r = 1.5$, $a = 0.05$ and $D_{0X} = D_{0Y} = 2$, with k_g taking respectively the values 4.7 $((a)_1 - (c)_1)$ and 5 $((a)_2 - (c)_2)$, the same for the stability/instability diagrams, where red regions are for instability and the blue ones are those where the plane wave solution is expected to remain stable under modulation.

3.2.2.1 The synchronization factor R

The synchronous and asynchronous behavior of a system, is one phenomenon significant in physics for understanding waves in different mediums. Here we numerically analyze the behavior of certain parameter according to the synchronization factor R. In this framework the spatial synchronization factor R [233–235] is adopted and calculated as follow:

$$R = \frac{\langle F^2 \rangle - \langle F \rangle^2}{\frac{1}{N}\sum_{n=1}^{N}[\langle x_n(t)^2 \rangle - \langle x_n(t) \rangle^2]} \tag{3.2}$$

With $F = \frac{1}{N}\sum_{n=1}^{N} x_n(t)$

where $\langle \cdot \rangle$ denotes the time averaging. The value of R is between 0 and 1, and it increases with decreasing average cAMP concentration errors. That is to say, perfect synchronization is realized when the synchronization factor is close to 1 and non-perfect synchronization is reached when the factor of synchronization is close to 0. Recently, much of the studies carried out to understand coordination between the amoebas through the diffusion to synchronize of cAMP oscillation [236, 237]. Here, in order to study the stability of spiral waves, the synchronization factor R is highlighted according to certain parameters of control for know the fields of appearance of the spirals waves , when a value close to zero of this function suggests the emergence of spiral waves in the medium, whereas a value of R close to unity supposes the absence of blocking waves to the detriment of synchronous patterns in the network [238].

Fig.3.9, we plot synchronization factor R versus parameter k_g for the HF and LF regimes. The panel Fig.3.9(a) correspond to HF regime, R tend to 0 although for some values $k_g \in [4.7 - 5.15]$ of this parameter. In this interval the oscillations of the cAMP concentrations of n-cell become asynchronous, while for $k_g > 5.15$ R tend to 1 the patterns tend to synchronize itself. In the LF regime R tend to 1 for different values of $k_g \geq 4.7$, The oscillations of the cAMP concentrations show synchronous behavior.

Figure 5 and 6 describes different features of the cAMP concentration, both for the HF and LF modes. In figure 5, The Figure 6 the time series is plot to the LF mode, the panels ((a)-(c)) display a behavior quasi-synchronous in times, this that produces target waves in the region of aggregation.

3.2.2.2 Patterns cAMP waves in HF mode

In this part, the behavior of cAMP waves represented in HF frequency mode. we plot Time series of cAMP concentration $g(n, m, t)$ according to the HF mode at various node (200,200) for line blue and (350,350) line red; the periods and amplitudes of waves propagating varying when

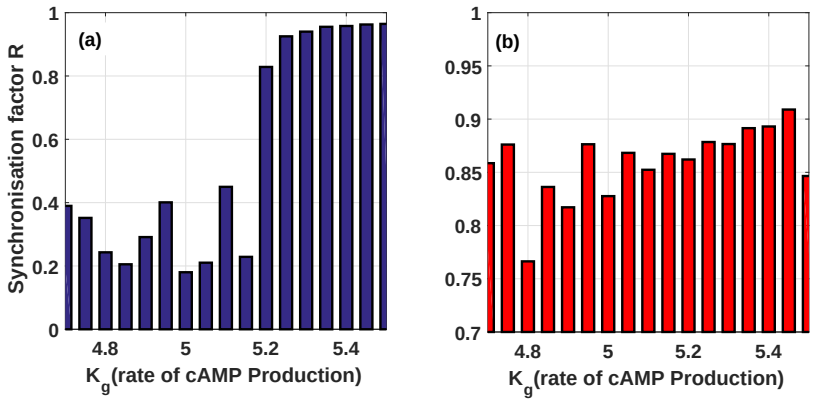

Figure 3.9: Bands diagrams of synchronisation factor R versus the rate of cAMP production k_g for both HF (a) and LF (b) modes. (a) when $k_g \in [4.7 - 5.15]$ the feature illustrates asynchrony state of oscillations cAMP concentration as R decreases towards 0, at $k_g > 5.15$ the cAMP oscillations stretch at this synchronized when R increasing. (b) synchronisation factor R is raising the cAMP oscillations illustrates the values synchronous in their propagating. We have fixed $k = 0.25\pi$, $k_r = 1.5$, $a = 0.05$, $\tau = 4.8$, $D_x = 2$ and $D_y = 2$.

k_g decreasing (see fig 3.10(a-c)), this predicts that an initial target wave would encounter an obstacles in the region of aggregation, which leads to the birth of multi-spiral waves. In Fig.3.11, the spatiotemporal structures of cAMP waves are depicted in the (n, t)-plane for different values of the cell number m = 100, 200 and 350, corresponding respectively to panels 3.11((A)-(I)) in HF mode. Therein, we observe the emergence of nonlinear asynchronous patterns which are scattered in the cAMP concentration. Such asynchronous structures could be considered as the true precursors of spiral waves. How do planes waves break up to form spirals ? When cAMP waves collide they annihilate, since cells on both sides of a wave are refractory to cAMP stimulation. Thus, collision between two waves cannot explain the origin of spirals. Rather, they form when a new pulse is emitted shortly after a wave has passed. When this happens, double spirals form Fig.3.12. The features of Fig.3.12 show how the multi-spirals waves are developed in the region of aggregation through the spatiotemporal dynamics of cAMP waves in the (n,m)-plane at different time in FH mode. When we vary the production rate of $g(n, m, t)$ with time we observe a different excitability: $k_g = 5$ in 3.12((A)-(C)), $k_g = 4.86$ in 3.12((D)-(F)) and $k_g = 4.7$ in 3.12((G)-(I)).

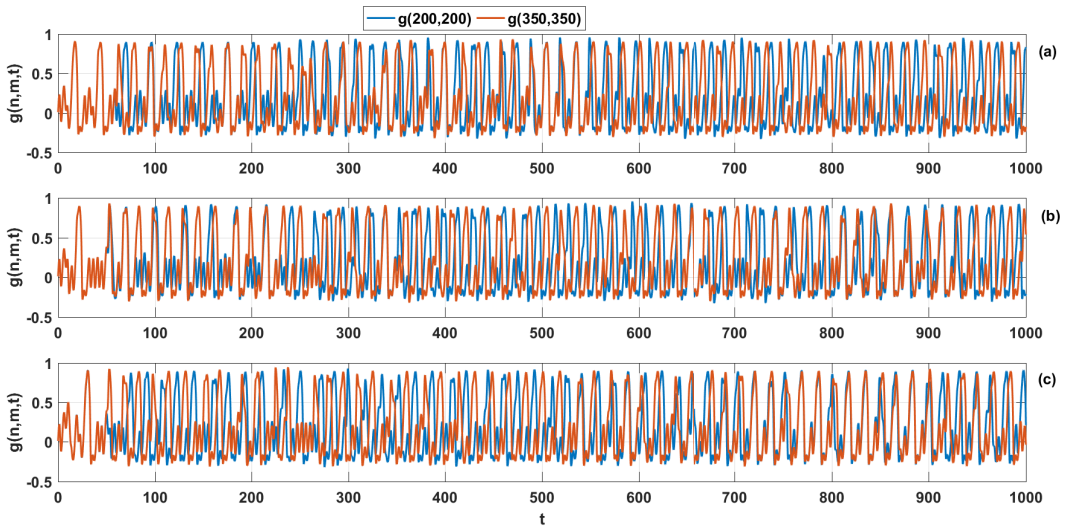

Figure 3.10: Time series of cAMP concentration $g(n, m, t)$ according to the HF mode at various node (200,200) for line blue and (350,350) line red. We varying the parameter k_g from top to bottom as: (a) $k_g = 5$, (b) $k_g = 4.86$, (c) $k_g = 4.7$. We have fixed $k = 0.25\pi$, $k_r = 1.5$, $a = 0.05$, $\tau = 4.8$, $D_x = 2$ and $D_y = 2$.

3.2.2.3 Patterns cAMP waves in LF mode

In order to be convinced of the existence of such patterns, the time series of cAMP concentration in node (200,200) for line blue and (350,350) line red displayed in Fig. 3.13 in LH mode. the periods and amplitudes of waves propagating varying when k_g decreasing (see fig 3.13(a-c)). We observed the nonlinear patterns in the cAMP concentration. the fig.3.14 confirmed the diagrams of fig.3.13, what show the reappearance of a nonlinear patterns no break in times and suggests the absence of spiral waves within the system, while target waves are expected(see. fig.3.14((A)-(I))). In panels 3.15 The patterns in the LF mode forme the unstable and target waves when k_g with time vary (see. Fig.3.15((A)-(I))). $k_g = 5$ in 3.15((A)-(C)), $k_g = 4.86$ in 3.15((D)-(F)) and $k_g = 4.7$ in 3.15((G)-(I)).

3.2.3 Concluding remarks

In summary this study focused on the propagation of cAMP waves in two-dimensional FHN model. For this purpose, we have shown using the analytical analysis that, there are two propagation frequency regimes of the cAMP waves in colony of Dd amoebae, the HF and the LF regimes. Key experiments published independently in 1975 by two groups showed that cAMP signals in Dictyostelium are frequency encoded. In a mutant of D. discoideum unable to aggregate, cAMP pulses administered at the physiological frequency of one pulse every 5 min are capable of rescu-

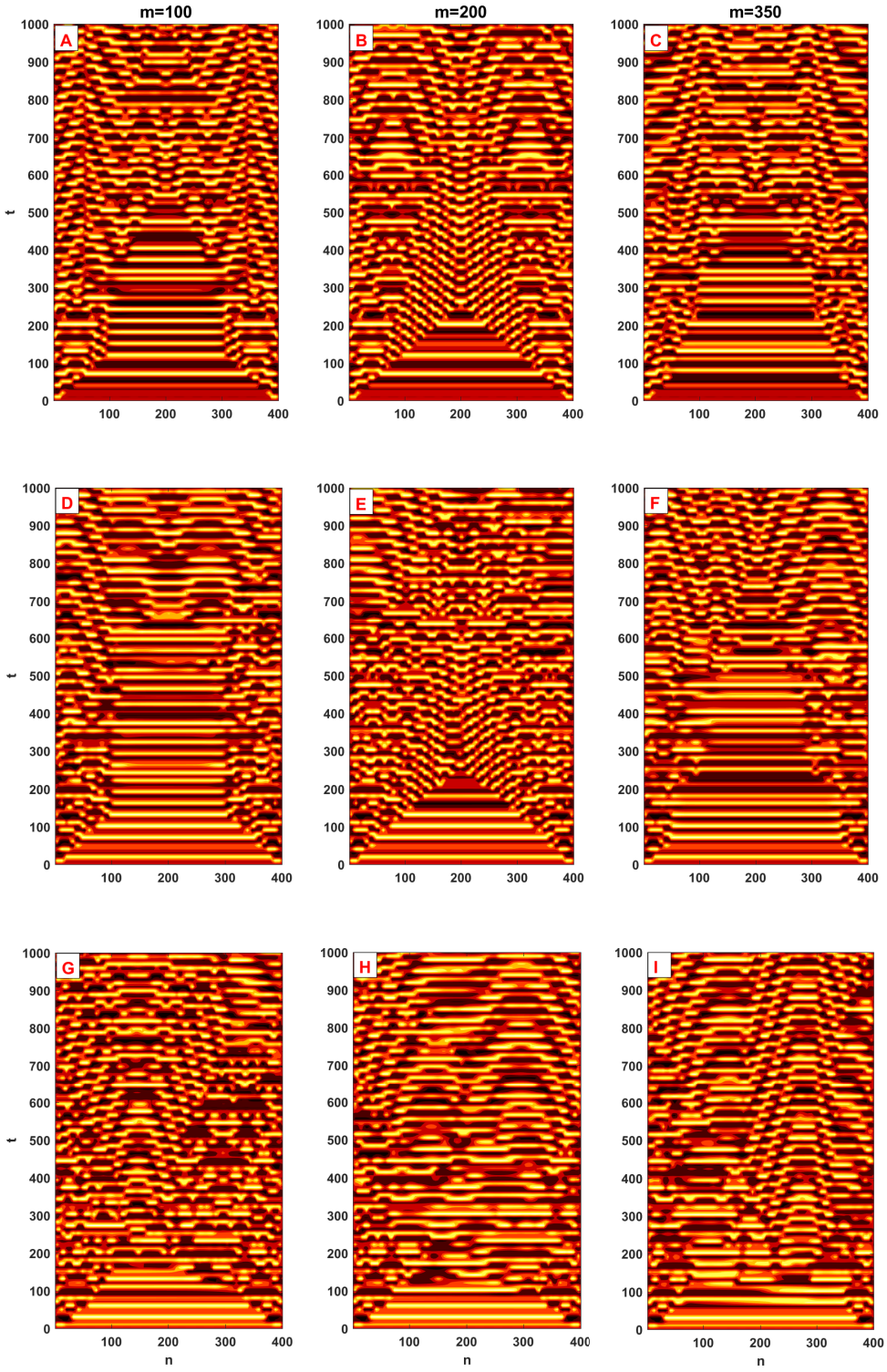

Figure 3.11: Space-time plots of cAMP concentration $g_{n,m}(t)$ in $(n,t)-$ plane according to the HF mode, under the change of the $m-space$ in the tranverse direction as $m = 100$ in columns (A), $m = 200$ in columns (B) and $m = 350$ in columns (c). We have fixed $k = 0.25\pi$, $k_r = 1.5$, $a = 0.05$, $\tau = 4.8$, $D_x = 2$ and $D_y = 2$. We varying the parameter k_g from top to bottom as: line (A) $k_g = 5$, line (D) $k_g = 4.86$, line (G) $k_g = 4.7$.

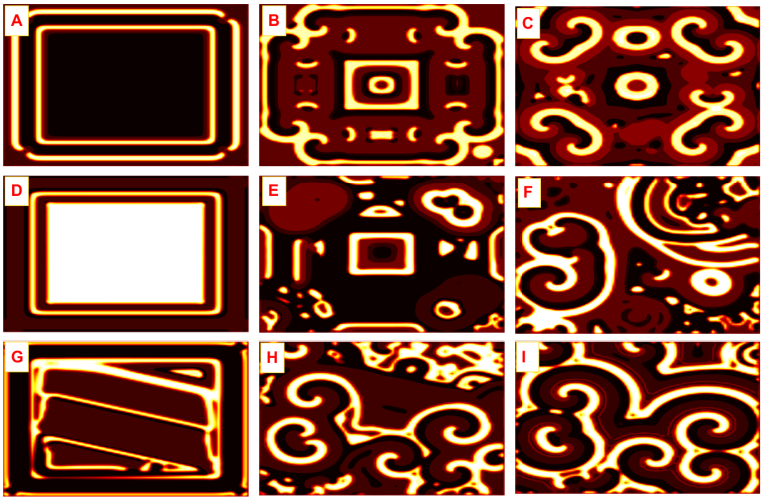

Figure 3.12: Space-temporal patterns of cAMP concentration $g_{n,m}(t)$ in 400×400 according to the HF mode array at different times: $t = 100$ in columns (A), $t = 500$ in columns (B) and $t = 900$ in columns (c). We have fixed $k = 0.25\pi$, $k_r = 1.5$, $a = 0.05$, $\tau = 4.8$, $D_x = 2$ and $D_y = 2$. We varying the parameter k_g from top to bottom as: line (A) $k_g = 5$, line (D) $k_g = 4.86$, line (G) $k_g = 4.7$.

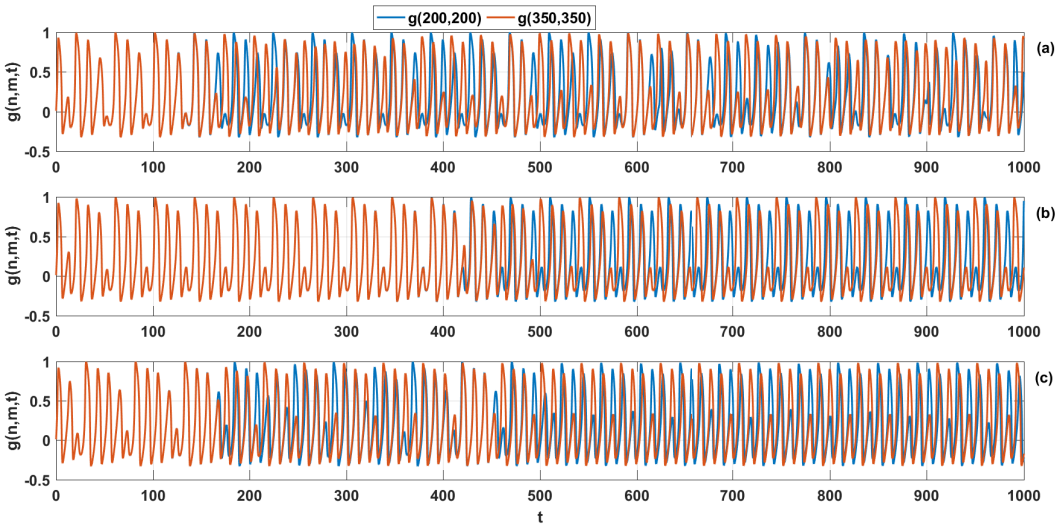

Figure 3.13: Time series of cAMP concentration $g(n, m, t)$ according to the LF mode at various node (200,200) for line blue and (350,350) line red. We varying the parameter k_g from top to bottom as: (a) $k_g = 5$, (b) $k_g = 4.86$, (c) $k_g = 4.7$. We have fixed $k = 0.25\pi$, $k_r = 1.5$, $a = 0.05$, $\tau = 4.8$, $D_x = 2$ and $D_y = 2$.

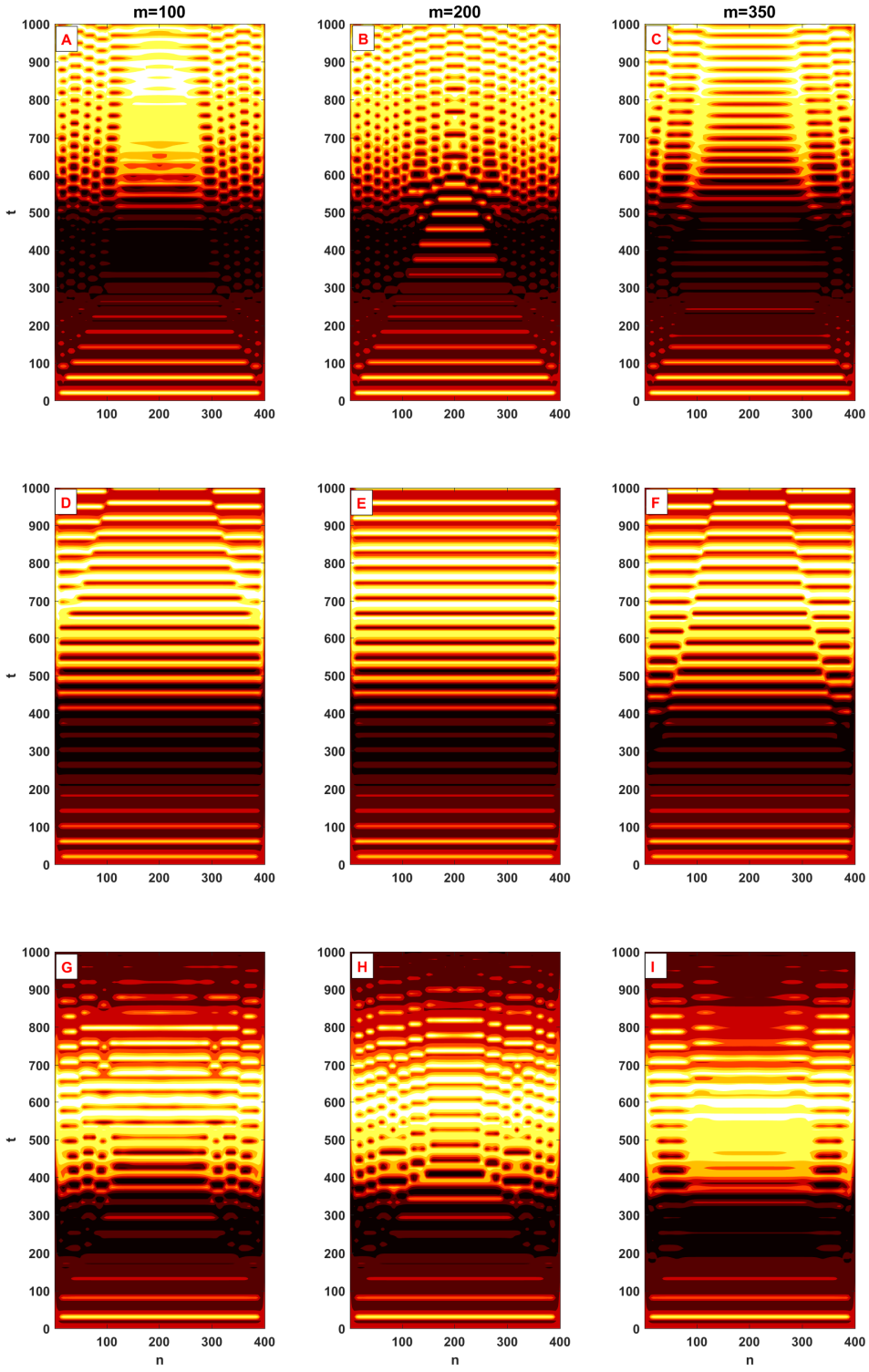

Figure 3.14: Space-time plots of cAMP concentration $g_{n,m}(t)$ in $(n,t)-$ plane according to the LF mode, under the change of the $m-space$ in the tranverse direction as $m = 100$ in column (A), $m = 200$ in column (B) and $m = 350$ in column (c). We have fixed $k = 0.25\pi$, $k_r = 1.5$, $a = 0.05$, $\tau = 4.8$, $D_x = 2$ and $D_y = 2$. We varying the parameter k_g from top to bottom as: line (A) $k_g = 5$, line (D) $k_g = 4.86$, line (G) $k_g = 4.7$.

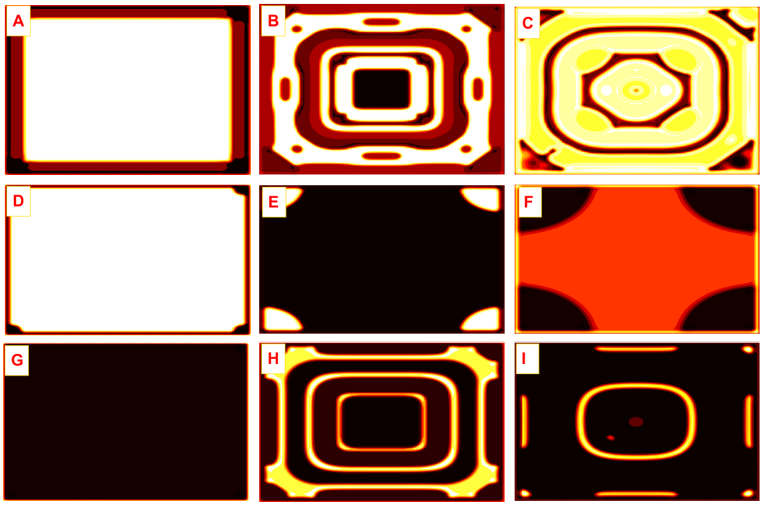

Figure 3.15: Space-temporal patterns of cAMP concentration $g_{n,m}(t)$ in 400×400 according to the LF mode array at different times: $t = 100$ in columns (A), $t = 500$ in columns (B) and $t = 900$ in columns (c). We have fixed $k = 0.25\pi$, $k_r = 1.5$, $a = 0.05$, $\tau = 4.8$, $D_x = 2$ and $D_y = 2$. We varying the parameter k_g from top to bottom as: line (A) $k_g = 5$, line (D) $k_g = 4.86$, line (G) $k_g = 4.7$.

ing the mutant and lead to multicellular aggregation [240]. In contrast, continuous stimulation by cAMP does not lead to aggregation. In the wild type, the administration of cAMP pulses after starvation accelerates development in the phase leading to aggregation. This effect is obtained with cAMP pulses delivered every 5 min but not when the interval between pulses is reduced to 2 min, or when the cAMP signal becomes continuous [39]. Pulses of cAMP administered at random intervals in wild type are likewise less effective [40]. These observations demonstrate the importance of the frequency of pulsatile cAMP signals. In fact, cAMP oscillations are electrical activities that take place by the receptors cells of cAMP at different frequencies divided into two bands: LH and HF bands. Moreover, we found that under some conditions and values of generic parameters, the two regimes might share a few common instability/stability regions. In this respect, the cAMP concentration, in the HF and LF regimes, has been found to display not only envelopes and asymmetric envelopes solitons, but also trains of waves, whose biological implications in aggregation process has been discussed. The effect of the k_g parameters has also been debated, and the solutions found have appeared to be sensitive to two-dimensional diffusive effects. Our results suggest that in the aggregation process of dictyostelium discoideum amoeba the chemotaxis movement of cells through cAMP pulsation occurs in two frequency modes. HF mode produces multi-spiral waves (medium more excited) and LH mode gives unstable or target waves (medium less excited).

3.3 Long-range interaction of multi-spiral cAMP waves in Dictyostelium discoideum aggregation.

The long-rang interaction of cAMP spiral waves is studied in the process of aggregation of dictyostelium discoideum cells. Numerically, we find the values range of external periodic signal that support the formation of long-range instabilities patterns within the network. Moreover, the main features of cAMP waves are found to be qualitatively and quantitatively altered by the change of the long-range parameter.

3.3.1 Numerical results

Our numerical computations were performed on the generic model (2.33) using the fourth-order Runge-Kutta computational scheme with, $N \times M = 200 \times 200$ the total number of Dd amoebae cells in the network, J = 10 the interaction range, $\Delta t = 0.05$ the time step and no-flux boundary conditions, $g(N+j,m) = g(N+j-1,m)$, $g(1-j,m) = g(2-j,m)$, $g(n,M+j) = g(n,M+j-1)$, $g(n,1-j) = g(n,2-j)$ have been adopted as well as for the variable r of indexes n, m and j. Throughout the simulations, we fix $f_0 = 1$, A_0 and $k_g = 4.72$ and We use the parameter s as the bifurcation parameter. The values of the parameters k_g, s and A_0 in the interval where the system is in an asynchronous state is obtained by using the synchronization factor [239, 241]. Fig.3.16 diagrams synchronization factor R versus parameters k_g (Fig.3.16a), s (Fig.3.16b) and A_0 (Fig.3.16c). Fig.3.16a shows that the synchronization factor R decreases when the value of k_g increases. Explicitly the value of kg in the interval of $[4-6]$ presents an asynchronous system in the cAMP concentration. the LR parameter s shows a weak synchronization factor when s varies in the interval $[2-10]$, an increase for $s = 1$, which leads to an asynchronous state diffused completely in the cAMP concentration (see Fig.3.16b). In Fig.3.16c when $A_0 \in [0.25-0.65]$ the feature illustrates asynchrony state of oscillations cAMP concentration as R decreases towards 0, the cAMP oscillations stretch at this synchronized when R increasing for $k_g < 0.25$ and $k_g > 0.65$.

3.3.1.1 stability of multi-spiral waves under effects of weak LRI

Here, we fix the long-range parameters $s = 10$. In the weak LRI the results suggests that by the voice of cAMP signalization, the amoebas communicate thanks to the nearest-neighbor connections, in various sites of aggregation. The time series of extracellular cAMP concentration displayed in Fig.3.17 are consistent with the results of Fig.3.16, the curves of cAMP concentration at the different nodes $(100, 100)$ and $(150, 150)$ displays oscillations shape without any change, but with varying periods and amplitudes. Fig.3.17(D) the feature shows for a weak LR parameter

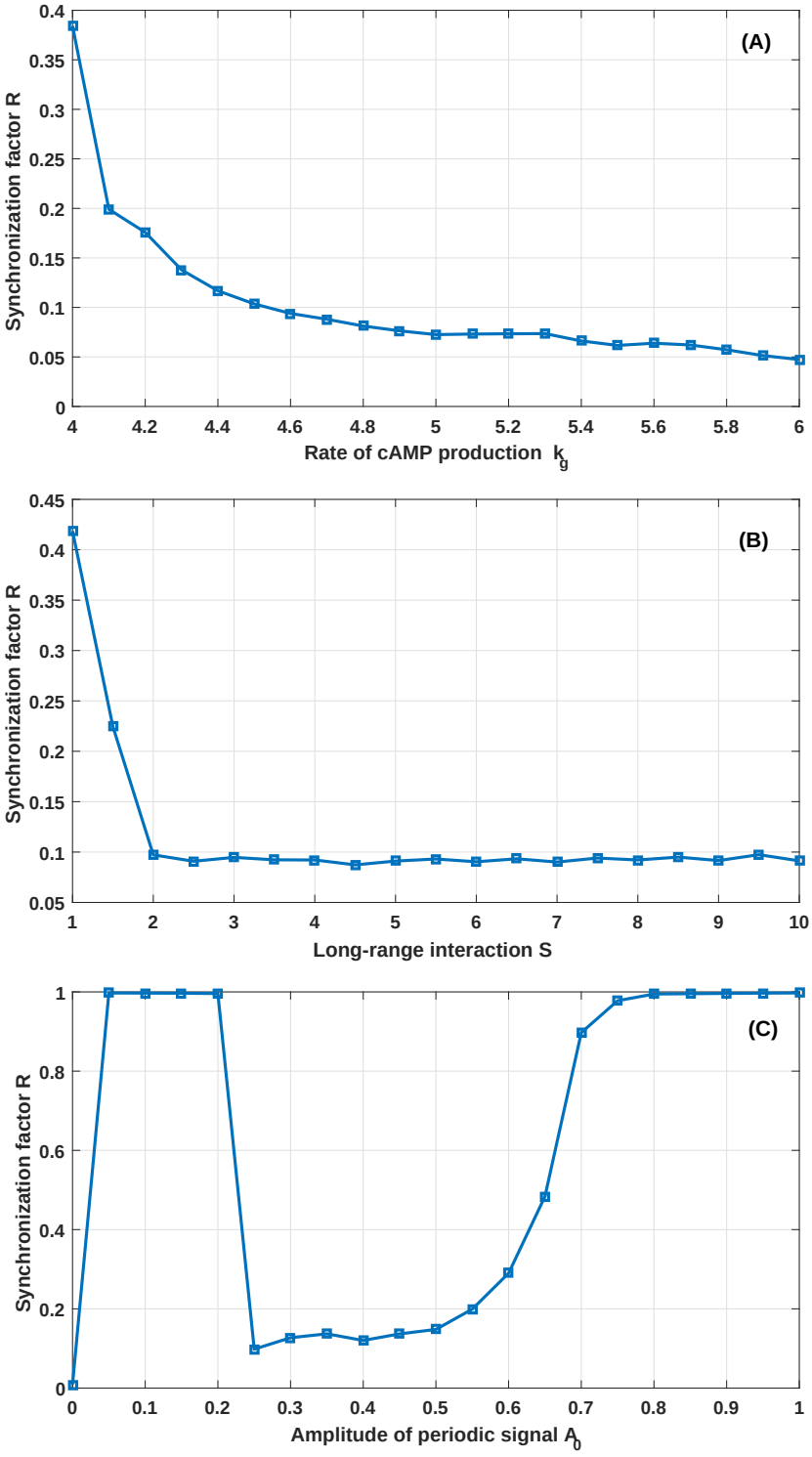

Figure 3.16: Bands diagrams of synchronisation factor R versus the rate of cAMP production k_g panel (A), long-range interaction parameter s panel (B) and amplitude of periodic signal A_0 panel (C). We have fixed $f_0 = 1$, $k_g = 4.72$ $k_r = 1.35$, $a = 0.05$, $\tau = 4.82$,and $D = 0.26$.

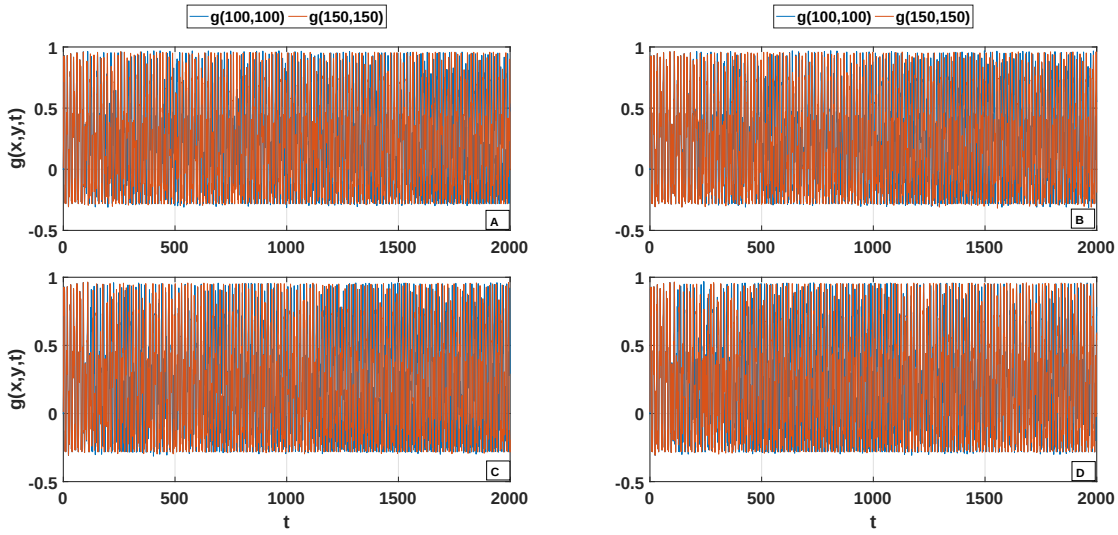

Figure 3.17: Time series of cAMP concentration $g_{n,m}(t)$ recorded for node (100,100) for line blue and (150,150) line red. We varying the long-range parameter s from top to bottom as: (A) $s = 0$, (B) $s = 1$, (C) $s = 3$, (D) $s = 10$. We have fixed $A_0 = 0.38$, $f_0 = 1$, $k_g = 4.72$, $k_r = 1.35$, $a = 0.05$, $\tau = 4.82$, and $D = 0.26$. The values of A_0 and k_g were selected in agreement with the synchronization diagrams of FIG.1.

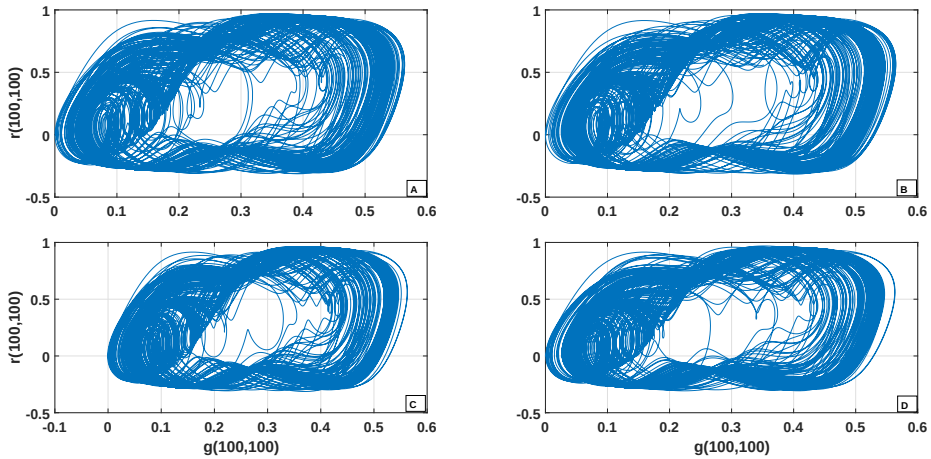

Figure 3.18: The phase portraits show the evolution of the cAMP concentration g versus the the number of desensitized cAMP receptors r while considering node (100,100). We varying the long-range parameter s from top to bottom as: (A) $s = 0$, (B) $s = 1$, (C) $s = 3$, (D) $s = 10$. We have fixed $A_0 = 0.38$, $f_0 = 1$, $k_g = 4.72$, $k_r = 1.35$, $a = 0.05$, $\tau = 4.82$, and $D = 0.26$. The obtained features reflect the same scenarios as in FIG.2. The chaotic attractorlike profiles of these features highly predict the asynchronous states within amoebae population.

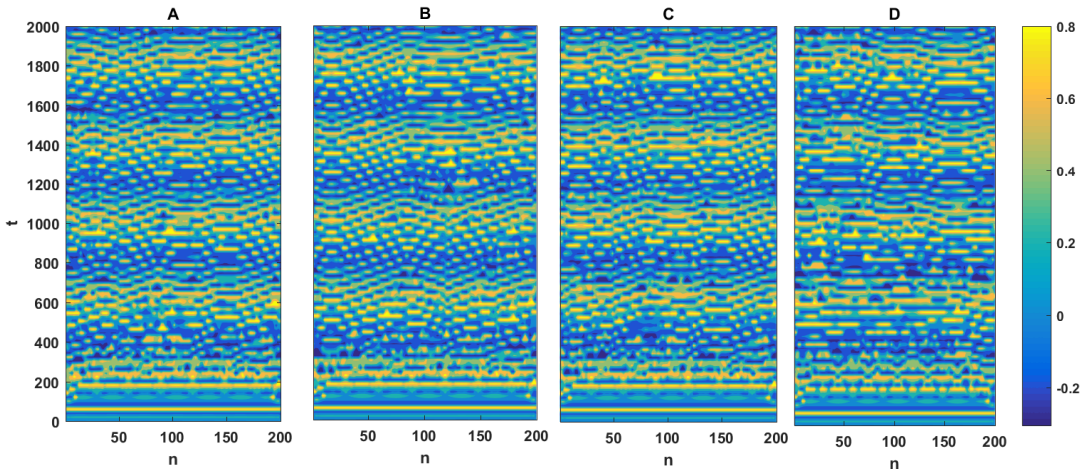

Figure 3.19: Spatiotemporal patterns of cAMP concentration $g_{n,m}(t)$ in (n,t)-plan under the change of the cell number m in the transverse direction as m = 50 in panel (A), m = 100 in panel (B), m = 150 in panel (C) and m = 180 in panel (D). The features are obtained in the case of strong LR $s = 10$. We observe the emergence of nonlinear patterns by random pulsations.

$s = 10$, shows a variation of the period of different the nodes oscillates in an asynchronous stat. The panel of Fig.3.18(D) depicting the phase portraits in $g-r$ plane allow to predict the collective dynamical behavior of one hundred cells in the network under the same scenarios as in Fig.3.17. The obtained irregular attractors which is especially sensitive to the change of parameter s predict the asynchronous states in the network. In Fig.3.19, Spatiotemporal structures of cAMP concentration $g_{n,m}(t)$ in (n,t)-plan for different values of the cell number $m = 50, 100, 150, 180$ corresponding respectively to panels (A), (B), (C) and (D). Therein, we observe the emergence of nonlinear asynchronous patterns which are scattered in the network. Such asynchronous structures could be considered as the true precursors of multi-spiral waves. In Fig.20(A)-(D), the features show evolution at times of multi-spirals waves cAMP concentration $g_{n,m}(t)$ for $s = 0$. In fact, weak LRI produces the emergence of multi-spiral waves-like patterns which from randomly firing amoebae [242]

3.3.1.2 stability of multi-spiral waves under effects of Coulomb LRI

In this section we consider successively the Coulomb LRI, i.e $s = 3$. The time series of extracellular cAMP concentration displayed in Fig.3.17 C are consistent with the results of Fig.3.16 C, the curves of cAMP concentration at the different nodes $(100, 100)$ and $(150, 150)$ displays oscillations shape without any change, but with varying periods and amplitudes. Fig.3.17(C) the feature shows for a weak LR parameter $s = 3$, shows a variation of the period of different the

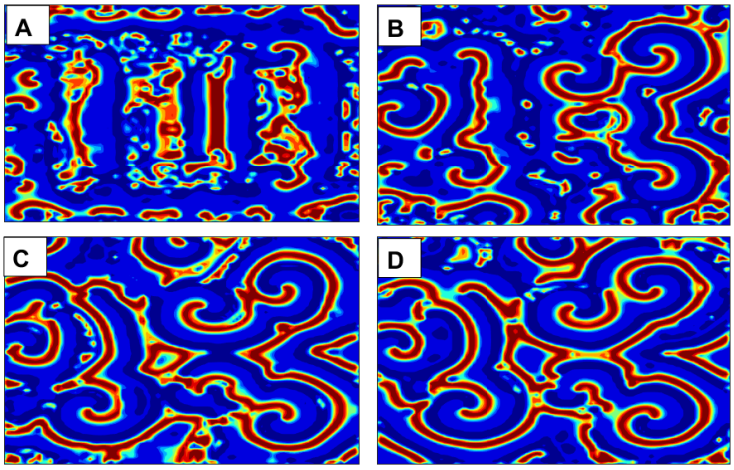

Figure 3.20: Evolution of multi-spirals waves cAMP concentration $g_{n,m}(t)$ in 200×200 cells array at different times:(A) $t = 500$, (B) $t = 1000$, (C) $t = 1500$ and (D) $t = 1800$. The features are obtained in the case of weak interaction $s = 10$. We have fixed $f_0 = 1$, $k_r = 1.35$, $a = 0.05$, $\tau = 4.82$, $D = 0.26$. As time increases, the spatiotemporal dynamics of cAMP concentration in medium becomes more excitable.

nodes oscillates in an asynchronous stat. The panel of Fig.3.18(C) depicting the phase portraits in $g - r$ plane allow to predict the collective dynamical behavior of one hundred cells in the network under the same scenarios as in Fig.3.17. In Fig.3.21, Spatiotemporal structures of cAMP concentration $g_{n,m}(t)$ in (n,t)-plan for different values of the cell number $m = 50, 100, 150, 180$ corresponding respectively to panels (A), (B), (C) and (D). Therein, We observe the emergence of asynchronous structures which are localized in some space regions over the time. In Fig.22(A)-(D), the features show as time increases, we observed inhibition in the excitable medium of cAMP concentration. $g_{n,m}(t)$ for $s = 3$, the Wavelength tend at increasing.

3.3.1.3 stability of multi-spiral waves under effects of strong LRI

In the case of strong LRI, i.e., $s = 1.0$, we obtain the features of Fig.17B, represent time series of extracellular cAMP concentration where the number of spikes tends to decrease. The panels of Fig.3.18B depicting the phase portraits in $g - r$ plane. The chaotic attractor like profiles of these features highly predict the asynchronous states within amoebae population. The change in cAMP concentration behavior shows that in aggregation surface amoebaes communication is sensitive to the effects of LRI as that has been proved previously [243]. Panels of Fig.23 exemplify asynchronous spatiotemporal dynamics of cAMP concentration $g_{n,m}(t)$ in the (n, t)-plane, while

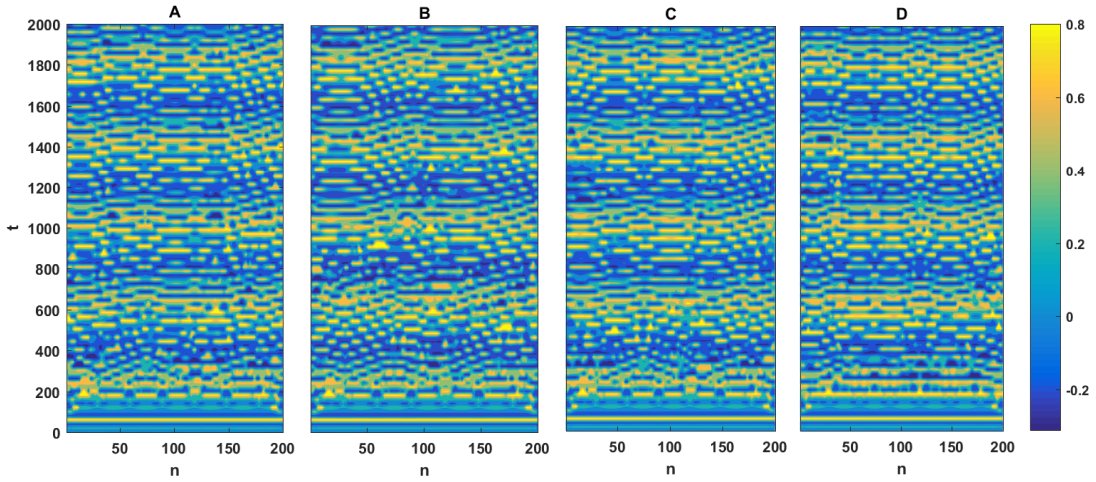

Figure 3.21: Spatiotemporal patterns of cAMP concentration $g_{n,m}(t)$ in (n,t)-plan under the change of the cell number m in the transverse direction as m = 50 in panel (A), m = 100 in panel (B), m = 150 in panel (C) and m = 180 in panel (D). The features are obtained in the case of strong LR $s = 3$. We observe asynchronous nonlinear patterns show a collision between two or more waves followed by new pulsations in the cAMP concentration.

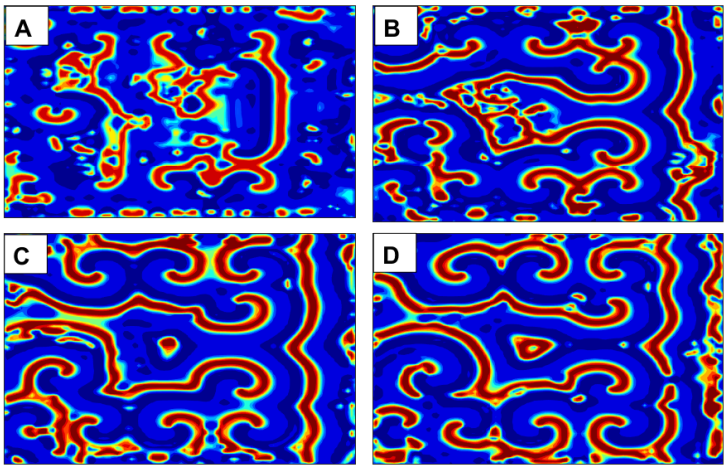

Figure 3.22: Evolution of multi-spirals waves cAMP concentration $g_{n,m}(t)$ in 200×200 cells array at different times:(A) $t = 500$, (B) $t = 1000$, (C) $t = 1500$ and (D) $t = 1800$. The features are obtained in the case for nearest neighbors interaction $s = 3$. We have fixed $f_0 = 1$, $k_r = 1.35$, $a = 0.05$, $\tau = 4.82$, $D = 0.26$. As time increases, the spatiotemporal dynamics of cAMP concentration in medium show emergence of excitability.

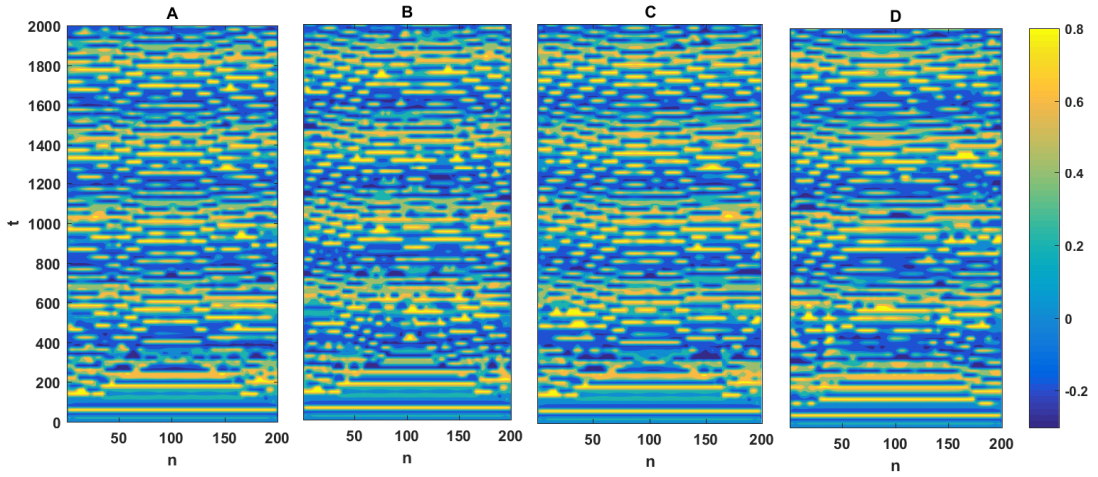

Figure 3.23: Spatiotemporal patterns of cAMP concentration $g_{n,m}(t)$ in (n,t)-plan under the change of the cell number m in the transverse direction as m = 50 in panel (A), m = 100 in panel (B), m = 150 in panel (C) and m = 180 in panel (D). The features are obtained in the case for nearest neighbors interaction $s = 1$. We observe the emergence of asynchronous structures which are localized in some space regions over the time.

panels of Fig.24 present the formation of double spirals by interaction of a new pulse with a recently passed wave. Thus, a wave in the form of a half circle is created (Fig. 24a). The ends of the half circle begin to curl inward, and a double spiral begins to form (Fig. 24b). The arms of the doubles spirals continue to curl and eventually collide and annihilate one another. The ends, however, survive (Fig. 24c-d) and again generate a new doubles spirals. The process repeats itself. The resulting pattern are the doubles spirals in the center of concentric elliptical waves of cAMP. Notice that the doubles spirals regenerates.

3.3.1.4 stability of multi-spiral waves under effects of ultra LRI

We have previously examined the effects of the ultra LRI on the stability of the multi-spiral waves i.e the case $s = 0$. In Fig.3.17A, the time series of the cAMP concentration $g_{n,m}(t)$ of node (100,100) displays the trains of extracellular cAMP concentration are consistent with the results of Fig.3.16, the curves of cAMP concentration at the different nodes $(100, 100)$ and $(150, 150)$ displays oscillations shape without any change, but with varying periods and amplitudes. Fig.3.17(a) the feature shows for a ultra LRI parameter $s = 0.0$, shows a variation of the period of different the nodes oscillates in an asynchronous stat. The panel of Fig.3.18(A) depicting the phase portraits in $g - r$ plane allow to predict the collective dynamical behavior of one hundred cells in the network under the same scenarios as in Fig.3.17. The obtained irregular attractors which is especially sensitive to the change of parameter s predict the asynchronous

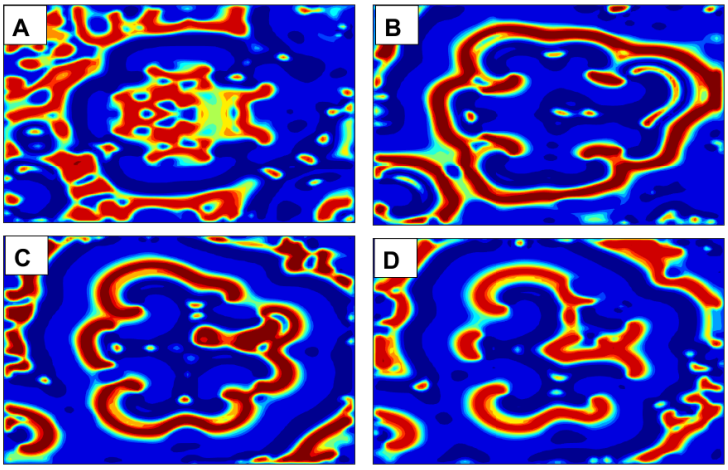

Figure 3.24: Evolution of multi-spirals waves cAMP concentration $g_{n,m}(t)$ in 200×200 cells array at different times:(A) $t = 500$, (B) $t = 1000$, (C) $t = 1500$ and (D) $t = 1800$. The features are obtained in the case for strong interaction $s = 1$. We have fixed $f_0 = 1$, $k_r = 1.35$, $a = 0.05$, $\tau = 4.82$, $D = 0.26$. As time increases, we observed less excitation in medium of cAMP concentration.

states in the network. In Fig.3.25, Spatiotemporal structures of cAMP concentration $g_{n,m}(t)$ in (n,t)-plan for different values of the cell number $m = 50, 100, 150, 180$ corresponding respectively to panels (A), (B), (C) and (D). Therein, the change of cell number m gives a qualitative insight on the heterogeneous nature of the network, which remains asynchronous during a time, and could be considered as the true precursors of multi-spiral waves. In Fig.26(A)-(D), the features show evolution at times of multi-spirals waves cAMP concentration $g_{n,m}(t)$ for $s = 0$. This is highlighted by the windows of Fig.26, where the spatial patterns of the cAMP concentration are represented at different times. There, we observe the emergence of Multi-spiral-like turbulence waves that become increasingly robust over the time.In short, ultra LRI can be useful for increasing excitability in cAMP concentration.

3.3.2 Concluding remarks

In this section the dependence of Dictyostelium discoideum aggregation with long-range cell-to-cell communication have been highlighted in an amoebae network. Based on the improved FitzHugh-Nagumo type equations which describe with a high accuracy the spatiotemporal dynamics of cAMP signaling. Furthermore by changing the long-range parameter s in each panel, various patterns with the same amplitudes but different phases and frequencies propagation are

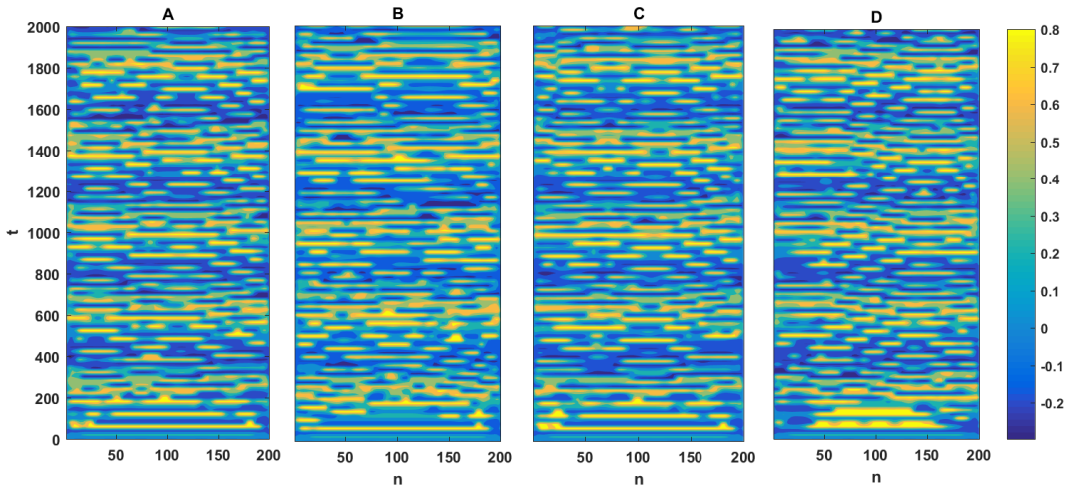

Figure 3.25: Spatiotemporal patterns of cAMP concentration $g_{n,m}(t)$ in (n,t)-plan under the change of the cell number m in the transverse direction as m = 50 in panel (A), m = 100 in panel (B), m = 150 in panel (C) and m = 180 in panel (D). The features are obtained in the case of weak LR $s = 0$. The change of cell number m gives a qualitative insight on the heterogeneous nature of the network, which remains asynchronous during a time, and could be considered as the true precursors of multi-spiral waves.

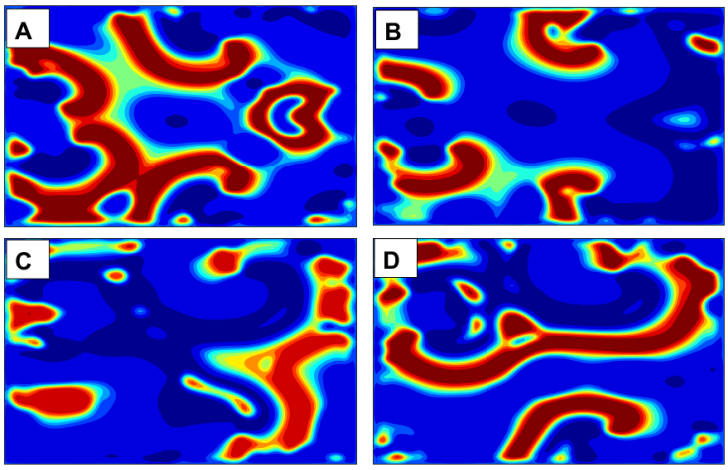

Figure 3.26: Evolution of multi-spirals waves cAMP concentration $g_{n,m}(t)$ in 200×200 cells array at different times:(A) $t = 500$, (B) $t = 1000$, (C) $t = 1500$ and (D) $t = 1800$. The features are obtained in the case for global interaction $s = 0$. We have fixed $f_0 = 1$, $k_r = 1.35$, $a = 0.05$, $\tau = 4.82$, $D = 0.26$. As time increases, we observed a disintegration of the multi-spiral wave in the spatiotemporal dynamics of cAMP concentration in medium.

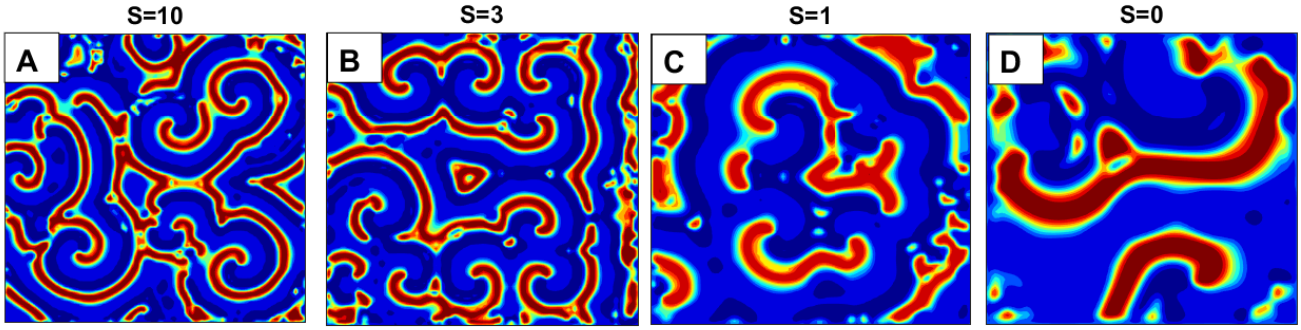

Figure 3.27: Simulation results of spatially extended multi-spiral waves at different values of the parameters long-range interaction at time t = 1900. The features presents influence of parameters long-range: (A) $s = 10$ (see Fig.8.D), (B) $s = 3$ (see Fig.9.D), (C)$s = 1$ (see Fig.10.D), (D) $s = 0$(see Fig.11.D).

obtained. the long-range interaction carried influence on certain parameters such as: Decrease the wavelength thus the excitability of the system and increases the speed of wave in the process of aggregation (see Fig.3.27). We observe how the impulses emitted during weak and strong long-range interaction experience a certain time delay relatively to those generated during ultra long-range interaction. As well weak long-range interaction patterns also experiences a time delay relatively to strong long range interaction patterns. Finally more the long-range interaction is emphasized more a great number of cAMP impulses is generated in a given time period. These findings suggest that more than weak long-range interaction which results from local coupling, weak-and strong long range interaction which result from strong and ultra coupling could well speed up the aggregation phenomenon in a starving Dd amoebae population.

3.4 Conclusion

In this chapter the transport and transfer of S-cAMP in the colony of D.D. amoebae are two important physical phenomena that have been studied to better understand their aggregation

processes in presence of flow-driven, HF frequency regimes and LRI. The phenomenon of MI due to the combined effects between nonlinearity and the dispersion of the explored systems, allowed to realize that the transport and the transfer of the S-cAMP can be ensured by a soliton-like solitary wave, thus consolidating the theory on the solitonic essence of S-cAMP. Especially we have shown that, the MI phenomenon is amplified, by the advective flow, HF frequency regimes and strong LRI. It was shown that MI phenomenon and cAMP-O are complementary phenomena since MI can be used analytically to predict the emergence of nonlinear patterns in colony of D.D. Additionally, numerical simulations have been performed in a square channel and different types oscillations were observed. Indeed, we have shown that in the case of aggregation two oscillations possible, in the presence of flow and in the absence of flow. Different wave models have been chosen which have biological meanings. Numerically, we have performed the bifurcation theory analysis and unveiled the values range of external stimulus which activate and sustain activity-dependence of starving amoebae. Then, we have shown these oscillations obeyed in two frequency modes. We have studied numerically the long-range parameter effects on non-linear models of cAMP. The values of certain parameters were obtained as a function of the synchronization factor. The long-range parameter decrease, leads to some characteristics of cAMP signaling. These results support that the accomplishment of Dd aggregation process may be accurately improved during the long-range communication by a starving population of amoebae.

General Conclusion

Summary

In this thesis, we have studied waves propagation and phenomena of aggregation of the amoeba D.D in the context of transport and transfer of S-cAMP in the surface of aggregation in order to highlight the complex dynamical behaviors of these systems as well as their biological implications. Using the continuous version of the three-dimensional MG cAMP model and FHN model. We have developed two discrete FHN models that provide an overview of the collective dynamic of cAMP signaling. MG and FHN models were improved both analytically and numerically, the cAMP dynamic under effects of flow external, frequency modes and LRI, not only for a better understanding of the studied phenomena, but also to highlight the main properties of the explored cAMP model.

To achieve our main goals, the work of this thesis has been subdivided into three chapters. The first one has dealt with an overview on cAMP signaling in colony of amoeba D.D. Here some generalities have been presented with emphasis on the functioning of cAMP as the that chemoattractant in the processus of aggregation. cAMP plays a crucial role in differentiation of a lower eukaryote, the amoeba D.D. The interest of this organism resides in the fact that it is a simple system, differentiating itself synchronously in only two cell types in response to cAMP. We have also reviewed some phenomenological mathematical of cAMP signaling models. Among them, we found that only MG and FHN models are biophysically meaningful since they were developed by means of experimentation procedures. Besides, both models are able to describe oscillations in the cAMP level in cell suspensions as well as cAMP wave propagation in a dispersed cell population. That why it was adopted in this thesis in order to better analyze waves propagation and the phenomena of aggregation by chemotaxis.

In chapter 2, we have presented the improved MG mathematical model which have been developed along with both analytical and numerical methods. The models investigated present : a reaction-diffusion-advection system or one or more reacting species are advected downstream with an externally imposed velocity. This advective flow can induce unique emergent phenomena. Nonlinear modulated synchronous patterns were investigated taking into account effects of flow

for the formation of such structures. Nonlinear modulated synchronous patterns were investigated taking into account effects of the change of the extracellular cAMP degradation rate (k_e), the production rate of cAMP (σ) and the advection flow velocity (V_f) for the formation of such structures.The model of FHN was finally discretized to study the frequency mode as well as LRI.The above model have been handled by means of some analytical and numerical methods. In that context, the CGL equation describing the spatiotemporal dynamics of envelop soliton has been derived in the DA expansion and SDA approximation. In LRI diffusive S-cAMP allowing to investigate effects of, LR parameter s and stimulus A_0 on, multi-spirals waves of cAMP. The RK4 method with periodic boundary conditions has been used in the numerical simulations for integrating of original models. As initial conditions usually are known to be influenced by CGL equation coefficients, the comparison between both analytical and numerical analysis has been done and suggests a perfect correlation between the found results

Chapter 3 presents the main results. Through MI phenomenon, the transport and the transfer of the S-cAMP can be ensured by a soliton-like solitary wave. This phenomenon is sustained by diffusion spatio-temporal of cAMP concentration and advective flow. This during the pulsatile secretion of cAMP triggers a chemotaxic response and creates a wave of cellular movement. These patterns can be concentric or spiral shaped. the influence of advective flow can generate quasi-periodic waves, spiral grains and chaotic patterns. D.D amoeba cell movement waves are superimposed on cAMP waves. These are due to the pulsatile secretion of cAMP by the aggregation centers and to the relays of these signals which thus propagate through the aggregation territory. The results of this study confirmed : (I) In aggregation under the influence of flow, the shape of the cAMP waves changes with higher imposed flow speeds, transitioning from a planar wave to a erratic patterns and spiral seeds . that becomes increasingly longer the higher the flow rate. Since the cells move against cAMP gradients when aggregating, the shape of the cAMP waves have an important role on the aggregation process, in regards to this, it is noteworthy that even without the presence of wave centers such as target centers and spirals, the cells are still capable of aggregation. This also shows the capability of D. discoideum to signal even in extremely adverse conditions. (II) Moreover, cAMP activities are governed by two frequency regimes where the HF regime is known to generate cAMP oscillations in the form of multi-spirals waves. However the LF regime causes the formation of asymmetric patterns in the form of cAMP oscillatin of trains or targets waves. (III) These results imply that the presence of LRI could better regulate information processing between the cells-cells level long-range and then protect some aggregation regions against the harmful effects of spiral waves in critical processes. This work allows to explore the structures accompanying the cellular aggregation in order to predict bacterial attacks, one of the technological doors being the design of micro-robots for endoscopic medical practices.

Future orientations

The work of this thesis has contributed to the improvement of mathematical MG and FHN models to better understand the dynamics of cAMP oscillation across the aggregation territory. Most of the investigations carried out aimed at studying the phenomena of wave propagation and chemiotaxi as a function of certain parameters, the number of which is not exhaustive. That is why we are prospecting other research directions that include:

- thermal fluctuations effects , during patterns formation of Dictyostelium discoideum
- Magnetic field effects during aggregation of Dictyostelium discoideum cells.
- Synchronized nonlinear patterns in colonies of dictyostelium discoideum with long-range diffusive interactions.
- Patterns formation in process aggregation of dictyostelium discoideum under noise effects.

Bibliography

[1] A.Goldbeter, LA Segel , *Unified mechanism for relay and oscillation of cyclc AMP in Dictyostelium* .Proc Natl Acad Sci USA,**74** (1977) 1543

[2] J.L.Martiel and A.Goldbeter,*A model based on receptor desensitization for cycle AMP signaling in dictyostelium cells.* cells. Biophys. J. **52** (1987) 807

[3] P.B.Monk and H.G.Othmer, *Cylcic AMP oscillation in suspension of dictyostelium.* Phil. Trans. R. Soc. lond. B **323** (1989) 185

[4] Y. Tang and H.G. Othmer, *Excitation, oscillations and wave propagation in a G-protein-based model of signal transduction in Dictyostelium discoideum.* Math. Biosci **120** (1994) 25

[5] R. FitzHugh, *Impulses and physiological states in theoretical models of nerve membrane.* Biophys. J. **1** (1961) 445

[6] I. Nagumo, S. Arimoto, S. Yoshizava, *An active pulse transmission line simulating nerve axon.* Proc. IRE **50** (1962) 2061

[7] B. Vasiev, F. Siegert, C. Weijer, *Multiarmed spirals in excitable media* Phys. Rev. Lett **28** (1997) 2489

[8] E. Palsson and E.C. Cox, *Origin and evolution of circular waves and spirals in Dictyostelium discoideum territories.* Proc. Natl. Acad. Sci. USA **93** (1996) 1151

[9] J. J. Tyson, K. A. Alexander, V. Manoranjan, and J. Murray, *Spontaneous center formation in Dictyostelium discoideum.* Phys. D: Nonlinear Phenom. **34** (1989) 193

[10] A. Goldbeter, *Bulletin of Mathematical Biology.* **68** (2006) 1095

[11] G. Gerisch,*Current Topics in Developmental Biology* **3** (1968) 157

[12] P. Devreotes, *Dictyostelium discoideum: a model system for cell-cell interactions in development.* Science **245** (1989) 1054

[13] W.F. Loomis, *Genetic networks that regulate development in Dictyostelium cells.* Microbiol. Rev. **60** (1996) 135

[14] L. Eichinger, *The genome of the social amoeba Dictyostelium discoideum.* Nature. **435** (2005) 43

[15] D. Y. Shao, H. Levine, and W. J. Rappel, *Coupling actin flow, adhesion, and morphology in a computational cell motility model.* Proc. Natl. Acad. Sci. U.S.A. **109** (2012) 6851

[16] N.W. Goehring, P.K. Trong, J.S. Bois, D. Chowdhury, E.M. Nicola, A.A. Hyman, and S.W. Grill, *Polarization of PAR proteins by advective triggering of a pattern-forming system.* Science **334** (2011) 1137

[17] S. Luther, F.H. Fenton, B.G. Kornreich, A. Squires , *Low-energy Control of Electrical Turbulence in the Heart.* Nature (London) **475** (2011) 235

[18] P. Stoodley, Z. Lewandowski, J. D. Boyle, and H. M.Lappin-Scott, *The formation of migratory ripples in a mixed species bacterial biofilm growing in turbulent flow.* Environ. Microbiol. **1** (1999) 447

[19] L. J. Shimkets and D. Kaiser, *Induction of coordinated movement of Myxococcus xanthus cells.* Journal of Bacteriol.**152** (1982) 451

[20] J. D. Murray, Mathematical Biology (Springer-Verlag,Berlin) (1989)

[21] A. T. Winfree, The Geometry of Biological Time (Springer, New York) (2010)

[22] A. B. Rovinsky and M. Menzinger, *Chemical instability induced by a differential flow.* Phys. Rev. Lett. **69** (1992) 1193

[23] A. B. Rovinsky and M. Menzinger, *Differential flow instability in dynamical systems without an unstable (activator) subsystem.* Phys. Rev. Lett. **72** (1994) 2017

[24] A. B. Rovinsky and M. Menzinger, *Self-organization induced by the differential flow of activator and inhibitor.* Phys. Rev. Lett. **70** (1993) 778

[25] M. Kaern, M. Menzinger, R. Satnoianub, and A. Hunding, Faraday Discuss. **120** (2001) 295

[26] P. Turing, *The chemical basis of morphogenesis.* Trans. R. Soc. B **37** (1952) 237

[27] A. Gholami, O. Steinbock, V. Zykov, E. Bodenschatz, *Flow-Driven Waves and Phase-Locked Self-Organization in Quasi-One-Dimensional Colonies of Dictyostelium discoideum.* Phys. Rev. Lett. **114** (2015) 018103

[28] A. Gholami, O. Steinbock, V. Zykov, E. Bodenschatz, *Flow-driven instabilities during pattern formation of Dictyostelium discoideum.* New Journal of Physics.**17** (2015) 063007

[29] A. Gholami, O. Steinbock, V. Zykov, E. Bodenschatz, *Flow-driven two-dimensional waves in colonies of Dictyostelium discoideum.* New Journal of Physics.**17** (2015) 093040

[30] T. Eckstein, E. Vidal-Henriquez, A. Bae, V. Zykov, E.Bodenschatz, A. Gholami, *Influence of fast advective flows on pattern formation of Dictyostelium discoideum.* PLoS ONE **13** (2018) 0194859

[31] P. J. Ortoleva, *Chemical emplacement of magma.* New York, **4** (1992) 475-487

[32] H. SevcLkova and M. Marek,*Quantum tunnelling in a dissipative system.* Physica D **9** (1983) 149

[33] O. Steinbock, J. Schuĺtze, and S. C. Muller, *Electric-field-induced drift and deformation of spiral waves in an excitable medium.* Phys. Rev. Lett. **68** (1992) 248

[34] J. J. Taboada, A. P. MunŸuzuri, V. Perez-Munuzuri, M. Gomez Gesteira, and V. Peťrez-Villar,*From oscillations to excitability: A case study in spatially extended systems.* Chaos **4** (1994) 519

[35] J. Kosek, H. S . evc..ĄLkovaĄL and M. Marek, *Scanning Electrochemical Microscopy. 31. Application of SECM to the Study of Charge Transfer Processes at the Liquid/Liquid Interface.* J. Phys. Chem. **99** (1995) 16033

[36] H.SevcLkovaĄL, I. Schreiber, and M. Marek, J. Phys. Chem. **100** (1996) 19153

[37] J. Lindner, H. SevcLkova, M. Marek, *Influence of an external electric field on cAMP wave patterns in aggregating Dictyostelium discoideum.* Physical Review E, **63** (2001) 041904

[38] Wagner, T. O. F. Filicori, Episodic Hormone Secretion: From Basic Science to Clinical Application. Hameln (FRG): TM-Verlag. (1987)

[39] Gerisch and U.Wick, *Intracellular oscillations and release of cyclic AMP from Dictyostelium cells* Bioch. and Bioph. Research Communications **65** (1975) 364

[40] V. Nanjundiah, *Periodic stimuli are more successful than randomly spaced ones for inducing development in Dictyostelium discoideum* . Bioscience Reports **8** (1988) 571

[41] G. Leendecker L. Wildt and M. Hansmaan, *Pregnancies followinf chronic intermittant (pulsatil) administration of Gn-RH by means of a portable pump (ŞZYKLOMATŤ) - a new approache to the treatment of infertility in hypothalamic amenorrhea.* Clin. Endocr. Metabol. **51** (1980) 1214

[42] N. Santoro, M. Filicori and W. F. JR Crowley , *Hypogonadotropic disorders in men and women: diagnosis and therapy with pulsatile gonadotropin-releasing hormone*. Endocr. Rev. **7** (1986) 11

[43] A.S. Eteme, C.B. Tabi, and A. Mohamadou, *Long-range patterns in HindmarshÛRose networks*. Commun.Nonlinear Sci. Numer. Simul. **43** (2017) 211

[44] C.B. Tabi, A.S. Eteme, A. Mohamadou, and T.C. Kofane,*Unstable discrete modes in Hindmarsh-Rose neural networks under magnetic flow effect*. Chaos Solitons Fractals **123** (2019) 116

[45] C.B. Tabi, I. Maïna, A. Mohamadou, H.P.F. Ekobena and T.C. Kofané, *Long-range intercellular Ca2+ wave patterns*. Physica A. **435** (2015) 1

[46] G. De Palo, D. Yi, and R.G. Endres, *A critical-like collective state leads to long-range cell communication in Dictyostelium discoideum aggregation*. PLoS Biol. **15** (2017) e1002602

[47] G. Singer, T. Araki, and C. J. Weijer, *Oscillatory cAMP cell-cell signalling persists during multicellular Dictyostelium development*. Commun. Biol., **2** (2019) 139

[48] T.B. Benjamin and J.E. Feir, *The disintegration of wave trains on deep water Part 1. Theory*. J. Fluid Mech. **27** (1967) 417-430

[49] A.D. Koko, C.B. Tabi, H.P.F. Ekobena, A. Mohamadou and T.C. Kofané, Chaos **22** (2012) 043110

[50] A. Mohamadou, B.E. Ayissi and T.C. Kofané, *Instability criteria and pattern formation in the complex Ginzburg-Landau equation with higher-order terms*. Phys. Rev. E **74** (2006) 046604

[51] C.B. Tabi, I. Maïna, A. Mohamadou, H.P.F. Ekobena and T.C. Kofané,*Wave instability of intercellular Ca^{2+} oscillation*. EPL. **106** (2014) 18005

[52] G.R.Y. Mefire, C.B. Tabi, A. Mohamadou, H.P.F. Ekobena andT.C.Kofané, Chaos. **123** (2013) 033128

[53] C.B. Tabi, A. Mohamadou and T.C. Kofané, *Long-range interactions and wave patterns in a DNA model*. Eur. Phys. J. E.**32** (2010) 327

[54] C.B. Tabi, Armand S. Eteme and T.C. Kofané,*Unstable cardiac multi-spiral waves in a FitzHugh-Nagumo soliton model under magnetic flow effect* Nonlinear Dyn **20** (2020) 05750

[55] I. Maïna, C.B. Tabi, A. Mohamadou, H.P.F. Ekobena and T.C. Kofané,*Discrete impulses in ephaptically coupled nerve fibers*. Chaos **25** (2015) 043118

[56] E. W. Sutherland, *On the biological role of Cyclic AMP*. JAMA **214** (1970) 1281

[57] B. Lubamba, B. Dhooghe, S. Noël and T. leal, *Cystic fibrosis: insight into CFTR pathophysiology and pharmacotherapy*. Clin. Biochem. (2012)

[58] R. W. Butcher and E. W. Sutherland, *Enthalpy of hydrolysis of the* 3' *bond of Adenosine* 3', 5'- *Monophosphate and Guanosine* 3', 5'-*Monophosphate*. J. bio. Chem. **237** (1962) 1244

[59] J. Kohyama and al *Epigenetic regulation of neural cell differentiation plasticity in the adult mammalian brain*. Proc. Natl. Acad. Sci. USA **105** (2008) 18012

[60] S. Rangarajan and J. M. Enserink, *Cyclic AMP induces integrin-mediated cell adhesion through Epac and Rap1 upon stimulation of the* β_2*-adrenergic receptor*. JCB **160** (2003) 487

[61] J. M. Enserink and L. S. Price, *The cAMP-Epac-Rap1 pathway regulates cell spreading and cell adhesion to laminin-5 through the* $\alpha 3\beta 1$ *integrin but not the* $\alpha 6\beta 4$ *integrin*. JBC **279** (2004) 44889

[62] X. Cullere and S. K. Shaw, Blood **105** (2005) 950

[63] N. Ozaki and T. Shibasaki, *cAMP-GEGII is a direct target of cAMP in regulated exocytosis*. Nature cell biology **11** (2000) 805

[64] F. Geissmann and S. Jung, *Blood monocytes consist of two principal subsets with distinct migratory properties*. Immunity **1** (2003) 71

[65] M. Métrich and A. Lucas, *Epac mediateds* β*-Adrenergic receptor-induced cardiomyocyte hypertrophy*. Circulation research **8** (2008) 959

[66] U. B. Kaupp and R. Seifert, *Cyclic nucleotide-gated ion channels*. Physiological reviews **3** (2002) 769

[67] W. Wong and J. D. Scott, *AKAP signalling complexes: focal points in space and time*. Molecular cell biology **12** (2004) 959

[68] M. D. Houslay, *Underpinning compartmentalised cAMP signalling through target cAMP breakdown*. Trends in biochemical sciences **2** (2010) 91

[69] G. S. Baillie and M. D. Houslay, *Arrestin times for compartmentalised cAMP signalling and phosphodiesterase-4 enzymes*. Current opinion in cell biology **17** (2005) 129

[70] G. S. Baillie, *Compartementalized signalling: spatial regulation of cAMP by the action of compartmentalied phosphodiesterases*. The FEBS journal **276** (2009) 1790

[71] D. M. Cooper, *Compartmentalization of adenylate cyclase and cAMP signaling.* Biochemical Society transactions **33** (2005) 1319

[72] M. Arnold, V. Sophie and M. Joelle, médecine/science 4 (1985) 192

[73] E. Krebs and J. Beavo, Annu Rro Biochem **48** (1979) 923.

[74] B. De Crombrugghe and S. Busby, H. Buc, *Cyclic AMP receptor protein: role in transcription activation.* Science 224 (1984) 831.

[75] G. M. Kammer, *The adenlate cyclase-cAMP-protein kinase A pathway and regulation of the immune response.* Immunology today **9** (1988) 222

[76] T. Vang, K.M. Torgersen, V. Sundvold, M. Saxena, F.O. Levy, B.S. Skalhegg, V. Hansson, T. Mustelin and K. Tasken, *Activation of the Cooh-Terminal Src Kinase (Csk) by Camp-dependent protein kinase inhibits signaling through the t cell receptor.* Journal of experimental medicine **193** (2001) 497

[77] N. Hermann-Kleiter and N. Thuille, *PKCtheta and PKA are antagonistic partners in the NF-AT transactivation pathway of primary mouse $CD3^+$ T lymphocytes.* Blood **107** (2006) 4841

[78] B.S. Skalhegg, B.F. Landmark, S.O. Doskeland, V. Hansson, T. Lea and T. Jahnsen, *Cyclic cAMP-dependent protein kinase type I mediates the inhibitory effects of $3', 5'$-cyclic adenosine monophosphate on cell replication in human T lymphocytes.* The Journal of biological chemistry **267** (1992) 15707

[79] K. Tasken and A. Ruppelt, Frontiers in bioscience : a journal and virtual library **11** (2006) 2929

[80] C.S. Henney and L.M. Lichtenstein, *The role of cyclic-AMP in the cytolytic activity of lymphocytes.* Journal of immunology **107** (1971) 610

[81] M. Betz and B.S. Fox, *Prostaglandin E2 inhibits production of th1 lymphokines but not of th2 lymphokines.* Journal of immunology **146** (1991) 108

[82] F.G. Snijdewint, P. Kalinski, E.A. Weirenga, J.D. Bos and M.L. Kapsenberg, *Prostaglandin E2 differentially modulates cytokine secretion profiles of human T helper lymphocytes.* journal of immunology **150** (1993) 5321

[83] S. Haraguchi and R.A. Good, *Immunosuppressive retroviral peptides: cAMP and cytokine patterns* Immunology today **16** (1995) 595

[84] C.M. Hilkens and A. Snijders, C.M. Hilkens and A. Snijders, *Modulation of T-cell cytokine secretion by accessory cell-derived products.* The European respiratory journal. Supplement **22** (1996) 90

[85] C. Conche and G. Boulla, *T cell adhesion primes antigen receptor-induced calcium responses through a transient rise in adenosine* $3^{'},5^{'}$*-cyclic monophosphate.* Immunity **30** (2009) 33

[86] C. Randriamampita and G. Boulla, *T cell adhesion lowers the threshold for antigen detection.* European journal of immunology **33** (2003) 1215

[87] C. Yue, K. L. Dodge, *Phosphorylation of Serine 1105 by Protein Kinase A Inhibits Phospholipase CSS3 Stimulation by* $G\alpha_q^*$. The Journal of biological chemistry **273** (1998) 18023

[88] K. Kaibuchi, S. Kuroda, *Regulation of the Cytoskeleton and Cell Adhesion by the Rho Family GTPases in Mammalian Cells.* Annual review of biochemistry **68** (1999) 459

[89] G. A. Marchildon, J. E. Casnellie, *Covalently bound myristate in a lymphoma tyrosine protein kinase.*. Proceedings of the National Academy of Sciences of the United States of America **81** (1984) 7679-7682

[90] M. Okada, S. Nada, *CSK: a protein-tyrosine kinase involved in regulation of src family kinases.* The Journal of biological chemistry **266** (1991) 24249

[91] T. Brdicka, D. Pavlistova, *Phosphoprotein Associated with Glycosphingolipid-Enriched Microdomains (Pag), a Novel Ubiquitously Expressed Transmembrane Adaptor Protein, Binds the Protein Tyrosine Kinase Csk and Is Involved in Regulation of T Cell Activation.* The Journal of experimental medicine **191** (2000) 1591

[92] M. Kawabuchi, Y. Satomi, . Nature **334** (2000) 1137

[93] M. Nokta and R. Pollard, *Human immunodeficiency virus infection: Association with altered intracellular levels of CAMP and cGMP in MT-4 cells.* Virology **181** (1991) 211

[94] B. Hofmann, P. Nishanian, *Human immunodeficiency virus proteins induce the inhibitory cAMP/protein kinase A pathway in normal lymphocytes.* Proceedings of the National Academy of Sciences of the United States of America **90** (1993) 6676-6680

[95] E. M. Aandahl, P. Aukrust, *Protein kinase A type I antagonist restores immune responses of T cells from HIV-infected patients.* FASEB journal **12** (1998) 855

[96] A. M. Masci, M. Galgani, *HIV-1 gp120 induces anergy in naive T lymphocytes through CD4-independent protein kinase-A-mediated signaling.*Journal of leukocyte biology **74** (2003) 1117

[97] C. Becker, C. Taube, *Protection from graft-versus-host disease by HIV-1 envelope protein gp120-mediated activation of human $CD4^+CD25^+$ regulatory T cells.* Blood **114** (2009) 1263

[98] B. Hofmann, P. Nishanian, *Restoration of T-cell function in HIV infection by reduction of intracellular cAMP levels with adenosine analogues.*. Europe PMC **7** (1993) 659

[99] C. Becker, C. Taube, *Protection from graft-versus-host disease by HIV-1 envelope protein gp120-mediated activation of human $CD4^+CD25^+$ regulatory T cells.* Blood **114** (2009) 1263

[100] J. Navarro, C. Punzon, *Inhibition of Phosphodiesterase Type IV Suppresses Human Immunodeficiency Virus Type 1 Replication and Cytokine Production in Primary T Cells: Involvement of $NF-\kappa B$ and NFAT.* Journal of virology **72** (1998) 4712-4720

[101] Y. Sun and al. *Infection of $CD4^+$ Memory T Cells by HIV-1 Requires Expression of Phosphodiesterase 4.* Journal of immunology **165** (2000) 1755

[102] M. Thivierge and al. *Cell-Type-Dependent Effect of Transforming Growth Factor β, a Major Cytokine in Breast Milk, on Human Immunodeficiency Virus Type 1 Infection of Mammary Epithelial MCF-7 Cells or Macrophages.* Blood **92** (1998) 40-45

[103] Y. By and al. *Monoclonal antibody-assisted stimulation of adenosine A2A receptors induces simultaneous downregulation of CXCR4 and CCR5 on $CD4^+$ T-cells.*. Human immunology **71** (2010) 1073

[104] Kenneth B. Rapper and Nathan R. Smith, *Design, Synthesis and Structural Analysis of Cyclopeptides Against VEGF-Receptor.* J Bacteriol. 38(4)(1939) 431

[105] L. Eichinger and J.A. Pachebat, *The genome of the social amoeba Dictyostelium discoideum.* Nature. 435(7038) (2005) 43

[106] J.E. Strassman ,Zhu Y, and D.C. Queller , *Altruism and social cheating in the social amoeba Dictyostelium discoideum.* Nature (2000)

[107] D. L. Williams, R. Von Herzen, J. Sclater and R. Anderson, *The Galapagos Spreading Centre: Lithospheric Cooling and Hydrothermal Circulation.* Geophysical Journal International 38(3), (1974) 587

[108] C. Juliet Coates and J. Adrian Harwood, *Cell-cell adhesion and signal transduction during Dictyostelium development.* Journal of Cell Science **114**, (2001) 4349

[109] K.S. Uchida, T. Kitanishi-Yumura, and S. Yumura. *Turnover and flow of the cell membrane for cell migration.*. J Cell Sci **116** (2003) 51.

[110] A.J. Ridley, M.A. Schwartz, K. Burridge, R.A. Firtel, M. H. Ginsberg,G. Borisy, J.T. Parsons, A.R. Horwitz, *Cell migration: integrating signals from front to back.* Science **302**(2003)1704

[111] G.S. Pitt, N. Milona, J. Borleis, K.C. Lin, R.R. Reed, *Structurally distinct and stage-specific adenylyl cyclase genes play different roles in Dictyostelium development.* P.N. Cell **69** (1992) 305

[112] S. Saran, M.E. Meima, E. Alvarez-Curto, K.E. Weening, D.E. Rozen, P. Schaap, J. Muscle Res. *Overexpression of Sphingosine-1-Phosphate Lyase or Inhibition of Sphingosine Kinase in Dictyostelium discoideum Results in a Selective Increase in Sensitivity to Platinum-Based Chemotherapy Drugs.* Cell Motil. **23** (2002) 793

[113] A.J. Durston, *Dictyostelium discoideum aggregation fields as excitable media.* J. Theor. Biol. **42** (1973) 483

[114] G.L. Garcia, C.A. Parent, *Signal relay during chemotaxis.* J. Microsc. **231**, (2008) 529

[115] J. Lauzeral, J. Halloy and A. Goldbeter, *Desynchronization of cells on the developmental path triggers the formation of spiral waves of cAMP during Dictyostelium aggregation.* Proc. Natl. Acad. Sci. USA **94** (1997) 9153

[116] F.I. Comer, C.A. Parent, *Phosphoinositide 3-Kinase Activity Controls the Chemoattractant-mediated Activation and Adaptation of Adenylyl Cyclase.* Mol. Biol. Cell **94** (2006) 357-366

[117] C. J. Weijer, . Springer International Publishing. **16** (2019) 193

[118] Alcantara and Monk, *Signal propagation during aggregation in the slime mould Dictyostelium discoideum.* Microbiology Society. **85** (1974) 321

[119] M. Tiziana Baratta H. J. Damien Dorman,Stanley G. Deans,A. Cristina Figueiredo,José G. Barroso and Giuseppe Ruberto, *Antimicrobial and antioxidant properties of some commercial essential oils.*Flavour and Fragrance Journal **13** (1998) 235

[120] F. Höfer,P. Warbichler,W. Grogger and O. Lang, *On the application of energy filtering TEM in materials science: I. Precipitates in a Ni/Cr-alloy.* Micron.**26** (1995) 377

[121] Michael S. Levine, Katharine L. Altemus, Carlos Cepeda, Howard C.Cromwell, Cynthia Crawford, Marjorie A. Ariano, John Drago, David R.Sibley and Heiner Westphal, *Modulatory Actions of Dopamine on NMDA Receptor-Mediated Responses Are Reduced in D1A-Deficient Mutant Mice.* Journal of Neuroscience. **18** (1996) 5870

[122] C. J. Dallon and H. G. Othmer, . Royal Society. **352** (1997) 1471

[123] E. Pálsson and E. C. Cox, . Journal of Neuroscience. **93** (1996) 1151

[124] J. Lauzeral, J. Halloy, and A. Goldbeter, *Desynchronization of cells on the developmental path triggers the formation of spiral waves of cAMP during Dictyostelium?aggregation.* PNAS. **94** (1997) 9153

[125] M. Halloy, R. Etheridge and G. M.Burghardt, *Herpetological Monographs.* JSTOR. **12** (1998) 1

[126] R.M. Macnab and D.E. Jr. Koshland, *The gradient-sensing mechanism in bacterial chemotaxis.* Proc. Natl. Acad. Sci. USA **69** (1972) 2509

[127] M. Dinauer, T.L. Steck and P.N. Devreotes, *Cyclic* $3^{'}, 5$,*-AMP relay in Dictyostelium discoideum. III. The relationship of cAMP synthesis and secretion during the cAMP signaling response.* Biophys Chem. **72** (1980) 21

[128] A. Goldbeter, D.E. Jr. Koshland, . Proc. Natl. Acad. Sci. USA **74** (1977) 1543

[129] B.E. Knox, P.N. Devreotes, A. Goldbeter, L.A. Segel , *A molecular mechanism for sensory adaptation based on ligand-induced receptor modification* . Proc. Natl. Acad. Sci. USA **83** (1986) 2345

[130] U. Alon, M.G. Surette, N. Barkai and S. Leibler, *Robustness in bacterial chemotaxis.* Nature **397** (1999) 168-171

[131] L. Ma, C. Janetopoulos, L. Yang, P.N. Devreotes and P.A. Iglesias, *Two Complementary, Local Excitation, Global Inhibition Mechanisms Acting in Parallel Can Explain the Chemoattractant-Induced Regulation of* $PI(3,4,5)P_3$ *Response in Dictyostelium Cells.* Biophys.J. **87** (2004) 3764-3774

[132] G.L. Garcia and C.A. Parent, *Signal relay during chemotaxis.* J. Microsc. **231** (2008) 529-534

[133] J. Lauzeral, J. Halloy and A. Goldbeter, *Desynchronization of cells on the developmental path triggers the formation of spiral waves of cAMP during Dictyostelium?aggregation.* Proc. Natl.Acad. Sci. USA **94** (1997) 9153-9158

[134] F.I. Comer and C.A. Parent, *Phosphoinositide 3-Kinase Activity Controls the Chemoattractant-mediated Activation and Adaptation of Adenylyl Cyclase.* Mol. Biol. Cell **17** (2006) 357

[135] G. Gerisch, D. Malchow, W. Roos, and U. Wick, *Oscillations of cyclic nucleotide concentrations in relation to the excitability of Dictyostelium cells.* J. Exp. Biol.**81** (1979) 33

[136] K.J. Tomchik and P.N. Devreotes, . Science. **212** (1982) 443

[137] T. Gregor,K. Fujimoto, N. Masaki and S. Sawai, *The onset of collective behavior in social amoebae.* Science. **328** (2010) 1021

[138] H. Cai, M. Katoh-Kurasawa, T. Muramoto, B. Santhanam, Y. Long, L. Li, M. Ueda, P.A. Iglesias, G. Shaulsky and P.N. Devreotes, *Nucleocytoplasmic shuttling of a GATA transcription factor functions as a development timer.* Science **343**(2014) 1249531

[139] A.J. Durston, *Pacemaker activity during aggregation in Dictyostelium discoideum.* Dev. Biol. **37** (1974) 225

[140] P. Foerster, S.C. Müller and B. Hess, *Curvature and spiral geometry in aggregation patterns of Dictyostelium discoideum.* Development. **109** (1990) 11

[141] M. Darmon, P. Brachet and L.H. Pereira da Silva, *Cell differentiation in the absence of intracellular cyclic AMP pulses in Dictyostelium discoideum.* Proc. Natl. Acad. Sci. USA **72** (1975) 3163

[142] D. Dormann, J.Y. Kim, P.N. Devreotes and C.J. Weijer, *cAMP receptor affinity controls wave dynamics, geometry and morphogenesis in Dictyostelium.* J. Cell Sci. **114**, (2001) 2513

[143] G. Gerisch and U. Wick, *Intracellular oscillations and release of cyclic AMP from Dictyostelium cells.* Biophys. Res. Commun. **65** (1975) 364

[144] V. Nanjundiah, *Periodic stimuli are more successful than randomly spaced ones for inducing development inDictyostelium discoideum.* Biosci. Rep. **8** (1988) 571

[145] Y.X. Li, A. Goldbeter, *Frequency encoding of pulsatile signals of cAMP based on receptor desensitization in Dictyostelium cells.* J. Theor. Biol. **146** (1990) 355

[146] Y.X. Li, A. Goldbeter, . Biophys. J. **55** (1989) 125

[147] Y.X. Li, A. Goldbeter, *Pulsatile signaling in intercellular communication Periodic stimuli are more efficient than random or chaotic signals in a model based on receptor desensitization.* Biophys. J. **61** (1992) 161

[148] A. Goldbeter, T. Erneux and L. A. egel, *Pulsatile signaling in intercellular communication Periodic stimuli are more efficient than random or chaotic signals in a model based on receptor desensitization.* FEBS Lett, **89** (1978) 231

[149] A. Gholami, O. Steinbock, V. Zykov, and E. Bodenschatz, *Flow-driven instabilities during pattern formation of Dictyostelium discoideum.* New J. Phys.**17** (2015) 063007

[150] A. Gholami, O. Steinbock, V. Zykov, and E. Bodenschatz, *Flow-Driven waves and Phase-Locked Self-Organization in Quasi-One-Dimensional Colonies of Dictyostelium discoideum.* Phys. Rev. Lett. **114** (2015) 018103

[151] A. Goldbeter and L. A Segel, *Unified mechanism for relay and oscillation of cyclic AMP in Dictyostelium discoideum.* Proc. Natl. Aad. Sci. U.S.A. **74** (1977) 1543

[152] A. Goldbeter and L. A Segel, . Proc. Natl. Aad. Sci. U.S.A. **17** (1980) 127

[153] M. Dinauer, T. Steck, and Devreotes, *Skip Nav Destination Article/August 01 1980 Cyclic* $3',5'$*-AMP relay in dictyostelium discoideum. IV. Recovery of the cAMP signaling response after adaptation to cAMP.* J. Cell Biol **86** (1980a) 545

[154] M. Dinauer, T. Steck, and Devreotes, *Cyclic 3', 5'-AMP relay dictyostelium discoideum. V. Adaptation of the cAMP signaling response during cAMP stimulation.* J. Cell Biol **86** (1980b) 554

[155] J.Lindner, S. Hana and M. Milos, *Quantum-fluctuation-induced spatial stochastic resonance at zero temperature.* Physical Review E, **63** (2001) 041904

[156] J. Leon and M. Manna, *Multiscale analysis of discrete nonlinear evolution equations.* J. Phys. A: Math. Gen.**32** (1999) 2845

[157] C. B. Tabi, I. Maĺýna, A. Mohamadou, H.P. F. Ekobena and T. C. Kofanťe, *Long-range intercellular Ca2+ wave patterns.* Physica A **435** (2015) 1

[158] I. Maïna, C. B. Tabi, A. Mohamadou, H. P. F. Ekobena and T. C. Kofanťe, *Discrete impulses in ephaptically coupled nerve fibers.* Chaos **25** (2015) 043118

[159] A.S. Etémé, C. B. Tabi, and A. Mohamadou, *Long-range patterns in HindmarshŰRose networks.* Commun. Nonlinear Sci. Numer. Simul **43** (2017) 211

[160] C. S. Panguetna, C. B. Tabi, and T. C. Kofane, *Two-dimensional modulated ion-acoustic excitations in electronegative plasmas.* PHYSICS OF PLASMAS **24** (2017) 092114

[161] D. Bensimon, P. Kolodner, C.M. Surko, H. Williams, V. Croquette, *Competing and coexisting dynamical states of travelling-wave convection in an annulus.* J.Fluid Mech. **217** (2006) 441

[162] J.J. Niemela, G. Ahlers, D. Cannell, *Localized travaling-wave states in Binary-fluid convection.* Phys. Rev. Lett **64** (1990) 1365

[163] R. Graham, in: Riste (Ed.), Fluctuations, Instabilities and Phase Transitions, Springer, Berlin (1975)

[164] J.J. Hegseth, C.D. Andereck, F. Hayot, Y. Pomeau, *Spiral turbulence and phase dynamics.* Phys. Rev. Lett. **62** (1989) 257

[165] C.B. Tabi, A.S. Etémé, A. Mohamadou, *Frequency mode excitations in two-dimensional HindmarshŰRose neural networks.* Physica A **474** (2017) 186

[166] C.N. Takembo, A. Mvogo, H.P.F. Ekobena, T.C. Kofané, *Effect of electromagnetic radiation on the dynamics of spatiotemporal patterns in memristor-based neuronal network.* Nonlinear Dynam. **95** (2018) 1067

[167] A. Mohamadou, B.E. Ayissi and T.C. Kofané. *Instability criteria and pattern formation in the complex Ginzburg-Landau equation with higher-order terms.* Phys. Rev. E **74** (2006) 046604

[168] T.B. Benjamin and J.E. Feir, *The Disintegration of Wa-vetrains on Deep Water.* J. Fluid Mech **27** (1967) 417

[169] F.II Ndzana, A. Mohamadou and T.C. Kofané, *Modulational instability in a purely nonlinear coupled complex GinzburgŰLandau equations through a nonlinear discrete transmission line.* Chaos **18** (2008) 043121

[170] F.II Ndzana, A. Mohamadou, T.C. Kofané and L.Q. English, *Transmission-line analysis of e -near-zeroŰfilled narrow channels.* Phys. Rev. E. **78** (2008) 016606

[171] F.II Ndzana, A. Mohamadou and T.C. Kofané, *Modulated waves and chaotic-like behaviours in the discrete electrical transmission line.* J. Phys. D: Appl. Phys. **40** (2007) 3254

[172] A.D. Koko, C.B. Tabi, H.P.F. Ekobena, A. Mohamadou and T.C. Kofané, . Chaos **22** (2012) 043110

[173] J.D. Murray, , . (Springer-Verlag, Berlin) (1989)

[174] A.S. Mikhailov, *Foundations of Synergetics II: Complex Patterns.* (Springer-Verlag, Berlin) (1991) 1

[175] A.S. Mikhailov, and I.V. Uporov, *Foundations of Synergetics II: Complex Patterns.* (Springer-Verlag, Berlin) (1991) 138

[176] G. Nicolis, *Introduction to Nonlinear Science.*(Cambridge University Press, Cambridge) (1995) 13

[177] Y. Kuramoto, *Chemical Oscillations, Waves, Turbulence.* (Springer-Verlag, Berlin). (1984) 193

[178] H. Mori, and Y. Kuramoto, *Dynamics of Coupled Oscillator Systems.* (Springer-Verlag, Berlin) (1998)119

[179] R. Kapral and K. Showalter, *Chemical Waves and Patterns.* (Kluwer Academic Publishers, Dordrecht) (1995)

[180] D. Walgraef, *Spatiotemporal pattern formation.* (Springer-Verlag, Berlin) (1996) 503

[181] H. Meinhardt, *Models of Biological Pattern Formation.* (Academic Press, London) (1982)

[182] P. N. Devreotes, and J. A. Sherring, *Kinetics and concentration dependence of reversible cAMP-induced modification of the surface cAMP receptor in Dictyostelium.* J. Biol. Chem. **6378** (1985) 260

[183] P. M. Conn, D. C. Rogers, and R. McNeil, *Hormones and their Actions, Part 2: Specific action of protein hormones.* Endocrinology.**335** (1982) 111

[184] G. Nicolis, and I. Prigogine, J. Wiley and Sons, *Self organization in nonequilibrium systems.* Inc., New York (1977)

[185] J. L. Martiel, and A. Goldbeter, . C. R. Acad. Sci. (Paris) Ser. III. **549** (1984) 298

[186] B. Coukell, *Developmental regulation and properties of the cGMP-specific phosphodiesterase in dictyostelium discoideum.* Differentiation. **103** (1984) 246

[187] P. N. Devreotes, and T. L. Steck, *Cyclic* $3^{'}, 5^{'}$ *AMP relay in Dictyostelium discoideum. II. Requirements for the initiation and termination of the response.* J. Cell Biol. **80** (1979) 300

[188] P. J. M. Van Haastert, *Alteration of receptor/G-protein interaction by putative endogenous protein kinase activity in Dictyostelium discoideum membranes.* J. Biol. Chem. **262** (1987) 3239

[189] D. R. Sibley, J. R. Peters, P. Nambi, M. G. Caron, and R. J.Lefkowitz, *Cyclic nucleotide-dependent phosphorylation in Dictyostelium discoideum.* J. Biol. Chem. **259** (1984) 9742-9749

[190] J. Lubs-Haukeness, and C. Klein, *Cyclic nucleotide-dependent phosphorylation in Dictyostelium discoideum amoebae.* J. Biol. Chem. **257** (1982) 12204

[191] M. Dinauer, S. MacKay, and P. N. Devreotes, *Cyclic* $3^{'}, 5^{'}$*-AMP relay in Dictyostelium discoideum. IV. Recovery of the cAMP signaling response after adaptation to cAMP.* J. Biol. Chem. **86** (1980a) 537-544

[192] M. C. Cross and P. C. Hohenberg, *Pattern formation outside equilibrium*. Rev. Mod. Phys. **65** (1993) 851.

[193] B. A. Malomed , *Complex Ginzburg-Landau Equation, in Encyclopedia of Nonlinear Science*, (Routledge, New York, 2005) 157.

[194] A. Gasri, . Thesis (2018)

[195] R. FitzHugh, *Impulses and Physiological States in Theoretical Models of Nerve Membrane*. Biophys. J. **1** (1961) 445

[196] J.S. Nagumo, S. Arimoto and S. Yoshizawa, *An active pulse transmission line simulating nerve axon*. Proc. IRE **50** (1962) 2061

[197] A.T. Winfree, *Varieties of spiral wave behavior: An experimentalist's approach to the theory of excitable media*. Chaos **1** (1991) 303

[198] A. Mvogo, A. Tambue, G. H. Ben-Bolie and T. C. Kofané, *Fractional nonlinear dynamics of DNA breathing*. Commun. Nonlinear Sci. Numer. Simulat **39** (2016) 396

[199] T. Banerje, P.S. Dutta, A. Zakharova and E. Schöll, *Chimera patterns induced by distance-dependent power-law coupling in ecological networks*. Phys. Rev. E **94** (2016) 032206

[200] S.F. Mingaleev, P.L. Christiansen, Y.B. Gaididei, M. Johansson and K.Ø. Rasmussen, *Models for energy and charge transport and storage in biomolecules*. JBP **25** (1999) 41

[201] I. Daumont, T. Dauxois, M. Peyrard, *Modulational instability: first step towards energy localization in nonlinear lattices*. Nonlinearity **10** (1997) 617

[202] Y.S. Kivshar, M. Peyrard, *Modulational instabilities in discrete lattices*. Phys. Rev. A **46** (1992) 3198

[203] C.B. Tabi, A. Mohamadou, T.C. Kofane, *Modulational Instability and Pattern Formation in DNA Dynamics with Viscosity*. J. Comput. Theor. Nanosci. **8** (2008) 647

[204] R. J. Field, and M. Burger, *Oscillations and traveling waves in chemical systems*. Eds, Wiley, New York, (1985)

[205] J. J. Tyson and J. P. Keener, *Singular perturbation theory of traveling waves in excitable media (a review)*. Physica D **32** (1988) 327

[206] S. C. Muller, P. Coullet, and D. Walgraef, *From oscillations to excitability: A case study in spatially extended systems*. Chaos **4** (1994) 439

[207] J. Rinzel, *Electrical excitability of cells, theory and experiment: Review of the Hodgkin-Huxley foundation and an update.* B. Math. Biol. **52** (1990) 5

[208] A. L. Hodgkin and A. F. Huxley, *A quantitative description of membrane current and its application to conduction and excitation in nerve.* J. Physiol. **117** (1952) 500

[209] M. A. Allessie, F. I. M. Bonke, and F. J. G. Schopman, *Circus movement in rabbit atrial muscle as a mechanism of trachycardia.* Circ. Res. **33** (1973) 54

[210] M. A. Allessie, F. I. M. Bonke, and F. J. G. Schopman, *Circus movement in rabbit atrial muscle as a mechanism of tachycardia. II. The role of nonuniform recovery of excitability in the occurrence of unidirectional block, as studied with multiple microelectrodes.* Circ. Res. **39** (1976) 168

[211] M. A. Allessie, F. I. M. Bonke, and F. J. G. Schopman, *Circus movement in rabbit atrial muscle as a mechanism of tachycardia. III. The "leading circle" concept: a new model of circus movement in cardiac tissue without the involvement of an anatomical obstacle.* Circ. Res. **41** (1977) 9

[212] A. T. Winfree, *The Three-Dimensional Dynamics of Electrochemical Waves and Cardiac Arrhythmias.* (Princeton University Press, Princeton) (1987)

[213] J. M. Davidenko, A. V. Pertsov, R. Salomonsz, W. Baxter, and J. Jalife, *Interactions of spiral waves in inhomogeneous excitable media.* Nature **335** (1992) 349

[214] V. I. Koroleva and J. Burès, *Circulation of cortical spreading depression around electrically stimulated areas and epileptic foci in the neocortex of rats.* Brain Res. **173** (1979) 209

[215] N. A. Gorelova and J. Burès, *Spiral waves of spreading depression in the isolated chicken retina.* J. Neurobiol **14** (1983) 353

[216] M. Lauritzen, *Cortical spreading depression in migraine.* Cephalalgia **21** (2001) 757

[217] A. J. Durston, *Dictyostelium discoideum aggregation fields as excitable media.* J. Theor. Biol. **42** (1973) 483

[218] K. J. Tomchik and P. N. Devreotes, *Adenosine* 3′, 5′*-monophosphate waves in Dictyostelium discoideum: a demonstration by isotope dilution–fluorography.* Science **212** (1981) 443

[219] F. Siegert and C. Weijer, *Digital image processing of optical density wave propagation in Dictyostelium discoideum and analysis of the effects of caffeine and ammonia.* J. Cell Sci. **93** (1989) 325

[220] J. Lechleiter, S. Girard, E. Peralta, and D. Clapham, *Spiral Calcium Wave Propagation and Annihilation in Xenopus laevis Oocytes*. Science **252** (1991) 123

[221] A. Z. Zaikin and A. Zhabotinsky, *Concentration Wave Propagation in Two-dimensional Liquid-phase Self-oscillating System*. Nature **225** (1970) 535

[222] A. T. Winfree, *Spiral Waves of Chemical Activity*. Science **175** (1972) 634

[223] S. Jakubith, H. H. Rotermund, W. Engel, A. von Oertzen, and G. Ertl, *Spatiotemporal concentration patterns in a surface reaction: Propagating and standing waves, rotating spirals, and turbulence*. Phys. Rev. Lett. **65** (1990) 3013

[224] S. Nettesheim, A. von Oertzen, H. H. Rotermund, and G. Ertl, *Reaction Diffusion Patterns in the Catalytic CO-oxidation on Pt(110): Front Propagation and Spiral Waves*. J. Chem. Phys. **98** (1993) 9977

[225] A. B. Carey, R. H. Giles, Jr., and R. G. McLean, *The landscape epidemiology of rabies in Virginia*. Am. J. Trop. Med. Hyg. **27** (1978) 573

[226] J. D. Murray, E. A. Stanley, and D. L. Brown, *On the spatial spread of rabies among foxes*. Proc. Roy. Soc. Lond B **229** (1986) 111

[227] M. Kuperman and G. Abramson, *Small World Effect in an Epidemiological Model*. Phys. Rev. Lett. **86** (2001) 2909

[228] L. S. Schulman and P. E. Seiden, *Percolation and Galaxies*. Science **233** (1986) 425

[229] B. F. Madore and W. L. Freedman, *Self-Organizing Structures*. Am. Sci. **75** (1987) 252

[230] P. Parmananda, *Generalized synchronization of spatiotemporal chemical chaos*. Phys. Rev. E **56** (1997) 1595

[231] B. F. Edwards, *Poiseuille Advection of Chemical Reaction Fronts*. Phys. Rev. Lett. **89** (2002) 104501.

[232] M. Leconte ,J. Martin, N. Rakotomalala and D. Salin, *Pattern of reaction diffusion fronts in laminar flows*. Phys. Rev. Lett. **90** (2003) 128302.

[233] A. S. Etémé , C. B. Tabi and A. Mohamadou, *Synchronized nonlinear patterns in electrically coupled HindmarshÛRose neural networks with long-range diffusive interactions*. Chaos Solitons and Fractals **104** (2017) 813

[234] M. D. hamala, V. K. Jirsa and M. Ding , *Enhancement of Neural Synchrony by Time Delay*. Phys. Rev. Lett. **92** (2004) 074104

[235] W. T. Yu , J. Tang , MaJ and X. Yang, *Heterogeneous delay-induced asynchrony and resonance in a small-world neuronal network system*. EPL **114** (2016) 50006

[236] S. Nagano, *Diffusion-Assisted Aggregation and Synchronization in Dictyostelium discoideum*. Phys. Rev. Lett. **80** (1998) 4826-4829

[237] W. Rappel, A. Nicol, A. Sarkissian, and H. Levine, *Self-organized Vortex State in Two-Dimensional Dictyostelium Dynamics*. Phys. Rev. Lett. **83,** (1999) 1247-1250

[238] M. Shafiei, F. Parastesh, M. Jalili, S. Jafari, M. Perc and M. Slavinec, *Effects of partial time delays on synchronization patterns in Izhikevich neuronal networks*. Eur. Phys. J. B **92** (2019) 36

[239] R. FitzHugh, *Impulses and Physiological States in Theoretical Models of Nerve Membrane*. Biophys.J.,**1** (1961) 445

[240] D. P. Brachet, and L. H. Pereira Da Silva, *Chemotactic signals induce cell differentiation in Dictyostelium discoideum*. Cell Biology **8** (1975) 3163

[241] J. Ma, J. Tang, A. Zhang, Y. Jia, *Robustness and breakup of the spiral wave in a two-dimensional lattice network of neurons*. Sci. China Phys. Mech. Astron. **53** (2010) 672

[242] E. Palssan and E. C. Coxt, *Origin and evolution of circular waves and spirals in Dictyostelium discoideum territories*. Proc. Natl. Acad. Sci. USA, 93 1996 1151

[243] G. De Palo Darvin Yi and R. G. Endres, *A Critical-like Collective State Leads to Long-range Cell Communication in Dictyostelium discoideum Aggregation*. PLOS Biology **15** (2017) 1

List of publication

N.R.Zaoro, C.B. Tabi, A.S.Etémé, T.C.Kofané *"Unstable cAMP wave patterns during aggregation of Dictyostelium discoideum cells"*, Physics Letters A **384** (2020)126133 .

Appendix

APPENDIX A

$a_0 = \lambda_1 S/\epsilon_1\lambda_2,\ a_1 = 2\frac{\lambda_1 S}{\epsilon_1\lambda_2} - 1,\ a_2 = \frac{\lambda_1 S}{\epsilon_1\lambda_2} - 2,\ a_3 = S/\epsilon_1\lambda_2,\ a_4 = -1/\lambda_2,$

$b_1 = 1 + L_1,\ b_2 = L_1 + \kappa L_2 c,\ b_3 = L_2 c\kappa,\ b_4 = c + \kappa + L_2 c\kappa + L_1,\ b_5 = c\kappa + cL_2\kappa.$

APPENDIX B

$c_0 = a_0 + a_1\gamma_0 + a_2\gamma_0^3 - \gamma_0^3 + a_4\gamma_0^2\rho_0^2 + a_4\rho_0^2\gamma_0^3;$

$c_1 = a_1 + 2a_2\gamma_0 + 3\gamma_0^2 + 2a_3\gamma_0\rho_0^2 + 3a_4\gamma_0^2\rho_0^2;$

$c_2 = a_2 - 3\gamma_0 + a_3\rho_0^2 + 3a_4\gamma_0\rho_0^2;$

$c_3 = a_4\rho_0^2 - 1;$

$c_4 = 2a_3\gamma_0\rho_0 + 4a_4\gamma_0^2\rho_0;$

$c_5 = 2a_3\gamma_0^2 + 2a_4\gamma_0^3\rho_0;$

$c_6 = a_3\gamma_0^2 + a_4\gamma_0^3;$

$c_7 = 2a_3\rho_0 + 4a_4\gamma_0\rho_0;$

$c_8 = 2a_3\gamma_0 + 3a_4\gamma_0^2;$

$d_0 = L_1 - b_1\rho_0 + b_2\gamma_0 + b_3\gamma_0^2 + b_4\gamma_0\rho_0 + b_5\rho_0\gamma_0^2;$

$d_1 = -b_1 + b_4\gamma_0 + b_5\gamma_0^2;$

$d_2 = b_2 + b_4\rho_0 + 2b_5\gamma_0\rho_0 + 2b_3\gamma_0;$

$d_3 = b_3 + b_5\rho_0;\ d_4 = b_4 + 2b_5\gamma_0;$

$d_5 = b_5$

APPENDIX C

$\Omega_0^2 = (\frac{2c_1c_4d_0}{c_5} + c_1d_1) - (c_4d_0 + c_5d_2);$

$e_0 = -c_5d_0;\ e_1 = \frac{c_1c_4d_1}{c_5} + c_1d_4 + \frac{2c_1c_6d_2}{c_5} + \frac{2c_1c_8d_0}{c_5} - c_4d_2 - c_5d_3 - \frac{2c_1^2c_6d_1}{c_5^2} - c_7d_0;$

$e_2 = \frac{c_1c_4d_4}{c_5} + c_1d_5 + \frac{2c_1c_6d_3}{c_5} + \frac{2c_1^2c_6d_4}{c_5^2} + \frac{c_1c_7d_1}{c_5} + \frac{2c_1c_8d_2}{c_5} - c_4d_2 - c_7d_2 - \frac{2c_1^2c_8d_1}{c_5^2};$

$f_0 = -(c_1 + d_1 + \frac{2c_6d_0}{c_5})$; $f_1 = \frac{c_1c_4}{c_5} + \frac{4c_1c_6d_1}{c_5^2} - 2c_2 - \frac{c_4d_1}{c_5} - d_4 - \frac{2c_6d_2}{c_5} - \frac{2c_8d_0}{c_5}$;

$f_2 = \frac{4c_1c_6d_4}{c_5^2} + \frac{2c_1c_7}{c_5} + \frac{4c_1c_8d_1}{c_5^2} - 3c_3 - \frac{c_4d_4}{c_5} - d_5 - \frac{2c_6d_3}{c_5} - \frac{c_7d_1}{c_5} - \frac{2c_8d_2}{c_5} - \frac{c_1^2c_8}{c_5^2}$;

$g_0 = -(\frac{c_4}{c_5} + \frac{2c_6d_1}{c_5^2})$; $g_1 = \frac{2c_1c_8}{c_5^2} - \frac{2c_7}{c_5} - \frac{2c_8d_1}{c_5^2} - \frac{2c_6d_4}{c_5^2}$; $g_2 = -\frac{c_8}{c_5^2}$;

$h_0 = d_1v + \frac{2c_6d_0v}{c_5}$; $h_1 = \frac{c_4d_1v}{c_5} + d_4v + \frac{2c_6d_2v}{c_5} + \frac{2c_8d_0v}{c_5} - \frac{4c_1c_6d_1v}{c_5^2}$;

$h_2 = \frac{c_4d_4v}{c_5} + d_5v + \frac{2c_6d_3v}{c_5} + \frac{c_7d_1v}{c_5} + \frac{2c_8d_2v}{c_5} - \frac{4c_1c_6d_4v}{c_5^2} - \frac{4c_1c_8d_1}{c_5^2}$; $h_3 = \frac{c_4v}{c_5} + \frac{4c_6d_1v}{c_5^2}$; $h_4 = \frac{2c_8v}{c_5^2}$;

$h_5 = \frac{2c_6d_4v}{c_5^2} + \frac{2c_7v}{c_5} + \frac{4c_8d_1v}{c_5^2} - \frac{2c_1c_8v}{c_5^2}$;

$i_0 = -\frac{2c_6d_1v^2}{c_5^2}$; $i_1 = -(\frac{2c_6d_4v^2}{c_5^2} + \frac{2c_8d_1v^2}{c_5^2})$; $i_2 = -\frac{c_8v^2}{c_5^2}$;

$D_0 = -(\epsilon_1d_1 + \frac{2c_6\epsilon_1d_0}{c_5})$; $D_1 = \frac{4c_1\epsilon_1c_6d_1}{c_5^2} - \frac{c_4d_1\epsilon_1}{c_5} - \epsilon_1d_4 - \frac{2c_6d_2\epsilon_1}{c_5} - \frac{2c_8d_0\epsilon_1}{c_5}$;

$D_2 = \frac{4c_1c_6d_4\epsilon_1}{c_5^2} + \frac{4c_1c_8d_1\epsilon_1}{c_5^2} - \frac{c_4d_4\epsilon_1}{c_5} - d_5\epsilon_1 - \frac{2c_8d_1\epsilon_1}{c_5} - \frac{2c_6d_3\epsilon_1}{c_5} - \frac{c_7d_1\epsilon_1}{c_5}$;

$D_3 = -(\frac{c_4\epsilon_1}{c_5} + \frac{4c_6d_1\epsilon_1}{c_5^2})$; $D_4 = -\frac{2c_8\epsilon_1}{c_5^2}$; $D_5 = \frac{2c_1c_8\epsilon_1 - 4c_6d_4\epsilon_1 - 4c_8d_1\epsilon_1}{c_5^2} - \frac{2c_7\epsilon_1}{c_5}$;

$D_6 = \frac{4c_6d_1v\epsilon_1}{c_5^2}$; $D_7 = \frac{4c_6d_4v\epsilon_1 + 4c_8d_1v\epsilon_1}{c_5^2}$; $D_8 = \frac{2c_8v\epsilon_1}{c_5^2}$; $\lambda_0 = v$; $\mu_0 = \epsilon_1$;

$H_0 = \frac{2c_6d_1\epsilon_1^2}{c_5^2}$; $H_1 = \frac{2c_6d_4\epsilon_1^2 + 2c_8d_1\epsilon_1^2}{c_5^2}$; $H_2 = \frac{c_8\epsilon_1^2}{c_5^2}$;

Appendix D

$$\sum_{p=1}^{\infty}\epsilon^p\sum_{l=-\infty}^{+\infty}\Bigg(-l^2\omega^2\psi_p^{(l)}(\xi,\eta,\tau)+2il\omega\upsilon_g\varepsilon\frac{\partial}{\partial\xi}\psi_p^{(l)}(\xi,\eta,\tau)+\varepsilon^2\upsilon_g^2\frac{\partial^2}{\partial\xi^2}\psi_p^{(l)}(\xi,\eta,\tau)$$
$$-2il\omega\varepsilon^2\frac{\partial}{\partial\tau}\psi_p^{(l)}(\xi,\eta,\tau)\Bigg)A^{(l)}(x,t)+\Omega_0^2\left(\sum_{p=1}^{\infty}\epsilon^p\sum_{l=-\infty}^{+\infty}\psi_p^{(l)}(\xi,\eta,\tau)A^{(l)}(x,t)\right)+e_1\times$$
$$\left(\sum_{p=1}^{\infty}\epsilon^p\sum_{l=-\infty}^{+\infty}\psi_p^{(l)}(\xi,\eta,\tau)A^{(l)}(x,t)\right)^2+e_2\left(\sum_{p=1}^{\infty}\epsilon^p\sum_{l=-\infty}^{+\infty}\psi_p^{(l)}(\xi,\eta,\tau)A^{(l)}(x,t)\right)^3$$
$$+\left[f_0+f_1\left(\sum_{p=1}^{\infty}\epsilon^p\sum_{l=-\infty}^{+\infty}\psi_p^{(l)}(\xi,\eta,\tau)A^{(l)}(x,t)\right)+f_2\left(\sum_{p=1}^{\infty}\epsilon^p\sum_{l=-\infty}^{+\infty}\psi_p^{(l)}(\xi,\eta,\tau)\right.\right.$$
$$\left.\left.A^{(l)}(x,t)\right)^2\right]\sum_{p=1}^{\infty}\epsilon^p\sum_{l=-\infty}^{+\infty}\Bigg(-il\omega\psi_p^{(l)}(\xi,\eta,\tau)-\varepsilon\upsilon_g\frac{\partial}{\partial\xi}\psi_p^{(l)}(\xi,\eta,\tau)$$
$$+\varepsilon^2\frac{\partial}{\partial\tau}\psi_p^{(l)}(\xi,\eta,\tau)\Bigg)A^{(l)}(x,t)+\left[g_0+g_1\sum_{p=1}^{\infty}\epsilon^p\sum_{l=-\infty}^{+\infty}\psi_p^{(l)}(\xi,\eta,\tau)A^{(l)}(x,t)\right]\times \tag{3.3a}$$
$$\left(\sum_{p=1}^{\infty}\epsilon^p\sum_{l=-\infty}^{+\infty}\Bigg(-il\omega\psi_p^{(l)}(\xi,\eta,\tau)-\varepsilon\upsilon_g\frac{\partial}{\partial\xi}\psi_p^{(l)}(\xi,\eta,\tau)+\varepsilon^2\frac{\partial}{\partial\tau}\psi_p^{(l)}(\xi,\eta,\tau)\Bigg)\times\right.$$
$$\left.A^{(l)}(x,t)\right)^2+\left[h_0+h_1\sum_{p=1}^{\infty}\epsilon^p\sum_{l=-\infty}^{+\infty}\psi_p^{(l)}(\xi,\eta,\tau)A^{(l)}(x,t)+h_2\left(\sum_{p=1}^{\infty}\epsilon^p\sum_{l=-\infty}^{+\infty}\times\right.\right.$$
$$\left.\left.\psi_p^{(l)}(\xi,\eta,\tau)A^{(l)}(x,t)\right)^2+h_3\sum_{p=1}^{\infty}\epsilon^p\sum_{l=-\infty}^{+\infty}\Bigg(-il\omega\psi_p^{(l)}(\xi,\eta,\tau)-\varepsilon\upsilon_g\frac{\partial}{\partial\xi}\psi_p^{(l)}(\xi,\eta,\tau)\right.$$
$$\left.+\varepsilon^2\frac{\partial}{\partial\tau}\psi_p^{(l)}(\xi,\eta,\tau)\Bigg)A^{(l)}(x,t)+h_4\left(\sum_{p=1}^{\infty}\epsilon^p\sum_{l=-\infty}^{+\infty}\times\Bigg(-il\omega\psi_p^{(l)}(\xi,\eta,\tau)-\varepsilon\upsilon_g\frac{\partial}{\partial\xi}\times\right.$$
$$\left.\psi_p^{(l)}(\xi,\eta,\tau)+\varepsilon^2\frac{\partial}{\partial\tau}\psi_p^{(l)}(\xi,\eta,\tau)\Bigg)A^{(l)}(x,t)\right)^2+$$

$$h_5\left(\sum_{p=1}^{\infty}\epsilon^p\sum_{l=-\infty}^{+\infty}\psi_p^{(l)}(\xi,\eta,\tau)A^{(l)}(x,t)\right)\left(\sum_{p=1}^{\infty}\epsilon^p\sum_{l=-\infty}^{+\infty}\left(-il\omega\psi_p^{(l)}(\xi,\eta,\tau)-\varepsilon\upsilon_g\frac{\partial}{\partial\xi}\times\right.\right.$$
$$\left.\left.\psi_p^{(l)}(\xi,\eta,\tau)+\varepsilon^2\frac{\partial}{\partial\tau}\psi_p^{(l)}(\xi,\eta,\tau)\right)A^{(l)}(x,t)\right)\Bigg]\sum_{p=1}^{\infty}\epsilon^p\sum_{l=-\infty}^{+\infty}\left(ilk\psi_p^{(l)}(\xi,\eta,\tau)+\varepsilon\frac{\partial}{\partial\xi}\times\right.$$
$$\left.\psi_p^{(l)}(\xi,\eta,\tau)+\varepsilon\frac{\partial}{\partial\eta}\psi_p^{(l)}(\xi,\eta,\tau)\right)A^{(l)}(x,t)+\Bigg[i_0+i_1\sum_{p=1}^{\infty}\epsilon^p\sum_{l=-\infty}^{+\infty}\psi_p^{(l)}(\xi,\eta,\tau)A^{(l)}(x,t)$$
$$+i_2\sum_{p=1}^{\infty}\epsilon^p\sum_{l=-\infty}^{+\infty}\left(-il\omega\psi_p^{(l)}(\xi,\eta,\tau)-\varepsilon\upsilon_g\frac{\partial}{\partial\xi}\psi_p^{(l)}(\xi,\eta,\tau)+\varepsilon^2\frac{\partial}{\partial\tau}\psi_p^{(l)}(\xi,\eta,\tau)\right)\times$$
$$A^{(l)}(x,t)\Bigg]\left(\sum_{p=1}^{\infty}\epsilon^p\sum_{l=-\infty}^{+\infty}\left(ilk\psi_p^{(l)}(\xi,\eta,\tau)+\varepsilon\frac{\partial}{\partial\xi}\psi_p^{(l)}(\xi,\eta,\tau)+\varepsilon\frac{\partial}{\partial\eta}\psi_p^{(l)}(\xi,\eta,\tau)\right)\times\right.$$
$$\left.A^{(l)}(x,t)\right)^2+e_0=\Bigg[D_0+D_1\sum_{p=1}^{\infty}\epsilon^p\sum_{l=-\infty}^{+\infty}\psi_p^{(l)}(\xi,\eta,\tau)A^{(l)}(x,t)+D_2\left(\sum_{p=1}^{\infty}\epsilon^p\times\right.$$
$$\left.\sum_{l=-\infty}^{+\infty}\psi_p^{(l)}(\xi,\eta,\tau)A^{(l)}(x,t)\right)^2+D_3\sum_{p=1}^{\infty}\epsilon^p\sum_{l=-\infty}^{+\infty}\left(-il\omega\psi_p^{(l)}(\xi,\eta,\tau)-\varepsilon\upsilon_g\frac{\partial}{\partial\xi}\psi_p^{(l)}(\xi,\eta,\tau)\right.\qquad(3.3b)$$
$$\left.+\varepsilon^2\frac{\partial}{\partial\tau}\psi_p^{(l)}(\xi,\eta,\tau)\right)A^{(l)}(x,t)+D_4\left(\sum_{p=1}^{\infty}\epsilon^p\sum_{l=-\infty}^{+\infty}\left(-il\omega\psi_p^{(l)}(\xi,\eta,\tau)-\varepsilon\upsilon_g\frac{\partial}{\partial\xi}\times\right.\right.$$
$$\left.\left.\psi_p^{(l)}(\xi,\eta,\tau)+\varepsilon^2\frac{\partial}{\partial\tau}\psi_p^{(l)}(\xi,\eta,\tau)\right)A^{(l)}(x,t)\right)^2+D_5\left(\sum_{p=1}^{\infty}\epsilon^p\sum_{l=-\infty}^{+\infty}\psi_p^{(l)}(\xi,\eta,\tau)A^{(l)}(x,t)\right)\times$$
$$\left(\sum_{p=1}^{\infty}\epsilon^p\sum_{l=-\infty}^{+\infty}\left(-il\omega\psi_p^{(l)}(\xi,\eta,\tau)-\varepsilon\upsilon_g\frac{\partial}{\partial\xi}\psi_p^{(l)}(\xi,\eta,\tau)+\varepsilon^2\frac{\partial}{\partial\tau}\psi_p^{(l)}(\xi,\eta,\tau)\right)A^{(l)}(x,t)\right)$$
$$+D_6\sum_{p=1}^{\infty}\epsilon^p\sum_{l=-\infty}^{+\infty}\left(ilk\psi_p^{(l)}(\xi,\eta,\tau)+\varepsilon\frac{\partial}{\partial\xi}\psi_p^{(l)}(\xi,\eta,\tau)+\varepsilon\frac{\partial}{\partial\eta}\psi_p^{(l)}(\xi,\eta,\tau)\right)A^{(l)}(x,t)$$
$$+D_7\left(\sum_{p=1}^{\infty}\epsilon^p\sum_{l=-\infty}^{+\infty}\psi_p^{(l)}(\xi,\eta,\tau)A^{(l)}(x,t)\right)\sum_{p=1}^{\infty}\epsilon^p\sum_{l=-\infty}^{+\infty}\left(ilk\psi_p^{(l)}(\xi,\eta,\tau)+\varepsilon\frac{\partial}{\partial\xi}\right.$$
$$\left.\psi_p^{(l)}(\xi,\eta,\tau)+\varepsilon\frac{\partial}{\partial\eta}\psi_p^{(l)}(\xi,\eta,\tau)\right)A^{(l)}(x,t)$$

$$+ D_8 \sum_{p=1}^{\infty} \epsilon^p \sum_{l=-\infty}^{+\infty} \left(- il\omega \psi_p^{(l)}(\xi,\eta,\tau) - \varepsilon \upsilon_g \frac{\partial}{\partial \xi} \psi_p^{(l)}(\xi,\eta,\tau) + \varepsilon^2 \frac{\partial}{\partial \tau} \psi_p^{(l)}(\xi,\eta,\tau) \right)$$

$$A^{(l)}(x,t) \sum_{p=1}^{\infty} \epsilon^p \sum_{l=-\infty}^{+\infty} \left(ilk\psi_p^{(l)}(\xi,\eta,\tau) + \varepsilon \frac{\partial}{\partial \xi} \psi_p^{(l)}(\xi,\eta,\tau) + \varepsilon \frac{\partial}{\partial \eta} \psi_p^{(l)}(\xi,\eta,\tau) \right) \times$$

$$A^{(l)}(x,t) \Bigg] \sum_{p=1}^{\infty} \epsilon^p \sum_{l=-\infty}^{+\infty} \Big(- l^2 k^2 \psi_p^{(l)}(\xi,\eta,\tau) A^{(l)}(x,t) + 2ilk\varepsilon \frac{\partial}{\partial \xi} \psi_p^{(l)}(\xi,\eta,\tau) A^{(l)}(x,t) +$$

$$\varepsilon^2 \frac{\partial^2}{\partial \xi^2} \psi_p^{(l)}(\xi,\eta,\tau) A^{(l)}(x,t) + \varepsilon^2 \frac{\partial^2}{\partial \eta^2} \psi_p^{(l)}(\xi,\eta,\tau) A^{(l)}(x,t) \Big) + \Bigg[H_0 + H_1 \sum_{p=1}^{\infty} \epsilon^p \sum_{l=-\infty}^{+\infty}$$

$$\psi_p^{(l)}(\xi,\eta,\tau) A^{(l)}(x,t) + H_2 \sum_{p=1}^{\infty} \epsilon^p \sum_{l=-\infty}^{+\infty} \left(- il\omega \psi_p^{(l)}(\xi,\eta,\tau) - \varepsilon \upsilon_g \frac{\partial}{\partial \xi} \psi_p^{(l)}(\xi,\eta,\tau) \right.$$

$$\left. + \varepsilon^2 \frac{\partial}{\partial \tau} \psi_p^{(l)}(\xi,\eta,\tau) \right) A^{(l)}(x,t) \Bigg] \left(\sum_{p=1}^{\infty} \epsilon^p \sum_{l=-\infty}^{+\infty} \Big(- l^2 k^2 \psi_p^{(l)}(\xi,\eta,\tau) A^{(l)}(x,t) + \right. \tag{3.3c}$$

$$2ilk\varepsilon \frac{\partial}{\partial \xi} \psi_p^{(l)}(\xi,\eta,\tau) A^{(l)}(x,t) + \varepsilon^2 \frac{\partial^2}{\partial \xi^2} \psi_p^{(l)}(\xi,\eta,\tau) A^{(l)}(x,t) + \varepsilon^2 \frac{\partial^2}{\partial \eta^2} \psi_p^{(l)}(\xi,\eta,\tau) \times$$

$$\left. A^{(l)}(x,t) \Big) \right)^2 + \lambda_0 \sum_{p=1}^{\infty} \epsilon^p \sum_{l=-\infty}^{+\infty} \left(ilk\epsilon^2 \frac{\partial}{\partial \tau} \psi_p^{(l)}(\xi,\eta,\tau) - \epsilon^2 \upsilon_g \frac{\partial^2}{\partial \xi^2} \psi_p^{(l)}(\xi,\eta,\tau) - il\omega\epsilon \frac{\partial}{\partial \xi} \times \right.$$

$$\left. \psi_p^{(l)}(\xi,\eta,\tau) - il\omega\epsilon\upsilon_g \frac{\partial}{\partial \xi} \psi_p^{(l)}(\xi,\eta,\tau) + l^2 k\omega \psi_p^{(l)}(\xi,\eta,\tau) \right) A^{(l)}(x,t) + \mu_0 \sum_{p=1}^{\infty} \epsilon^p \sum_{l=-\infty}^{+\infty} \times$$

$$\Bigg(- l\omega\epsilon^2 \frac{\partial}{\partial \tau} \psi_p^{(l)}(\xi,\eta,\tau) - l^2 k^2 \epsilon^2 \frac{\partial}{\partial \tau} \psi_p^{(l)}(\xi,\eta,\tau) - 2il\epsilon^2 \upsilon_g \frac{\partial}{\partial \xi^2} \psi_p^{(l)}(\xi,\eta,\tau) +$$

$$2l^2 k\omega\epsilon \frac{\partial}{\partial \xi} \psi_p^{(l)}(\xi,\eta,\tau) + l^2 k^2 \epsilon \upsilon_g \frac{\partial}{\partial \xi} \psi_p^{(l)}(\xi,\eta,\tau) + il^3 k^2 \omega \psi_p^{(l)}(\xi,\eta,\tau) \Bigg) A^{(l)}(x,t)$$

Appendix E: The leading order (1,l)

$$\sum_{l=-1}^{1} l^2 \omega^2 \psi_l^1 A^l(\xi,\eta,t) + \Omega_0^2 \sum_{l=-1}^{1} l^2 A^l(n,t) = -D_0 \sum_{l=-1}^{1} l^2 A^l(\xi,\eta,t) \tag{3.4a}$$

Appendix F: The leading order (2,l)

$$
\begin{aligned}
&\sum_{l=-1}^{1} 2il\omega v_g \frac{\partial \psi_l^1}{\partial \xi} A^l(\xi,\eta,t) - \sum_{l=-1}^{1} l^2\omega^2 \psi_l^2 A^l(\xi,\eta,t) + \Omega_0^2 \sum_{l=-1}^{1} \psi_l^2 A^l(\xi,\eta,t) \\
&e_1 \left(\sum_{l=-1}^{1} \psi_l^2 A^l(\xi,\eta,t) \right) \left(\sum_{l=-1}^{1} \psi_l^2 A^l(\xi,\eta,t) \right) \\
&+ f_1 \left(\sum_{l=-1}^{1} \psi_l^1 A^l(\xi,\eta,t) \right) \left(\sum_{l=-1}^{1} -il\omega \psi_l^1 A^l(\xi,\eta,t) \right) + g_0 \left(\sum_{l=-1}^{1} il\omega \psi_l^1 A^l(\xi,\eta,t) \right)^2 \\
&h_1 \left(\sum_{l=-1}^{1} \psi_l^1 A^l(\xi,\eta,t) \right) \left(\sum_{l=-1}^{1} ilk \psi_l^1 A^l(\xi,\eta,t) \right) \\
&h_3 \left(\sum_{l=-1}^{1} il\omega \psi_l^1 A^l(\xi,\eta,t) \right) \left(\sum_{l=-1}^{1} ilk \psi_l^1 A^l(\xi,\eta,t) \right) + i_0 \left(\sum_{l=-1}^{1} ilk \psi_l^1 A^l(\xi,\eta,t) \right)^2 = \qquad (3.5a) \\
&- D_o \sum_{l=-2}^{2} l^2 k^2 \psi_l^2 A^l(\xi,\eta,t) + D_0 \sum_{l=-1}^{1} 2ilk \frac{\partial \psi_l^1}{\partial \xi} A^l(\xi,\eta,t) \\
&+ D_1 \left(\sum_{l=-1}^{1} \omega \psi_l^1 A^l(\xi,\eta,t) \right) \left(\sum_{l=-1}^{1} -l^2 k^2 \psi_l^1 A^l(\xi,\eta,t) \right) \\
&+ D_3 \left(\sum_{l=-1}^{1} il\omega\omega \psi_l^1 A^l(\xi,\eta,t) \right) \left(\sum_{l=-1}^{1} l^2 k^2 \psi_l^1 A^l(\xi,\eta,t) \right) \\
&- D_6 \left(\sum_{l=-1}^{1} ilk\omega \psi_l^1 A^l(\xi,\eta,t) \right) \left(\sum_{l=-1}^{1} l^2 k^2 \psi_l^1 A^l(\xi,\eta,t) \right) - H_0 \left(\sum_{l=-1}^{1} l^2 k^2 \psi_l^1 A^l(\xi,\eta,t) \right)^2
\end{aligned}
$$

Appendix G: The leading order (3,l)

$$
\begin{aligned}
&\sum_{l=-1}^{1} \upsilon_g^2 \frac{\partial^2 \psi_l^1}{\partial \xi^2} A^l(\xi,\eta,t) + \sum_{l=-2}^{2} 2il\omega\upsilon_g \frac{\partial \psi_l^1}{\partial \xi} A^l(\xi,\eta,t) - \sum_{l=-1}^{1} 2il\omega \frac{\partial \psi_l^1}{\partial \tau} A^l(\xi,\eta,t) \\
&- \sum_{l=-3}^{3} l^2\omega^2 \psi_l^3 A^l(\xi,\eta,t) + \Omega_0^2 \sum_{l=-3}^{3} \psi_l^3 A^l(\xi,\eta,t) \\
&+ 2e_1 \left(\sum_{l=-1}^{1} \psi_l^1 A^l(\xi,\eta,t) \right) \left(\sum_{l=-2}^{2} \psi_l^2 A^l(\xi,\eta,t) \right) + e_2 \left(\sum_{l=-1}^{1} \psi_l^1 A^l(\xi,\eta,t) \right)^3 \\
&- f_0 \left(\sum_{l=-1}^{1} \psi_l^1 A^l(\xi,\eta,t) \right) + f_1 \Big[\left(\sum_{l=-1}^{1} \psi_l^1 A^l(\xi,\eta,t) \right) \left(\sum_{l=-2}^{2} -il\omega\psi_l^2 A^l(\xi,\eta,t) \right) \times \\
&\left(\sum_{l=-2}^{2} \psi_l^2 A^l(\xi,\eta,t) \right) \left(\sum_{l=-1}^{1} -il\omega\psi_l^1 A^l(\xi,\eta,t) \right) \Big] + f_2 \left(\sum_{l=-1}^{1} \psi_l^1 A^l(\xi,\eta,t) \right)^2 \times \\
&\left(\sum_{l=-1}^{1} -il\omega\psi_l^1 A^l(\xi,\eta,t) \right) + 2g_0 \left(\sum_{l=-1}^{1} -il\omega\psi_l^1 A^l(\xi,\eta,t) \right) \left(\sum_{l=-2}^{2} -il\omega\psi_l^1 A^l(\xi,\eta,t) \right) \qquad (3.6a) \\
&+ g_1 \left(\sum_{l=-1}^{1} \psi_l^1 A^l(\xi,\eta,t) \right) \left(\sum_{l=-1}^{1} -il\omega\psi_l^1 A^l(\xi,\eta,t) \right)^2 + g_2 \left(\sum_{l=-1}^{1} -il\omega\psi_l^1 A^l(\xi,\eta,t) \right)^3 \\
&+ h_0 \left(\sum_{l=-1}^{1} ilk\psi_l^1 A^l(\xi,\eta,t) \right) + h_1 \Big[\left(\sum_{l=-1}^{1} \psi_l^1 A^l(\xi,\eta,t) \right) \left(\sum_{l=-2}^{2} ilk\omega\psi_l^2 A^l(\xi,\eta,t) \right) \times \\
&\left(\sum_{l=-2}^{2} \psi_l^2 A^l(\xi,\eta,t) \right) \left(\sum_{l=-1}^{1} ilk\omega\psi_l^1 A^l(\xi,\eta,t) \right) \Big] + h_2 \left(\sum_{l=-1}^{1} \psi_l^1 A^l(\xi,\eta,t) \right) \times \\
&\left(\sum_{l=-1}^{1} ilk\omega\psi_l^1 A^l(\xi,\eta,t) \right) + h_3 \Big[\left(\sum_{l=-1}^{1} -il\omega\psi_l^1 A^l(\xi,\eta,t) \right) \left(\sum_{l=-2}^{2} ilk\omega\psi_l^2 A^l(\xi,\eta,t) \right) \times \\
&\left(\sum_{l=-2}^{2} -il\omega\psi_l^2 A^l(\xi,\eta,t) \right) \left(\sum_{l=-1}^{1} ilk\psi_l^1 A^l(\xi,\eta,t) \right) \Big]
\end{aligned}
$$

$$
\begin{aligned}
&h_4\left(\sum_{l=-1}^{1}-il\omega\psi_l^2A^l(\xi,\eta,t)\right)\times\\
&\left(\sum_{l=-1}^{1}ilk\psi_l^1A^l(\xi,\eta,t)\right)+h_5\left(\sum_{l=-1}^{1}\psi_l^1A^l(\xi,\eta,t)\right)\left(\sum_{l=-1}^{1}-il\omega\psi_l^1A^l(\xi,\eta,t)\right)\times\\
&\left(\sum_{l=-1}^{1}ilk\psi_l^1A^l(\xi,\eta,t)\right)+2i_0\left(\sum_{l=-1}^{1}ilk\psi_l^1A^l(\xi,\eta,t)\right)\left(\sum_{l=-2}^{2}ilk\psi_l^2A^l(\xi,\eta,t)\right)+\\
&i_1\left(\sum_{l=-1}^{1}\psi_l^1A^l(\xi,\eta,t)\right)\left(\sum_{l=-1}^{1}ilk\psi_l^1A^l(\xi,\eta,t)\right)+i_2\left(\sum_{l=-1}^{1}-il\omega\psi_l^1A^l(\xi,\eta,t)\right)\times\\
&\left(\sum_{l=-1}^{1}ilk\psi_l^1A^l(\xi,\eta,t)\right)^2=D_0\big[\sum_{l=-3}^{3}-l^2k^2\psi_l^3A^l(\xi,\eta,t)+\sum_{l=-2}^{2}2ilk\frac{\partial\psi_l^2}{\partial\xi}A^l(\xi,\eta,t)+\\
&\sum_{l=-1}^{1}\frac{\partial^2\psi_l^1}{\partial\xi^2}A^l(\xi,\eta,t)+\sum_{l=-1}^{1}\frac{\partial^2\psi_l^1}{\partial\eta^2}A^l(\xi,\eta,t)\big]+D_1\big[\left(\sum_{l=-1}^{1}\psi_l^1A^l(\xi,\eta,t)\right)\times\\
&\left(\sum_{l=-2}^{2}-l^2k^2\psi_l^2A^l(\xi,\eta,t)\right)\left(\sum_{l=-2}^{2}\psi_l^2A^l(\xi,\eta,t)\right)\left(\sum_{l=-1}^{1}-lk^2\psi_l^1A^l(\xi,\eta,t)\right)\big]+\\
&D_2\left(\sum_{l=-1}^{1}\psi_l^1A^l(\xi,\eta,t)\right)\left(\sum_{l=-1}^{1}-l^2k^2\psi_l^1A^l(\xi,\eta,t)\right)+D_3\big[\left(\sum_{l=-1}^{1}-il\omega\psi_l^1A^l(\xi,\eta,t)\right)\times\\
&\left(\sum_{l=-2}^{2}-l^2k^2\psi_l^2A^l(\xi,\eta,t)\right)\left(\sum_{l=-2}^{2}-il\omega\psi_l^2A^l(\xi,\eta,t)\right)\left(\sum_{l=-1}^{1}-l^2k^2\psi_l^1A^l(\xi,\eta,t)\right)\big]+\\
&D_4\left(\sum_{l=-1}^{1}-il\omega\psi_l^1A^l(\xi,\eta,t)\right)^2\left(\sum_{l=-1}^{1}-l^2k^2\psi_l^1A^l(\xi,\eta,t)\right)+D_5\left(\sum_{l=-1}^{1}-\psi_l^1A^l(\xi,\eta,t)\right)\times\\
&\left(\sum_{l=-1}^{1}-il\omega\psi_l^1A^l(\xi,\eta,t)\right)\left(\sum_{l=-1}^{1}-l^2k^2\psi_l^1A^l(\xi,\eta,t)\right)+D_6\big[\left(\sum_{l=-1}^{1}ilk\omega\psi_l^1A^l(\xi,\eta,t)\right)\times\\
&\left(\sum_{l=-2}^{2}-l^2k^2\psi_l^2A^l(\xi,\eta,t)\right)\left(\sum_{l=-2}^{2}ilk\psi_l^2A^l(\xi,\eta,t)\right)\left(\sum_{l=-1}^{1}-l^2k^2\psi_l^1A^l(\xi,\eta,t)\right)\big]+\\
&D_7\left(\sum_{l=-1}^{1}\psi_l^1A^l(\xi,\eta,t)\right)\left(\sum_{l=-1}^{1}ilk\psi_l^1A^l(\xi,\eta,t)\right)\left(\sum_{l=-1}^{1}-l^2k^2\psi_l^1A^l(\xi,\eta,t)\right)
\end{aligned}
\tag{3.6b}
$$

$$
\begin{aligned}
&D_8\left(\sum_{l=-1}^{1}-il\omega\psi_l^1A^l(\xi,\eta,t)\right)\times\left(\sum_{l=-1}^{1}ilk\psi_l^1A^l(\xi,\eta,t)\right)\left(\sum_{l=-1}^{1}-l^2k^2\psi_l^1A^l(\xi,\eta,t)\right)\\
&+2H_0\left(\sum_{l=-1}^{1}-l^2k^2\psi_l^1A^l(\xi,\eta,t)\right)\left(\sum_{l=-1}^{1}-l^2k^2\psi_l^1A^l(\xi,\eta,t)\right)\\
&+H_1\left(\sum_{l=-1}^{1}psi_l^1A^l(\xi,\eta,t)\right)\times\left(\sum_{l=-1}^{1}-l^2k^2\psi_l^1A^l(\xi,\eta,t)\right)^2\\
&+H_2\left(\sum_{l=-1}^{1}-il\omega\psi_l^1A^l(\xi,\eta,t)\right)\left(\sum_{l=-1}^{1}-l^2k^2\psi_l^1A^l(\xi,\eta,t)\right)^2\\
&+\lambda_0\sum_{l=-1}^{1}l^2k\omega\psi_l^1A^l(\xi,\eta,t)+\mu_0\sum_{l=-1}^{1}il^3k^2\psi_l^1A^l(\xi,\eta,t)
\end{aligned}
\tag{3.6c}
$$

Unstable cAMP wave patterns during aggregation of Dictyostelium discoideum cells

Article *in* Physics Letters A · November 2019

DOI: 10.1016/j.physleta.2019.126133

4 authors:

Rodax Nelson Zaoro
Université de Bangui
1 PUBLICATION **1** CITATION
SEE PROFILE

Conrad Bertrand Tabi
Botswana International University of Science and Technology
119 PUBLICATIONS **813** CITATIONS
SEE PROFILE

Armand Sylvin Eteme
University of Yaounde I
12 PUBLICATIONS **87** CITATIONS
SEE PROFILE

Timoleon Crepin Kofane
University of Yaounde I
443 PUBLICATIONS **3,971** CITATIONS
SEE PROFILE

Physics Letters A 384 (2020) 126133

Contents lists available at ScienceDirect

Physics Letters A

www.elsevier.com/locate/pla

Unstable cAMP wave patterns during aggregation of Dictyostelium discoideum cells

N.R. Zaoro [a,b], C.B. Tabi [c,*], A.S. Etémé [a], T.C. Kofané [c,d]

[a] Laboratoire de Biophysique, Département de Physique, Faculté des Sciences, Université de Yaoundé I, B.P. 812 Yaoundé, Cameroon
[b] Department of Physics, Faculty of Science, University of Bangui, P. O. Box 1450, Bangui, Central African Republic
[c] Department of Physics and Astronomy, Botswana International University of Science and Technology, Private Bag 16, Palapye, Botswana
[d] Laboratoire de Mécanique, Département de Physique, Faculté des Sciences, Université de Yaoundé I, B.P. 812 Yaoundé, Cameroon

ARTICLE INFO

Article history:
Received 14 September 2019
Received in revised form 1 November 2019
Accepted 7 November 2019
Available online 12 November 2019
Communicated by M. Perc

Keywords:
Dictyostelium discoideum
Modulational instability
Patterns

ABSTRACT

Flow-driven formation of unstable patterns of cyclic adenosine monophosphate (cAMP) is investigated in the Martiel-Goldbeter (MG) model. This is predicted via a complex Ginzburg-Landau equation, derived from the MG model, under the so-called modulational instability process. Regions of parameters where patterns exist are discussed analytically and verified numerically. Quasi-periodic waves, spiral seeds and chaotic patterns are found to control information driven in a colony of homogeneously distributed *Dictyostelium discoideum* cells under the change of the extracellular cAMP degradation rate (k_e), the production rate of cAMP (σ) and the advection flow velocity (V_f). Our results suggest that these quantities play a key role in the efficient regulation of communication within an amoeba colony, and the presence of the flow makes it possible to understand pattern formation process among D. *discoideum* cells under spontaneous fluid flow in their natural environment.

1. Introduction

Biological pattern formation usually takes place as a consequence of the interaction of individual cells to create multicellular structures. One of the fascinating dynamics of such entities, both for biologists and nonequilibrium physicists, is offered by the aggregation of amoebae in *Dictyostelium*, a process which has some similarities with Belousov-Zhabotinsky reactions [1,2]. In fact, under favorable conditions of life, such as the presence of food in the soil, *Dictyostelium* amoebae grow and divide individually. However, after a short period of starvation, they have to aggregate and create a multicellular slug, thanks to a substance that has been recognized as cyclic adenosine $3', 5'-$monophosphate (cAMP) which is initially released by some of the amoebae and then relayed by the others, thus controlling chemotaxis in the course of aggregation. More precisely, there exists a cellular rhythm in the production of cAMP which supports the wave-like nature of aggregation in D. *discoideum* [3,4]. This represents one of the most striking examples of spiral waves and target patterns in nature which have attracted considerable attention from the pattern formation community. Recent experimental results on flow-driven waves in the signaling of the amoebae D. *discoideum* have shown that cAMP wave patterns may develop spontaneously under the effect of a flow and propagate with a velocity proportional to the driving flow velocity [5]. Due to nature exposure, many factors are expected to significantly change the wave generation processes of D. *discoideum*, including advective flows [6], external magnetic forces during the early stage of D. *discoideum* morphogenesis [7], just to name a few.

Many models have been used over the years to describe the cAMP patterns in D. *discoideum* [8–10]. Among these, the most widely utilized are Martiel-Goldbeter (MG) model [8], Monk-Othmer model [11] and Tang-Othmer model [12]. Most of these are capable of accounting for the most important features of cAMP signals through the process of cell aggregation. Moreover, each particular model possesses its singular way of breaking the homogeneity and producing wave patterns. However, the MG model has been extensively used, under different contexts. Initially, the MG model was formulated as a set of three ordinary differential equations for intracellular cAMP, extracellular cAMP and the membrane receptors. The same kinetic laws were adopted and extended by Tyson and coworkers to a field of stationary signaling cells by taking into account spatial diffusion of cAMP through the extracellular medium [13]. Along the same line, the effect of advection on the pattern formation in a colony of homogeneously distributed D. *dis-*

* Corresponding author.
E-mail addresses: zaoronelson@yahoo.fr (N.R. Zaoro), conrad@aims.ac.za, tabic@biust.ac.bw (C.B. Tabi), etemearmand@yahoo.fr (A.S. Etémé), tckofane@yahoo.com (T.C. Kofané).

https://doi.org/10.1016/j.physleta.2019.126133
0375-9601/

coideum cells was studied using the standard two-component MG model in one dimension. In order to address the experimentally reported flow-driven waves, the effect of the flow profile on the flow-driven waves was studied numerically, where the MG model was extended to its two-dimensional formulation through the following two-component set of equations [14]:

$$\frac{\partial \gamma}{\partial t} = \epsilon_1 \nabla^2 \gamma + \overrightarrow{\upsilon} \cdot \overrightarrow{\nabla} \gamma + \frac{1}{\epsilon_1}[s\phi(\rho,\gamma) - \gamma], \tag{1}$$

$$\frac{\partial \rho}{\partial t} = -f_1(\gamma)\rho + f_2(\gamma)(1-\rho), \tag{2}$$

with $f_1(\gamma) = \frac{1+\kappa\gamma}{1+\gamma}$, $f_2(\gamma) = \frac{L_1+\kappa L_2 c\gamma}{1+c\gamma}$, $\phi(\rho,\gamma) = \frac{\lambda_1+Y^2}{\lambda_2+Y^2}$, $Y = \frac{\rho\gamma}{1+\gamma}$, where ρ is the fraction of active receptors on the membrane, γ is the dimensionless extracellular cAMP concentration and $\overrightarrow{\nabla} = \frac{\partial}{\partial x}\overrightarrow{i} + \frac{\partial}{\partial y}\overrightarrow{j}$. $\epsilon_1 = \frac{k_1}{k_e}$, $\epsilon_2 = \frac{k_1}{k_i+k_t}$, $\kappa = \frac{k_2}{k_1}$, with k_1 being the desensitization rate of active receptors and k_e, the degradation rate of extracellular cAMP. $s = \frac{qk_t\alpha\sigma}{k_e(k_t+k_i)h(1+\alpha)}$ depends on σ, the production rate of cAMP. We should stress that the term $\overrightarrow{\upsilon} \cdot \overrightarrow{\nabla}\gamma$ represents the effect of the external flow and was initially introduced by Gholami et al. [14], as said so far. In this work, we also adopt the same model and we use the theory of modulational instability (MI) to predict and characterize pattern formation of *D. discoideum*, which, to the best of our knowledge, has not yet been reported in the literature.

MI is in fact a process closely related to pattern and soliton formation [15–18]. Thanks to the interplay between nonlinear and dispersion effects, self-induced modulation of the steady state emerges, causing a quasi-continuous wave pulse to disintegrate during propagation. Under a broad range of contexts, MI takes place both in continuous models and discrete systems that are usually described by the nonlinear Schrödinger (NLS) or the complex Ginzburg-Landau (CGL) equations. Reaction-diffusion equations contain many parameters that are specific to each system, which renders the possibility of making general predictions of pattern formation in oscillatory media very limited. However, it was shown by Kuramoto [19] that all reaction-diffusion systems, with a reaction dynamics close to the onset of oscillations, can be reduced to a universal envelope equation, with a great predictive power, which is the CGL equation with rich pattern formation. Therefore, many physical factors can affect the dynamics of the system competitively or cooperatively such as diffusion, nonlinearity, inhomogeneities, advection and noise or thermal fluctuations, just to name a few. Recent contributions by Tabi and co-workers go that directions, with very good applications to neural networks [20], energy transport and storage in biomolecules [21] and blood flow in elastic tubes [22]. In this letter, albeit in an approximate way, we relate all the coefficients of the CGL equation to the physical parameters of the MG model for pattern formation in D. *discoideum*, through an averaging method known as the multiple-scale expansion. The theory of MI is then used to predict the emergence of wave patterns, followed by direct numerical simulation of the generic MG model. The effect of factors like the degradation rate of extracellular cAMP (k_e) and the production rate of cAMP (σ) is studied. The whole work ends with some concluding remarks on the results and their biological implications.

2. CGL equation and linear stability analysis

In order to proceed, we first introduce dimensionless time and space as $t \to k_1 t'$ and $(x,y) \to \frac{k_1}{\sqrt{Dk_e}}(x',y')$. Additionally, the dimensionless flow velocity is such that $\overrightarrow{\upsilon} = \left(V_f/\sqrt{k_e D}\right)\overrightarrow{e_x}$, where V_f is dimensionless, with $D = 0.024\ \text{mm}^2.\text{min}^{-1}$ being the diffusion coefficient of cAMP. Values of other parameters are detailed in Ref. [14], except the values of $k_1 = 0.09\,\text{min}^{-1}$ and $k_2 = 1.665\,\text{min}^{-1}$ which can be suitably adjusted to obtain waves with a period of approximately 5 min. In order to study nonlinear effects and obtain the corresponding CGL from Eqs. (1) and (2), trial solutions γ and ρ are decomposed as

$$\begin{pmatrix} \gamma(x,y,t) \\ \rho(x,y,t) \end{pmatrix} = \begin{pmatrix} \gamma_0 \\ \rho_0 \end{pmatrix} + \sum_{p=1}^{\infty} \epsilon^p \sum_{l=-\infty}^{+\infty} \begin{pmatrix} \psi_l^{(p)}(\xi,\eta,\tau) \\ \phi_l^{(p)}(\xi,\eta,\tau) \end{pmatrix} A^l(x,t), \tag{3}$$

where γ_0 and ρ_0 are steady-state solutions. $A^l(x,t) = e^{il(kx-\omega t)}$ represents the carrier wave solution, with the frequency $\omega = \sqrt{\Omega_0^2 + D_0 k^2}$. Spatial variables are scaled as $\xi = \varepsilon(x - v_g t)$, $\eta = \varepsilon y$ and the slow time scale $\tau = \varepsilon^2 t$ has been applied, with $v_g = \frac{D_0 k}{\omega}$ being the group velocity. The frequency ω and the corresponding group velocity v_g are plotted in Fig. 1 versus the wavenumber k, for different values of the degradation rate of the intracellular cAMP k_e. For $k = 0$, we have $\omega = \Omega_0$ which is not sensitive to the change in k_e. However, when $k \neq 0$, the frequency decreases with increasing k_e due to the parameter D_0 which depends on system parameters (see Fig. 1(a)). Although $v_g = 0$ for $k = 0$, its value is also found to be sensitive to the change in k_e for $k > 0$. Fig. 1(b) shows that v_g is a decreasing function of the degradation rate of the intracellular cAMP. Using the multiple-scale expansion and after cumbersome and long calculations, the corresponding CGL equation that combines Eqs. (1) and (2) is obtained at order the order (ϵ^3, A^1) in the form

$$i\frac{\partial \psi}{\partial \tau} + \frac{P_1}{2}\frac{\partial^2 \psi}{\partial \xi^2} + \frac{P_2}{2}\frac{\partial^2 \psi}{\partial \eta^2} + (Q_r + iQ_i)\,|\,\psi\,|^2\,\psi + i\frac{(R_r + iR_i)}{2}\psi = 0, \tag{4}$$

where the coefficient $P_1, P_2, Q_r, Q_i, R_r, R_i$ are given by

$$\begin{aligned}
P_1 &= \frac{1}{\omega}(D_0 - v_g^2), \quad P_2 = \frac{D_0}{\omega}, \\
Q_r &= \frac{1}{2\omega}[3g_1\omega^2 + h_5 k\omega + 3D_4 k^2\omega^2 + D_8 k^3\omega + 3H_1 k^4 - 3e_2 \\
&\quad - 3D_2 k^2 - 2e_1 m_1 + (2h_3 k\omega + 3D_1 k^2 + 4H_0 k^4 - 2e_1 \\
&\quad - 2g_0\omega^2 - 4i_0 k^2)m_r + 6m_i(D_6 k^3 - D_3 k^2\omega)], \\
Q_i &= \frac{1}{2\omega}[\omega f_2 + 3g_2\omega^3 + h_4 k\omega^2 + 3i_2 k^2\omega \\
&\quad + D_5 k^2\omega - h_2 k - D_7 k^3 - H_2 k^4\omega + (\omega f_1 - h_1 k)m_1 \\
&\quad + (2h_3 k\omega + 3D_1 k^2 + 4H_0 k^4 - 2e_1 - 2g_0\omega^2 - 4i_0 k^2)m_i \\
&\quad + 6m_r(D_3 k^2\omega - D_6 k^3)] \\
R_r &= \frac{\omega f_0 - h_0 k + \mu_0 k^2\omega}{\omega}, \quad R_i = \lambda_0 k.
\end{aligned} \tag{5}$$

Except for P_1, P_2 all the other parameters are complex and the subscripts r and i denote their real and imaginary parts, respectively (For detailed expressions of parameters, see *Appendix*). They are plotted in Fig. 2, versus the wavenumber k, and show different features when k_e changes. In fact, except Q_r and Q_i that have some negative values, the rest of the coefficients remain positive. This shows that the found CGL equation remains linked to system parameters and gives credit to the linear stability analysis that will be performed. The CGL equation is a universal model that gives the possibility to predict pattern formation in reaction-diffusion models [23]. The applicability of the CGL equations goes far beyond reaction-diffusion systems to cover other research areas actually related to superconductivity, nonlinear optics, plasmas,

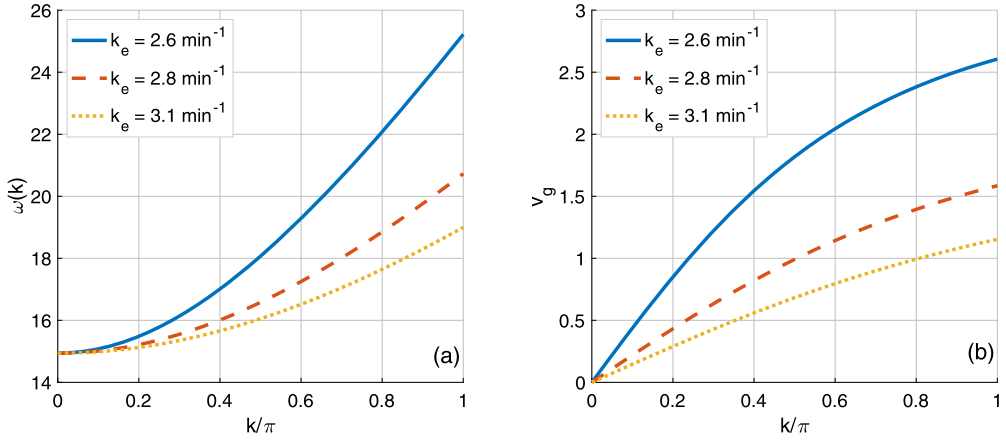

Fig. 1. The angular wave frequency ω and the group velocity v_g are plotted against the wavenumber k. The influence of the degradation rate of extracellular cAMP by the enzyme phosphodiesterase k_e is studied for a fixed value $\sigma = 0.2$ min^{-1} of the production rate of intercellular cAMP.

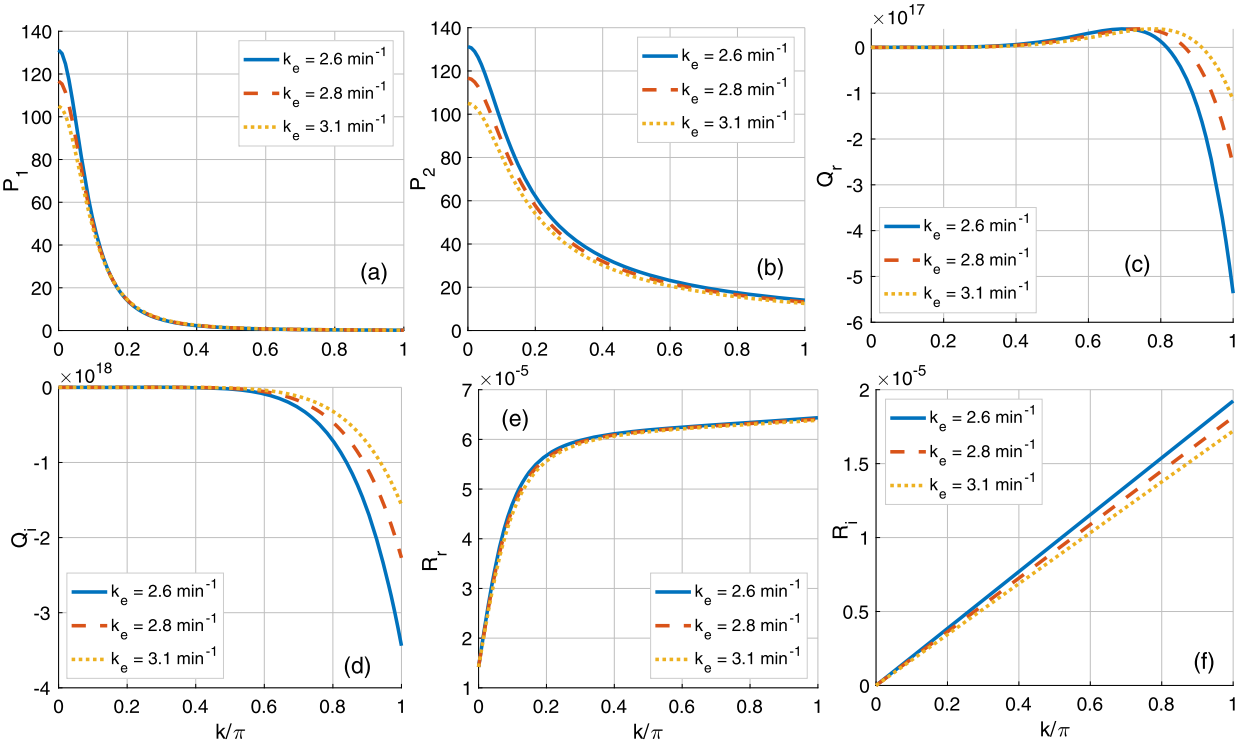

Fig. 2. Variations of the coefficients of the CGL Eq. (4) versus the wavenumber k, with changing the degradation rate of extracellular cAMP by the enzyme phosphodiesterase k_e. The dispersion coefficient P_1, P_2, as well the dissipative coefficients R_r and R_i remain positive for any k and k_e. However, the real and imaginary parts of the nonlinearity coefficient Q_r and Q_i are positives for some values of k and negatives for others. All the panels have been plotted for a fixed value $\sigma = 0.2$ min^{-1} of maximum activity of adenylate cyclase.

Bose-Einstein condensates, and quantum field theories [24]. Using Eq. (4), we want to predict the occurrence of nonlinear patterns, through the MI process, and their response to model parameters over long periods of time. We assume a plane wave $\psi(\xi,\eta,\tau) = \phi_0 e^{i(q_1\xi+q_2\eta-\varpi\tau)}$ to be solution of Eq(4), where the wavenumbers q_1 and q_2, the frequency ϖ and the amplitude ϕ_0, after separating the real and imaginary parts, satisfy the relations $\varpi = \frac{P_1}{2}q_1^2 + \frac{P_2}{2}q_2^2 + \frac{Ri}{2} - Q_r\phi_0^2$ and $Q_i\phi_0^2 + \frac{R_r}{2} = 0$. The solution is then perturbed as $\psi(\xi,\eta,\tau) = [\phi_0 + \Phi(\xi,\eta,\tau)]e^{i(q_1\xi+q_2\eta-\varpi\tau+\mu(\xi,\eta,\tau))}$, where $\Phi(\xi,\eta,\tau)$ and $\mu(\xi,\eta,\tau)$ are, respectively, the amplitude and phase perturbations, considered to be small with respect to the unperturbed amplitude and phase of the wave. This leads to a set of equations for the perturbations Φ and μ whose solutions are taken as $\Phi(\xi,\eta,\tau) = \Phi_0 e^{i(K_1\xi+K_2\eta-\nu\tau)} + cc$ and $\mu(\xi,\eta,\tau) = \mu_0 e^{i(K_1\xi+K_2\eta-\nu\tau)} + cc$, with K_1 and K_2 being the wavenumbers of the perturbations and ν their angular frequency. Making use of these leads to a homogeneous system for Φ_0 et μ_0 whose determinant should be zero for non-trivial solution to exist. This gives a nonlinear dispersion relation for the perturbation frequency ν from which the growth rate of MI is derived in the form

$$\Gamma(K_1,K_2) = \frac{1}{2}\left[R_r + \sqrt{R_r^2 + (P_1K_1^2 + P_2K_2^2)\left(\frac{4Q_r\phi_0^2}{P_1K_1^2 + P_2K_2^2} - 1\right)}\right]. \quad (6)$$

In order for Γ to be positive, we should have $\frac{4Q_r\phi_0^2}{P_1K_1^2+P_2K_2^2} - 1 > 0$, which will be possible only if the amplitude goes beyond a thresh-

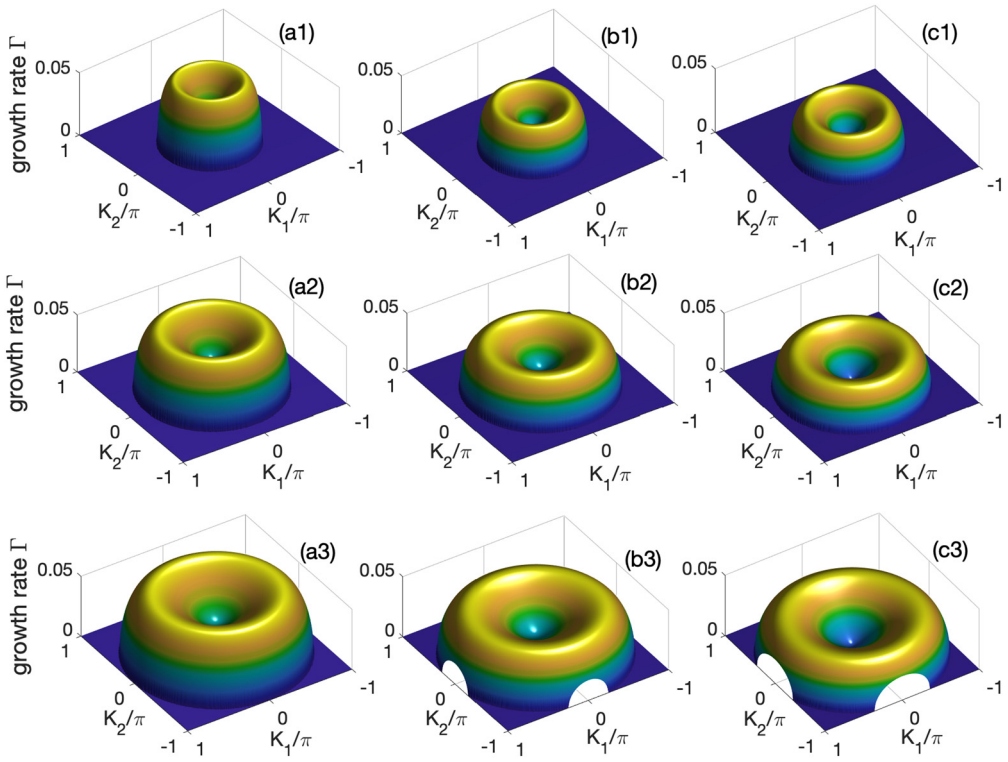

Fig. 3. The MI growth rate Γ versus the wavenumbers K_1 and K_2. Panels $(aj)_{j=1,2,3}$ corresponds to $\sigma = 0.2$ min^{-1}, panels $(bj)_{j=1,2,3}$ to $\sigma = 0.3$ min^{-1} and panels $(cj)_{j=1,2,3}$ gives the MI growth rate for $\sigma = 0.6$ min^{-1}. From top to bottom, the different rows have been, respectively, computed for $k_e = 2.6$ min^{-1} $(j = 1)$, 2.8 min^{-1} $(j = 2)$ and 3.1 min^{-1} $(j = 3)$.

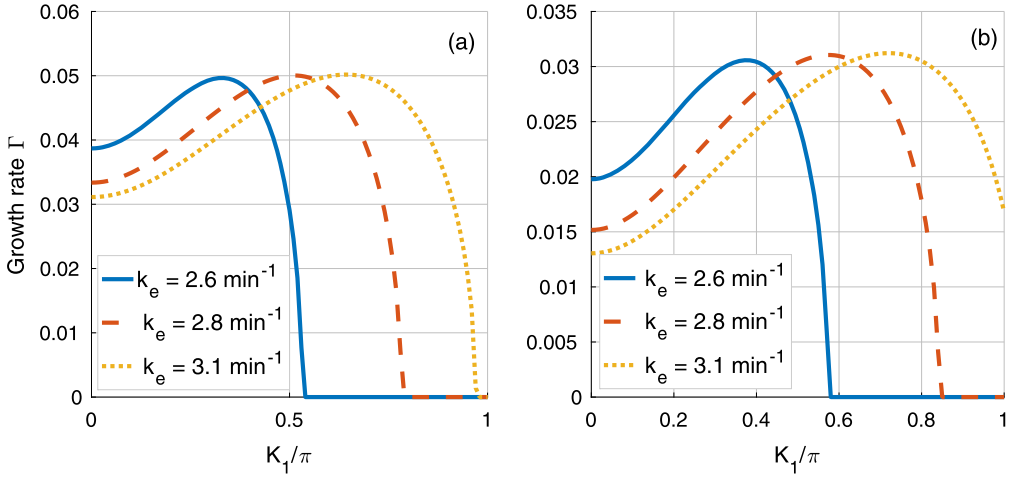

Fig. 4. The MI growth rate $\Gamma(K_1, K_2)$ versus the longitudinal wavenumber K_1, with $K_2 = 0.1\pi$. Each panel corresponds to a fixed value of σ, while Γ is plotted for three different values of k_e. Panel (a) corresponds to $\sigma = 0.2$ min^{-1} and panel (b) to $\sigma = 0.6$ min^{-1}. $\Gamma > 0$ is delimited by the intervals $0 < K_1 < K_{1,cr}$, where the plane wave is expected to be unstable under slight modulation.

old $\phi^2_{0,cr} = \frac{P_1 K_1^2 + P_2 K_2^2}{4Q_r}$. When values for ϕ_0 are suitably chosen, we obtain the MI growth rate shown in Fig. 3, where panels $(aj)_{j=1,2,3}$ corresponds to $\sigma = 0.2$ min^{-1}, panels $(bj)_{j=1,2,3}$ to $\sigma = 0.3$ min^{-1} and panels $(cj)_{j=1,2,3}$ gives the MI growth rate for $\sigma = 0.6$ min^{-1}. In the $(K_1, K_2)-$plane, it is obvious from the two sets of diagrams that the area of instability, i.e., where $\Gamma(K_1, K_2) > 0$, gets expanded with increasing k_e. However, regions of instability are more larger for $\sigma = 0.6$ min^{-1} than for the other values. This shows that both the production and degradation rates of cAMP may deeply influence pattern formation. Fixing $K_2 = 0.1\pi$, the same regions are clearly depicted in Fig. 4, where Γ is plotted versus K_1. Fig. 4(a) shows results for $\sigma = 0.2$ min^{-1}, and $\Gamma > 0$ is delimited by the intervals $0 < K_1 < K_{1,cr}$, where the plane wave becomes unstable under slight modulations. $K_{1,cr}$, in Fig. 4(a), increases when k_e takes the respective value 2.6 min^{-1}, 2.8 min^{-1} and 3.1 min^{-1}. The same behaviors appear for $\sigma = 0.6$ min^{-1}. However, for $k_e = 3.1$ min^{-1}, there is marginal instability, which corresponds to what is shown in Fig. 3(c3).

3. Unstable wave patterns of cAMP

In the following, our analysis and numerical simulations are focused on pattern formation in order to bring out the effect of the external flow on the spatiotemporal development of MI. The MG model of Eqs. (1) and (2) has been used in the simulations, with the initial conditions being the perturbed plane waves, with

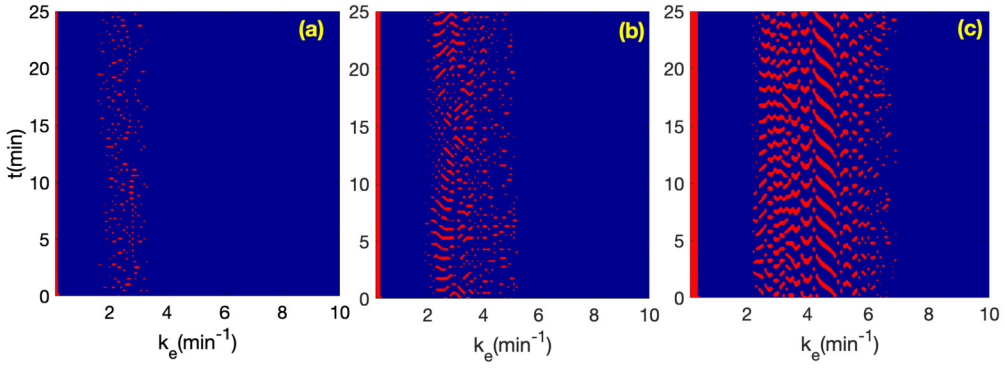

Fig. 5. The bifurcation diagrams of cAMP extracellular concentration $\gamma(50,50)$ in the $(k_e,t)-$plane with increasing σ (i.e., higher activity of the enzyme adenylate cyclase) as: $\sigma=0.1$ min^{-1} in panel (a), $\sigma=0.15$ min^{-1} in panel (b) and $\sigma=0.2$ min^{-1} in panel (c). The diagrams allow to find the threshold value k_e above which the dynamical activity of D. *discoideum* is switched on. (For interpretation of the colors in the figure(s), the reader is referred to the web version of this article.)

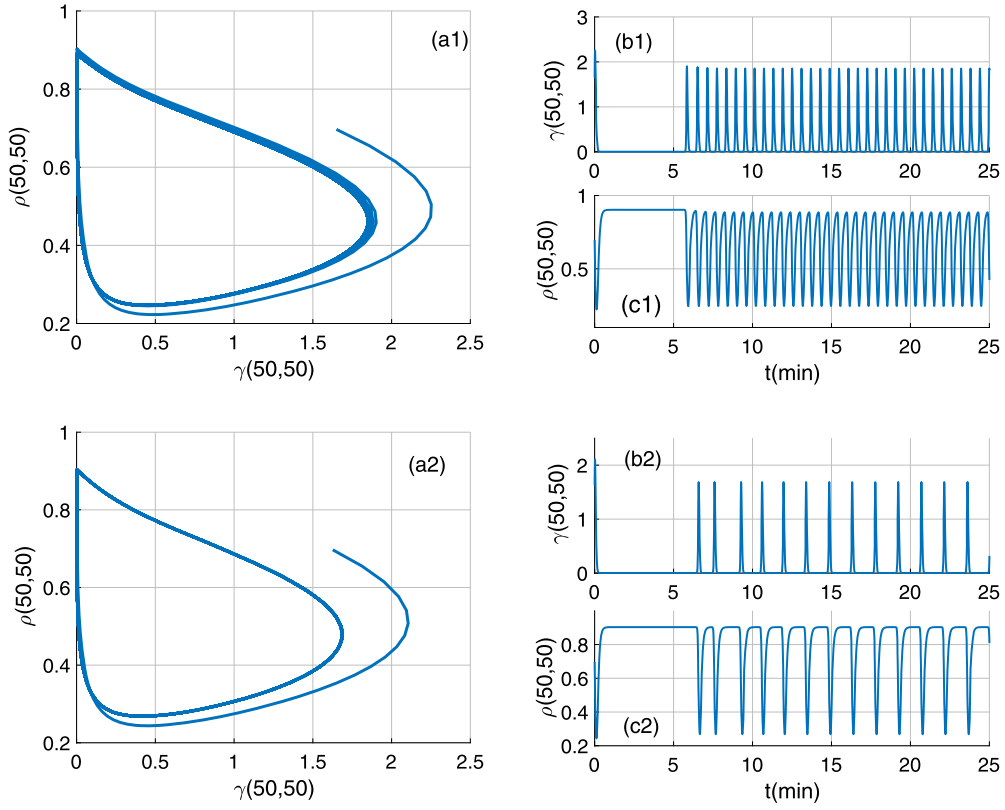

Fig. 6. The phase portraits in the $(\gamma,\rho)-$plane are depicted in panels $(\text{aj})_{j=1,2}$. Time series for cAMP concentration γ are displayed in panels $(\text{bj})_{j=1,2}$, while time series for the fraction of receptors in the active state ρ are shown in panels $(\text{cj})_{j=1,2}$. The features are obtained in absence of the advective flow, with $\sigma=0.2$ min^{-1} and k_e taking the values 2.8min^{-1} $(j=1)$ and 3.1 min^{-1} $(j=2)$.

wavenumbers $K_1=0.4\pi$ and $K_2=0.1\pi$ belonging to the instability areas depicted in Figs. 3 and 4. No-flux boundary conditions have been considered in the Merson modification of the Runge-Kutta computational scheme, with a time step $\Delta t=10^{-4}$ min and spatial meshes $\Delta x=\Delta y=0.01$ mm. Simulation results giving lower and higher threshold values of k_e which support cAMP pattern formation via MI process are shown in the bifurcation diagram of Fig. 5, with red regions being where wave patterns are expected. The bifurcation behaviors of the system show clearly that the interval for active k_e is very sensitive to the change in σ, as expected, since the activity of adenylate cyclase, which produces intracellular cAMP, controls the rate at which the extracellular cAMP gets degraded. The balance between the two parameters may then play an important role in the occurrence of wave patterns. Based on the results of Fig. 5, the time series and phase diagrams describing the dynamics of both the cAMP concentration γ and the fraction of receptors in the active state ρ are depicted in Figs. 6 and 7. In order to get the results of Fig. 6, we have fixed $\sigma=0.2$ min^{-1}, and values for k_e have been picked from the active region of Fig. 5. In this regard, Panels (a1), (b1) and (c1) of Fig. 6 have been obtained $k_e=2.8$ min^{-1}, while panels (a2), (b2) and (c2) were obtained for $k_e=3.1$ min^{-1}. The dynamics of γ and ρ is in general quasi-periodic, but with increasing the degradation rate of cAMP, the wave frequency drops. On the other hand, when the production rate of intercellular cAMP is increased to $\sigma=0.25$ min^{-1}, the wave frequencies for γ and ρ increase, although there is some wave modulation for $k_e=2.8$ min^{-1}, as depicted in Figs. 7(b1) and (c1), in the time interval 12 min$<t<$18 min, followed by quasi-periodic oscillations of the concentration γ and ρ for $t<18$ min. These modulations disappear when k_e increases to 3.1 min^{-1}, and

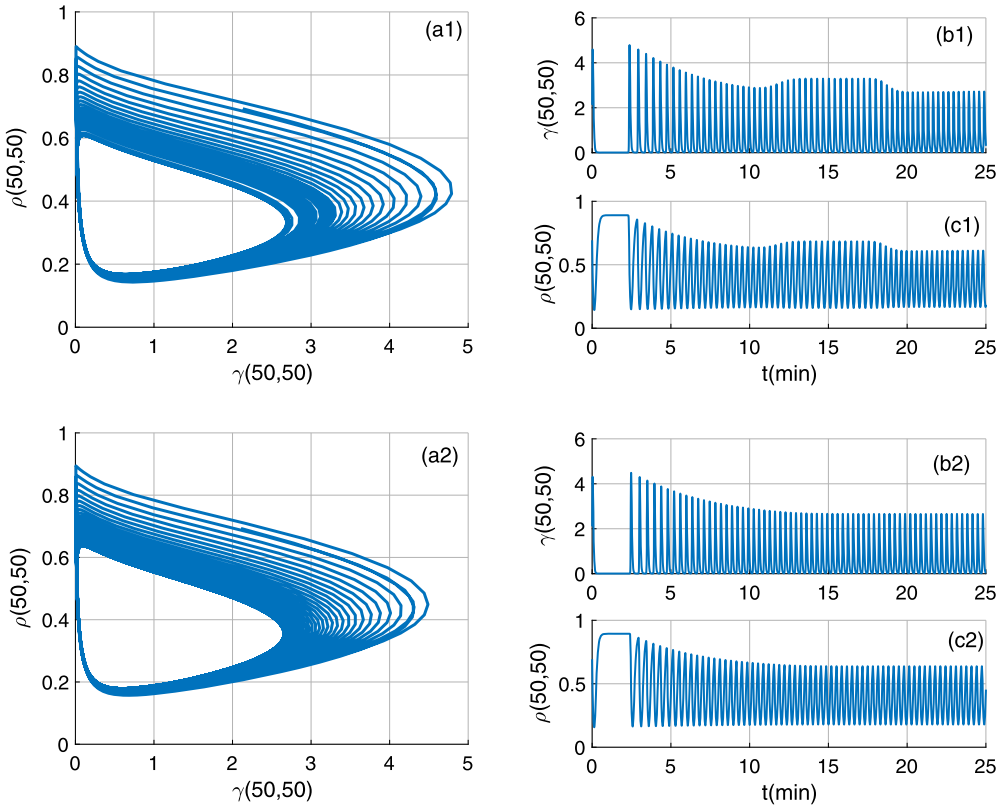

Fig. 7. The phase portraits in the $(\gamma, \rho)-$plane are depicted in panels $(\text{aj})_{j=1,2}$. Time series for cAMP concentration γ are displayed in panels $(\text{bj})_{j=1,2}$, while time series for the fraction of receptors in the active state ρ are shown in panels $(\text{cj})_{j=1,2}$. These results have been obtained in the absence of the advective flow, with $\sigma = 0.25$ min^{-1} and k_e taking the values 2.8 min^{-1} $(j = 1)$ and 3.1 min^{-1} $(j = 2)$.

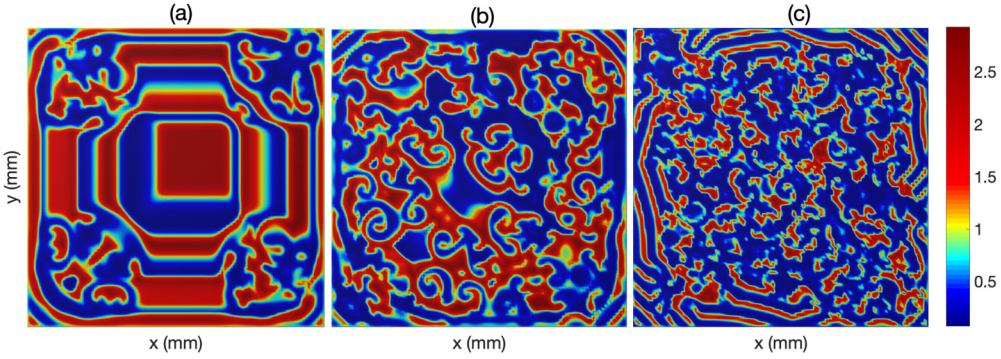

Fig. 8. The panels show the manifestation of MI through pattern formation in absence of the external flow, for different values of the degradation rate of the intracellular cAMP k_e: (a) $k_e = 2.6$ min^{-1}, (b) $k_e = 2.8$ min^{-1} and (c) $k_e = 3.1$ min^{-1}, with $\sigma = 0.3$ min^{-1}. All the panels have been recorded at time $t = 60$ min.

the wave amplitude decreases and becomes constant at $t > 12$ min (see Figs. 7(b2) and (c2)). This shows the effect of each of the parameters, which may contribute to balance nonlinear and dispersive effects for nonlinear modes to emerge in the system. In the rest of this letter, we fixed $\sigma = 0.3$ min^{-1} and used different values of k_e. Also, most of the simulations were recorded at time $t = 60$ min.

In absence of the advective flow, i.e., $V_f = 0$, typical examples of simulation results are given in Fig. 8, where panels (a), (b) and (c) correspond to the respective values 2.6 min^{-1}, 2.8 min^{-1} and 3.1 min^{-1} of k_e. Initially, as predicted by the linear stability analysis on the 2D CGL equation, the plane wave solution breaks up into wave patterns in panel (a), then forms localized patterns that are a mixed-up of unstable patterns and spiral seeds (see Fig. 8(b)). The later scenario tends to disappear when the degradation rate k_e increases, leading to erratic structures and sporadic bands along the boundaries of the system (see Fig. 8(c)). Also, one can still see some spots of high cAMP concentration that confirm the robust tendency of the amoeba to aggregate under any starvation situation.

We now consider a flow that goes from left to right, in the $x-$direction. Figs. 9$(\text{aj})_{j=1,2,3}$ show the corresponding spatiotemporal behaviors of the dimensionless concentration of cAMP for $k_e = 2.6$ min^{-1}, which corresponds to the case of Fig. 8(b). Panels $(\text{aj})_{j=1,2,3}$ have been recorded, respectively, from left to right, for the flow velocities $V_f = 0.2$ mm.min^{-1}, 1 mm.min^{-1} and 1.8 mm.min^{-1}. Obviously, the disintegration of the initial plane wave importantly depends on the imposed flow velocity. For example, in Fig. 9(a1), cooperative patterns appear in the system for $V_f = 0.2$ mm.min^{-1}, with large spots of high cAMP concentration. By increasing the flow velocity to 1 mm.min^{-1}, one obtains the wave patterns of Fig. 9(a2), characterized by trains of upstream

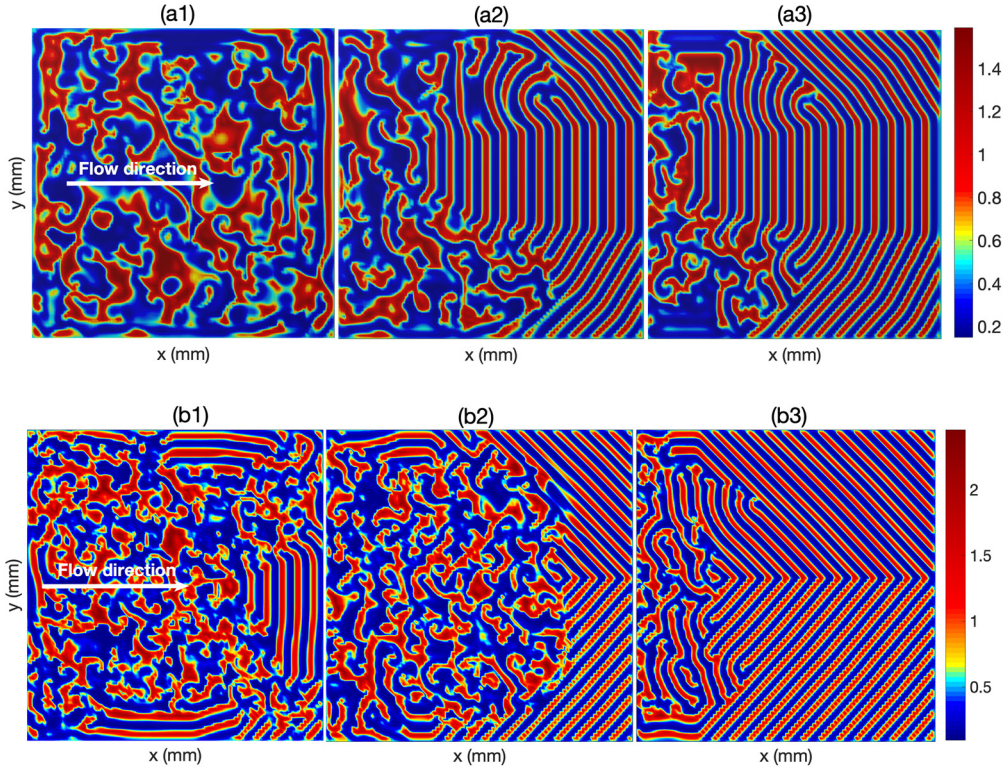

Fig. 9. Two-dimensional patterns of cAMP concentration $\gamma(x, y, t)$. Panels $(\mathrm{aj})_{j=1,2,3}$ show results for $k_e = 2.6$ min^{-1} and panels $(\mathrm{bj})_{j=1,3}$ correspond to $k_e = 3.1$ min^{-1}. From left to right, panels in each set correspond respectively to $V_f = 0.2$ mm.min^{-1}, 1 mm.min^{-1} and 1.8 mm.min^{-1}, with $\sigma = 0.3$ min^{-1} and $t = 60$ min.

peaks with flat tops, followed by a zone of erratic patterns of high cAMP concentration. Additionally, one can notice the disappearance of the spiral seeds, which corroborate the fact that advective flows are not favorable to spiral wave formation. This gets more pronounced in Fig. 9(a3), with $V_f = 1.8$ mm.min^{-1}. This phenomenon, to our modest opinion, may be due to the fact that the production rate of cAMP being unchanged, the degradation rate which is increased, along with the flow velocity, brings about important changes in the balance between nonlinear and dispersive effects, and therefore affects the process of MI. This suitably agrees with the patterns of Figs. $9(\mathrm{bj})_{j=1,2,3}$, where the degradation rate k_e has been increased to 3.1 min^{-1}. As in the previous case, the flow velocity takes the same values and increases from left to right. This case corresponds to Fig. 8(c), in absence of the advection flow. Obviously, the propagating cAMP waves respond to the flow. In this case, the spectrum of behaviors obtained in Fig. 9 remains, except that the trains of upstream peaks acquire a triangular shape, as a response to the high velocity of the flow. This was already predicted numerically by Edwards [25] and confirmed experimentally by Leconte et al. [26] in the case of an autocatalytic reaction. In general, when the flow velocity increases, the wave patterns are restrained to the left area of the medium, where there are probably multiple interactions between the upstream peaks and other types of patterns that are due to the instability of the initial plane wave solutions. Remarkably, all such modes of oscillation can be obtained through the activation of MI, but their long-time behaviors cannot be predicted by the linear stability analysis. However, when wave parameters are well-chosen in the area of instability, one expects some correlation between the analytical and numerical calculations, which is, once more, satisfactorily confirmed by the above-discussed results.

4. Conclusion

In this letter, the collective behavior of D. *discoideum* was studied. During starvation, D. discoideum amoeba release periodic spikes of cAMP in response to extracellular cAMP levels and interact by propagating cAMP waves throughout space. Starting with the pioneering work by Martiel and Goldbeter [8], there has been several contributions on modeling the D. *discoideum* signaling network. We have considered the same model in the present work. We have shown that the reaction-diffusion equations modeling the chemical cAMP concentration and cAMP receptors, can be reduced to a CGL equation, on which we conducted the linear stability analysis of MI. Regions of parameters that support the MI process have been discussed via the MI growth rate. Additionally, numerical simulations have been performed in a square channel and two oscillation cases have been considered: **(i)** cAMP oscillations in absence of the advective flow and **(ii)** in presence of the flow. In the absence of the flow, we considered as control parameters the production rate of intercellular cAMP (σ) and degradation rate of extracellular cAMP (k_e) that are among important parameters governing the system dynamics. In the first case, in agreement with the calculations on the CGL equation, the plane wave solutions were found to disintegrate into wave patterns, that are very sensitive to the change in control parameters. In that context, we obtained erratic patterns and spiral seeds. On the other hand, in presence of the flow, especially when the flow velocity was increased, an instability appeared, which generated wave trains upstream, followed again by erratic patterns. For some values of the degradation rate of extracellular cAMP, one obtained upstream traveling peaks of different shapes, which is in agreement with several experiments. In fact, Gholami and co-workers already obtained such results either through experiment [5] or through direct numerical simulation [14,27] in straight microfluidic devices, where flow-driven waves with a parabolic and triangular

flow profiles were reported. Under fast advective flows, Eckstein et al. [6] compared numerical and experimental results on pattern formation of self-organizing D. *discoideum* amoeba in a microfluidic setup, using a modified MG model, for a better understanding of the aggregation process, through waves patterns of cAMP of D. *discoideum* in its natural environment. However, our approach has shown that MG equations, when parameters related to MI are well-chosen, the same wave patterns of D. *discoideum* aggregation can be retrieved, which once more confirms their robustness in the studied system, and may give some substantial hint in this research field. Our investigations have also raised many interesting questions, some of which have been discussed in this letter, and which require to be fully addressed when D. *discoideum* cells are exposed to some other physical factors such as thermal fluctuations, time-delay, inhomogeneity of the medium, just to cite a few.

Declaration of competing interest

The authors certify that they have NO affiliations with or involvement in any organization or entity with any financial interest (such as honoraria; educational grants; participation in speakers' bureaus; membership, employment, consultancies, stock ownership, or other equity interest; and expert testimony or patent-licensing arrangements), or non-financial interest (such as personal or professional relationships, affiliations, knowledge or beliefs) in the subject matter or materials discussed in this manuscript.

Acknowledgements

The work of RNZ was supported in part by Campus France for the promotion of the higher education, the reception and the international mobility under the grant **946130B**. The work of CBT was supported by the Botswana International University of Science and Technology under the grant **DVC/RDI/2/1/16I (25)**.

Appendix

The following CGL equation has been obtained

$$i\frac{\partial\psi}{\partial\tau}+\frac{P_1}{2}\frac{\partial^2\psi}{\partial\xi^2}+\frac{P_2}{2}\frac{\partial^2\psi}{\partial\eta^2}+(Q_r+iQ_i)\mid\psi\mid^2\psi + i\frac{(R_r+iR_i)}{2}\psi=0, \tag{7}$$

with the coefficient $P_1, P_2, Q_r, Q_i, R_r, R_i$ being given by

$$P_1=\frac{1}{\omega}(D_0-\upsilon_g^2),\quad P_2=\frac{D_0}{\omega},$$

$$Q_r=\frac{1}{2\omega}[3g_1\omega^2+h_5k\omega+3D_4k^2\omega^2+D_8k^3\omega+3H_1k^4-3e_2 - 3D_2k^2-2e_1m_1+(2h_3k\omega+3D_1k^2+4H_0k^4-2e_1-2g_0\omega^2 - 4i_0k^2)m_r+6m_i(D_6k^3-D_3k^2\omega)],$$

$$Q_i=\frac{1}{2\omega}[\omega f_2+3g_2\omega^3+h_4k\omega^2+3i_2k^2\omega + D_5k^2\omega-h_2k-D_7k^3-H_2k^4\omega+(\omega f_1-h_1k)m_1 + (2h_3k\omega+3D_1k^2+4H_0k^4-2e_1-2g_0\omega^2-4i_0k^2)m_i + 6m_r(D_3k^2\omega-D_6k^3)]$$

$$R_r=\frac{\omega f_0-h_0k+\mu_0k^2\omega}{\omega},\quad R_i=\lambda_0k. \tag{8}$$

The different intermediary coefficients due to the application of the multiple-scale expansion procedure are:

$$\Omega_0^2=\left(\frac{2c_1c_4d_0}{c_5}+c_1d_1\right)-(c_4d_0+c_5d_2),\quad e_0=-c_5d_0,$$

$$e_1=\frac{c_1c_4d_1}{c_5}+c_1d_4+\frac{2c_1c_6d_2}{c_5}+\frac{2c_1c_8d_0}{c_5}-c_4d_2-c_5d_3 - \frac{2c_1^2c_6d_1}{c_5^2}-c_7d_0$$

$$e_2=\frac{c_1c_4d_4}{c_5}+c_1d_5+\frac{2c_1c_6d_3}{c_5}+\frac{2c_1^2c_6d_4}{c_5^2}+\frac{c_1c_7d_1}{c_5}+\frac{2c_1c_8d_2}{c_5} - c_4d_2-c_7d_2-\frac{2c_1^2c_8d_1}{c_5^2}$$

$$f_0=-(c_1+d_1+\frac{2c_6d_0}{c_5}),\quad f_1=\frac{c_1c_4}{c_5}+\frac{4c_1c_6d_1}{c_5^2}-2c_2-\frac{c_4d_1}{c_5} - d_4-\frac{2c_6d_2}{c_5}-\frac{2c_8d_0}{c_5}$$

$$f_2=\frac{4c_1c_6d_4}{c_5^2}+\frac{2c_1c_7}{c_5}+\frac{4c_1c_8d_1}{c_5^2}-3c_3-\frac{c_4d_4}{c_5}-d_5-\frac{2c_6d_3}{c_5} - \frac{c_7d_1}{c_5}-\frac{2c_8d_2}{c_5}-\frac{c_1^2c_8}{c_5^2}$$

$$g_0=-(\frac{c_4}{c_5}+\frac{2c_6d_1}{c_5^2}),\quad g_1=\frac{2c_1c_8}{c_5^2}-\frac{2c_7}{c_5}-\frac{2c_8d_1}{c_5^2}-\frac{2c_6d_4}{c_5^2},$$

$$g_2=-\frac{c_8}{c_5^2}$$

$$h_0=d_1v+\frac{2c_6d_0v}{c_5},$$

$$h_1=\frac{c_4d_1v}{c_5}+d_4v+\frac{2c_6d_2v}{c_5}+\frac{2c_8d_0v}{c_5}-\frac{4c_1c_6d_1v}{c_5^2}$$

$$h_2=\frac{c_4d_4v}{c_5}+d_5v+\frac{2c_6d_3v}{c_5}+\frac{c_7d_1v}{c_5}+\frac{2c_8d_2v}{c_5}-\frac{4c_1c_6d_4v}{c_5^2} - \frac{4c_1c_8d_1}{c_5^2}$$

$$h_3=\frac{c_4v}{c_5}+\frac{4c_6d_1v}{c_5^2},\quad h_4=\frac{2c_8v}{c_5^2},$$

$$h_5=\frac{2c_6d_4v}{c_5^2}+\frac{2c_7v}{c_5}+\frac{4c_8d_1v}{c_5^2}-\frac{2c_1c_8v}{c_5^2}$$

$$i_0=-\frac{2c_6d_1v^2}{c_5^2},\quad i_1=-(\frac{2c_6d_4v^2}{c_5^2}+\frac{2c_8d_1v^2}{c_5^2}),\quad i_2=-\frac{c_8v^2}{c_5^2}$$

$$D_0=-(\epsilon_1d_1+\frac{2c_6\epsilon_1d_0}{c_5}),$$

$$D_1=\frac{4c_1\epsilon_1c_6d_1}{c_5^2}-\frac{c_4d_1\epsilon_1}{c_5}-\epsilon_1d_4-\frac{2c_6d_2\epsilon_1}{c_5}-\frac{2c_8d_0\epsilon_1}{c_5}$$

$$D_2=\frac{4c_1c_6d_4\epsilon_1}{c_5^2}+\frac{4c_1c_8d_1\epsilon_1}{c_5^2}-\frac{c_4d_4\epsilon_1}{c_5}-d_5\epsilon_1-\frac{2c_8d_1\epsilon_1}{c_5} - \frac{2c_6d_3\epsilon_1}{c_5}-\frac{c_7d_1\epsilon_1}{c_5}$$

$$D_3=-(\frac{c_4\epsilon_1}{c_5}+\frac{4c_6d_1\epsilon_1}{c_5^2}),\quad D_4=-\frac{2c_8\epsilon_1}{c_5^2},$$

$$D_5=\frac{2c_1c_8\epsilon_1-4c_6d_4\epsilon_1-4c_8d_1\epsilon_1}{c_5^2}-\frac{2c_7\epsilon_1}{c_5}$$

$$D_6=\frac{4c_6d_1v\epsilon_1}{c_5^2},\quad D_7=\frac{4c_6d_4v\epsilon_1+4c_8d_1v\epsilon_1}{c_5^2},\quad D_8=\frac{2c_8v\epsilon_1}{c_5^2}$$

$$\lambda_0 = v,\ \ \mu_0 = \epsilon_1,\ \ H_0 = \frac{2c_6 d_1 \epsilon_1^2}{c_5^2},\ \ H_1 = \frac{2c_6 d_4 \epsilon_1^2 + 2c_8 d_1 \epsilon_1^2}{c_5^2},$$

$$H_2 = \frac{c_8 \epsilon_1^2}{c_5^2},$$

with $c_0 = \lambda_1 S/\epsilon_1\lambda_2 + (2\frac{\lambda_1 S}{\epsilon_1\lambda_2} - 1)\gamma_0 + (\frac{\lambda_1 S}{\epsilon_1\lambda_2} - 2)\gamma_0^3 - \gamma_0^3 - (1/\lambda_2)\gamma_0^2\rho_0^2(1+\gamma_0)$, $c_1 = (2\frac{\lambda_1 S}{\epsilon_1\lambda_2} - 1) + 2(\frac{\lambda_1 S}{\epsilon_1\lambda_2} - 2)\gamma_0 + 3\gamma_0^2 + (2S/\epsilon_1\lambda_2)\gamma_0\rho_0^2 - (3/\lambda_2)\gamma_0^2\rho_0^2$, $c_2 = (\frac{\lambda_1 S}{\epsilon_1\lambda_2} - 2) - 3\gamma_0 + (S/\epsilon_1)\lambda_2\rho_0^2 - (3/\lambda_2)\gamma_0\rho_0^2$, $c_3 = (-1/\lambda_2)\rho_0^2 - 1$, $c_4 = 2(S/\epsilon_1\lambda_2)\gamma_0\rho_0 - (4/\lambda_2)\gamma_0^2\rho_0$, $c_5 = (2S/\epsilon_1\lambda_2)\gamma_0^2 - (2/\lambda_2)\gamma_0^3\rho_0$, $c_6 = (S/\epsilon_1\lambda_2)\gamma_0^2 - (1/\lambda_2)\gamma_0^3$, $c_7 = (2S/\epsilon_1\lambda_2)\rho_0 - (4/\lambda_2)\gamma_0\rho_0$, $c_8 = 2(S/\epsilon_1\lambda_2)\gamma_0 - (3/\lambda_2)\gamma_0^2$, $d_0 = L_1 - (1+L_1)\rho_0 + (L_1 + \kappa L_2 c)\gamma_0 + L_2 c\kappa\gamma_0^2 + (c + \kappa + L_2 c\kappa + L_1)\gamma_0\rho_0 + (c\kappa + cL_2\kappa)\rho_0\gamma_0^2$, $d_1 = -(1+L_1) + (c + \kappa + L_2 c\kappa + L_1)\gamma_0 + (c\kappa + cL_2\kappa)\gamma_0^2$, $d_2 = L_1 + \kappa L_2 c + (c + \kappa + L_2 c\kappa + L_1)\rho_0 + 2(c\kappa + cL_2\kappa)\gamma_0\rho_0 + 2(L_2 c\kappa)\gamma_0$, $d_3 = L_2 c\kappa + (c\kappa + cL_2\kappa)\rho_0$, $d_4 = c + \kappa + L_2 c\kappa + L_1 + 2(c\kappa + cL_2\kappa)\gamma_0$, $d_5 = c\kappa + cL_2\kappa$.

References

[1] A.T. Winfree, Science 175 (1972) 634.
[2] A. Zaikin, Zhabotinsky, Nature 225 (1970) 535.
[3] G. Gerisch, Curr. Top. Dev. Biol. 3 (1968) 157.
[4] F. Alcantara, M. Monk, J. Gen. Microbiol. 85 (1974) 321.
[5] A. Gholami, O. Steinbock, V. Zykov, E. Bodenschatz, Phys. Rev. Lett. 114 (2015) 018103.
[6] T. Eckstein, E. Vidal-Henriquez, A. Bae, V. Zykov, E. Bodenschatz, A. Gholami, PLoS ONE 13 (2018) e0194859.
[7] C. Wilhelm, C. Riviere, N. Biais, Phys. Rev. E 75 (2007) 041906.
[8] J.L. Martiel, A. Goldbeter, Biophys. J. 52 (1987) 807.
[9] H. Levine, I. Aranson, L. Tsimring, T.V. Truong, Proc. Natl. Acad. Sci. 93 (1996) 6382.
[10] J. Noorbakhsh, D.J. Schwab, A.E. Sgro, T. Gregor, P. Mehta, Phys. Rev. E 91 (2015) 062711.
[11] P.B. Monk, H.G. Othmer, Philos. Trans. R. Soc. Lond. 323 (1989) 185.
[12] H.G. Othmer, G. Tang, Math. Biosci. 120 (1994) 25.
[13] J.J. Tyson, K.A. Alexander, V.S. Manoranjan, J.D. Murray, Physica D 34 (1989) 193.
[14] A. Gholami, V. Zykov, O. Steinbock, E. Bodenschatz, New J. Phys. 17 (2015) 093040.
[15] I. Maïna, C.B. Tabi, A. Mohamadou, H.P.F. Ekobena, T.C. Kofané, Chaos 25 (2015) 043118.
[16] A.S. Etémé, C.B. Tabi, A. Mohamadou, Commun. Nonlinear Sci. Numer. Simul. 43 (2017) 211.
[17] C.B. Tabi, R.Y. Ondoua, H.P. Ekobena, A. Mohamadou, T.C. Kofané, Phys. Lett. A 380 (2016) 2374.
[18] G.R.Y. Mefire, C.B. Tabi, A. Mohamadou, H.P.F. Ekobena, T.C. Kofané, Chaos 23 (2013) 033128.
[19] Y. Kuramoto, Chemical Oscillations, Waves and Turbulence, Springer-Verlag, Berlin, 1984.
[20] A.S. Etémé, C.B. Tabi, A. Mohamadou, Chaos Solitons Fractals 104 (2017) 813.
[21] C.B. Tabi, A. Mohamadou, T.C. Kofané, J. Comput. Theor. Nanosci. 5 (2008) 647.
[22] C.D.K. Bansi, C.B. Tabi, A. Mohamadou, Chaos Solitons Fractals 109 (2019) 170.
[23] M.C. Cross, P.C. Hohenberg, Rev. Mod. Phys. 65 (1993) 851.
[24] B.A. Malomed, Complex Ginzburg-Landau equation, in: Encyclopedia of Nonlinear Science, Routledge, New York, 2005, pp. 157–160.
[25] B.F. Edwards, Phys. Rev. Lett. 89 (2002) 104501.
[26] M. Leconte, J. Martin, N. Rakotomalala, D. Salin, Phys. Rev. Lett. 90 (2003) 126.
[27] E. Vidal-Henriquez, T. Eckstein, V. Zykov, E. Bodenschatz, A. Gholami, Chaos 27 (2017) 103110.